

# **Nitrogen-bridged Polyphenylene-based Materials for Electronic Applications**

Dissertation

Zur Erlangung des Grades

“Doktor der Naturwissenschaften”

am Fachbereich Chemie, Pharmazie und Geowissenschaften der  
Johannes Gutenberg-Universität

**Ashok Kumar Mishra**  
Geboren in Saharsha / India

Mainz, 2006

## Table of Content

<b>1. General introduction and Motivation</b>	
1.1 Overview of $\pi$ -conjugated polymers.....	1
1.2 Poly(p-phenylene) .....	2
1.2.1 Synthesis of PPP.....	3
1.2.1.1 Electrochemical Synthesis.....	3
1.2.1.1.1 Oxidative polymerization.....	3
1.2.1.1.2 Reductive polymerization.....	4
1.2.1.2 Chemical Synthesis.....	5
1.2.1.2.1 Kovacic's Synthesis.....	6
1.2.1.2.2 Catalytic and thermal dehydrogenation.....	7
1.2.1.2.3 Metal catalyzed coupling reaction.....	8
1.3 Organic light emitting diodes.....	13
1.3.1 Electroluminescence device.....	14
1.3.1.1 Basic processes.....	14
1.3.1.2 Basic parameters.....	14
1.3.1.3 Blue-emitting materials.....	15
1.3.1.4 Device structure.....	17
1.4 Polymeric solar cell.....	21
1.4.1 Advantage of organic solar cell over Si cell.....	21
1.4.2 Disadvantage of organic cell over Si cell.....	22
1.4.3 Basic working principle.....	23
1.4.4 Device parameters.....	24
1.4.5 Materials Used in organic solar cell.....	25
1.4.6 Device architecture.....	28
1.4.7 Current challenges.....	31
1.5 Organic thin field-effect transistors.....	31
1.5.1 Basic operation.....	32
1.5.2 Materials used in OFETs.....	33
1.5.2.1 p-Type semiconductor.....	34
1.5.2.2 n-Type semiconductor.....	36
1.6 Motivation of this work.....	38
1.6.1 Nitrogen-bridged semi-ladder-type polymers.....	38
1.6.2 Carbazole-thiophene fused molecule for OFETs.....	42
1.6.3 Aminocarbazole-anthraquinone fused dyes and polymers.....	43
1.7 References.....	45
<b>2. Nitrogen-bridged ladder-type polyphenylenes</b>	
2.1 Introduction.....	50
2.1.1 Ladder-type polymers.....	50
2.1.1.1 Heteroatomic ladder-type polymers by multifunctional polycondensation route.....	51
2.1.1.2 Conjugated ladder-type polymers by polymer analogous cyclization.....	53
2.1.1.2.1 Carbon-bridged ladder-type polymers.....	53
2.1.1.2.2 Nitrogen-bridged ladder-type polymers.....	55

2.2	Synthesis and characterization.....	60
2.2.1	Synthesis of poly(ladder-type tetraphenylene).....	62
2.2.1.1	Nitrogen-bridged poly(ladder-type tetraphenylene).....	62
2.2.1.2	Carbon-bridged poly(ladder-type tetraphenylene).....	63
2.2.1.3	Fully arylated carbon-bridged poly(ladder-type tetraphenylene)....	64
2.2.2	Synthesis of nitrogen-bridged poly(ladder-type pentaphenylene).....	66
2.2.3	Synthesis of poly(ladder-type hexaphenylene).....	69
2.2.3.1	Poly(ladder-type hexaphenylene) with three nitrogen bridges.....	69
2.2.3.2	Poly(ladder-type hexaphenylene) with one nitrogen bridges.....	70
2.3	Photophysical properties.....	72
2.3.1	Ladder-type monomers.....	72
2.3.1.1	All carbon-bridged ladder-type monomers.....	72
2.3.1.2	Nitrogen-bridged ladder-type monomers.....	74
2.3.2	Ladder-type polymers.....	76
2.3.2.1	Poly(ladder-type tetraphenylene).....	76
2.3.2.2	Poly(ladder-type pentaphenylene).....	80
2.3.2.3	Poly(ladder-type hexaphenylene).....	83
2.3.2.4	All carbon-bridged ladder-type polymers.....	87
2.3.2.5	Nitrogen-bridged ladder-type polymers.....	91
2.4	Electrochemical properties of ladder-type polymers.....	94
2.4.1	Poly(ladder-type tetraphenylene)s.....	94
2.4.2	Poly(ladder-type pentaphenylene).....	96
2.4.3	Poly(ladder-type hexaphenylene)s.....	97
2.4.4	Comparison between all nitrogen-bridged polymers.....	98
2.5	Stability of ladder-type polymers under oxidative environment.....	99
2.5.1	Poly(ladder-type tetraphenylene).....	99
2.5.1.1	Nitrogen-bridged poly(ladder-type tetraphenylene).....	99
2.5.1.2	Carbon-bridged poly(ladder-type tetraphenylene).....	100
2.5.2	Poly(ladder-type hexaphenylene) with one nitrogen bridge.....	101
2.6	Supramolecular organization of ladder-type polymers.....	104
2.7	Application of ladder-type polymers in FETs.....	113
2.8	Application of ladder-type polymers in PLEDs.....	122
2.8.1	Poly(ladder-type tetraphenylene).....	123
2.8.1.1	Nitrogen-bridged poly(ladder-type tetraphenylene).....	123
2.8.1.2	Carbon-bridged poly(ladder-type tetraphenylene).....	124
2.8.1.3	Fully arylated carbon-bridged poly(ladder-type tetraphenylene)...	126
2.8.2	Poly(ladder-type hexaphenylene) with one nitrogen bridges.....	128
2.9	Application of nitrogen-bridged polymers in solar cell.....	130
2.9.1	Photoquenching in the film.....	131
2.9.2	Photovoltaic devices with PCBM.....	132
2.9.3	Relation between the polymer design, supramolecular order and phovoltaic performance.....	134
2.9.4	Optimization of devices.....	136
2.10	Application of ladder-type polymers as gain medium in amplification of blue light by amplified spontaneous emission.....	138
2.11	Conclusions.....	147

2.12	References.....	150
<b>3.</b>	<b>Carbazole and thiophene fused oligomers</b>	
3.1	Introduction.....	153
3.2	Synthesis and optical properties.....	154
3.3	2D-WAXS and POM studies.....	158
3.4	Application of oligomers in OFETs.....	171
3.5	Conclusions.....	175
3.6	References.....	176
<b>4.</b>	<b>Aminocarbazole-anthraquinone fused dyes and polymers</b>	
4.1	Introduction.....	178
4.1.1	Carbazole azo dyes.....	179
4.1.2	Carbazole dyes with quinone groups.....	181
4.1.3	Dioxazine dyes.....	182
4.2	Synthesis and optical properties.....	184
4.3	Explanation of optical properties by resonance theory.....	188
4.4	Synthesis of novel red-emitting material .....	191
4.5	Unsuccessful attempt of dehydration on compound 61.....	194
4.6	Polymer based on diaminocarbazole and dichloroanthraquinone.....	197
4.7	Conclusions.....	200
4.8	References.....	201
<b>5.</b>	<b>Experimental details</b>	
5.1	Apparatus for analysis.....	202
5.2	General procedures.....	203
5.2.1	Electroluminescence devices.....	203
5.2.2	Solar cell devices.....	203
5.2.3	FET devices.....	203
5.3	Synthetic procedures.....	204
<b>6.</b>	<b>Acknowledgement.....</b>	<b>251</b>

## Chapter 1

### Introduction

#### 1.1 Overview of $\pi$ -conjugated polymers

Conjugated polymers are macromolecules that possess alternating single and double bonds along the main chain. These polymers combine the optoelectronic properties of semiconductors with the mechanical properties and processing advantages of plastics. When functionalized with flexible side groups, these materials become soluble in organic solvents and can be solution processed at room temperature into large-area, optical-quality thin films; such films are readily fabricated into desired shapes that are useful in novel devices. The ease of polymer processing compared with conventional inorganic semiconductors offers the potential for enormous cost-savings in applications that require visible band-gap semiconductors. Some common conjugated polymers are poly(acetylene) (PA), poly(thiophene) (PT), poly(pyrrole) (PPy), poly(*p*-phenylene) (PPP), poly(*p*-phenylenevinylene) (PPV), poly(fluorene) (PF), poly(carbazole) (PCz) and poly(phenanthrene) (PPh), which are illustrated in Figure 1.1.

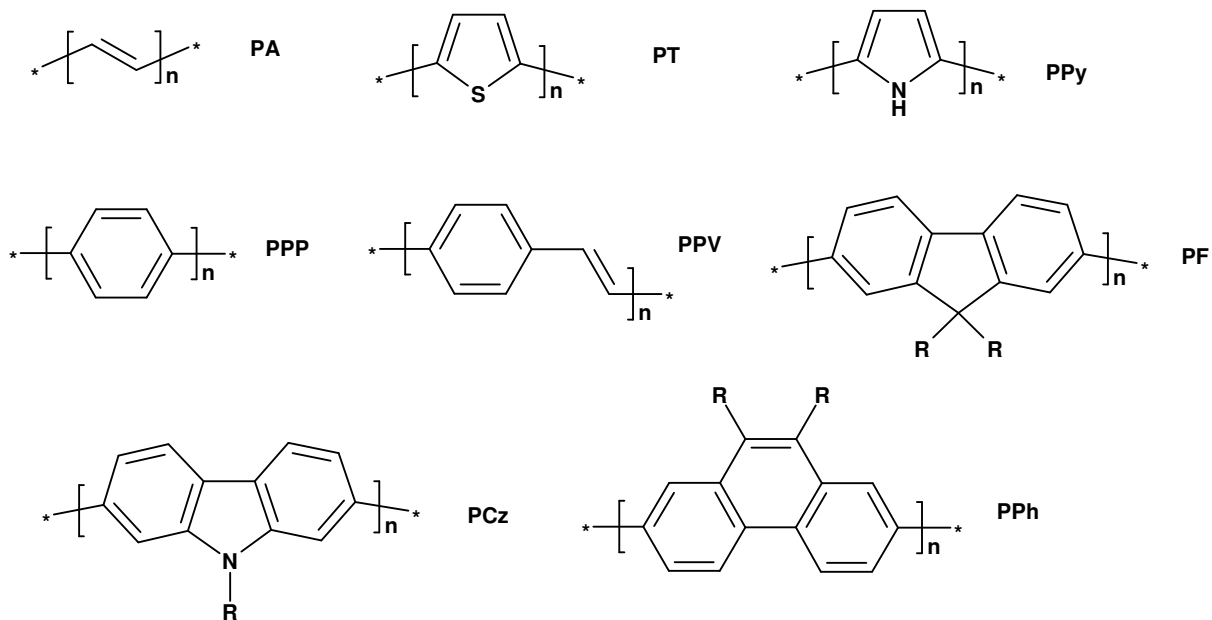


Figure 1.1 Structures of conjugated polymers

The potential use of conjugated polymers in electronic devices was realized in the late 1970s when electrically conductive polymers were discovered; i.e. Polyacetylene doped with iodine.<sup>1</sup> In recognition of this extraordinary discovery, the scientists (Shirakawa, MacDiarmid, and Heeger) were jointly awarded the 2000 Nobel Prize in Chemistry.

Many conjugated polymers that were studied in the early 1980s were based on heterocyclic compounds which were synthesized using chemical and electrochemical means.<sup>2</sup> Chemically synthesized conjugated polymers resulted in powders, which were insoluble and uncharacterizable using conventional analytical techniques. The primary interest in these powders was their electrical conductivity and their corresponding electronic structure. Alternatively, electrochemical synthesis of conjugated polymers was a more attractive approach because films were formed on the electrode.<sup>3</sup> Significant research on these polymer films was therefore performed to understand their spectrochemical and electrochemical properties. In the mid 1980s, Elsenbaumer reported the ground breaking synthesis of soluble conjugated polymers by attaching an alkyl side chain on polythiophene. The solubility of the polymers allowed structural characterization and polymer processing using spin or drop cast methods.<sup>4-6</sup>

To date, a surge of research on soluble conjugated polymers has been performed, due to their potential use as components in electronic applications, such as field effect transistors (FETs),<sup>7-12</sup> light emitting diodes (LEDs),<sup>13-22</sup> actuators,<sup>23</sup> and solar cells.<sup>24-28</sup> The development of these soluble conjugated polymers has led to significant improvement in their properties, including their high electrical conductivity (up to 2000 S/cm),<sup>29</sup> high field effect mobility ( $\sim 0.12 \text{ cm}^2 \text{ V}^{-1} \text{ s}^{-1}$ ) with excellent on/off ratios in FETs ( $10^7$ ),<sup>12</sup> high solid state photoluminescent<sup>30</sup> and LED efficiencies (10 % photons/electrons, external),<sup>17</sup> and significant solar conversion efficiencies (4.2 %).<sup>24</sup>

### **1.2 Poly(*p*-phenylene); A promising material for polymer electronics**

In the field of conjugated polymers, poly(*p*-phenylene) (PPP) continues to receive considerable attention due to its outstanding physical and chemical properties. In particular, it is known for its exceptional thermal stability in the neutral state, its

resistance to environmental oxidation and photo irradiation, its very wide window of conductivity range (from  $10^{-18}$  Scm<sup>-1</sup> in the pristine form to more than  $10^2$  S cm<sup>-1</sup> in the doped state), the possibility of carrying out chemical or electrochemical n- or p- doping of the polymer similar to that of polyacetylene and its application in electronic devices such as LEDs, FETs and solar cells.

### **1.2.1 Synthesis of Poly(*p*-phenylene)**

There are two main methods to synthesize conjugated *p*-phenylene polymers (i) electrochemical (ii) chemical

#### **1.2.1.1 Electrochemical synthesis**

Electrochemical oxidation of benzene was first investigated in the 1960s. The formation of black deposits was observed but it was realized only much later that benzene was being polymerized, and it was not until the beginning of the 1980s that electrosynthesis was developed for producing PPP films on metallic substrate. These methods are useful in producing films of controlled thickness and various morphology in a single step. Electrosynthesis of PPPs may be classified into two main reaction families

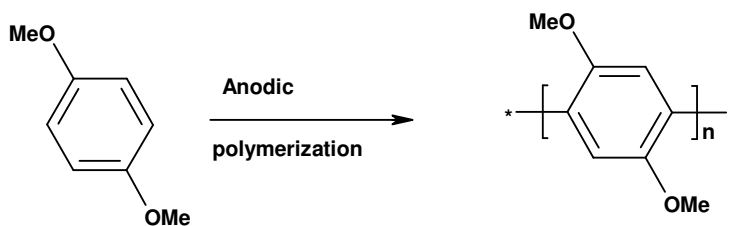
- (1) Oxidative electropolymerization,
- (2) Reductive electropolymerization.

##### **1.2.1.1.1 Oxidative polymerization**

This is a very valuable technique to obtain PPP films of controlled thickness.<sup>31</sup> Although it is similar to chemical methods like Kovacic's which follow the same oxidation mechanism, the material so obtained is an insulating polymeric powder which has to be processed further to make homogeneous films but in the case of anodic electropolymerization (oxidative polymerization) a one-step process provides a conductive polymer film with controlled thickness. However, the structure and properties

is highly influenced by many experimental conditions like the electrolytic medium and electrolysis conditions.

Various 1,4-disubstituted benzenes were anodically polymerized in acetonitrile with the usual electrolytes TBABF<sub>4</sub> and yielded regular chains of poly(1,4-phenylene) but with small degree of polymerization, typically not higher than 10 (Scheme 1.1)<sup>31</sup>



**Scheme 1.1** Synthesis of 1,4-disubstituted PPP

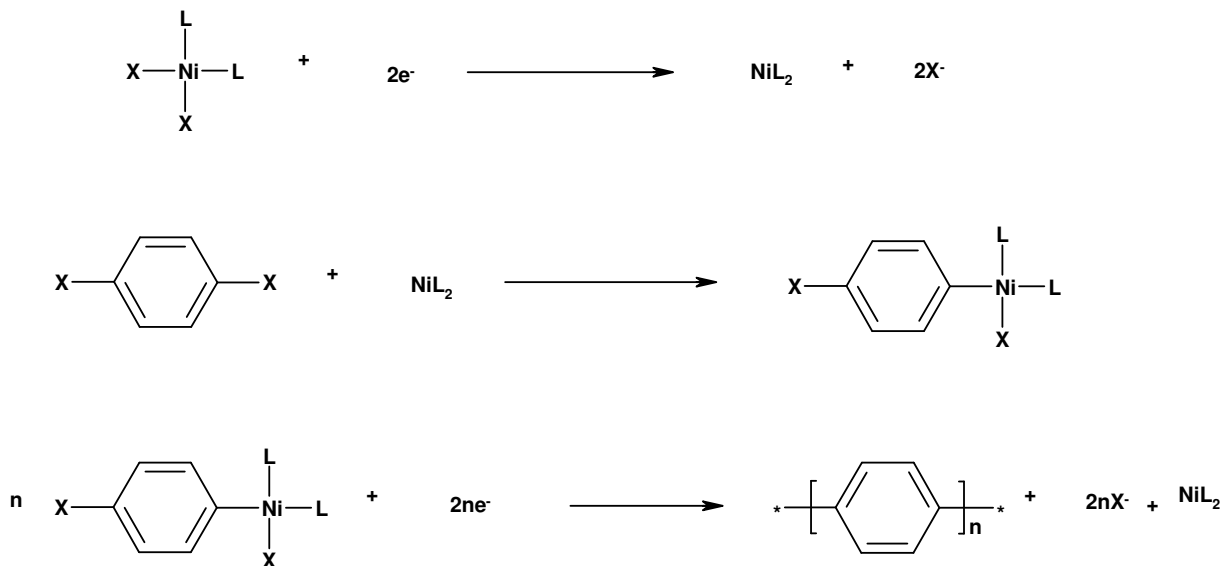
#### 1.2.1.1.2 Reductive electropolymerization

The reductive electropolymerization is similar to their chemical counter part like Yamamoto, Suzuki polymerization in the sense that both use the reducing conditions. The active catalytic species in the polymerization reaction are low-valent metal complexes. They can be used directly or can be generated *in situ* by reaction with a reducing agent such as magnesium or zinc. In the first case the active catalytic species is generated by the electrochemical reduction instead of using a reducing metal.

Synthesis of PPP is done mainly by using Ni complexes during reductive electropolymerization.<sup>32-34</sup> It involves two main steps<sup>35</sup> (Scheme 1.2)

- (i) Generation of the zero-valent nickel complex by electroreduction,
- (ii) Reduction of above complex leading to polymerization.





**Scheme 1.2** Mechanism of reductive electropolymerization

This technique is well adapted for the synthesis of linear polyphenylene oligomers. *p*-Sexi-, octa- and undecaphenylenes can be easily generated by electrochemical reduction of bromo-oligophenyl in the presence of catalytic amounts of  $\text{NiBr}_2(\text{bipy})$ .<sup>36</sup> This technique also has been used to generate copolymers by reducing a solution of 3, 6-dibromo-9-ethylcarbazole and 4,4'-dibromobiphenyl on a mercury pool. Doping the copolymers with  $\text{AsF}_5$  led to materials with conductivities increasing from  $10^{-5}$  to  $1 \text{ Scm}^{-1}$  when the amount of nitrogen in the polymer decreased from 4.5 % to 0.5 %.<sup>37</sup>

### 1.2.1.2 Chemical synthesis

- There are three main reactions typically used to synthesize PPP chemically. They are
- (1) Direct oxidation of benzene with a suitable catalyst-oxidant system also commonly known as Kovacic reaction,
  - (2) Catalytic and thermal dehydrogenation of poly(1,3-cyclohexadiene),
  - (3) Metal catalyzed coupling reaction (Grignard, Ullmann, Yamamoto and Suzuki).

### 1.2.1.2.1 Kovacic's method

In this method the carbon-carbon bond is formed by dehydro-coupling of benzene nuclei by a catalyst-oxidant system. The reagent used is either a binary system consisting of a Lewis acid and an oxidant or a single reagent with both Lewis acid and oxidizing properties. Aluminum chloride ( $\text{AlCl}_3$ ) as the Lewis acid (catalyst) with cupric chloride as oxidant is the best known catalyst-oxidant combination for polymerization of PPP by Kovacic's method (Scheme 1.3).<sup>38-40</sup> Polymerization occurs under mild conditions with water as a cocatalyst, and the yield of PPP depends on the ratio of catalyst to oxidant.<sup>41</sup>



**Scheme 1.3** Synthesis of PPP by Kovacic route

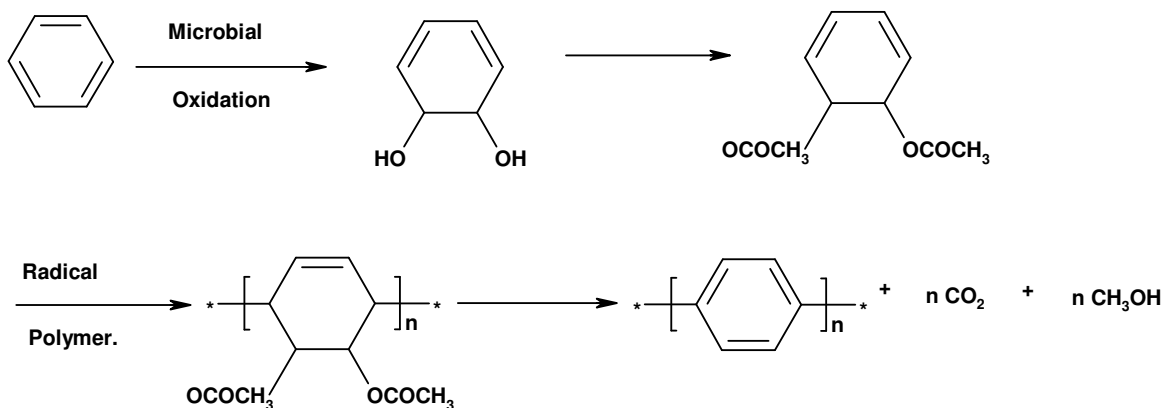
Usually, PPP obtained under Kovacic's conditions are powdery materials with some crystallinity which could be increased by annealing at 400 °C. The degree of polymerization achieved in this case was typically less than 15.<sup>42</sup> An interesting improvement of Kovacic reaction was reported by Arnautov et. al. where an ionic liquid was used instead of organic solvent which increased the degree of polymerization upto 25.<sup>43</sup> The increase in molecular weight was attributed to the improved solubility of the polymer in the ionic liquid than organic solvent. A second type of catalyst can also be used to polymerize the benzene where the catalyst functions both as Lewis acid as well as an oxidizing agent such as  $\text{FeCl}_3$ ,  $\text{MoCl}_5$ ,  $\text{AsF}_5$  and  $\text{SbF}_5$  together with water as a cocatalyst.<sup>40</sup>

Kovacic's method suffered from disadvantages like low molecular weights and the presence of large amounts of impurities such as oxygen, chlorine and catalyst residues in PPP.

### 1.2.1.2.2 Catalytic and thermal dehydrogenation of poly(1,3-cyclohexadiene)

The reaction was based on the aromatization of a soluble poly(1,3-cyclohexadiene) precursor, which was heated to give PPP. The dehydrogenation reaction was done in the presence of a mild oxidant, at a temperature which depends on the medium<sup>44-46</sup> and the nature of substituents attached with the cyclohexadiene moiety.<sup>47, 48</sup>

In early attempts, polymerization of 1,3-cyclohexadiene to a linear polymer containing cyclohexane as repeating unit was achieved by using a Ziegler catalyst consisting of a mixture of tri-isobutyl aluminum and titanium tetrachloride.<sup>44 46</sup> However, the polymer synthesized was low molecular weight ranging from 5000 to 10000 g/mol. Treatment of this polymer with chloranil as a dehydrogenating agent resulted in insoluble material.<sup>44</sup>



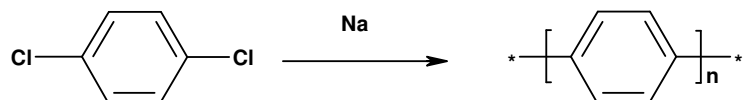
**Scheme 1.4** Synthesis of PPP by Ballard et. al.<sup>48</sup>

Lately, Ballard et. al. reported an improved synthesis where benzene was first oxidized to 5,6-cis-dihydroxycyclohexa-1,3-diene by microbial oxidation and subsequently polymerized using a free radical initiator. In this process high molecular weight (DP around 150) was achieved which further aromatized to PPP by elimination of two ROH group either by heating in solid state or solution (Scheme 4).<sup>48</sup> The disadvantage of this synthesis was the cyclohexadiene not only produced the 1,4- linkage but also some 1,2- linkages.

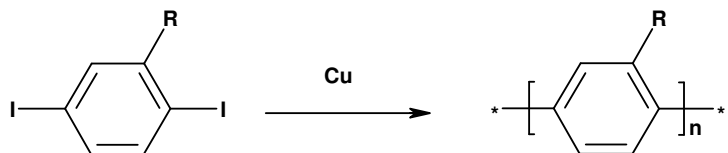
### 1.2.1.2.3 Metal-catalyzed coupling reaction

A great variety of reactions based on the coupling of 1,4-disubstituted aromatic monomers in the presence of various metals, mostly transition metals have been reported in order to generate high molecular weight 1,4-linked poly(*p*-phenylene). These reactions can be classified in to two main families (a) polymerization of 1,4-disubstituted aromatic monomers such as dihalides, bistriflates and bisalkylsulfonates using Ni compounds (b) Suzuki reaction which is the coupling between aromatic boronic acids or esters with halogenated aromatic compounds in the presence of Pd(0). There are also some attempts to make PPP by Wurtz-Fittig reaction<sup>49</sup> and also by Ullman reaction.<sup>50-52</sup> However, both methods resulted in low molecular weight PPP with structural irregularities (Scheme 5).

#### Wurtz-Fittig reaction



#### Ullmann reaction

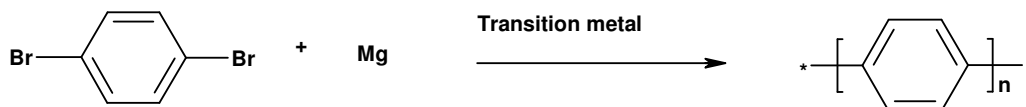


**Scheme 1.5** Synthesis of PPP by Wurtz-Fittig and Ullman route

#### (a) Ni-based catalytic systems (Yamamoto polymerization)

In the late 1970s, Yamamoto et. al. reported a more versatile and more efficient synthetic route to synthesize PPP.<sup>53</sup> The initial discovery that transition metals or their complexes catalyze the coupling of Grignard reagents with aryl halides were extended to the coupling of dihaloaromatic compounds.<sup>54-56</sup> The reaction yielded high selectivity, and quantitative yield under mild conditions. Particularly, the use of NiCl<sub>2</sub>(bpy) was more

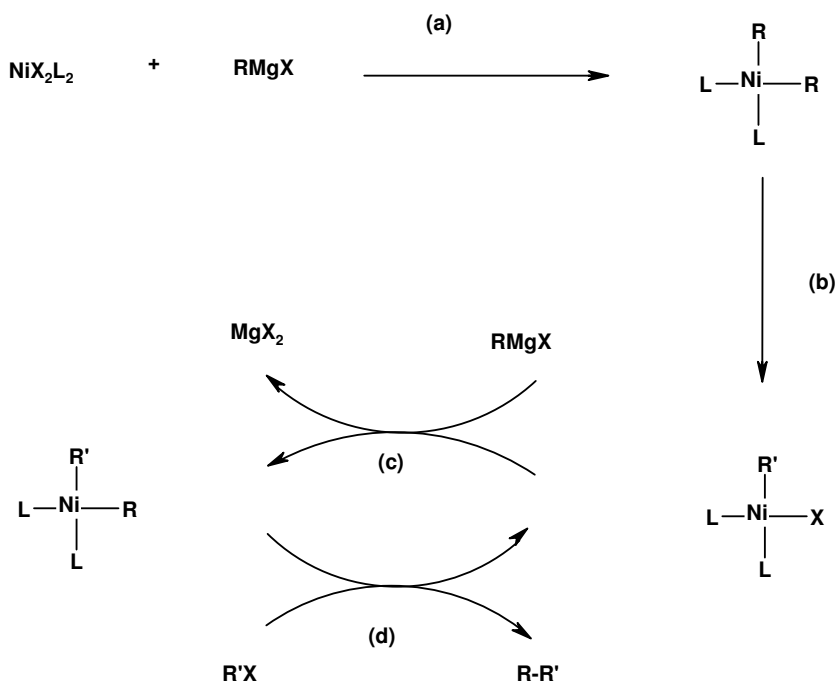
successful. The PPP obtained following this procedure was much less colored than prepared by the Kovacic route (Scheme 1.6). However, again the molecular weight was low but polymer was free from meta- or ortho- links which suggested that the reaction was highly regioselective.



**Scheme 1.6** Synthesis of PPP by Yamamoto route

The mechanism postulated for the reaction was an extension of the earlier proposed catalytic reaction of nickel catalysts for the coupling of Grignard reagents,  $\text{RMgX}$  with an aryl halide,  $\text{R}'\text{X}$ . The mechanism consists of four steps<sup>56</sup> (Scheme 1.7).

- Formation of  $\text{NiR}_2\text{L}_2$  by reaction of  $\text{NiX}_2\text{L}_2$  and  $\text{RMgX}$ ,
- Reaction of  $\text{NiR}_2\text{L}_2$  with  $\text{R}'\text{X}$  to give  $\text{R-R}$  and  $\text{NiR}'\text{XL}_2$ ,
- Alkylation of  $\text{NiR}'\text{XL}_2$  with  $\text{RMgX}$  to yield  $\text{NiRR}'\text{L}_2$  and  $\text{MgX}_2$ ,
- Elimination of  $\text{R-R}'$  with formation of  $\text{NiR}'\text{XL}_2$  in the reaction of  $\text{NiRR}'\text{L}_2$  with  $\text{RX}$ .



**Scheme 1.7** Mechanism of Yamamoto coupling

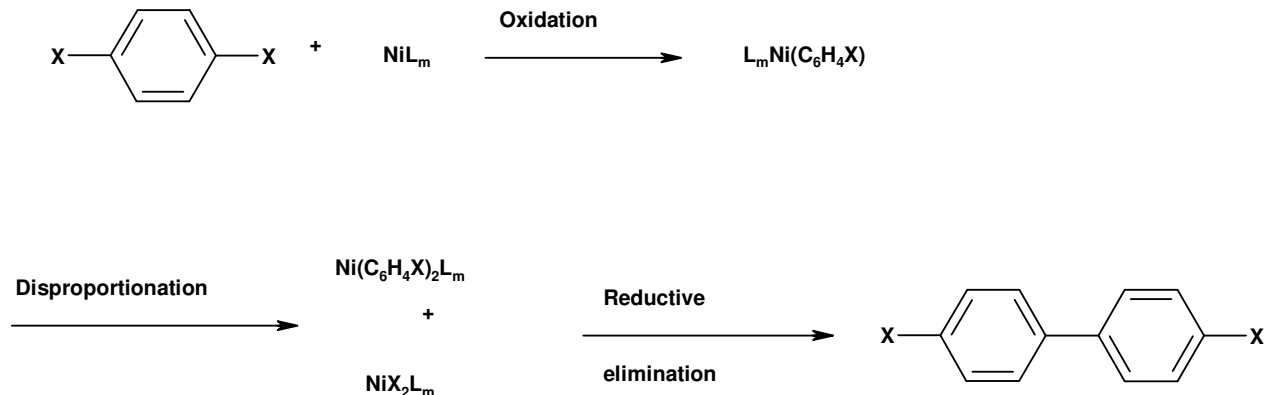
The  $\text{NiR}'\text{XL}_2$  was the active species and generated in situ by reactions (a) and (b). However, this method again resulted in only oligomers and the degree of polymerization (DP) was found to be of the order of 8.

Later, Yamamoto et. al. presented a new route to PPP by using Ni(0) as a coupling reagent for aryl halides<sup>57</sup> (Scheme 1.8).



**Scheme 1.8.** New route to PPP by Ni(0) by Yamamoto et. al.<sup>57</sup>

Polymerization was assumed to proceed through oxidative addition of Ni(0) to the carbon-halogen bond to form a (4-halophenyl)nickel complex  $\text{L}_m\text{Ni}(\text{C}_6\text{H}_4\text{X})_2$ , and reductive elimination of  $\text{XC}_6\text{H}_4\text{-C}_6\text{H}_4\text{X}$  from  $\text{L}_m\text{Ni}(\text{C}_6\text{H}_4\text{X})_2$ . Propagation occurs by coupling between  $\text{X}(\text{C}_6\text{H}_4)_x\text{X}$  and  $\text{X}(\text{C}_6\text{H}_4)_y\text{X}$  (Scheme 1.9).

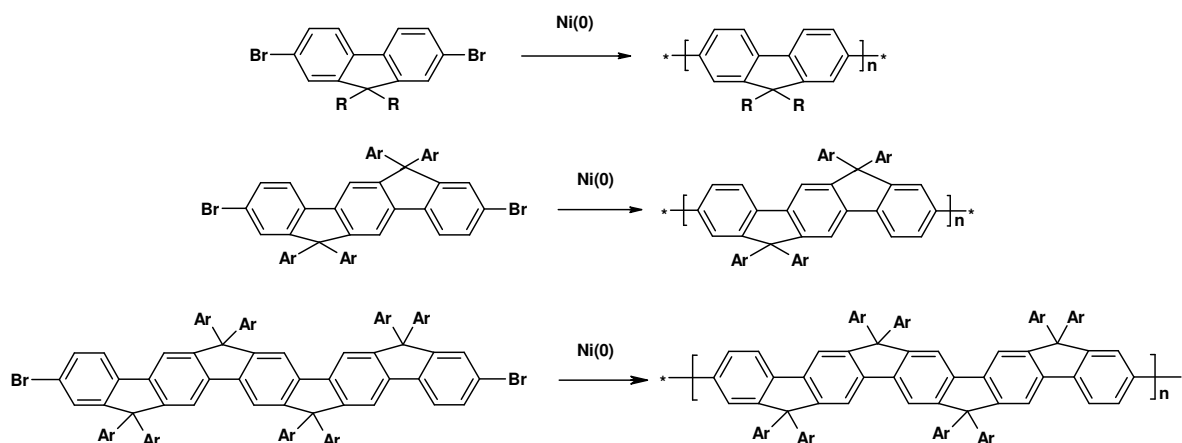


**Scheme 1.9** Mechanism of aryl-aryl coupling by Ni(0)

The PPP synthesized by this method had higher molecular weight compared to that synthesized by Kovacic. This reaction proceeded under mild conditions and can be applied to a wide range of aromatic compounds including those with carbonyl groups. However, it suffers from severe limitations like the need for stoichiometric amounts of the expensive Ni(0) reagents and the extreme air sensitivity of the reaction.

Recently, this method was used to synthesize a range of blue-emitting polymers starting from polyfluorene to ladder-type poly(pentaphenylene) as shown in scheme 10.<sup>20-</sup>

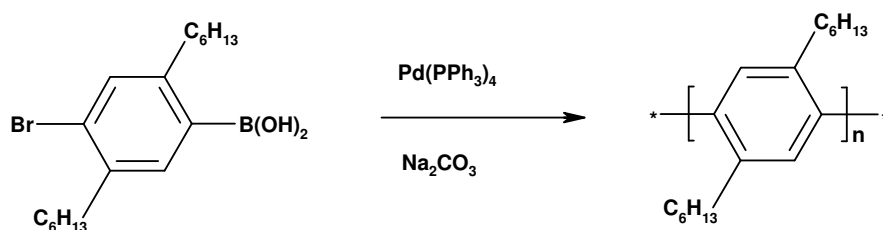
22

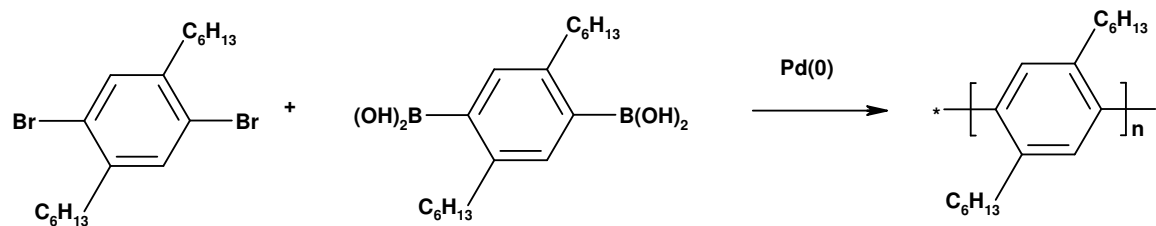


**Scheme 1.10** Synthesis of step ladder-type polyphenylene by Yamamoto polymerization

**(b) Pd-based catalytic systems (Suzuki Coupling reaction)**

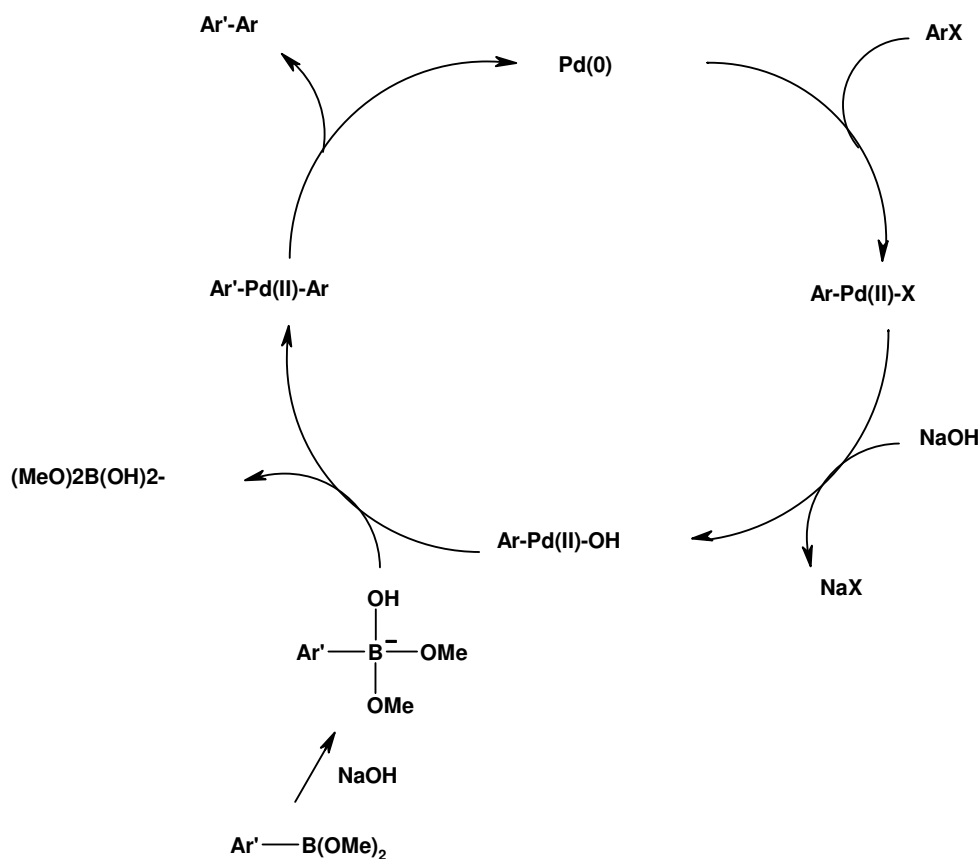
Suzuki reaction is considered to be one of the most versatile methods to form carbon-carbon bonds. This method is very useful when it comes to synthesize alternating copolymers which is not possible by Ni(0) catalyzed Yamamoto coupling which only leads to either homopolymer or random copolymer. This reaction was considered to be highly selective and quantitative. The influence of substituents attached at the ortho position was reported to be negligible. The 4-bromo-2,5-di-n-hexylbenzene boronic acid was synthesized and allowed to react in a heterogeneous system of aq.  $\text{Na}_2\text{CO}_3$  and benzene in the presence of  $\text{Pd}(\text{PPh}_3)_4$  under reflux for two days.<sup>58</sup> A colorless polymer was produced in 100 % yield shown in Scheme 1.11.





**Scheme 1.11** Synthesis of substituted PPP by Pd(0) catalyzed Suzuki reaction

This procedure has a clear advantage over Yamamoto polymerization which gave higher molecular weights than Yamamoto polycondensation. Osmometry and GPC experiments indicated a DP of over 28. Monomers containing nitro, keto or ether functions can be condensed without any complication. The mechanism of the Suzuki reaction is depicted in Scheme 1.12.



**Scheme 1.12** The mechanism of Suzuki coupling

This reaction was used in synthesizing various kinds of alternating copolymers as well as homopolymers. Some of them are shown in Figure 1.2.



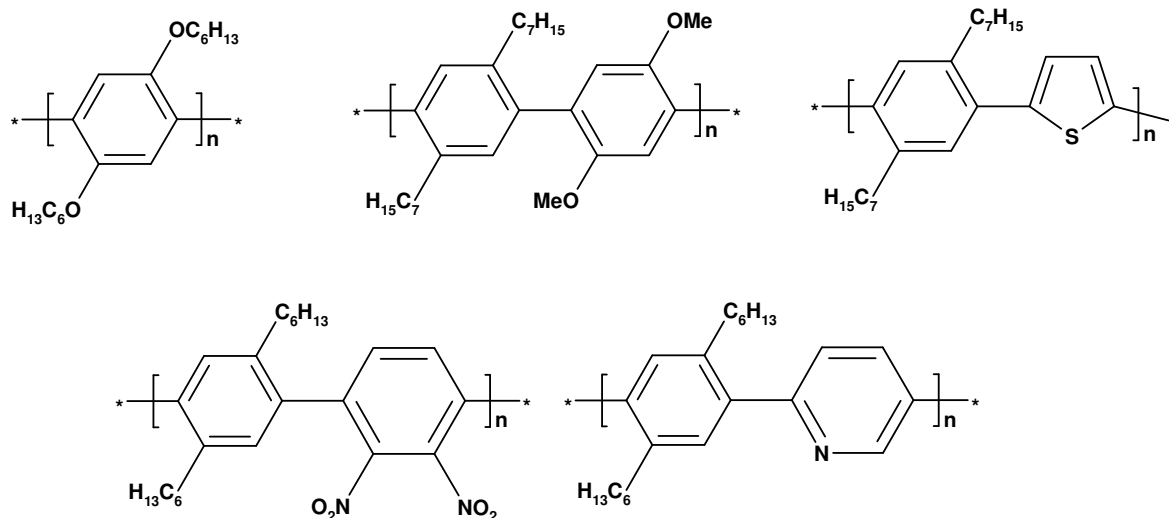


**Figure 1.2** Examples of homopolymers and copolymers synthesized by Suzuki reaction

Suzuki Coupling is also useful reaction in synthesizing ladder-type polymers. The optical, electrical, photoelectrical, and non-linear optical properties of these materials showed great promise. In the next chapter, the synthesis and characterization of ladder-type polymer will be discussed in more details.

### 1.3 Organic Light emitting diodes

#### 1.3.1 Electroluminescence

Electroluminescence is the emission of light from a material upon electrical excitation. In other words, electroluminescence results from the deexcitation of a solid that has been excited by electric current passing through it. The term electroluminescence has been known for a long time in inorganic semiconductors. Electroluminescence was observed for the first time in inorganic compounds (ZnS Phosphors) as early as 1936 by Destriau.<sup>59</sup> Shortly, inorganic light emitting diode was commercialized with a variety of applications. Pope et. al. first reported this phenomenon from organic semiconductors in 1963.<sup>60</sup> They observed emission from single crystals of anthracene, a few tens of micrometers in thickness, using silver paste electrodes and required large voltages to get emission, typically around 400 V. Development of organic thin-film electroluminescence

advanced in the 1970s with the study of thin-film devices. Vincett et. al. made devices using films of anthracene sublimed onto oxidized aluminum electrodes, with thermally evaporated semitransparent top gold electrodes, and were able to reduce the drive voltage considerably down to ~12 volt but with poor efficiency and lifetime.<sup>61</sup> Later on, Tang and Van Slyke demonstrated efficient electroluminescence in two layer sublimed molecular film devices consisting of a hole-transporting layer of an aromatic diamine and an emissive layer of 8-hydroxyquinolinealuminum (alq<sub>3</sub>).<sup>62</sup> Since the work of Tang and coworkers, a large number of other molecular materials have been used as the charge-transporting or emissive layer in LEDs. In 1990, a breakthrough came when Friend and coworkers at Cambridge university demonstrated green-yellow electroluminescence emission from the poly(paraphenylenevinylene) (PPV) during experiments on polymeric sandwich structures.<sup>19</sup>

### 1.3.2 Electroluminescent devices

#### 1.3.2.1 Basic processes

There are three basic processes occurring in an electroluminescent device

1. Charge carriers of opposite sign are introduced into the active layer,
2. Positive and negative charge carriers move in the active layer under the applied voltage,
3. Charge carriers of different sign interact with each other to form excited species called excitons which are short lived species and on radiative decay emit light corresponding to the band gap of polymer.

#### 1.3.2.2 Basic parameters

1. **Internal efficiency** The most common measure of quantum efficiency is the internal efficiency, the ratio of the number of photons emitted per electron injected. This number cannot be measured directly.

- 2. External efficiency** Not all of the light generated reaches the viewer and so the external efficiency is a factor of  $2n^2$  lower than the internal efficiency, where  $n$  is the refractive index of the polymer. Typical values for the external quantum efficiency range between 0.1 - 5 %.<sup>63</sup>

$$\eta_{\text{int}} = 2n^2 \eta_{\text{ext}}$$

- 3. Power efficiency** The ratio of output light power to the input electric power, known as power efficiency ( $\text{cdA}^{-1}$ ), can be calculated by multiplying the external efficiency by the ratio of the mean photon energy ( $E_p$ ) and the drive voltage ( $U$ ). High power efficiency is required for long device lifetimes.

$$\eta_{\text{pow}} = E_p U^{-1} \eta_{\text{ext}}$$

- 4. Luminous efficiency** The luminous efficiency, measured in lumens per watt ( $\text{lmW}^{-1}$ ) takes into account that the human eye is more sensitive to certain colors. The luminous efficiency is determined by multiplying the power efficiency by the luminous efficacy ( $S$ ), as defined by the Commission de L'Eclairage (CIE).<sup>64</sup>

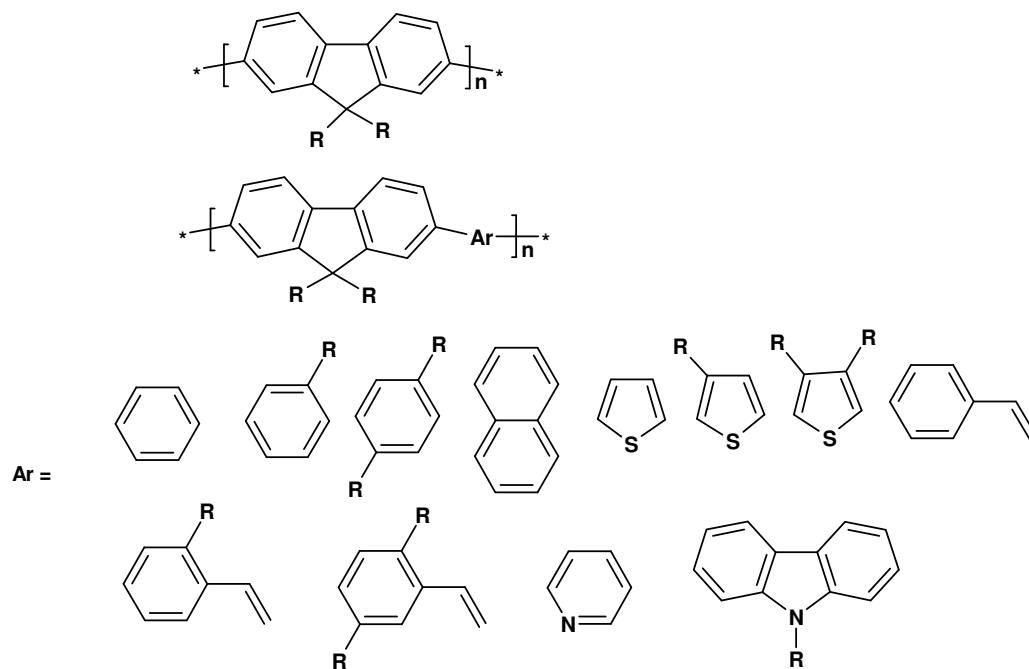
$$\eta_{\text{lum}} = \eta_{\text{pow}} S$$

- 5. Luminance** The brightness of a device, in  $\text{cdm}^{-2}$ , is also used to estimate the efficiencies of devices. The Luminance is sometimes reported as a function of current density. An average laptop display has a luminance in the order of 100  $\text{cdm}^{-2}$ .<sup>15, 65</sup>

### 1.3.2.3 Blue-emitting Materials

Blue emission is the most difficult to achieve not only in PLEDs but also in inorganic semiconductor-based LEDs.

## Group A



## Group B

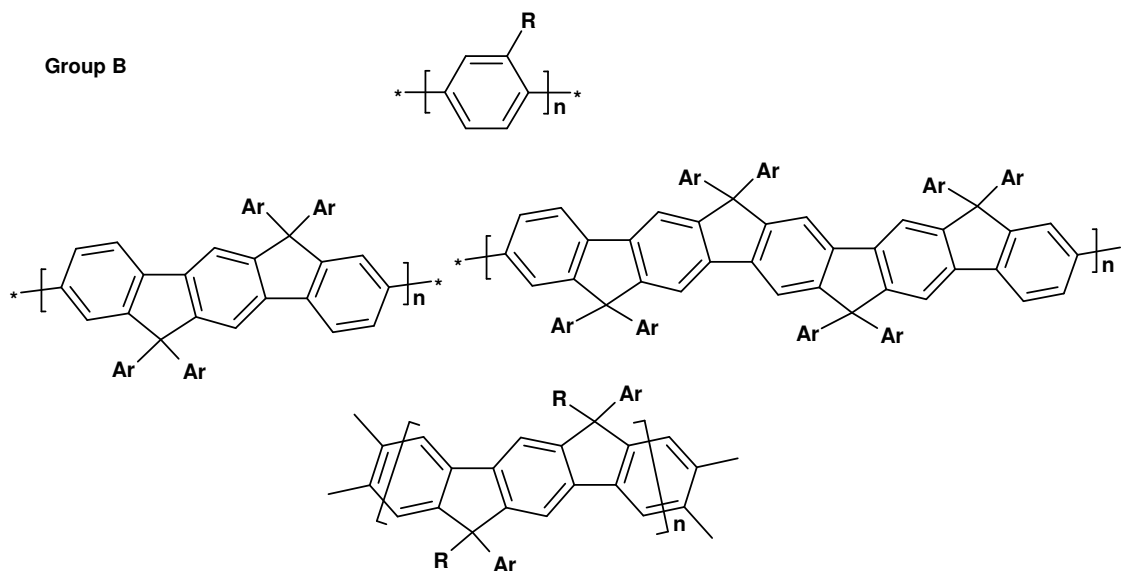


**Figure 1.3** Blue-emitting materials used in PLEDs

Polymers suitable for the fabrication of blue emitting PLEDs must show a high band gap. Two groups of polymers (Figure 1.3) can be used for this purpose, namely poly(fluorene) homopolymers/copolymers<sup>66</sup> and substituted ladder-type poly(p-phenylenes)<sup>15, 20, 22</sup>.

Due to solution processability of new generations of electroluminescent polymers, ink-jet techniques can be applied in the fabrication of PLED-based multicolor displays. Commercial application of PLED-based devices requires materials with high purity, facile processability, and good thermal and oxidative stability. Industrially produced multicolor displays based on PLEDs have been demonstrated by CDT/SEIKO/Epson, Philips, Toshiba and other companies (Figure 1.4).



**Figure 1.4** OLEDs based display from LG electronics

### 1.3.2.4 Device structure

Depending upon the number of layers, LED devices can have either single layer or multilayer configuration.

#### (1) Single-Layer LED devices

In this device configuration the emitting layer (conjugated polymer) is sandwiched between cathode and anode, where cathode is the electron injecting electrode (usually a

low work function alkali metal such as Ca, Mg or Ba) and anode is the hole injecting electrode, indium tin oxide being the most commonly used one as shown in Figure 1.5.

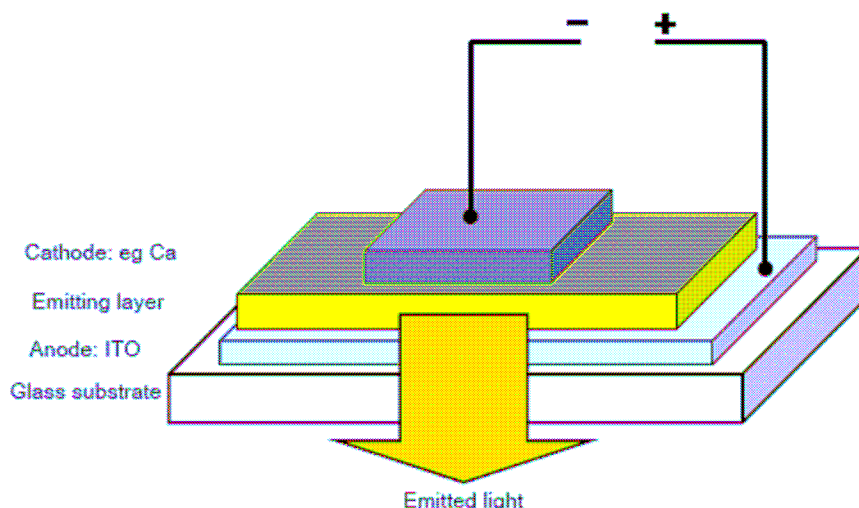


**Figure 1.5** Schematic diagram of single layer OLEDs

The EL emission process in the single layer device can be described as follows. When an electric field is applied in the forward direction (the high work function contact is positive), positive charge carriers are injected into the layer from the high work function contact and electrons are injected from the low work function contact. These carriers move as polarons under the force of the applied electric field and meet each other within the emitting layer. Pairs of positive and negative charge carriers can form weakly or strongly bound states depending on the nature of the electronic structure of the active layer. These bound neutral excited states can either be singlet (spin 0) or triplet (spin 1) states, which determines whether the decay of these states into the ground state is dipole allowed (radiative decay results in emission of light) or dipole forbidden (nonradiative decay results in energy dissipation as heat). The dipole-allowed radiative recombination of these excited states finally causes the electroluminescence.

In a single-layer electroluminescent (EL) device, the region where the EL occurs is usually located near the cathode because of the better mobility of positive polaron (hole) in the conjugated polymer. This concentration of positive charges near the cathode is a drawback for producing efficient electroluminescence, as near the cathode

the probability for nonradiative recombination at defect site is quite high. In these cases, multi-layer devices are required to improve the electroluminescence efficiency and are built by introducing an electron transport layer between the polymer and cathode and a hole-transport layer between the polymer and anode.

## **(2) Multilayer LED devices**

Multilayer devices can be made by inserting an electron transport layer between the cathode and polymer, or a hole transport layer between the anode and polymer, or both. The type of multi layer device used in the fabrication of any device depends entirely on the intrinsic properties of the polymeric emissive material used.

### **(i) PLED devices with an electron transport layer**

As discussed before, the main drawback of single layer devices is that the exciton mainly forms near to the polymer and cathode interface due to the better hole mobility in the most conjugated polymers and hence nonradiative quenching takes place at this site because of high concentration of defects at the interface. This quenching effect can be decreased by introducing an electron transporting layer between the cathode and the polymer. This layer can significantly improve the EL efficiency when its LUMO is located below the conduction band (CB) edge of the polymer, so that the potential barrier at the interface to the low work function electrode is decreased. The electron injection is then facilitated, and the balance in the charge injection can be improved. Some of the electron transporting materials used in multilayer PLED devices are listed in Figure 1.6.

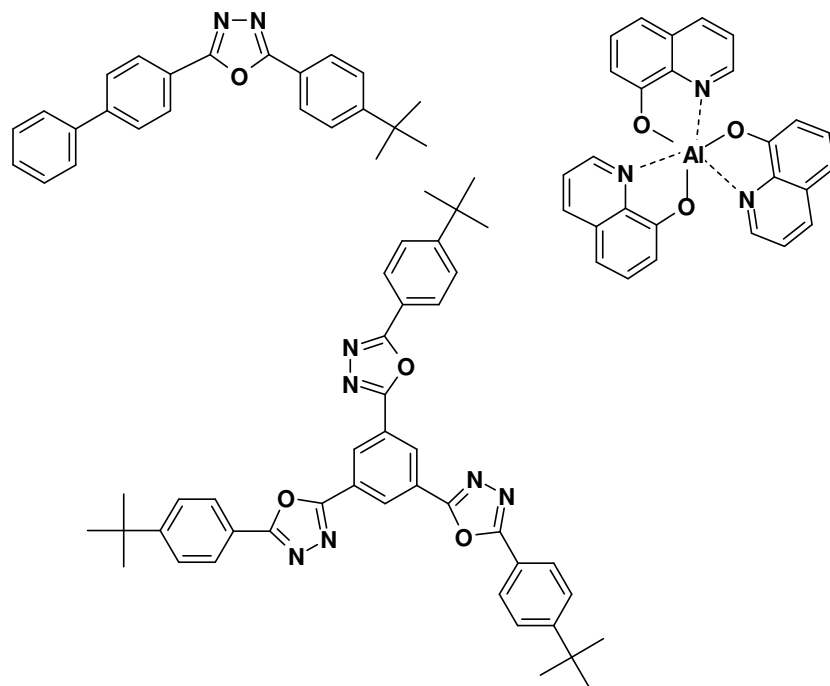


**Figure 1.6** Examples of electron-transporting materials<sup>15</sup>

(ii) **PLED devices with a hole transport layer**

To improve the stability and efficiency of PLEDs, it is very important to decrease the operating bias voltage so that the power consumption and hence the Joule heating of the devices is reduced.

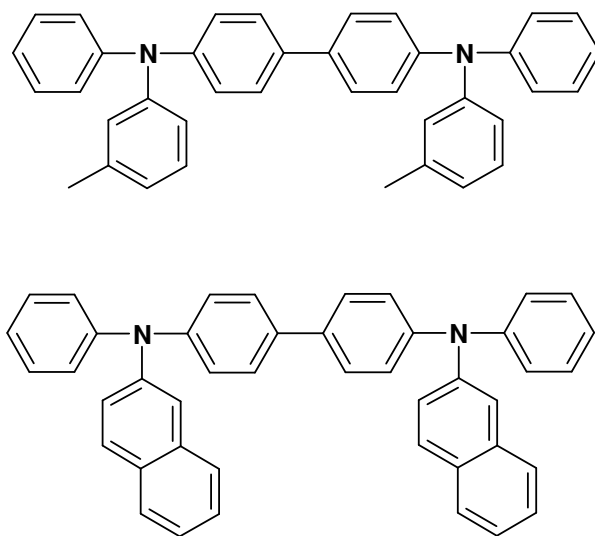


**Figure 1.7** Examples of hole-transporting materials



The stability of PLEDs is strongly influenced by malfunctions introduced by the high local temperature that occur during the operation of devices. These high temperatures are also a drawback for achieving high EL quantum efficiencies due to thermal quenching effects of the excited species. The bias voltage, i. e., the electric field required for the onset of current, and electroluminescence in the forward direction decrease when the potential barrier on the polymer/anode interface is reduced. A reduction of the barrier height can be obtained by introducing a hole transporting layer (HTL) between the anode and polymer. To lower the barrier height, the HOMO level of the HTL, which has a high hole mobility, has to be located above the valence band (VB) of the polymer and below the Fermi level of the metal. Some of the more common hole transporting materials are shown in Figure 1.7.

## **1.4 Polymeric solar cell**

A solar cell is a semiconductor device which converts solar energy into electrical energy. It is a pollution free and renewable source of energy. Currently, the main barrier that prevents photovoltaic technology from providing a large fraction of our electricity is the high cost of manufacturing crystalline silicon. Although the cost per peak watt of crystalline silicon photovoltaic (PV) cells has dropped significantly over the past decades<sup>67</sup>, these PV cells are still too expensive to compete with conventional grid electricity without the benefit of government subsidies.<sup>68</sup> One potential alternative to crystalline silicon PV cells is cells made from thin films (<1  $\mu\text{m}$ ) of conjugated (semiconducting) polymers, which can easily be cast onto flexible substrates over a large area using solution-processing techniques. These organic PV cells could provide electricity at a lower cost than crystalline silicon solar cells if a reasonable power efficiency (10 %) and lifetime (10 years) could be achieved on a large scale. However, the main limitations to their application now, are low power conversion efficiency (PCE) and instability compared to silicon-based solar cells.<sup>69</sup> Recently, PCEs of 5 % have been reported for polymer solar cell.<sup>70, 71</sup>

### 1.4.1 Advantage of polymeric solar cell over silicon based solar cell

- 1. Solvent processing :-** The conjugated polymer has the advantage that it can be casted from solution using wet-processing techniques such as spin casting, dip coating<sup>72</sup>, ink jet printing<sup>73, 74</sup>, screen printing<sup>75-77</sup>, and micromolding<sup>77</sup>. These techniques represent an enormously attractive route for producing large-area photovoltaic cells cheaply because they can be performed at ambient temperatures and pressure, and many of these techniques are scalable to larger area with little material loss. Also, many of these techniques can be applied to systems that require flexible substrates, such as roll-to-roll coaters.<sup>78</sup>
- 2. High absorption coefficient :-** A second major requirement for the active layer in a PV cell is that it should absorb a significant fraction of the solar radiation. The high ( $10^5 \text{ cm}^{-1}$ ) peak optical absorption coefficient of many conjugated polymers makes them excellent candidates in this regard. While crystalline silicon PV cells must be made  $\sim 100 \mu\text{m}$  thick to effectively absorb incident light, organic semiconductors have a direct band gap and generally must only be 100-500 nm thick to absorb most of the light at their peak absorption wavelength. However, one of the biggest existing hurdles to reaching high-efficiency PV cells with conjugated polymers is that the band gap of these semiconductors is too large and the absorption bandwidth of these materials too narrow to absorb a large fraction of the solar spectrum. While the photon flux of the AM 1.5G solar spectrum peaks around 700 nm (1.8 eV), P3HT, MEH-PPV, and OC1C10-PPV absorb strongly only over the wavelength range 350-650 nm (3.5-1.9 eV). As a result of this mismatch between the absorption spectrum of the organic semiconductor and the solar spectrum, a 240 nm thick film of P3HT only absorbs about 21 % of the solar photons.<sup>69</sup>
- 3. Low Cost:-** Polymer solar cells are expected to be cheaper compared to inorganic based solar cells because of low processing costs.

### 1.4.2 Disadvantages of polymeric solar cells over silicon based solar cells<sup>79</sup>

1. A strong driving force such as an electric field should be present to break up the photogenerated excitons. These excitons are strongly bound and do not spontaneously dissociate into charge pairs (Dissociation requires an input energy of  $\sim 100$  mV compared to a few meV for a crystalline semiconductor) and hence all excitons do not convert into charge carriers.
2. Charge transport proceeds in conjugated polymer by a *hopping* mechanism between localized states, rather than transport within a band like inorganic semiconductor and hence mobilities are low.
3. Limited light absorption across the solar spectrum limits the photocurrent.
4. Photocurrent is sensitive to temperature through hopping transport.
5. Many polymeric materials are susceptible to degradation in the presence of water and oxygen.

### 1.4.3 Basic working principle of a solar cell

The process of converting light energy into electrical energy mainly consists of four steps<sup>80</sup>

- (i) Absorption of a photon leading to the formation of an excited state called exciton (electron-hole pair),
- (ii) Exciton diffusion to a region where it can dissociate such as the interface between donor and acceptor molecule,
- (iii) Dissociation of exciton into charge carriers i.e. electron and hole,
- (iv) Charge transport to the anode(hole) and cathode(electron).

The electric current that a photovoltaic solar cell delivers corresponds to the number of created charges that is collected at the electrodes. This number depends on the fraction of photons absorbed ( $\eta_{\text{abs}}$ ), the fraction of electron-hole pairs that are dissociated ( $\eta_{\text{diss}}$ ), and finally the fraction of charge carriers reaching the corresponding electrodes ( $\eta_{\text{out}}$ ). The overall photocurrent efficiency ( $\eta_{\text{eff}}$ ) can be represented as

$$\eta_{\text{eff}} = \eta_{\text{abs}} \times \eta_{\text{diss}} \times \eta_{\text{out}}$$

The fraction of absorbed photons is a function of the absorption spectrum, the absorption coefficient, and the absorbing layer thickness. The fraction of dissociated electron-hole pairs is determined by the number of excitons that reach the donor-acceptor interface and the probability of charge separation there.<sup>81</sup> After dissociation, the charge carrier needs a net driving force, which generally results from a gradient in the electrochemical potentials of electrons and holes. Two forces contribute to this gradient

- (1) The internal electric field which leads to a field induced drift of charge carriers and mainly depends on the workfunction of the respective electrodes,
- (2) Concentration gradients of the respective charge carriers which leads to the diffusion current.

Usually, thin film devices (less than 100 nm) are mostly field drift dominated, whereas thick devices, having effective screening of electrical fields inside the bulk, are more dominated by the diffusion of charge carriers in concentration gradients at the selective contacts.<sup>80</sup>

#### 1.4.4 Solar cell device parameters

The typical current-voltage curves of an organic solar cell device are depicted in Figure 1.8. The most important device parameter in a solar cell is the power conversion efficiency ( $\eta_{\text{eff}}$ ) which can be defined as<sup>80</sup>

$$\eta = \frac{I_{\text{sc}} \times V_{\text{oc}} \times FF}{P_{\text{in}}}$$

Where **short-circuit current** ( $I_{\text{sc}}$ ) is the current produced when the positive and negative terminals of the cell are short-circuited, and the voltage between the terminals is zero.

**Open-circuit voltage ( $V_{oc}$ )** is the voltage across the positive and negative terminals under open-circuit conditions when the current flowing in circuit is zero.

**Fill factor (FF)** measures the "squareness" of the I-V curve and can be defined as shown below

$$FF = \frac{I_{mp} \times V_{mp}}{I_{sc} \times V_{oc}}$$

where  $I_{mp}$  and  $V_{mp}$  correspond to the current and voltage at maximum power point respectively.

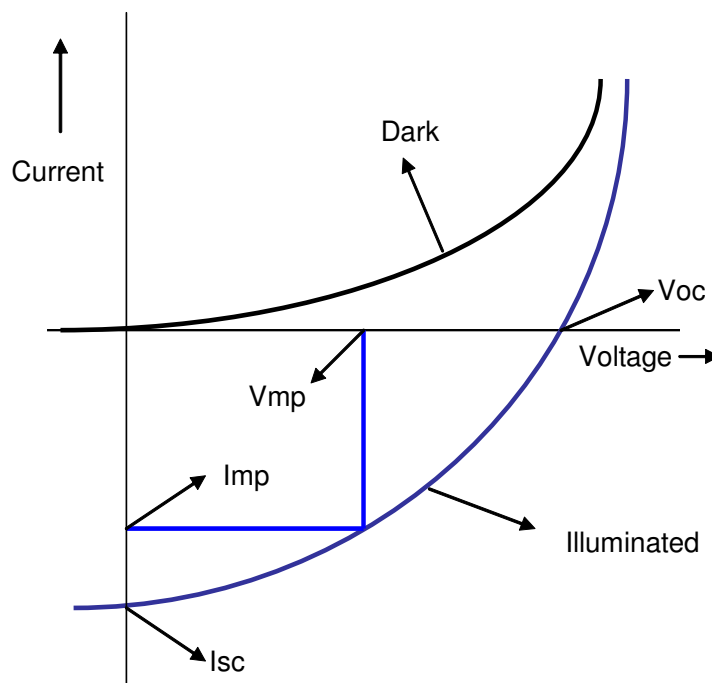


**Figure 1.8** Current-voltage curves of an organic solar cell

#### 1.4.5 Materials used in solar cell devices

Plants use the natural process of photosynthesis to convert sunlight into chemical energy, where the first step in this process is the absorption of light by chlorophyll molecules. In fact, chlorophyll pigments were also directly applied in a single layer solar

cell.<sup>82</sup> Besides the absorption of sunlight and creation of photogenerated charge carriers, a second requirement for solar cell materials is the ability to transport these charge carriers. Both properties are commonly found for materials that have an extended delocalized pi-electron system. Polymer solar cells are fabricated by inserting an active layer between two electrodes with one electrode transparent to incident light. The active layer is usually composed of two materials with different electron affinities. The composition of the active layer can be polymer/polymer or polymer/molecule, where a material with lower electron affinity acts as electron donor and another material, with high electron affinity, acts as electron acceptor. Some of the commonly used conjugated hole-conducting donor type polymers are shown in Figure 1.9.

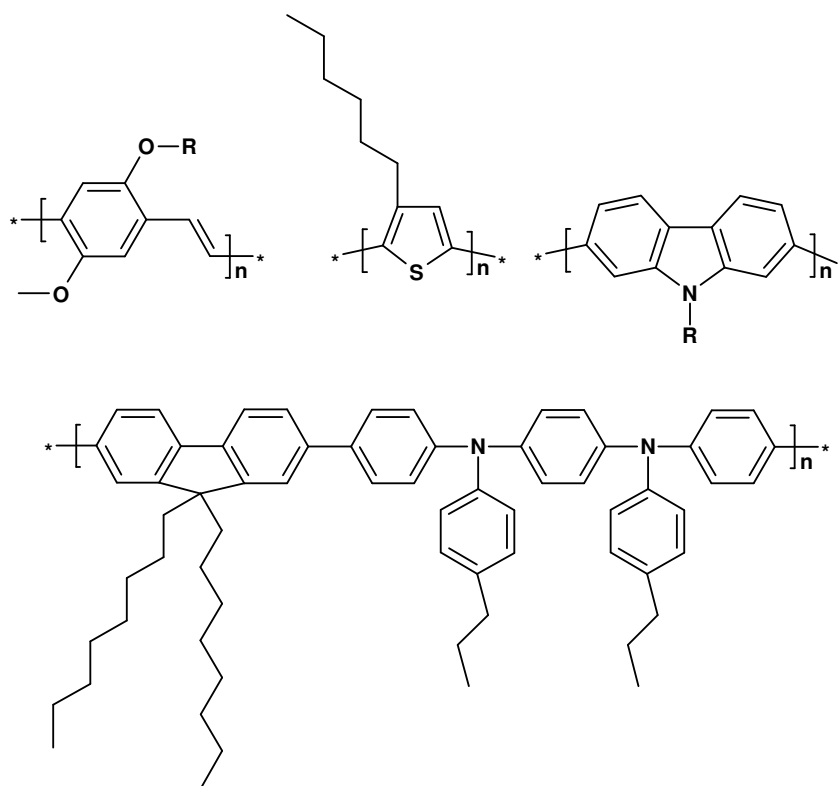


**Figure 1.9** Donor type conjugated polymers

Four important representatives of hole-conducting donor type polymers are MDMO-PPV (poly[2-methoxy-5-(3,7-dimethyloctyloxy)]-1,4-phenylenevinylene), P3HT (poly(3-hexylthiophene-2,5-diyl), PCz (polycarbazole) and PFB (poly(9,9'-dioctylfluorene-co-bis-N,N'-(4-butylphenyl)-bis-N-N'-phenyl-1,4-phenylenediamine)).<sup>25</sup>

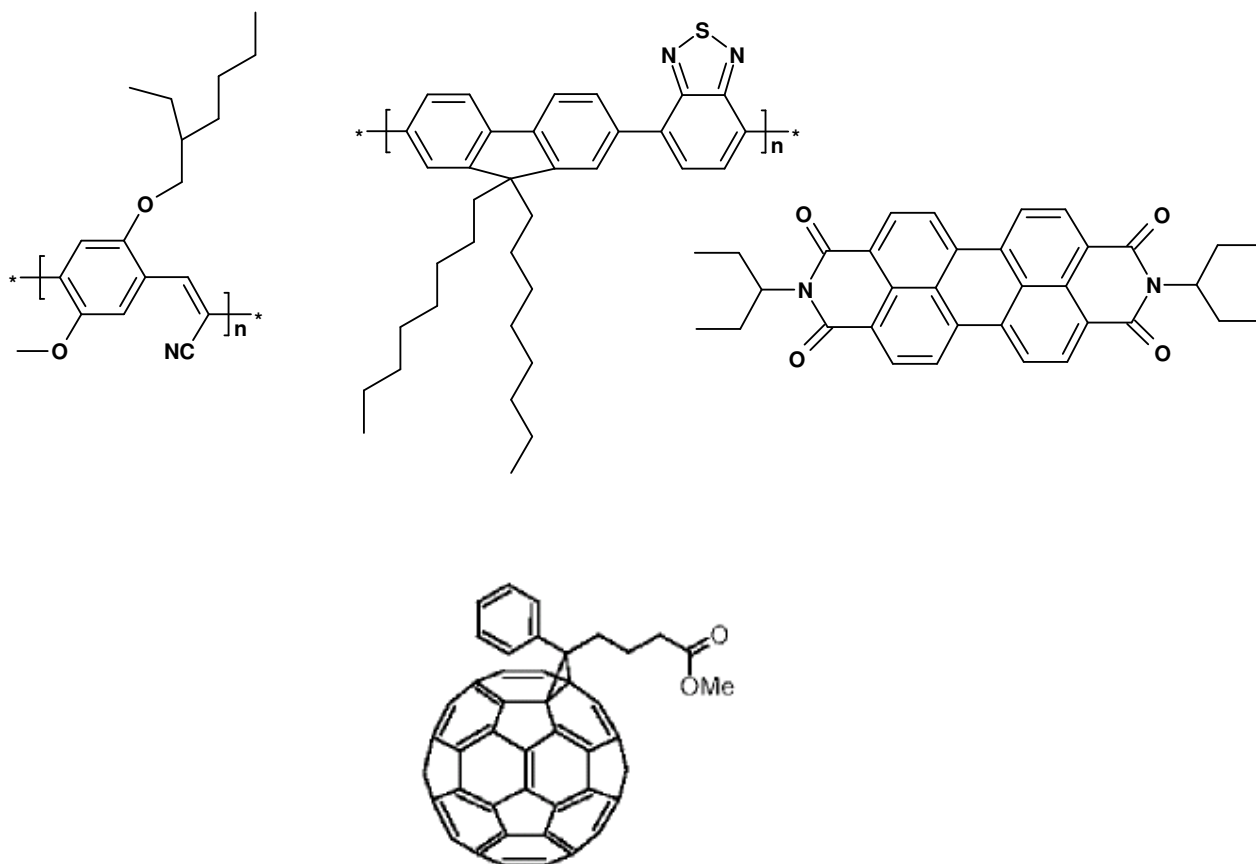


**Figure 1.10** Common electron-accepting materials used in a solar cell

Figure 1.10 depicts the commonly used electron-conducting acceptor polymers like CN-MEH-PPV (poly-[2-methoxy-5-(2'-ethylhexyloxy)-1,4-(1-cyanovinylene)-phenylene] and F8TB (poly(9,9'-dioctylfluorene-co-benzothiadiazole), a soluble derivative of  $C_{60}$ , namely PCBM (1-(3-methoxycarbonyl) propyl-1-phenyl[6,6] $C_{61}$ ) and PDI (parylene tetracarboxydiimide). All of these materials are solution processable due to their side-chain solubilization.<sup>19, 83</sup> For the construction of donor-acceptor solar cells, the donor polymers can be either combined with an acceptor polymer or with fullerenes either in planar or diffuse bilayer structures or in blends. One of the disadvantages of organic polymer-based photovoltaic cells is that it uses only the blue side of the solar spectrum in contrast to silicon whose absorption spectrum extends up to 1100 nm.

Charge carrier mobilities in films of molecules and conjugated polymers often depend on the nanoscopic order, which can be manipulated by the processing

conditions.<sup>84-87</sup> For example, a preferential orientation of polymer backbones parallel to the substrate gives rise to an anisotropic charge transport.<sup>88, 89</sup> An overview of some materials used for organic field-effect transistors is reported by Dimitrakopoulos.<sup>7</sup> However, charge transport in FETs is in lateral direction (parallel to the substrate) contrary to solar cells and most LEDs. For bulk heterojunction solar cells, it was observed that the charge transport in such blend structures is a sensitive function of the nanomorphology of the mixture.<sup>90, 91</sup>

### 1.4.6 Device Architecture

The solar cell device architecture can be divided into two classes (1) single layer device and (2) Bilayer device. Both devices are made by sandwiching the active layer between two electrodes having different work function. However, only a pure conjugated polymer is used as the active layer in the former whereas in the latter a mixture of donor and acceptor is used.

#### 1.4.6.1 Single layer device or Homojunction

The first organic solar cells were based on single thermally evaporated molecular organic layers sandwiched between two metal electrodes of different work functions (Figure 1.11). The difference in work function provides an electric field which drives separated charge carriers towards the respective contacts.

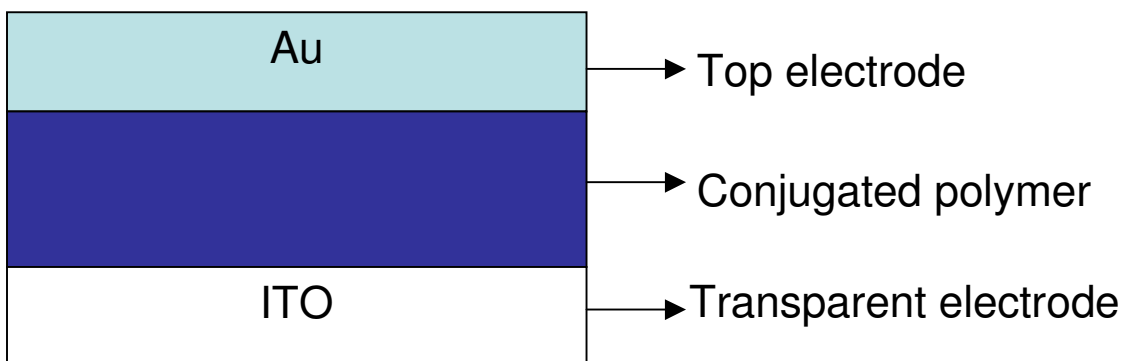


**Figure 1.11** Typical device architecture of single layer photovoltaic cell



The electric field is seldom sufficient to break up the photogenerated excitons. Instead, the excitation diffuses within the organic layer until it reaches a contact, where it may be broken up to supply separate charges, or recombine. Since exciton diffusion lengths are short, typically 1-10 nm,<sup>92-96</sup> exciton diffusion limits charge carrier generation in such a device. Single layer solar cells of this type deliver quantum efficiencies (QE) of less than 1 % and power conversion efficiencies of less than 0.1 %.<sup>97</sup> High QE is a necessary, though not sufficient condition for high power efficiencies. In organic and polymeric devices the value is still far from the value of 80-90 % typical in inorganic solar cells.<sup>79</sup>

#### 1.4.6.2 Bilayer device or Heterojunction devices

In a bilayer device, a donor and an acceptor material are stacked together with a planar interface. There the charge separation occurs,<sup>96, 98-100</sup> which is mediated by a large potential drop between donor and acceptor. The bilayer is sandwiched between two electrodes matching the donor HOMO and the acceptor LUMO, for efficient extraction of the corresponding charge carriers (Figure 1.12).

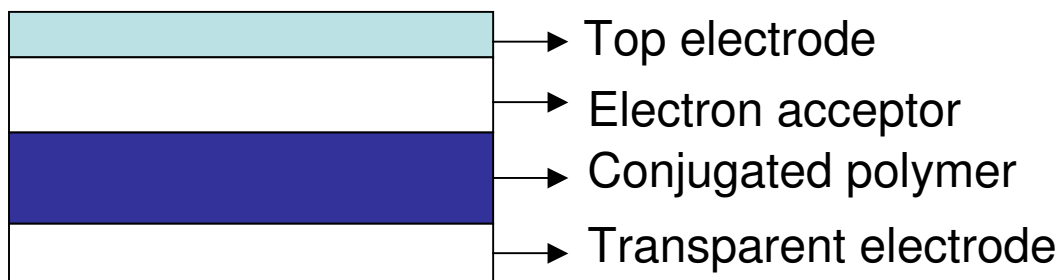


**Figure 1.12** Typical device architecture of bilayer photovoltaic cell

This concept was first introduced by C. W. Tang in 1985 when he discovered that, by making two-layer PV cells with organic semiconductors that have offset energy bands, the external quantum efficiency of PV cells could be improved to 15 % at the wavelength of maximum absorption.<sup>98, 99</sup> By analyzing the shape of the EQE spectrum for his two-layer device, Tang deduced that the improved efficiency resulted from exciton

dissociation at the interface between the two semiconductors. Excitons generated within a few nanometers of the heterojunction could diffuse to the interface and undergo forward electron or hole transfer. This process of forward charge transfer led to the spatial separation of the electron and hole, thereby preventing direct recombination and allowing the transport of electrons to one electrode and holes to the other.

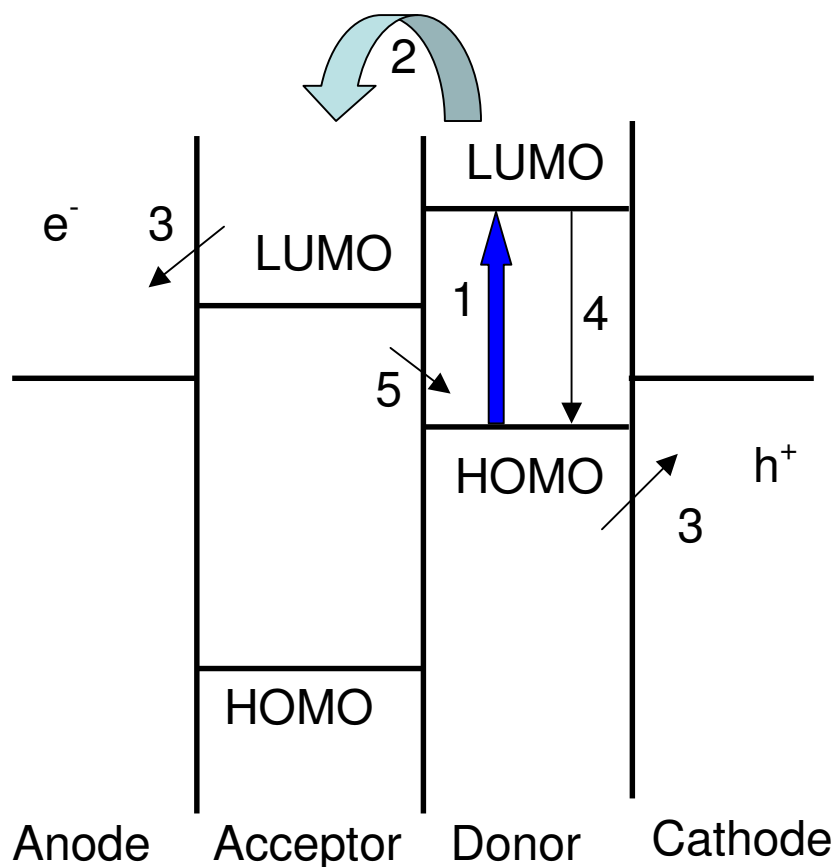


**Figure 1.13** Schematic energy-band diagram of donor-acceptor heterojunction. 1. Excitation of donor molecule after absorption of a photon, 2. Charge separation, 3. Transfer of charge to respective electrodes, 4. Geminate recombination, 5. Interfacial recombination.

Figure 1.13 depicts the basic processes in heterojunction solar cell devices. If both the excited state (LUMO) and ground state (HOMO) of the donor material lie at energies sufficiently higher than those of the acceptor material, then it is energetically favorable

for an exciton reaching the interface to dissociate, leaving a positive polaron on the acceptor and a negative polaron on the donor. For efficient photocurrent generation, charge separation (2) should compete successfully with geminate recombination (4) after a photon absorption event (1), and transfer to electrode (3) should compete with interfacial recombination (5).

### **1.4. 7 Current challenges**

While organic solar cells produce quite respectable open-circuit voltages, the short circuit photocurrent and fill factor are much lower than those available from silicon based devices. The lower photocurrent is due to poorer light absorption as well as photocurrent generation and transport, and the low fill factor is due to poor transport and recombination. To overcome these problems, future work should be focused on achieving the following goals<sup>79</sup>

- (i) Improving light harvesting,
- (ii) Improving photocurrent generation,
- (iii) Improving charge transport,
- (iv) Improving device architecture as well as stability of devices.

These are the four areas where the organic and polymeric materials lag behind silicon. The first three goals can be achieved by synthesizing new polymers or copolymers having low band-gap so that they match better with the solar spectrum and at the same time improve charge carrier mobility. Hence there is dire need to develop new materials to design more efficient solar cell devices with atleast 10 % power conversion efficiency which is the minimum cut off for commercialization.

## **1.5 Organic Thin Field-Effect Transistors (OFETs)**

Since John Bardeen, William Shockley, and Walter Brattain invented the world's first transistor in 1947, inorganic field-effect transistors (FETs) have dominated the

mainstream microelectronics industry. They are the fundamental building blocks for basic analytical circuits, such as amplifiers, as well as the key elements for digital combinational logic circuits, such as adders, shifters, inverters, and arithmetic logic units, and are used to build sequential logic circuits, such as flip-flops. Moreover, transistors are essential to the modern memory devices, integrated circuits, and microprocessors used in personal computers and laptops.<sup>101</sup> Organic thin film field-effect transistors (OTFTs) are particularly interesting as their fabrication processes are much less complex compared with conventional silicon technology, which involves high-temperature and high-vacuum deposition processes and sophisticated photolithographic patterning methods. In general, low-temperature deposition and solution processing can replace the more complicated processes involved in the conventional Silicon technology. In addition, the mechanical flexibility of organic materials makes them naturally compatible with plastic substrates for lightweight and foldable products. Since the report of the first organic field-effect transistor in 1986,<sup>102</sup> there has been great progress in both the materials' performance and development of new fabrication techniques. OTFTs have already been demonstrated in applications such as electronic paper<sup>103, 104</sup>, sensors<sup>105, 106</sup>, and memory devices including radio frequency identification cards (RFIDs)<sup>107, 108</sup>. Although OTFTs are not meant to replace conventional inorganic TFTs – because of the upper limit of their switching speed – they have great potential for a wide variety of applications, especially for new products that rely on their unique characteristics, such as electronic newspapers, inexpensive smart tags for inventory control, and large-area flexible displays.

### **1.5.1 Basic operation of OFETs**

An OTFT is analogous to its inorganic counterpart in basic design and function. It is a three-terminal device, in which a voltage applied to a gate electrode controls current flow between a source and drain electrode under an imposed bias. A basic schematic diagram is shown in Figure 1.14, where  $V_g$  and  $V_{ds}$  are the applied gate and source-drain voltages, respectively. The control of source-drain current in FETs via a third terminal has resulted in their widespread use as switches.

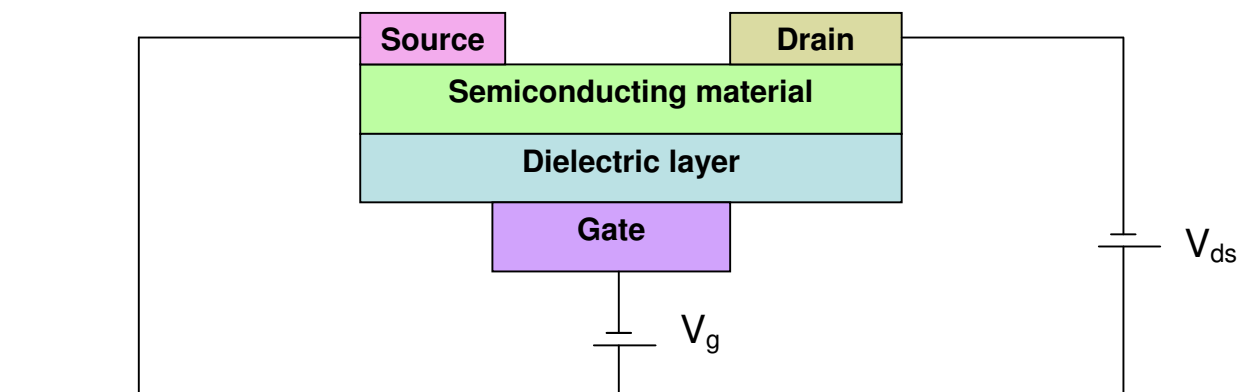


**Figure 1.14** Schematic device configuration of OFETs

Their utility in this capacity is gauged by several key measures of their performance. The mobility,  $\mu$ , describes how easily charge carriers can move within the active layer under the influence of an electric field and is, therefore, directly related to the switching speed of the device. This parameter can be extracted from current-voltage measurements, and would ideally be as large as possible. Typical values range from 0.1-1  $\text{cm}^2/\text{Vs}$  for amorphous-Si (a-Si) devices, with the best organic materials achieving mobilities of 1-10  $\text{cm}^2/\text{Vs}$ . The on/off ratio, defined as the ratio of the current in the ‘on’ and ‘off’ states, is indicative of the switching performance of OTFTs. A low off current is desired to eliminate leakage while in the inactive state. Ratios as high as  $10^6$  – suitable for most applications – can be reached by current-generation OTFTs.

### 1.5.2 Materials used in OFETs

Depending upon the nature of charge carrier, the organic semiconductor can function either as p-type or n-type. In p-type semiconductor the majority carriers are holes, while in n-type semiconductors, the majority carriers are electrons. Accordingly, the transistors are either p-type or n-type.

### 1.5.2.1 p-Type semiconductor

Most organic materials tend to transport holes better than electrons, thus there are more p-type materials and most work has been focused on them. p-Type semiconductors consist of large molecules like pentacene, tetracene, oligothiophenes and polymers like poly(3-alkylthiophenes) [P3ATs], poly(9,9-dioctylfluorene-co-bithiophene) [F8T2] (Figure 1.15). The synthesis and fabrication of organic thin film transistors (OTFTs) based on polycrystalline, vapor deposited sexithiophene and  $\alpha,\omega$ -dihexylsexithiophene films by Garnier et al. played a very important role in the evolution of the field of organic transistors.<sup>109</sup> This work showed not only that relatively high mobilities are attainable by polycrystalline organic semiconductors, but also delineated the strategies that should be followed in order to increase the performance of OTFTs. In the case of rod-like molecules, such as thiophene oligomers, large  $\pi$ -conjugation length along the long axis of the molecule and close molecular packing of the molecules along at least one of the short molecular axes ( $\pi$ -stacking) are two important conditions for high charge carrier mobilities.<sup>7</sup> One of the most studied organic molecule for OFETs is the pentacene.

Pentacene is an aromatic compound with five condensed benzene rings. The highest field effect mobilities so far have been recorded for pentacene ( $0.3\text{-}0.7\text{ cm}^2\text{V}^{-1}\text{s}^{-1}$  on  $\text{SiO}_2/\text{Si}$  substrates<sup>109</sup>,  $1.5\text{ cm}^2\text{V}^{-1}\text{s}^{-1}$  on chemically modified  $\text{SiO}_2/\text{Si}$  substrates<sup>110</sup> and  $3\text{ cm}^2\text{V}^{-1}\text{s}^{-1}$  on polymer gate dielectrics<sup>111</sup>). Pentacene was originally deposited by vacuum evaporation. However, recent advances in chemistry have made it possible to synthesize soluble pentacene precursors which gets converted to polycrystalline pentacene upon heating. Field-effect mobilities of  $0.1\text{ cm}^2\text{V}^{-1}\text{s}^{-1}$  and on/off ratios as high as  $10^4$  have been reported using this method<sup>112</sup>. Thiophene-based oligomers are also catching up as Halik and co-workers have reported mobilities as high as  $1.1\text{ cm}^2\text{V}^{-1}\text{s}^{-1}$  for an alkyl-substituted oligothiophene.<sup>113</sup>

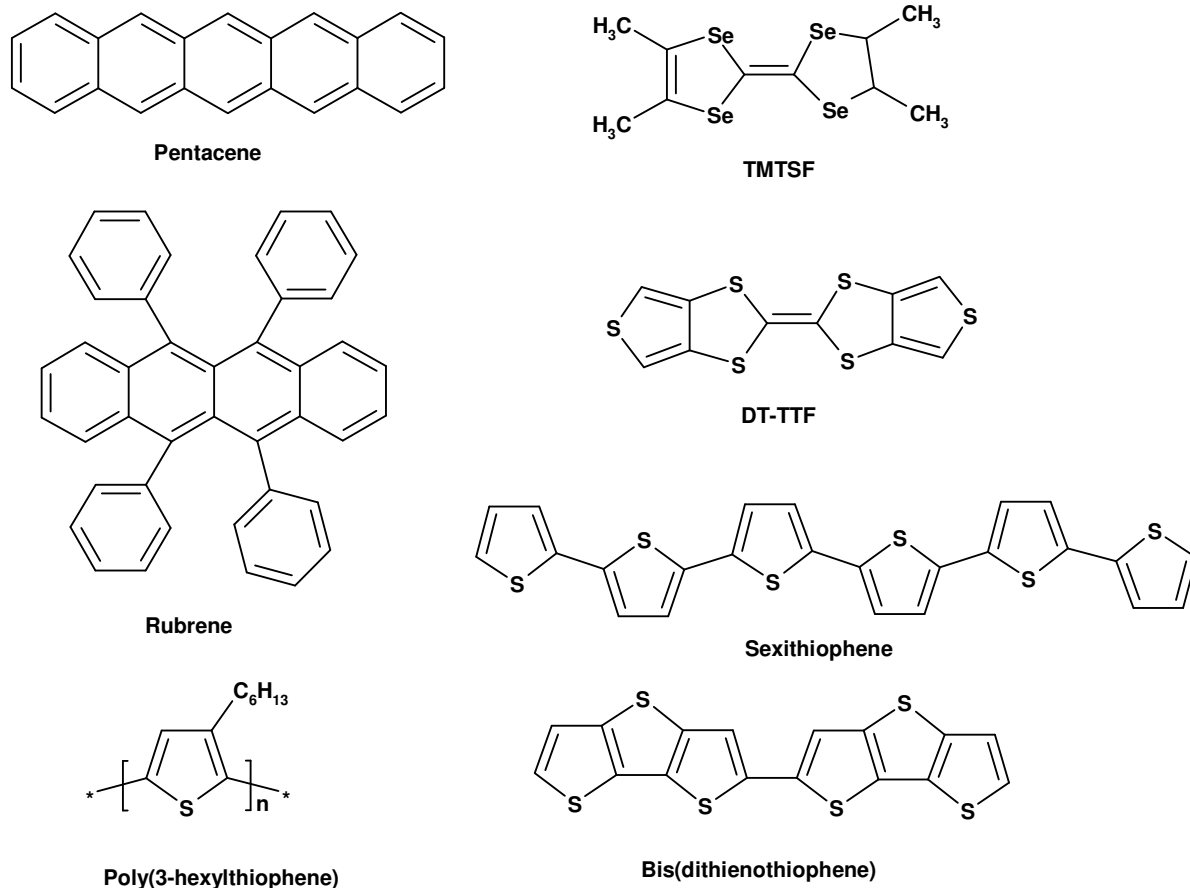


**Figure 1.15** Some of the p-type organic molecules and polymer used in FETs

Polymers are attractive for OFETs because thin films of these materials can be obtained through simple solution techniques such as drop casting, spin coating and ink printing etc. However, lower mobilities result on account of the poor molecular ordering and low crystallinity obtained by the solution processing. However, mobilities beyond  $0.1 \text{ cm}^2\text{V}^{-1}\text{s}^{-1}$  have been reported with regioregular polythiophene with structure optimization or annealing.<sup>112, 114</sup> Another way to increase performance is through doping (e.g. 2,3-dichloro-5,6-dicyanobenzoquinone [DDQ] is a dopant for P3HT), but this has a disadvantage of increasing the off-state leakage current. The latest materials being explored are organic single crystals. The highest charge mobility of  $15.4 \text{ cm}^2\text{V}^{-1}\text{s}^{-1}$  was reported for OFETs based on rubrene single crystals recently.<sup>115</sup> The high mobility of single crystals stems from good molecular ordering that permits good overlapping of  $\pi$ - $\pi$

orbitals. Compared to single crystals, organic thin films are often associated with grain boundaries and interfacial disorder which eventually decrease the charge carrier mobility.

### 1.5.2.2 n-Type semiconductor

High performance n-type semiconductors are important components of p-n junction diodes, bipolar transistors and complementary circuits. Besides the instability, another reason for n-type OFET materials lagging behind p-type materials is that the metals used for making contact to organic semiconductors have work functions better suited for injection of holes into the HOMO than of electrons into the LUMO, which associates with the band levels of the organic materials. For most p-type materials, the ionization potentials are about 5 eV, which is very close to noble metal's work functions. Low work function metals such as Al, Ca, Mg, which might be suitable for n-type semiconductors usually oxidize very easily and readily form reactive complexes with the organic semiconductor.<sup>116</sup> Therefore, the electron affinity of the semiconductor should be optimized such that the LUMO level offset with respect to the Fermi level of the source and drain electrodes does not limit the injection of electrons from the source into the semiconductor and from the semiconductor into the drain. For FET operation, electrons are conveniently injected into compounds with ionization potentials approximately 4 eV below vacuum using Au (work function 5 eV) for source/drain electrodes.<sup>117</sup> By adding strong electron-withdrawing groups such as -F, -CN, and -Cl on the backbone of the molecules, good candidates for n-type semiconductors may be synthesized. Hexadecahalogenated metallophthalocyanines like F16CuPc have been found to function as air-stable n-type semiconductors with a maximum electron mobility of  $0.03 \text{ cm}^2\text{V}^{-1}\text{s}^{-1}$ .<sup>118</sup> This represents an interesting line of study by which p-type semiconductors can be converted to n-type semiconductors. Recently, perfluoropentacene ( $\text{C}_{22}\text{F}_{14}$ ) has been designed as a potential n-type semiconductor for OFETs (Figure 1.16). Sakamoto et. al. have fabricated OFETs, bipolar OFETs and complementary circuits using perfluoropentacene and pentacene as the active materials.<sup>119</sup> Field effect mobility of  $0.11 \text{ cm}^2\text{V}^{-1}\text{s}^{-1}$  has been reported for this material. Another class of n-type materials being tested is perylene and its derivatives.



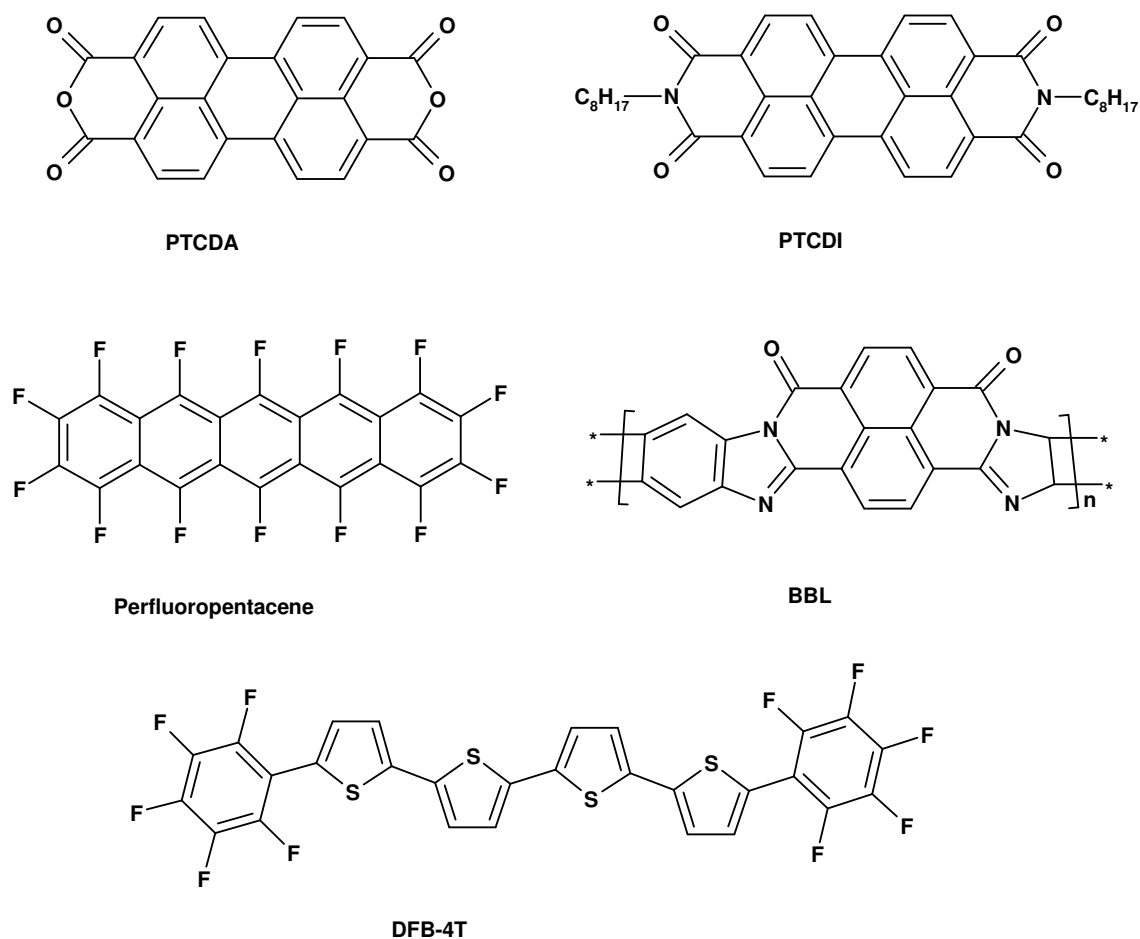


**Figure 1.16** Some of the n-type organic molecules and polymer used in FETs

Malenfant et. al. have reported that OFETs based on N,N'-dioctyl-3,4,9,10-perylenetetracarboxylic diimide (PTCDI-C8) as the organic semiconductor provided bottom contact devices with mobilities as high as  $0.6 \text{ cm}^2\text{V}^{-1}\text{s}^{-1}$  in the saturation regime and current on/off ratios of  $10^5$ .<sup>120</sup> It has also been reported recently that pentacene can be interface-doped with low work function metals like Ca to behave like a n-type semiconductor. An on/off ratio of  $10^4$  and field-effect mobility of  $0.19 \text{ cm}^2\text{V}^{-1}\text{s}^{-1}$  has been reported. Reports on n-type semiconducting polymers for OFET applications are scarce. However, Babel and Jenehke have reported the observation of field-effect electron mobility as high as  $0.1 \text{ cm}^2\text{V}^{-1}\text{s}^{-1}$  in a solution spin-coated conjugated ladder polymer, poly(benzobisimidazobenzophenanthroline).<sup>121</sup>

## 1.6 Motivation of this work

### 1.6.1 Synthesis of nitrogen-bridged semi-ladder-type polymers

Poly(2,7-carbazole)s have the potential to be useful as blue emitters, but also as donor materials in a solar cell due to their better hole-accepting properties due to the nitrogen bridges. However, they have two deficiencies as blue-emitters. First its emission maximum occurs at 421 nm, making it a violet-blue rather than a pure blue emitter. Secondly, the electron-rich nature of the 3- and 6- positions makes these materials susceptible to electrochemical degradation. To overcome the latter problem ladder-type polycarbazoles have been prepared, but these are blue-green emitters due to long extended conjugation, and also show marked aggregation even in solution which red-shifts their emission even further. For carbazole based materials to be useful as blue-emitters, it is necessary to fine tune the emission maximum closer to the pure blue (around 450 nm) and at the same time eliminate this aggregation which leads to undesirable long wavelength emission. In order to maximize their use as donor materials in photovoltaic device, it is highly desirable to redshift their absorption maximum so as to exploit more of the visible spectrum. I intend to address these problems in this work by the following ways:

**1 Aggregation of polymer chain:-** It can be eliminated in one of two ways; the first option is to alter the chain conformation of the polymer as less planar chains should aggregate less. This was achieved by Dierschke in a ladder-type polymer (Figure 1.17), whose polymer backbone has a helical structure.<sup>122</sup>

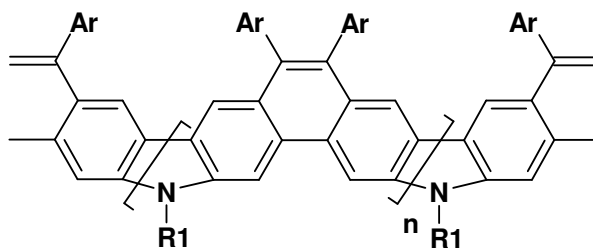


**Figure 1.17** Carbazole based ladder-type polymer synthesized by Dierschke et. al<sup>122</sup>

Recently, Qu et. al reported a novel kind of semi-ladder-type poly(p-phenylene) containing both carbazole and fluorene moieties (Figure 1.18).<sup>123</sup> In this case, the polymer had different building blocks or constituents in the backbone such as fluorene, ladder-type poly(tetraphenylene) and ladder-type poly(hexaphenylene). The absorption and PL spectra of the polymer in film were almost identical to those in solution, and no bathochromic shift was observed, The absence of aggregation in this case unlike the fully ladder-type polymers was ascribed to the irregular nature of the backbone. However, this method of preventing aggregation required greater synthetic effort and the structure of polymer was not well defined.

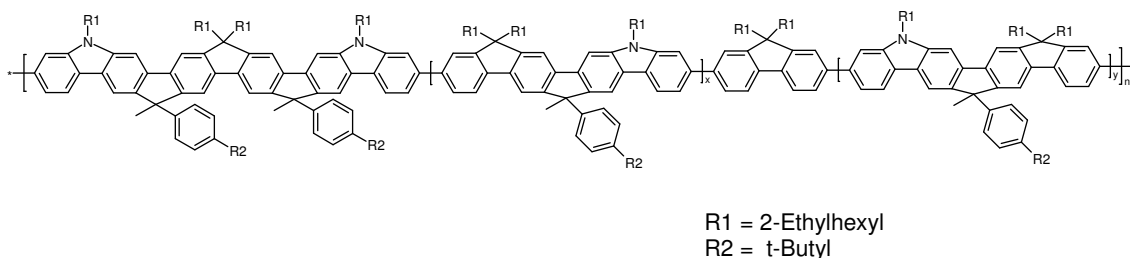
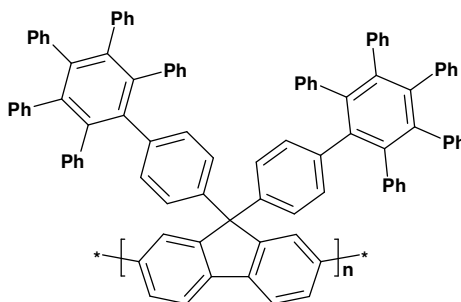


**Figure 1.18** Carbazole based ladder-type polymer synthesized by Qu et. al<sup>123</sup>

Another way to prevent aggregation is to attach polyphenylene dendrimers on the conjugated polymer chain (Figure 1.19). Setayesh et. al. reported dendronized polyfluorenes where dendrons were attached to the fluorene at the bridged carbon position which not only prevented the aggregation but also improved the color stability in electroluminescent devices by suppressing oxidation at carbon bridge position.<sup>124</sup>



14

**Figure 1.19** Dendronized poly(fluorene)

However, introduction also of bulky dendrons reduced the density of the electroactive material in the polymer bulk because of their large size and hence reduced the overall efficiency of electronic devices. Later, it was found that simple phenyl rings are sufficient to suppress the long wavelength emission. In our study, the concept of semi-ladder-type polymer is used to suppress the aggregation as well as improve the solubility, which will be discussed shortly.

**2 Tuning of emission maximum :-** A second problem associated with fully ladder-type polymers is that the emission maximum is too far red-shifted for them to be suitable for use as blue-emitter in PLEDs devices. Tuning the emission maximum can be done by bridging only some of the phenylenes – i. e. making semi-ladder-type polymers – or by incorporating some less conjugated moieties such as by *meta*-linkage or other nonconjugated groups into the polymer backbone. The first concept of moving from fully ladder to semi-ladder-type polymer was adopted for four main reasons

- (i) Emission maximum of bridged poly(phenylene)s has been shown to be tunable systematically over the blue region of the spectrum, from polyfluorene (421 nm) to poly(ladder-type pentaphenylene)<sup>22</sup> (445 nm),
- (ii) A single bond introduces some flexibility between two monomers and reduces the planarity which helps in solubility as well as reduces the aggregation,
- (iii) The monomers are highly pure and well characterized prior to polymerization so probability of chemical defects by incomplete reactions is less likely,
- (iv) Improved thermal stability of polymers as well as better electrical transport properties compared to polymers with a meta-linkage or a nonconjugated group in the backbone.

In order to address the problems of fully ladder-type polymers as well as of polycarbazole and exploring the advantages of semi-ladder-type polymer, a series of nitrogen-bridged semi-ladder-type polymers were synthesized - ladder-type poly(tetraphenylene), ladder type poly(pentaphenylene), and ladder-type poly(hexaphenylene) and their derivatives (Chart 1). These semi-ladder-type nitrogen-bridged polymers were expected to have several advantages **1**. All are carbazole

derivatives and so it was anticipated that these polymers would retain the good hole accepting and transporting properties of carbazole; 2. Unlike carbon-bridged polymers, nitrogen bridges cannot be oxidized to form emissive ketone defects and hence nitrogen-bridged polymers are expected to be more stable under device operational conditions; 3. Better solubility compared to fully ladder-type polymers (which exhibited poor solubility because of planar structure leading to aggregation) or polycarbazole where only one alkyl chain can be attached per monomer unit so less soluble than polyfluorenes; 4. Tuning of emission maximum in semi-ladder-type polymers is possible by changing the conjugation length in the monomers; 5. Suppressing the aggregation by the aryl or alkyl substitution at carbon bridges as well as by introducing the flexibility by single bond between two repeat units.

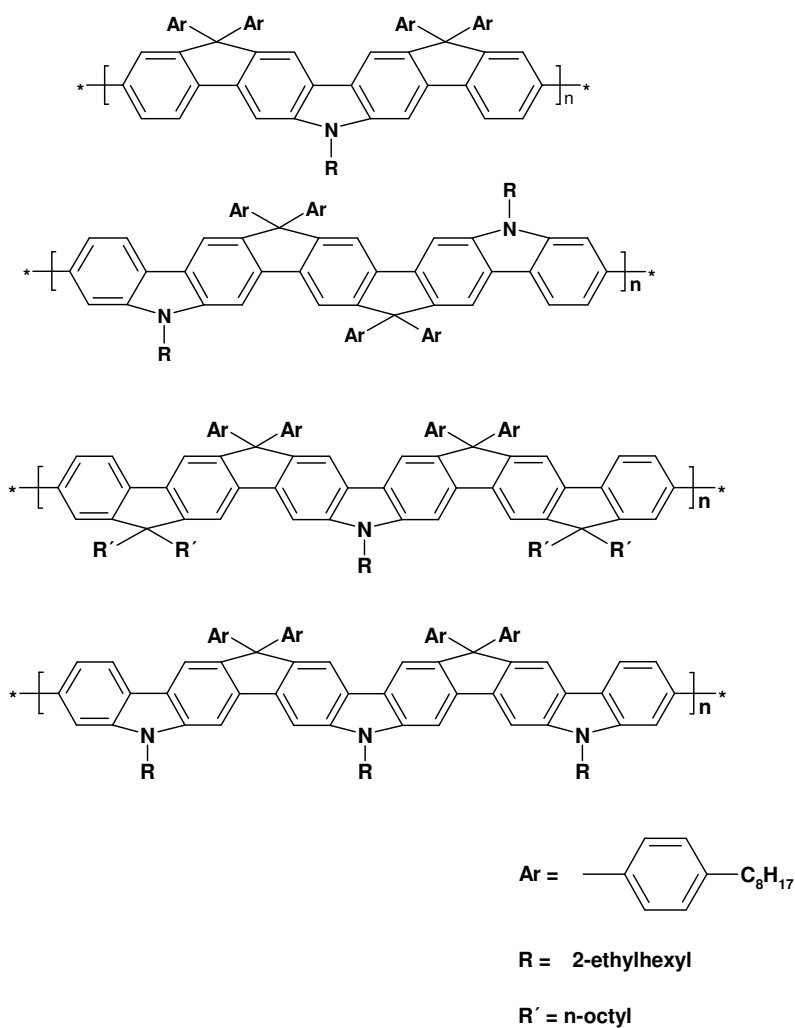


**Chart 1** Nitrogen-bridged semi-ladder-type polymers

To compare the properties and advantages of nitrogen-bridged ladder-type polymers over all carbon-bridged polymers, alkyl, aryl and fully arylated ladder-type poly(tetraphenylene)s were also synthesized (Chart 2)

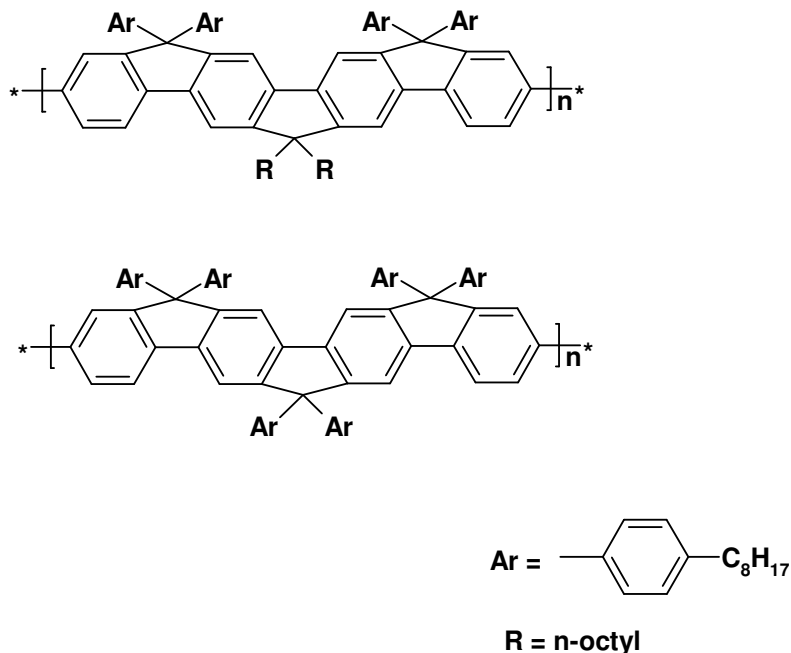


**Chart 2** Carbon-bridged ladder-type poly(tetraphenylene)s

### 1.6.2 Synthesis of solution and melt processible carbazole-thiophene fused molecules for field effect transistors

Polymers rarely give highly ordered structures. In general, layers of polymers are heterogeneous and consist of highly ordered areas of crystalline nature and less ordered amorphous zones. Of course charge mobility in ordered regions will be higher than in disordered ones. One solution to this problem is the synthesis of polymers having regular chain structure which help in forming ordered supramolecular structure. This importance of individual polymer chain regularity on the properties of the semiconducting layer can be demonstrated by a comparison of the charge carrier mobilities in FETs produced from regiorandom and regioregular poly(3-alkylthiophene)s.<sup>86</sup> In the latter charge carrier mobilities are much higher. Another solution to this problem is the synthesis of small molecules having enough alkyl chain on the backbone so that they can be solution or melt

processed and has the ability to form thin films like polymers as well as retain the structural order characteristic of small molecules. This may result in high charge carrier mobilities suitable for large area applications. The small molecule should be 1. Planar in shape so that they can form long range ordered structure 2. Electron rich to generate sufficient charge carriers in FET devices and 3. bearing sites on its backbone to attach solubilizing groups. To address all these problems, ladder type carbazole-thiophene fused aromatics were synthesized (Figure 1.20) and tested in FETs. The performance was also compared with nitrogen-bridged ladder-type hexaphenylene molecule.

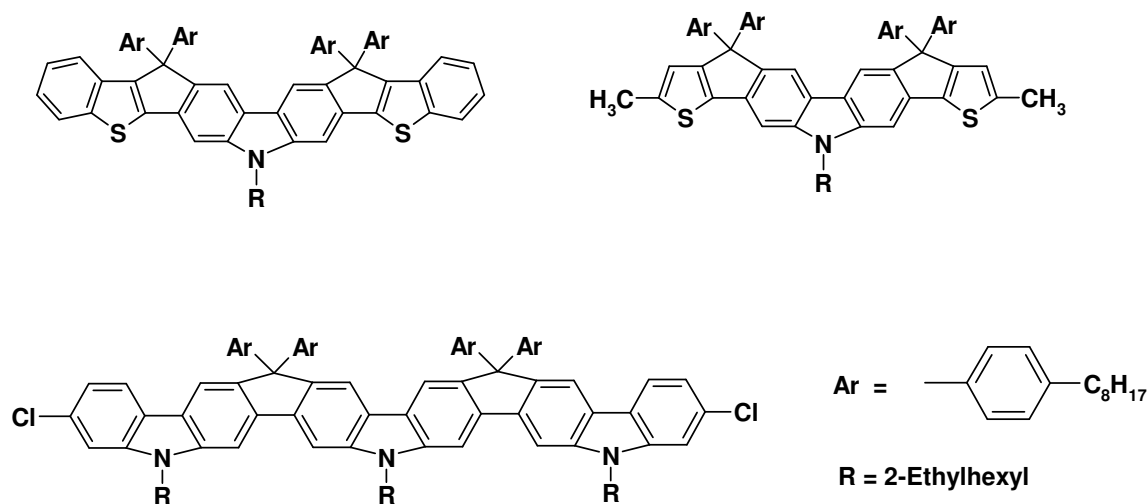


**Figure 1.20** Ladder-type carbazole-thiophene molecules for FETs devices

### 1.6.3 Aminocarbazole-anthraquinone fused dyes and polymers

Carbazole is an attractive raw material for the synthesis of dyes since it is cheap and readily available. Carbazolodioxazine (Figure 1.21), commercially known as violet 23 is a representative compound of dioxazine pigments. It is an important violet pigment, used as a coloring material for plastics and printing inks. Violet 23 is synthesized from 3-amino-9-ethylcarbazole by initial condensation with *p*-chloroanil to generate dicarbazolylaminochlorobenzoquinone and subsequent cyclization of the quinone gives carbazolodioxazine.<sup>125</sup> Recently, Ikeda et. al. have confirmed the structure spectroscopically by attaching a long alkyl chain at the nitrogen center of carbazole.<sup>126-128</sup>

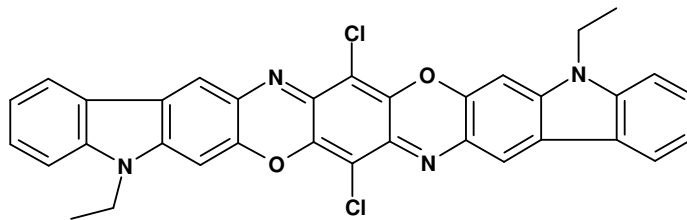


**Figure 1.21** Structure of violet 23

As part of our efforts into developing cheap alternatives to violet 23, we have focussed on the coupling of two readily available substrates, 3-aminocarbazole and chloroanthraquinones. Both 3-aminocarbazole and 3,6-diaminocarbazole are easy to synthesize and dichloroanthraquinones are readily available in various isomeric forms. The synthesis of 3,6-bis(1-anthraquinonylamino)carbazole has been reported either by the condensation of 3,6-diaminocarbazole with 1-chloroanthraquinone or by condensation of the more readily available dihalocarbazoles with 1-aminoanthraquinone.<sup>125</sup>

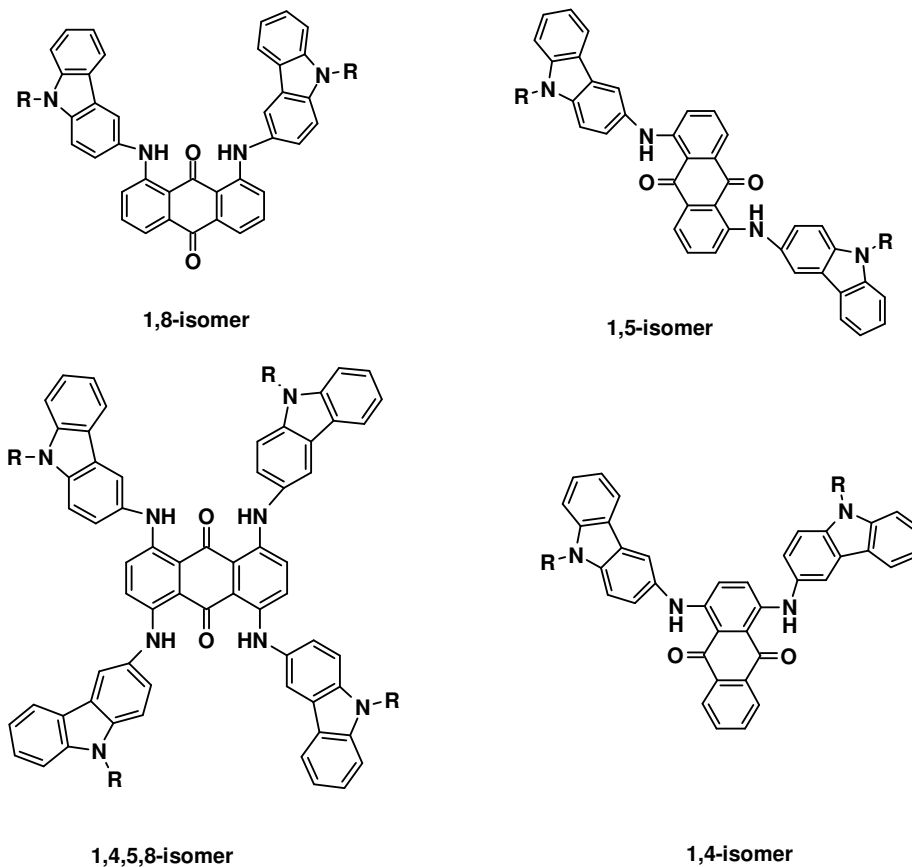


**Figure 1.22** Carbazole-anthraquinone fused compounds



The resulting pigment was violet in color ( $\lambda_{\max} = 513$  nm) but the absorbance maximum was too hypsochromic compared to violet 23 ( $\lambda_{\max} = 602$  nm). In the present study, we will report on the synthesis and characterization of dyes and pigments based on the coupling of 3-aminocarbazole with 1,4-, 1,5- and 1,8-dichloroanthraquinones (Figure 1.22), under palladium catalyzed Buchwald-Hartwig type amination conditions.<sup>129</sup> The synthesis and characterization of a series of soluble polymers by coupling of diamino-carbazole with 1,4-, 1,5- and 1,8-dichloroanthraquinones will be reported to compare the optical properties of polymers with their corresponding model compounds.

## 1.7 References

1. Shirakawa, H.; Louis, E. J.; MacDiarmid, A. G.; Chiang, C. K.; Heeger, A. J., *J. Chem. Soc.-Chem. Commun.* **1977**, (16), 578.
2. Tourillon, G., *Handbook of conducting polymers*. T A Stotheim: New York, 1986; p 294.
3. Diaz, A. F.; Kanazawa, K. K.; Gardini, G. P., *J. Chem. Soc., Chem. Commu.* **1979**, (14), 635.
4. Jen, K. Y.; Oboodi, R.; Elsenbaumer, R. L., *Polym. Mater. Sci. Eng.* **1985**, 53, 79.
5. Elsenbaumer, R. L.; Jen, K. Y.; Oboodi, R., *Synth. Met.* **1986**, 15, 169.
6. Milller, G. G.; Elsenbaumer, R. L., *J. Chem. Soc.-Chem. Commun.* **1986**, 1346.
7. Dimitrakopoulos, C. D.; Mascaro, D. J., *Adv. Mater.* **2002**, 14, 99.
8. Garnier, F.; Hajlaoui, R.; Yassar, A.; Srivastava, P., *Science* **1994**, 265, 1684.
9. Bao, Z., *Adv. Mater.* **2000**, 12, 227.
10. Gelinck, G. H.; Geuns, T. C. T.; Leeuw, D. M. d., *Appl. Phys. Lett.* **2000**, 77, 1487.
11. Huitema, H. E. A.; Gelinck, G. H.; van der Putten, J.; Kuijk, K. E.; Hart, C. M.; Cantatore, E.; Herwig, P. T.; van Breemen, A.; de Leeuw, D. M., *Nature* **2001**, 414, (6864), 599.
12. Ong, B. S.; Wu, Y. L.; Liu, P.; Gardner, S., *J. Am. Chem. Soc.* **2004**, 126, (11), 3378.
13. Akcelrud, L., *Progress in Polymer Science* **2003**, 28, (6), 875.
14. Friend, R. H.; Gymer, R. W.; Holmes, A. B.; Burroughes, J. H.; Marks, R. N.; Taliani, C.; Bradley, D. D. C.; Dos Santos, D. A.; Bredas, J. L.; Logdlund, M.; Salaneck, W. R., *Nature* **1999**, 397, (6715), 121.
15. Kraft, A.; Grimsdale, A. C.; Holmes, A. B., *Angew. Chem., Int. Ed. Engl.* **1998**, 37, (4), 402.
16. Sheats, J. R.; Chang, Y. L.; Roitman, D. B.; Stocking, A., *Acc. Chem. Res.* **1999**, 32, (3), 193.
17. Gong, X.; Robinson, M. R.; Ostrowski, J. C.; Moses, D.; Bazan, G. C.; Heeger, A. J., *Adv. Mater.* **2002**, 14, (8), 581.
18. Partridge, R. H., *Polymer* **1983**, 24, (6), 733.

19. Burroughes, J. H.; Bradley, D. D. C.; Brown, A. R.; Marks, R. N.; Mackay, K.; Friend, R. H.; Burns, P. L.; Holmes, A. B., *Nature* **1990**, 347, (6293), 539.
20. Jacob, J.; Zhang, J. Y.; Grimsdale, A. C.; Müllen, K.; Gaal, M.; List, E. J. W., *Macromolecules* **2003**, 36, (22), 8240.
21. Jacob, J.; Sax, S.; Piok, T.; List, E. J. W.; Grimsdale, A. C.; Müllen, K., *J. Am. Chem. Soc.* **2004**, 126, (22), 6987.
22. Jacob, J.; Sax, S.; Gaal, M.; List, E. J. W.; Grimsdale, A. C.; Müllen, K., *Macromolecules* **2005**, 38, (24), 9933.
23. Smela, E., *Adv. Mater.* **2003**, 15, (6), 481.
24. Xue, J. G.; Uchida, S.; Rand, B. P.; Forrest, S. R., *Appl. Phys. Lett.* **2004**, 84, (16), 3013.
25. Li, J. L.; Dierschke, F.; Wu, J. S.; Grimsdale, A. C.; Müllen, K., *J. Mater. Chem.* **2006**, 16, (1), 96.
26. Christoph, J.; Brabec, J.; Sariciftci, N. S.; Hummelen, J. C., *Adv. Funct. Mater.* **2001**, 11, 15.
27. Sariciftci, N. S.; Smilowitz, L.; Heeger, A. J.; Wudl, F., *Science* **1992**, 258, 1474.
28. Morita, S.; Zakhidov, A. A.; Yoshino, K., *Solid state Commun.* **1992**, 82, 249.
29. McCullough, R. D.; Lowe, R. D.; Jayaraman, M.; Anderson, D. L., *J. Org. Chem.* **1993**, 58, 904.
30. Kohle, A.; Wilson, J. S.; Friend, R. H., Fluorescence and phosphorescence in organic materials. *Adv. Mater.* **2002**, 14, (10), 701.
31. Roncali, J., *Chem. Rev.* **1992**, 92, (4), 711-738.
32. Schiavon, G.; Zotti, G.; Bontempelli, G., *J. Electroanal. Chem.* **1984**, 161, (2), 323.
33. Schiavon, G.; Zotti, G.; Bontempelli, G., *J. Electroanal. Chem.* **1985**, 186, (1-2), 191.
34. Fauvarque, J. F.; Petit, M. A.; Pfluger, F.; Jutand, A.; Chevrot, C.; Troupel, M., *Makromol. Chem.* **1983**, 4, (7), 455.
35. Froyer, G.; Maurice, F.; Goblot, J. Y.; Fauvarque, J. F.; Petit, M. A.; Digua, A., *Mol. Cryst. Liq. Cryst.* **1985**, 118, (1-4), 267.
36. Faid, K.; Siove, A.; Chevrot, C.; Riou, M. T.; Froyer, G., *J. Chim. Phys.* **1992**, 89, (5), 1305.
37. Faid, K.; Ades, D.; Siove, A.; Chevrot, C., *J. Chim. Phys.* **1992**, 89, (5), 1019.
38. Kovacic, P.; Kyriakis, A., *J. Am. Chem. Soc.* **1963**, 85, (4), 454.
39. Kovacic, P.; Lange, R. M., *J. Org. Chem.* **1963**, 28, (4), 968.
40. Kovacic, P.; Koch, F. W., *J. Org. Chem.* **1963**, 28, (7), 1864.
41. Kovacic, P.; Sparks, A. K., *J. Org. Chem.* **1963**, 28, (4), 972.
42. Froyer, G.; Maurice, F.; Mercier, J. P.; Riviere, D.; Lecun, M.; Auvray, P., *Polymer* **1981**, 22, (7), 992.
43. Kobryanskii, V. M.; Arnautov, S. A., *J. Chem. Soc., Chem. Comm.* **1992**, (9), 727.
44. Marvel, C. S.; Hartzell, G. E., *J. Am. Chem. Soc.* **1959**, 81, (2), 448.
45. Cassidy, P. E.; Marvel, C. S.; Ray, S., *J. Polym. Sci. A3* **1965**, 3, (4PA), 1553.
46. Lefebvre, G.; Dawans, F., *J. Poly. Sci. A2* **1964**, 2, (7PA), 3277.
47. Ballard, D. G. H.; Curtis, A.; Shirley, I. M.; Taylor, S. C., *J. Chem. Soc., Chem. Commun.* **1983**, (17), 954-955.

48. Ballard, D. G. H.; Courtis, A.; Shirley, I. M.; Taylor, S. C., *Macromolecules* **1988**, 21, (2), 294.
49. Claesson, S.; Gehm, R.; Kern, W., *Makromol. Chem.* **1951**, 7, (1), 46.
50. Kern, W.; Gehm, R., *Angew. Chem.* **1950**, 62, (13-1), 337.
51. Wirth, H. O.; Muller, R.; Kern, W., *Makromol. Chem.* **1964**, 77, 90.
52. Hellmann, M.; Bilbo, A. J.; Pummer, W. J., *J. Am. Chem. Soc.* **1955**, 77, (13), 3650.
53. Yamamoto, T.; Hayashi, Y.; Yamamoto, A., *Bull. Chem. Soc. Japan* **1978**, 51, (7), 2091.
54. Tamao, K.; Sumitani, K.; Kumada, M., *J. Am. Chem. Soc.* **1972**, 94, (12), 4374.
55. Morrell, D. G.; Kochi, J. K., *J. Am. Chem. Soc.* **1975**, 97, (25), 7262.
56. Sekiya, A.; Ishikawa, N., *J. Organomet. Chem.* **1976**, 118, (3), 349.
57. Yamamoto, T.; Morita, A.; Miyazaki, Y.; Maruyama, T.; Wakayama, H.; Zhou, Z.; Nakamura, Y.; Kanbara, T.; Sasaki, S.; Kubota, K., *Macromolecules* **1992**, 25, (4), 1214.
58. Rehahn, M.; Schlüter, A. D.; Wegner, G.; Feast, W. J., *Polymer* **1989**, 30, (6), 1060.
59. Destriau, G., *J. Chem. Phys.* **1936**, 33, 587.
60. Pope, M.; Kallmann, H. P.; Magnante, P., *J. Chem. Phys.* **1963**, 38, 2042.
61. Vincett, P. S.; Barlow, W. A.; Hann, R. A.; Roberts, G. G., *Thin Solid films* **1982**, 94, 476.
62. Slyke, S. A. v.; Tang, C. W., *Appl. Phys. Lett.* **1987**, 51, 913.
63. Greenham, N. C.; Friend, R. H.; Bradley, D. D. C., *Adv. Mater.* **1994**, 6, 491.
64. Sheats, J. R.; Antoniadis, H.; Hueschen, M.; Leonard, W.; Miller, J.; Moon, R.; Roitman, D.; Stocking, A., *Science* **1990**, 248, 884.
65. Mitschke, U.; Bauerle, P., *J. Mater. Chem.* **2000**, 10, 1471.
66. Bernius, M. T.; Inbasekaran, M.; O'Brien, J.; Wu, W., *Adv. Mater.* **2000**, 12, (23), 1737.
67. Shah, A.; Torres, P.; Tscharnner, R.; Wyrsh, N.; Keppner, H., *Science* **1999**, 285, 692.
68. Johnson, J. C., *Chem. Eng. News* **2004**, 82, 25.
69. Coakley, K. M.; McGehee, M. D., *Chem. Mater.* **2004**, 16, 4533.
70. Brabec, C. J., *Sol. Energy Mater. Sol. Cell* **2004**, 83, 273.
71. Schilinsky, P.; Waldauf, C.; Hauch, J.; Brabec, C. J., *Thin Solid films* **2004**, 105, 451.
72. Wang, G.; Swenson, J.; Moses, D.; Heeger, A. J., *J. Appl. Phys.* **2003**, 93, 6137.
73. Hebner, T. R.; Wu, C. C.; Marcy, D.; Lu, M. H.; Sturm, J., *Appl. Phys. Lett.* **1998**, 72, 519.
74. Chang, S.; Liu, J.; Bharathan, J.; Yang, Y.; Onohara, J.; Kido, J., *Adv. Mater.* **1999**, 11, 734.
75. Pschenitzha, F.; Sturm, J. C., *Appl. Phys. Lett.* **1999**, 74, 1913.
76. Shaheen, S. E.; Radspinner, R.; Peyghambarian, N.; Jabbour, G. E., *Appl. Phys. Lett.* **2001**, 2996.
77. Rogers, J. A.; Bao, Z.; Raju, V. R., *Appl. Phys. Lett.* **1998**, 72, 2716.
78. Gustafsson, G.; Cao, Y.; Treacy, G. M.; Klavetter, F.; Colaneri, N.; Heeger, A. J., *Nature* **1992**, 357, 477.

79. Nelson, J., *Curr. Opinion in solid state and Mater. Science* **2002**, 6, 87.
80. Hoppe, H.; Sariciftci, N. S., *J. Mater. Res.* **2004**, 19, (7), 1924.
81. Gregg, B. A., *J. Phys. Chem. B* **2003**, 107, 4688.
82. Tang, C. W.; Albrecht, A. C., *J. Chem. Phys.* **1975**, 62, 2139.
83. Braun, D.; Heeger, A. J., *Appl. Phys. Lett.* **1991**, 58, 1982.
84. Adam, D.; Schuhmacher, P.; Simmerer, J.; Häussling, L.; Siemensmeyer, K.; Eitzbachi, K. H.; Ringsdorf, H.; Haarer, D., **1994**, 141, 371.
85. Funahashi, M.; Hanna, J.-I., *Phys. Rev. Lett.* **1997**, 78, 2184.
86. Sirringhaus, H.; Brown, P. J.; Friend, R. H.; Nielsen, M. M.; Bechgaard, K.; Langeveld-Voss, B. M. W.; Spiering, A. J. H.; Janssen, R. A. J.; Meijer, E. W.; Herwig, P.; Leeuw, D. M. d., *Nature* **1999**, 401, 685.
87. Sirringhaus, H.; Wilson, R. J.; Friend, R. H.; Inbasekaran, M.; Wu, W.; Woo, E. P.; Grell, M.; Bradley, D. D. C., *Appl. Phys. Lett.* **2000**, 77, 406.
88. Aasmundtveit, K. E.; Samuelsen, E. J.; Guldstein, M.; Steinsland, C.; Floranes, O.; Fagermo, C.; Seeberg, T. M.; Pettersson, L. A. A.; Inganäs, O.; Feidenhans, R.; Ferrer, S., *Macromolecules* **2000**, 33, 3120.
89. Zhokhavets, U.; Gobsch, G.; Hoppe, H.; Sariciftci, N. S., *Synth. Met.* **2004**, 143, 113.
90. Choulis, S. A.; Nelson, J.; Kim, Y.; Poplavskyy, D.; Kreouzis, T.; Durrant, J. R.; Bradley, D. D. C., *Appl. Phys. Lett.* **2003**, 83, 3812.
91. Pacios, R.; Nelson, J.; Bradley, D. D. C.; Brabec, C. J., *Appl. Phys. Lett.* **2003**, 83, 4764.
92. Halls, J. M.; Pichler, K.; Friend, R. H.; Moratti, S. C.; Holmes, A. B., *Appl. Phys. Lett.* **1996**, 68, 3120.
93. Theander, M.; Yartsev, A.; Zigmantas, D.; Sundström, V.; Mammo, W.; Anderson, M. R.; Inganäs, O., *Phys. Rev. B* **2000**, 61, 12957.
94. Savenije, T. J.; Warman, J. M.; Goossens, A., *Chem. Phys. Lett.* **1998**, 287, 148.
95. Haugeneder, A.; Neges, M.; Kallinger, C.; Spirkl, W.; Lemmer, U.; Feldman, J.; Scherf, U.; Harth, E.; Gugel, A.; Müllen, K., *Phys. Rev. B* **1999**, 59, 15346.
96. Pettersson, L. A. A.; Roman, L. S.; Inganäs, O., *J. Appl. Phys.* **1999**, 86, 487.
97. Marks, R. N.; Halls, J. J. M.; Bradley, D. D. C.; Friend, R. H.; Holms, A. B., *J. Phys.: Condens. Matter* **1994**, 6, 1379.
98. Tang, C. W., *Appl. Phys. Lett.* **1986**, 48, 183.
99. Peumans, P.; Yakimov, A.; Forrest, S. R., *J. Appl. Phys.* **2003**, 93, 3693.
100. Rostalski, J.; Meissner, D., *Sol. Energy Mater. Sol. Cells* **2000**, 63, 3.
101. Reese, C.; Roberts, M.; Ling, M. M.; Bao, Z., *Materialstoday* **2004**, 20.
102. Tsumura, A.; Koezuka, H.; Ando, T., *Appl. Phys. Lett.* **1986**, 49, (18), 1210.
103. Gelinck, G. H.; Huitema, H. E. A.; Van Veenendaal, E.; Cantatore, E.; Schrijnemakers, L.; Van der Putten, J.; Geuns, T. C. T.; Beenhakkers, M.; Giesbers, J. B.; Huisman, B. H.; Meijer, E. J.; Benito, E. M.; Touwslager, F. J.; Marsman, A. W.; Van Rens, B. J. E.; De Leeuw, D. M., *Nature Mater.* **2004**, 3, (2), 106.
104. Sheraw, C. D.; Zhou, L.; Huang, J. R.; Gundlach, D. J.; Jackson, T. N.; Kane, M. G.; Hill, I. G.; Hammond, M. S.; Campi, J.; Greening, B. K.; Francl, J.; West, J., *Appl. Phys. Lett.* **2002**, 80, (6), 1088.

105. Zhu, Z. T.; Mason, J. T.; Dieckmann, R.; Malliaras, G. G., *Appl. Phys. Lett.* **2002**, 81, (24), 4643.
106. Crone, B. K.; Dodabalapur, A.; Sarpeshkar, R.; Gelperin, A.; Katz, H. E.; Bao, Z., *J. Appl. Phys.* **2002**, 91, (12), 10140.
107. Voss, D., Cheap and cheerful circuits. *Nature* **2000**, 407, (6803), 442.
108. Baude, P. F.; Ender, D. A.; Haase, M. A.; Kelley, T. W.; Muyres, D. V.; Theiss, S. D., *Appl. Phys. Lett.* **2003**, 82, (22), 3964.
109. Gundlach, D. J.; Lin, Y. Y.; Jackson, T. N.; Nelson, S. F.; Schlom, D. G., *IEEE Electron Device Lett.* **1997**, 18, (3), 157.
110. Lin, Y. Y.; Gundlach, D. J.; Nelson, S. F.; Jackson, T. N., *IEEE Electron Device Letters* **1997**, 18, (12), 606-608.
111. Klauk, H.; Halik, M.; Zschieschang, U.; Schmid, G.; Radlik, W.; Weber, W., *J. Appl. Phys.* **2002**, 92, (9), 5259.
112. Bao, Z.; Lovinger, A. J.; Dodabalapur, A., *Appl. Phys. Lett.* **1996**, 69, (20), 3066.
113. Halik, M.; Klauk, H.; Zschieschang, U.; Schmid, G.; Ponomarenko, S.; Kirchmeyer, S.; Weber, W., *Adv. Mater.* **2003**, 15, (11), 917.
114. Sirringhaus, H.; Tessler, N.; Friend, R. H., *Science* **1998**, 280, (5370), 1741.
115. Sundar, V. C.; Zaumseil, J.; Podzorov, V.; Menard, E.; Willett, R. L.; Someya, T.; Gershenson, M. E.; Rogers, J. A., *Science* **2004**, 303, (5664), 1644.
116. Newman, C. R.; Frisbie, C. D.; da Silva, D. A.; Bredas, J. L.; Ewbank, P. C.; Mann, K. R., *Chem. Mater.* **2004**, 16, (23), 4436.
117. Katz, H. E.; Bao, Z., *J. Phys. Chem. B* **2000**, 104, (4), 671.
118. Bao, Z.; Lovinger, A. J.; Brown, J., *J. Am. Chem. Soc.* **1998**, 120, 1998.
119. Sakamoto, Y.; Suzuki, T.; Kobayashi, M.; Gao, Y.; Fukai, Y.; Inoue, Y.; Sato, F.; Tokito, S., *J. Am. Chem. Soc.* **2004**, 126, (26), 8138.
120. Malenfant, P. R. L.; Dimitrakopoulos, C. D.; Gelorme, J. D.; Kosbar, L. L.; Graham, T. O.; Curioni, A.; Andreoni, W., *Appl. Phys. Lett.* **2002**, 80, (14), 2517.
121. Babel, A.; Jenekhe, S. A., *J. Am. Chem. Soc.* **2003**, 125, (45), 13656.
122. Dierschke, F.; Grimsdale, A. C.; Müllen, K., *Macromol. Chem. Phys.* **2004**, 205, 1147.
123. Qiu, S.; Liu, L. L.; Wang, B. L.; Shen, F. Z.; Zhang, W.; Li, M.; Ma, Y. G., *Macromolecules* **2005**, 38, (16), 6782.
124. Setayesh, S.; Grimsdale, A. C.; Weil, T.; Enkelmann, V.; Müllen, K.; Meghdadi, F.; List, E. J. W.; Leising, G., *J. Am. Chem. Soc.* **2001**, 123, (5), 946.
125. Pielichowski, J.; Polaczek, J.; Chrzaszcz, R.; Galka, S., *Carbazole dyes, pigments abd related products*. Cracow: Warsaw, 1996.
126. Ikeda, M.; Kitahara, K.; Nishi, H., *J. Heterocycl. Chem.* **1991**, 28, 1165
127. Ikeda, M.; Kitahara, K.; Nishi, H., *J. Heterocycl. Chem.* **1992**, 29, 289.
128. Ikeda, M.; Kitahara, K.; Nishi, H.; Kozawa, K.; Uchida, T., *J. Heterocycl. Chem.* **1990**, 27, 1575.
129. Wolfe, J. P.; Tomori, H.; Sadighi, J. P.; Yin, J.; Buchwald, S. L., *J. Org. Chem.* **2000**, 65, 1158.

## Chapter 2

### Nitrogen-Bridged ladder-type polyphenylenes

In this chapter, the synthesis and characterization of a series of nitrogen-bridged semi-ladder-type polymers are presented. A new synthesis is developed to prepare nitrogen-bridged monomers, where the end-functionalization is done at a precursor stage with chlorine atom and then polymerized by Yamamoto-type polycondensation. The resulting series of polymers, nitrogen-bridged poly(ladder-type tetraphenylene), nitrogen-bridged poly(ladder-type pentaphenylene), nitrogen-bridged poly(ladder-type hexaphenylene) and its derivatives are discussed in the light of photophysical and electrochemical properties and compared with the all carbon-bridged analogous ladder-type polymers as well as with fully ladder-type polymers reported in literature. All carbon-bridged poly(ladder-type tetraphenylene) was also synthesized to compare the properties with nitrogen-bridged poly(ladder-type tetraphenylene). 2D-WAX is performed on the nitrogen-bridged ladder-type polymers to study the packing behavior in the solid-state and finally, these polymers are tested in the various electronic devices such as light-emitting diode, solar cell, field effect transistor, and polymeric blue laser.

#### 2.1 Introduction

##### 2.1.1 Ladder-type polymers

Materials with a ribbon- or ladder-type framework possess a two-dimensional geometry and are thus intermediate between linear and three-dimensional systems. The limited conformational freedom of ladder-type polymers is particularly relevant in the case of conjugated systems since the steric inhibition of electron delocalization is drastically reduced. Until today two general routes have been used to synthesize ladder-type polymers<sup>1-3</sup>.

- a. A stepwise formation of the ladder-type polymers by polymer analogous conversion of a functionalized, single-stranded precursor polymer.

**b.** The synchronous, concerted construction of the ladder structure by way of suitable multi-centered reactions (*e.g.*, repetitive [4+2]- or [2+2+2]-cycloaddition steps).

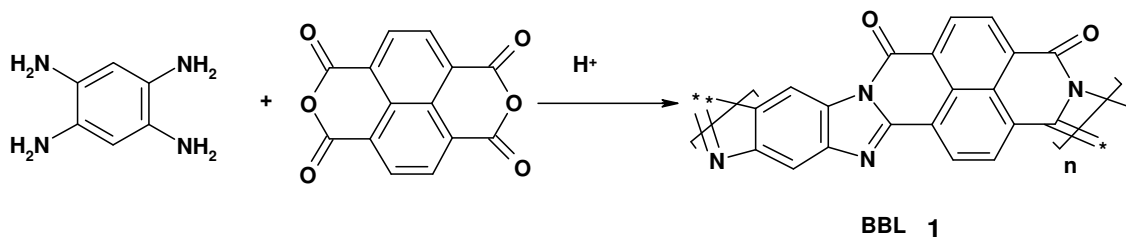
Of the two, the former method is more suitable to synthesize highly unsaturated, aromatic ladder-type polymers with  $\pi$ -conjugation throughout the main chain. By this it is possible to control the final, polymer-analogous reaction step so that it takes place quantitatively and with complete regioselectivity.

The latter concerted reaction variant is successfully applied to the synthesis of band polymers, which contain saturated,  $sp^3$ -carbon centers in the main chain. The Diels-Alder cycloaddition in particular has been used for the simultaneous connection for both strands of the ladder-type polymer. The required reaction steps often cannot be carried out quantitatively and hence lead to polymers with structural defects. These defects have adverse influence on the electronic properties such as electroluminescence, electrical and photoconductivity and extreme care must be taken to eliminate them during synthesis.

So, the development of synthetic methods for the generation of highly defined, molecular architecture with a high degree of homogeneity is of prime importance in the rapidly growing field of polymer electronics.

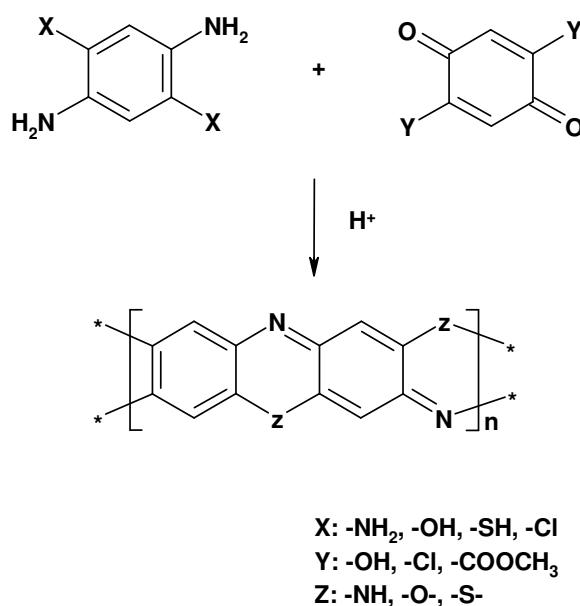
### **2.1.1.1 Heteroatomic ladder-type polymers by multifunctional polycondensation route**

Till the sixties, the synthetic approaches available in literature to make ladder-type polymers only resulted in incompletely formed double strands or partially cross-linked ladder structures rich in defects;<sup>4, 5</sup> the polymers synthesized via polymer-analogous aldol condensation of poly(vinyl methyl ketone) is an example.<sup>6, 7</sup> One of the earliest synthesis toward structurally defined, processable band polymers was achieved by the synthesis of poly(benzimidazobenzophenanthroline) (BBL) by Arnold and Vandeuessenin 1966 (Scheme 2.1).<sup>8-11</sup>



**Scheme 2.1** Synthesis of BBL

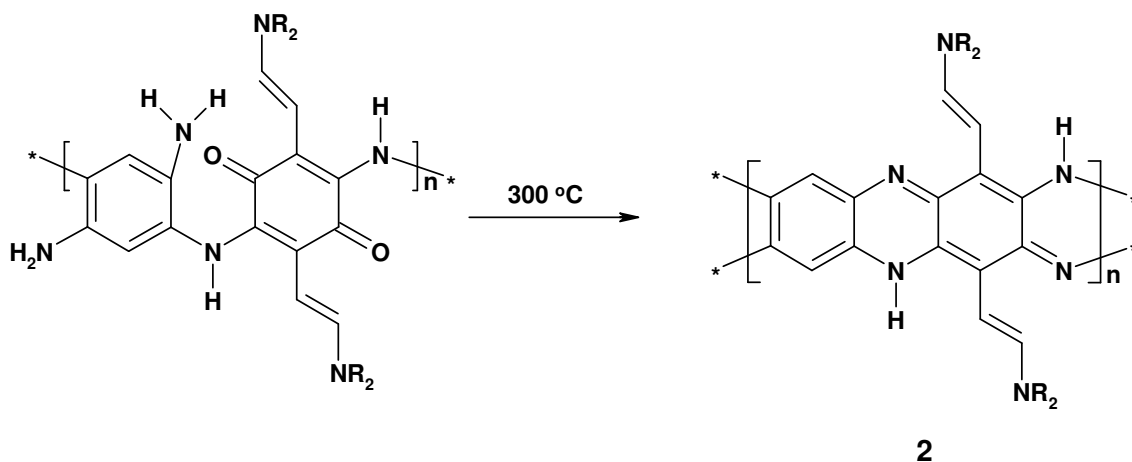
The BBL 1 was synthesized by polycondensation reaction between tetrafunctional monomers, in this case 1,2,4,5-tetraaminobenzene with naphthalene-1,4,5,8-tetracarboxylic anhydride in the presence of a protic solvent such as polyphosphoric or sulfuric acid. By optimizing the reaction conditions, it was possible to synthesize the completely soluble and unbranched polymers. It was processed from solution into high quality films by casting or spin coating. The cast BBL film exhibited an electrical conductivity of up to  $0.01 \text{ S cm}^{-1}$ .<sup>12</sup> These films were doped by ion implantation to high electrical conductivities about  $100 \text{ Scm}^{-1}$ .<sup>13, 14</sup>



**Scheme 2.2** Synthesis of heteroaromatic ladder-type polymers; poly(quinoxaline)s, poly(phenoxazine)s, and poly(phenothiazine)s.



At the same time, few more polymers were made following a similar synthetic methodology, which contained phenoxazine, phenothiazine, or quinoxaline as a structural Unit (Scheme 2.2).<sup>15-21</sup> However, the resulting polymers were only slightly soluble and made detailed characterization impossible. At the same time Yu and Dalton incorporated the solubilizing side group at the 3,6-positions of 2,5-dichlorobenzo-1,4-quinone building block to synthesize polyquinoxaline derivative **2** (Scheme 2.3).<sup>22, 23</sup> The resulting polymers were soluble and characterized by NMR and IR spectroscopy.



**Scheme 2.3** Synthesis of soluble poly(quinoxaline)s **2**

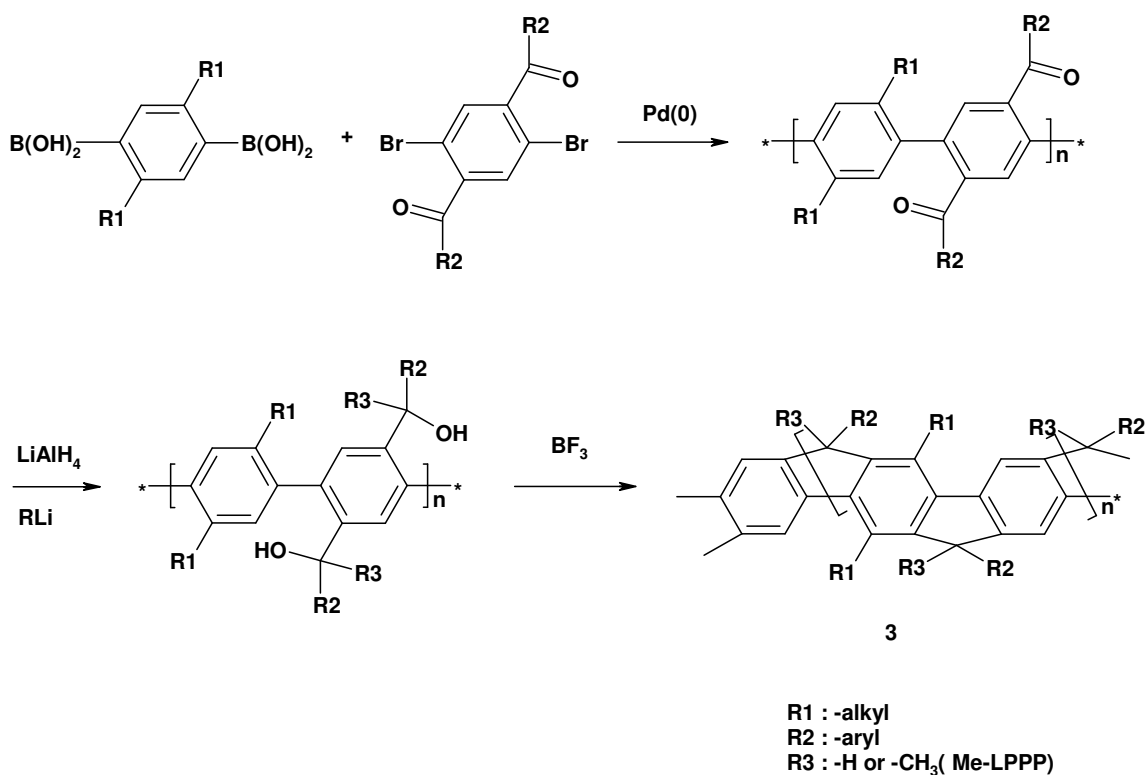
### 2.1.1.2 Conjugated ladder-type polymers by polymer-analogous cyclization

#### 2.1.1.2.1 Carbon-bridged ladder-type polymers

The optical and electronic properties of conjugated polymers frequently depend on the conformation of the main chain. Twisting of the monomeric units along the conjugated main chain leads to reduced conjugation and this is accompanied by drastic changes in the optical properties, along with a reduction of the photoluminescence quantum yield, and the electronic properties.<sup>24, 25</sup> One solution to this problem is the ladderization of the polymer backbone by appropriate carbon bridges. However, this often leads to poor solubility of the polymers since planar conjugated  $\pi$ -systems show high tendency toward stacking. The other alternative is to introduce solubilizing side chains on the polymer backbone so as to impart solubility

to the material. Ideally, it should be possible to design structures tuned for a particular absorption or emission wavelength without compromising on its solubility.

Müllen and coworkers introduced this strategy for the first time and synthesized soluble fully ladder-type poly(*p*-phenylene) from insoluble and infusible poly(*p*-phenylene).<sup>26</sup> It was a great success in the perspective of both synthetic methodology and material science.



**Scheme 2.4** Synthesis of poly(*p*-phenylene) ladder-type polymers **3**

The synthesis of LPPP **3** involved two main steps (Scheme 2.4)

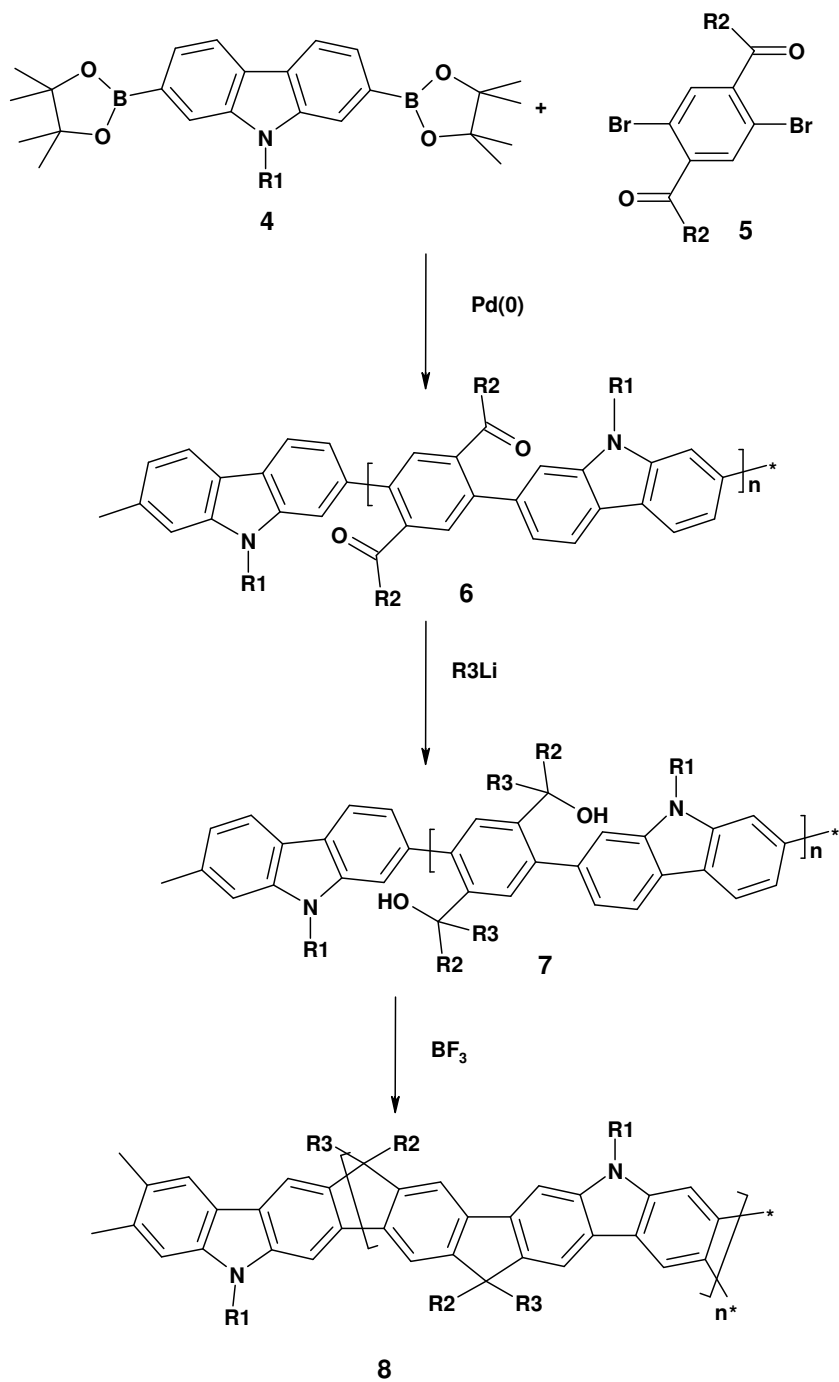
- (i) A keto functionalized, single stranded precursor polymer which was prepared by Suzuki coupling,
- (ii) The double strand of ladder-polymer was generated by two polymer analogous reaction (1) either reduction of keto group by LiAlH<sub>4</sub> or the addition of alkyllithium to give alcohol (2) and then polymer analogous Friedel-crafts Craft ring closure.

LPPP derivatives **3** were obtained with number average molecular weight ( $M_n$ ) of up to 50,000 ( $M_w/M_n = 2$ ), which corresponds to a linear coupling of up to 150 phenylene rings in the main chain of the double-stranded polymers. The transformation from conformationally twisted, single-stranded precursor to a rigid, double-stranded ladder-type polymer resulted in a drastic change in the optical properties of the polymer, as shown by a marked red shift of the absorption maximum as well as the appearance of a very intense blue photoluminescence. The polymer was characterized by mirror-plane symmetrical photoluminescence spectrum, a very small Stokes shift ( $150 \text{ cm}^{-1}$ )<sup>27</sup>, and high photoluminescence quantum yield (over 90 %), suggestive of a rigid polymer backbone that does not allow any geometrical relaxation. These properties were really interesting for the application of this material in blue light emitting diodes since stable blue color is very hard to obtain. However, in solid-state the polymer showed very intense aggregation which led to a significant change in optical properties. The emission spectrum was dominated by a red-shifted, unstructured broad emission band in the yellow region and the PL quantum yield was reduced to 10 %.<sup>28</sup> However, minor change in the substitution pattern on the polymer backbone where hydrogen at the bridged carbon atom was replaced by methyl group led to a significant suppression of the aggregation. The PL quantum yield also improved to 40 %.<sup>28-30</sup> LED devices demonstrated high electroluminescence (EL) quantum efficiency of up to 4 %.<sup>30</sup>

### 2.1.1.2.2 Nitrogen-bridged ladder-type polymers

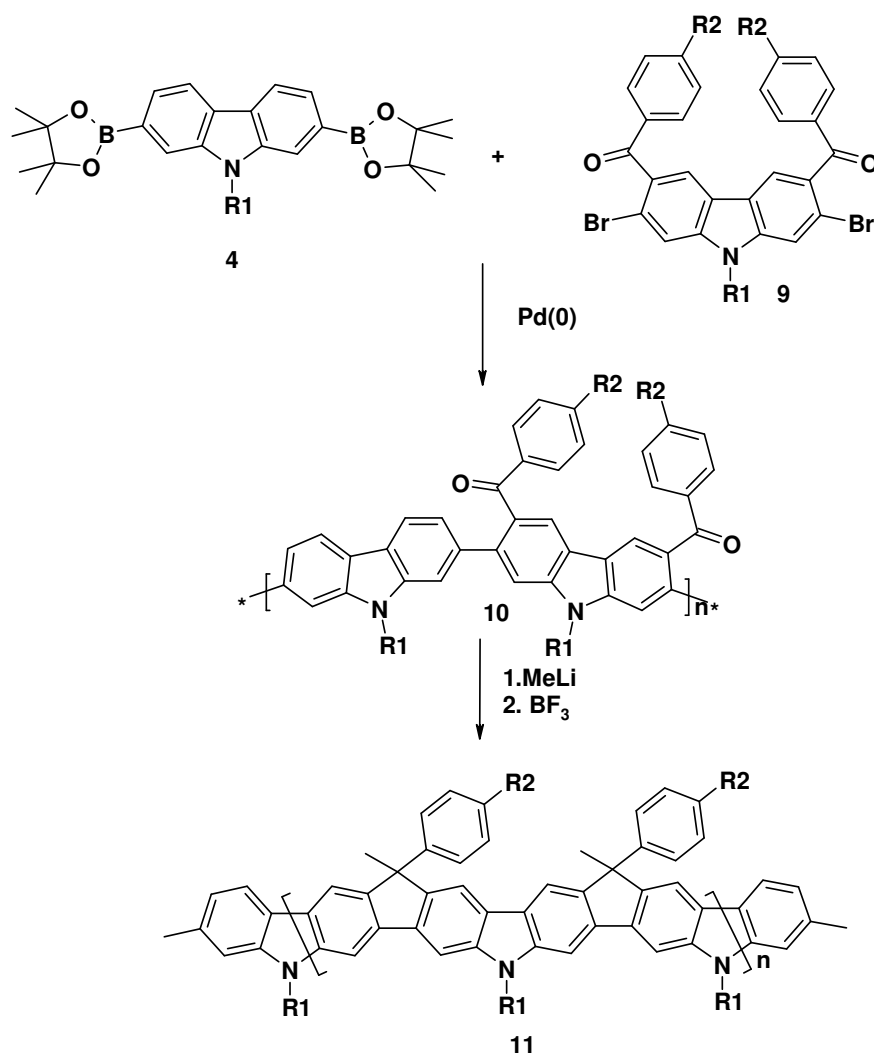
LPPP type polymers are excellent for optoelectronics applications but it suffers from disadvantages such as poor charge injection and susceptibility of the bridgehead 9-position toward oxidation to generate ketones, which leads to undesirable changes in their optical properties. Materials which avoid both of these problems are nitrogen-bridged ladder-type polymer since the nitrogen bridge is not oxidisable to the corresponding ketone and improves the hole-accepting and transporting properties by raising the highest occupied molecular orbital (HOMO). The first synthesis of the nitrogen bridged analogue of LPPP was reported by Scherf

and coworkers, who prepared the precursor alternating copolymer **6** by Suzuki polycondensation reaction of carbazole diboronic ester **4** and diketobenzene **5**, and then converted it to the ladder-polymer **8** by the polymer analogous addition of methyl lithium followed by ring closure with boron trifluoride (Scheme 2.5).<sup>31</sup>



**Scheme 2.5** Synthesis of carbazole based ladder-type polymer **8** reported by Scherf and coworkers<sup>31</sup>

The ring closure was assisted by the electron donating properties of the carbazole nitrogen which enhanced the susceptibility of the carbazole 3- and 6-positions toward electrophilic attack. The number average and weight average molecular weight of polymer **8** were found to be 35300 and 69100 g/mol, respectively, which corresponds to an average degree of polymerization of 45 units by GPC (Gel permeation chromatography) analysis against polystyrene as a standard. Absorption maximum and emission maximum of polymer **8** in chloroform solution was found to be at 460 nm and 468 nm, respectively, with a very small Stokes shift of 8 nm which is a characteristic of ladder-type polymers.



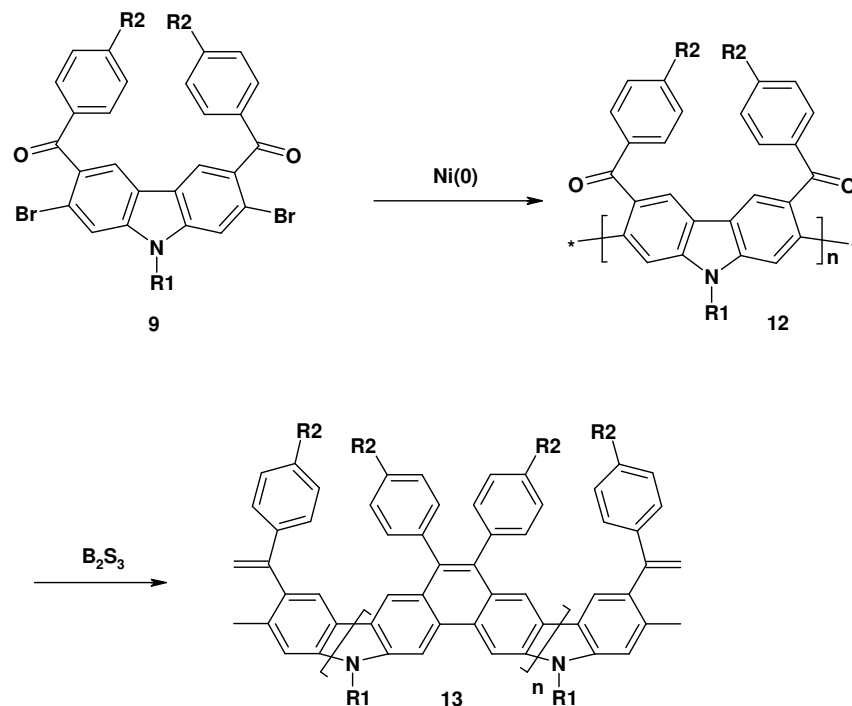
**Scheme 2.6** Synthesis of carbazole based ladder-type polymer **11**

In a similar attempt, Müllen and coworkers synthesized a carbazole based ladder-type polymer with higher carbazole content by taking the advantage that the carbazole 3, 6 positions can be easily functionalized by electrophilic substitution reaction (Scheme 2.6).<sup>32</sup> Then the precursor polymer **10** was made by the Suzuki polycondensation reaction of diacyl carbazole **9** with carbazole diboronic ester **4**. Finally, addition of methyllithium and ring closure by boron trifluoride resulted in ladder polymer **11** as shown in Scheme 2.6. This polymer was anticipated to be better hole transporter than ladder type polymer **8** made by Sherf and coworkers because of higher density of nitrogen in the polymer backbone as well as due to their asymmetry (all nitrogen are at same side of polymer), potentially useful for selective binding with an electrode or a nanoparticle or for layer-by-layer self assembly. The GPC measurements on polymer **11** displayed Mn and Mw of 13500 and 23000 g/mol respectively with a polydispersity index of 1.7. The optical properties were measured in chloroform solvent and found be highly dependent on the concentration of the polymer in solution. This concentration dependent optical behavior was a clear indication of the aggregation of the polymer chains in solution. At high concentrations of polymer (0.1 mg/mL), emission spectrum was featureless in shape and when concentration was reduced by 100 times, the broad featureless emission disappeared and a new blue-shifted sharp emission maximum at 473 nm appeared. This demonstrated that the polymer chains were interacting in solution and forming aggregates. The bulky aryl substituents were present only on one side of the the polymer chain which was proved insufficient to prevent aggregation. Polymer **11** showed green fluorescence in solution.

A similar polymer was also synthesized where the five membered ring was replaced by a six membered ring in the ladder-type polymer **13**.<sup>32</sup> In this case the precursor monomer was diacyl carbazole **9** which was polymerized by Yamamoto polycondensation reaction to give precursor polymer **12** and then ring closure by B<sub>2</sub>S<sub>3</sub> gave the desired polymer **13** (Scheme 2.7).

Polymer **13** was synthesized with Mn and Mw value of 11000 and 61000 g/mol respectively against polystyrene standard. In contrast to polymer **11**, polymer **13** displayed well resolved photoluminescence spectrum in solution with no

concentration dependence. The absence of aggregation was attributed to the helical structure of the polymer backbone unlike polymer **11**.



**Scheme 2.7** Synthesis of carbazole based ladder-type polymer **13**

Due to more extended conjugation, polymer **13** demonstrated a bathochromic shift of the emission maximum to 467 nm with secondary bands at 499 and 534 nm, so that the fluorescence was yellowish-green in color.

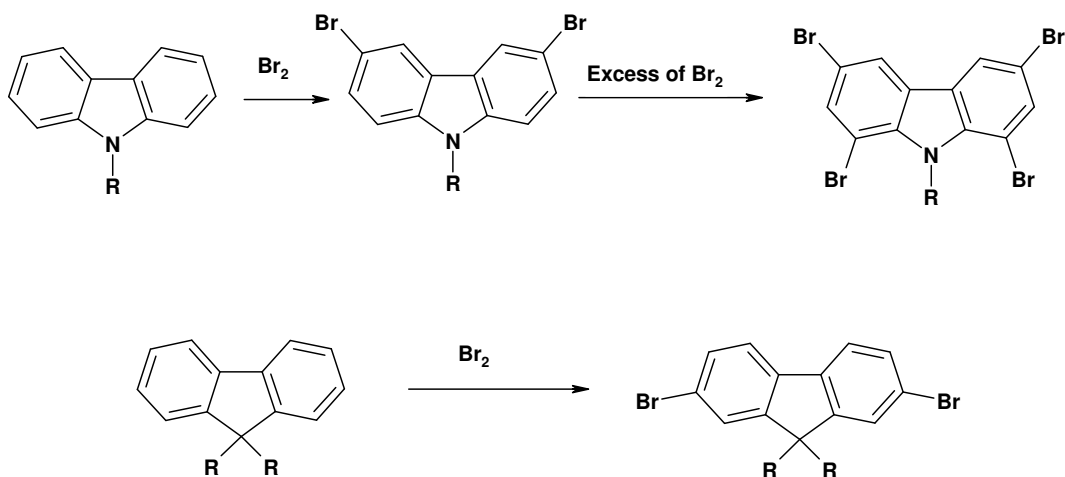
As mentioned above, the fully ladder type nitrogen-bridged polymers have the following disadvantages:

1. The solubility is so low that it is difficult to obtain good film from solution processing.
2. Aggregate formation leading to low energy emission in the solid-state
3. Emission maximum is bathochromically shifted (around 470 nm), and hence not suitable for use as a blue emitter.

To overcome these problems, a series of semi-ladder-type polymers were synthesized, characterized and, tested in various electronic devices as discussed below.

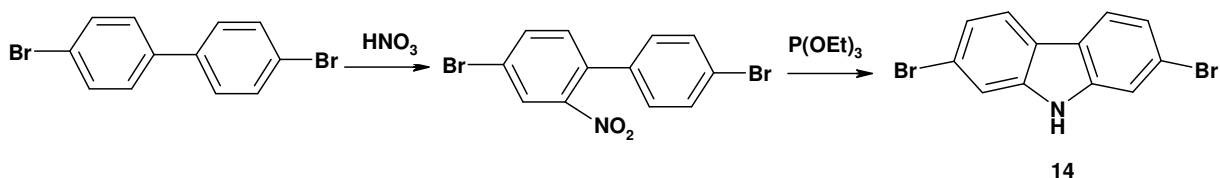
## 2.2 Synthesis and Characterization

One of the problems to synthesize nitrogen-bridged semi-ladder-type polymers is the strong directional property of nitrogen atom for electrophilic substitution reactions than carbon. For example, bromination of carbazole gives a 3,6-dibrominated product<sup>33</sup> and if excess of bromine is present then 1,3,6,8-tetrabromocarbazole is formed unlike fluorene (Scheme 2.9) which undergoes substitution at its 2,7-positions<sup>34</sup>.



**Scheme 2.9** Electrophilic substitution: Fluorene<sup>34</sup> vs Carbazole<sup>33</sup>

This is the reason 2,7-dibromocarbazole cannot be made directly from carbazole but it is made through a precursor route where end functionalization is done prior to the Cadogan ring closure as shown in Scheme 2.10.

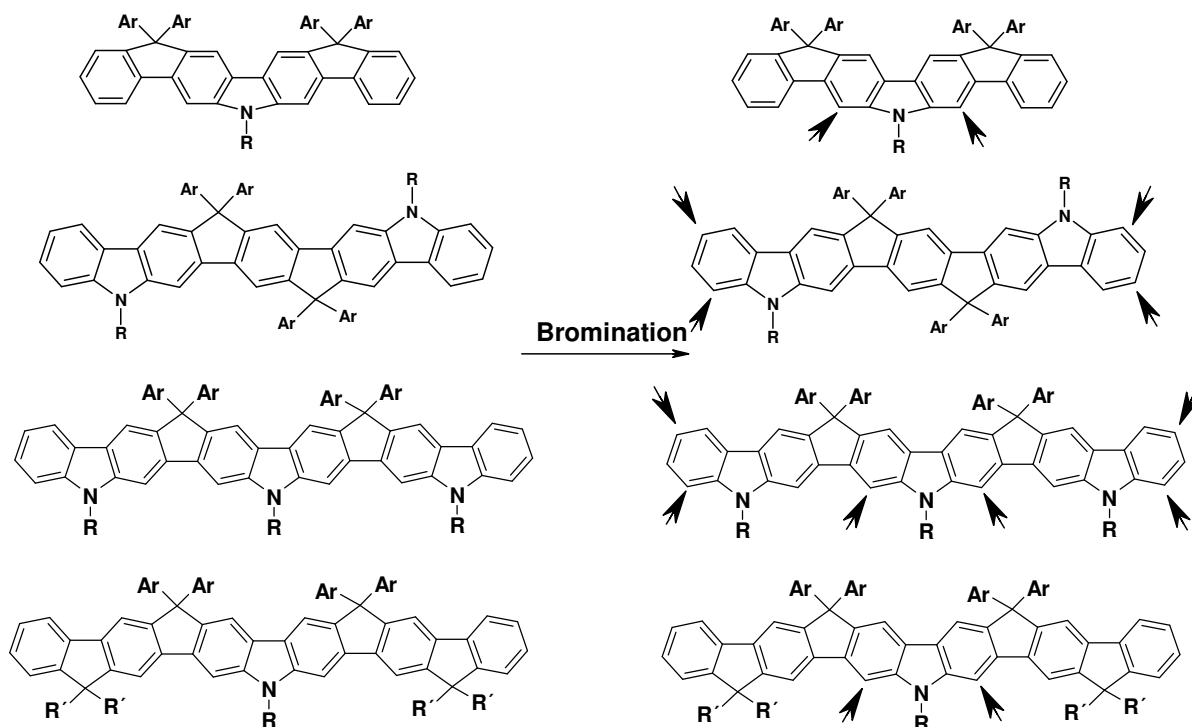


**Scheme 2.10** Synthesis of 2,7-dibromocarbazole by Müllen and coworkers<sup>35</sup>

In a similar way, for the synthesis of higher analogues of carbazole based monomers, it is very important to select appropriate precursor molecules which can



be easily end-functionalized otherwise it becomes difficult to achieve the desired substitution pattern as shown by the directionality of different monomers toward an electrophile (Scheme 2.11).



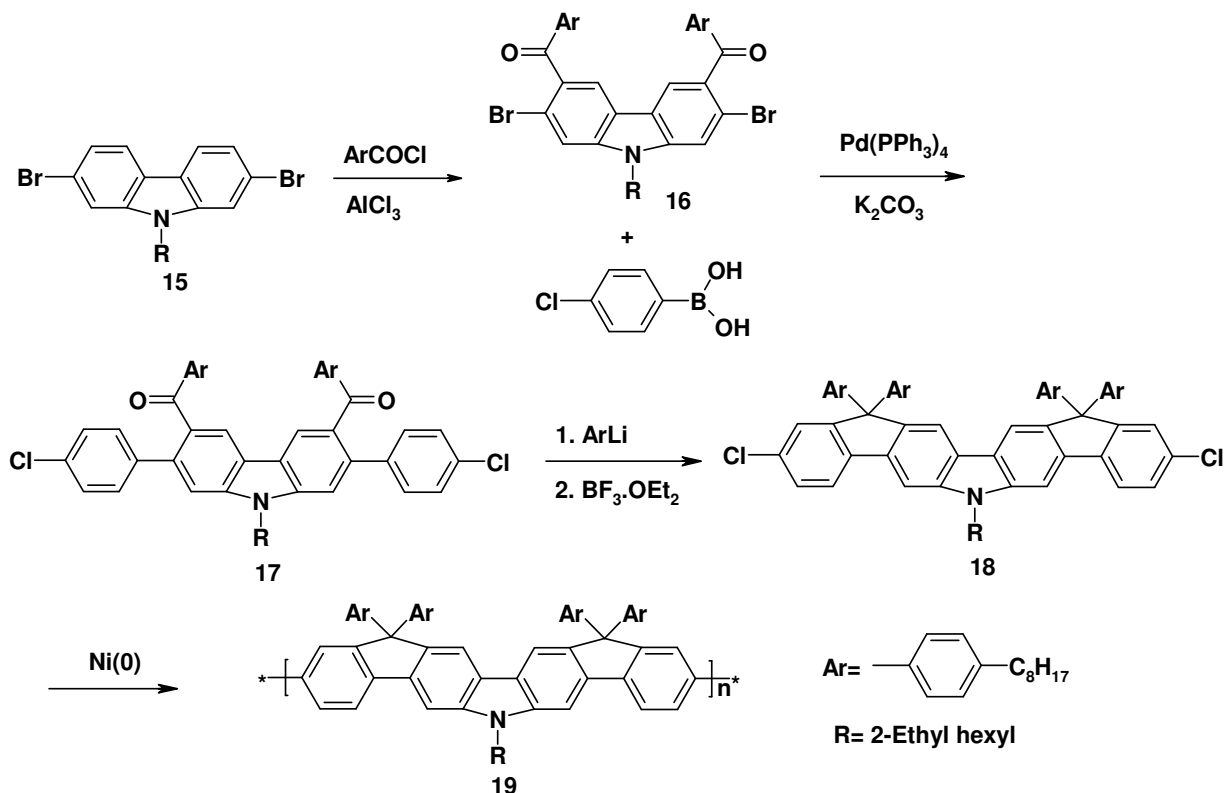
**Scheme 2.11** Preferred site on carbazole based monomers for electrophilic substitution reaction

To avoid these problems, a new synthetic methodology is developed where the precursor molecule was first end-functionalized with halogen preferably with chlorine atom because of two main reasons (i) Chlorine is less susceptible for exchange with phenyllithium than bromine during the conversion of the ester or keto group into alcohol as well as it is stable towards Suzuki coupling reaction and hence avoids polymerisation (ii) chlorine is preferred to bromine in Yamamoto polymerization because carbon-chlorine bond is stronger than C-Br, and so may be less susceptible to dehalogenation at the relatively long reaction times required for Yamamoto polycondensations at 70 °C. This decrease in dehalogenated side product would cause an increase in the molecular weight of the polymer.

## 2.2.1 Synthesis of poly(ladder-type tetraphenylene)

## 2.2.1.1 Synthesis of nitrogen-bridged poly(ladder-type tetraphenylene)

The synthetic approach towards carbazole based ladder-type poly(tetraphenylene) is shown in Scheme 2.12.



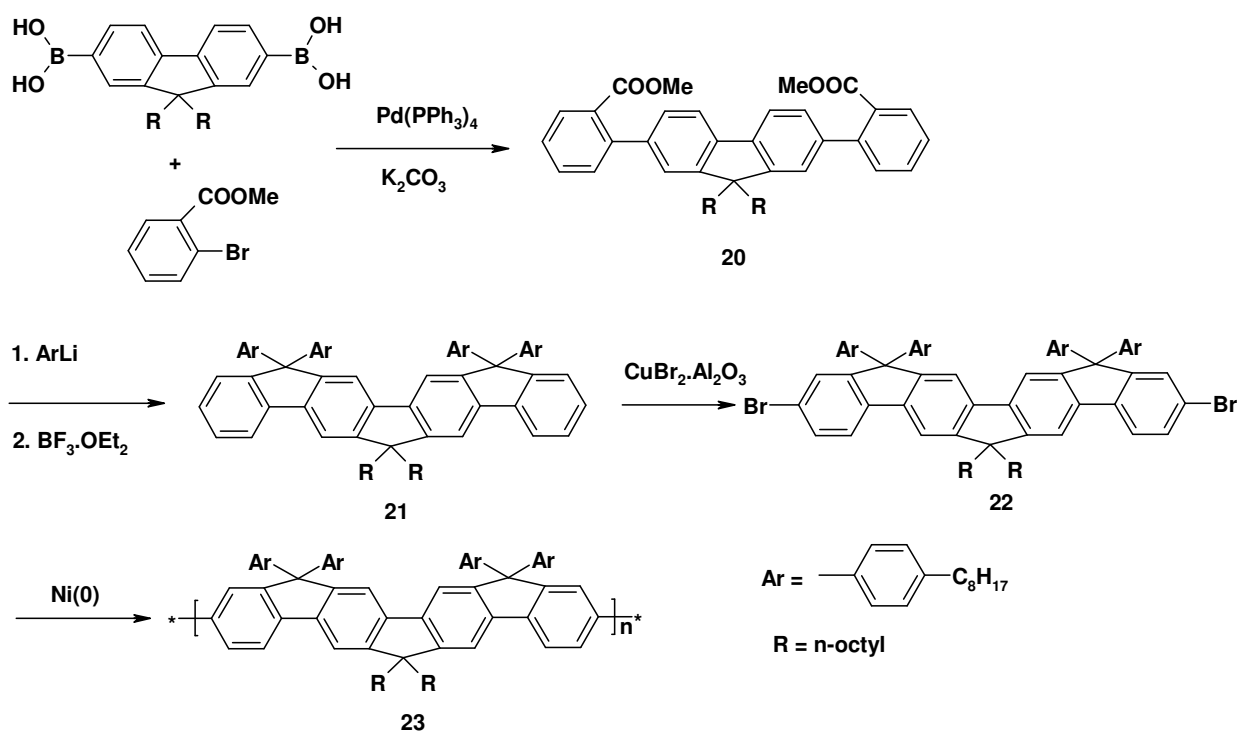
**Scheme 2.12** Synthesis of nitrogen-bridged poly(ladder-type tetraphenylene)

2,7-Dibromo-N-(2-ethylhexyl)carbazole (**15**) was synthesized according to the literature.<sup>35</sup> Friedel-Crafts acylation gave the 3,6-disubstituted carbazole **16** which was coupled with two equivalents of 4-chlorophenylboronic acid in the presence of  $\text{Pd}(\text{PPh}_3)_4$  as catalyst to generate the diketone **17** in 82 % yield. Treatment with a slight excess of 4-octylphenyllithium produced the corresponding diol which upon ring closure with  $\text{BF}_3$ -etherate gave the monomer **18** in 86 % combined yield. The polymer **19** was synthesized using nickel (0) mediated Yamamoto-type polymerization of monomer **18** in 77 % yield. GPC analysis against PPP standard showed a  $M_n$  value of  $4.6 \times 10^4 \text{ gmol}^{-1}$ , with a polydispersity index of 2.79. This

corresponds to a degree of polymerization of about 38 and the resulting polymer had very good solubility in common organic solvents like dichloromethane, tetrahydrofuran etc.

### 2.2.1.2 Synthesis of carbon-bridged poly(ladder-type tetraphenylene)

For comparison, a poly(ladder-type tetraphenylene) with all carbon bridges was also synthesized. The synthetic scheme is outlined in Scheme 2.13.



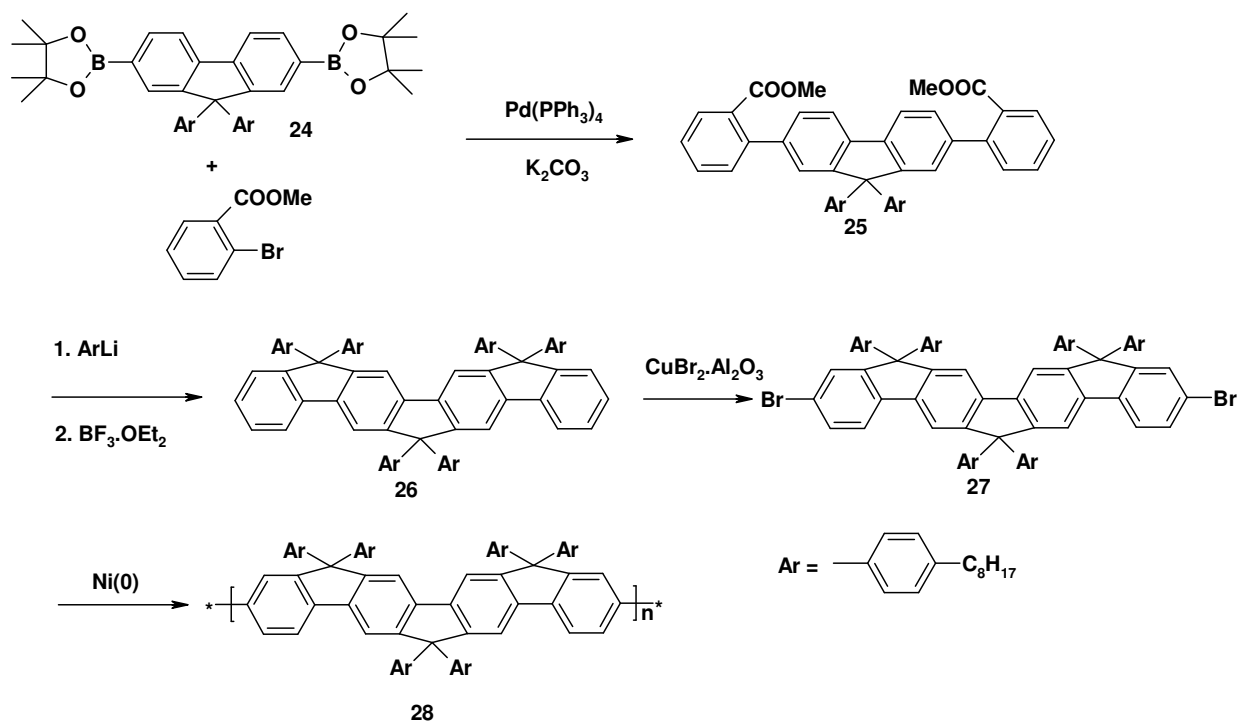
Scheme 2.13 Synthesis of polymer **23**

The diester **20** was synthesized in 71 % yield by standard Suzuki coupling of commercially available 9,9'-dioctyl-2,7-fluorene diboronic acid and methyl 2-bromobenzoate. Addition of four equivalents of 4-octylphenyl lithium generated the corresponding diol which was ring closed by  $\text{BF}_3 \cdot \text{etherate}$  to give the ladder-type tetraphenylene **21** in 82 % overall yield. In this case, the ring closure was obtained in quantitative yield by stirring the reaction mixture at room temperature. Although bromination using bromine liquid led to overbromination, use of  $\text{CuBr}_2$  on alumina

gave the desired monomer **22** in nearly quantitative yield. This was polymerized by Yamamoto-type polymerization to generate polymer **23** in 70 % yield. GPC analysis using PPP standard showed a  $M_n$  value of  $3.54 \times 10^4$  with a polydispersity index of 2.28. This corresponds to a degree of polymerization of about 27 and the material has good solubility in common organic solvents.

### 2.2.1.3 Synthesis of fully arylated poly(ladder-type tetraphenylene)

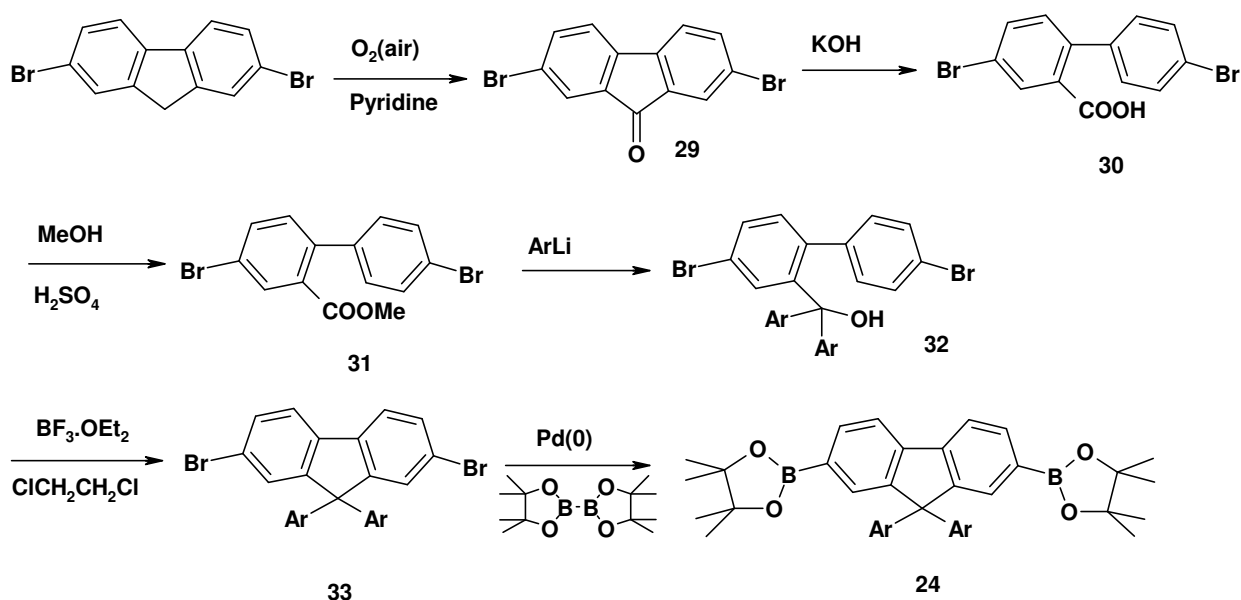
It is reported in literature that the alkylated phenylene based polymers such as polyfluorene, polyindeno fluorene and ladder-type polyphenylenes are prone to oxidative degradation at the carbon bridge, which results in fluorenone-type keto defect in the polymer backbone.<sup>36</sup> For comparison with nitrogen-bridged as well as alkylated, arylated poly(ladder-type tetraphenylene), a fully arylated poly(ladder-type tetraphenylene) was also synthesized (Scheme 2.14).



**Scheme 2.14** Synthetic route to fully arylated poly(ladder-type tetraphenylene)

The diester **25** was synthesized in 71 % yield by standard Suzuki coupling of fluorene diboronic ester **24** and commercially available methyl 2-bromobenzoate.

Addition of four equivalents of 4-octylphenyl lithium generated the corresponding diol which was ring closed by  $\text{BF}_3$ -etherate to give the fully arylated ladder-type tetraphenylene **26** in 78 % overall yield. The ring closure was obtained in quantitative yield by stirring the reaction mixture at room temperature.  $\text{CuBr}_2$  on alumina was used to give the desired monomer **27** in nearly quantitative yield. This was polymerized by Yamamoto-type polymerization to generate polymer **28** in 76 % yield. GPC analysis using PPP standard showed a  $M_n$  value of  $7.03 \times 10^4$  with a polydispersity index of 2.78. This corresponds to a degree of polymerization of about 47 and the material has good solubility in common organic solvents.



**Scheme 2.15** Synthesis of 9,9'-diaryl-2,7-fluorenediboronic ester **24**

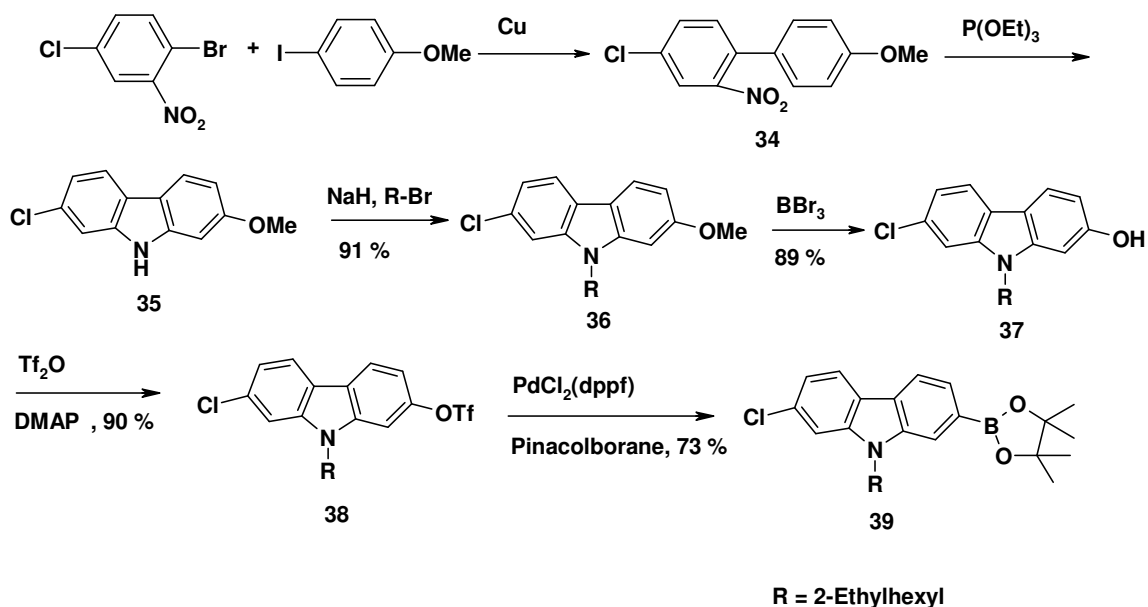
The intermediate **24** was made starting from commercially available 2,7-dibromofluorene as shown in Scheme 2.15. The dibromofluorene was oxidized in the presence of air and catalyzed by 0.8 M t-butylammonium hydroxide to give 2,7-dibromofluorenone (**29**) in 66 % yield. Compound **29** was converted to 4,4'-dibromobiphenyl-2-carboxylic acid (**30**) by KOH in diphenylether at 175 °C in 46 % yield. The resulting biphenyl acid **30** was refluxed in MeOH in the presence of sulfuric acid as catalyst to afford 4,4'-dibromo-biphenyl-2-carboxylic acid methyl ester (**31**) in 72 % yield. Addition of four equivalents of 4-octylphenyl lithium generated the corresponding diol **32** which was ring closed by  $\text{BF}_3$ -etherate to give the fully arylated

dibromofluorene **33** in 83 % overall yield. Again, the ring closure was obtained in quantitative yield by stirring the reaction mixture at room temperature. The fluorene diboronic ester **24** was obtained by the coupling of 2,7-diarylated dibromofluorene with bis-(pinacolato)diboron by Suzuki type coupling in 46 % yield.

## 2.2.2 Synthesis of nitrogen-bridged poly(ladder-type pentaphenylene)

### 2.2.2.1 The synthesis of intermediate 2-chloro-9-(2-ethylhexyl)-7-(4,4,5,5-tetramethyl-[1,3,2]dioxaborolan-2-yl)carbazole (**39**)

The synthesis of the key intermediate **39** for nitrogen-bridged poly(ladder-type pentaphenylene) is depicted in Scheme 2.16.



**Scheme 2.16** Synthesis of 2-chloro-9-(2-ethylhexyl)-7-(4,4,5,5-tetramethyl [1,3,2]dioxaborolan-2-yl)carbazole (**39**)

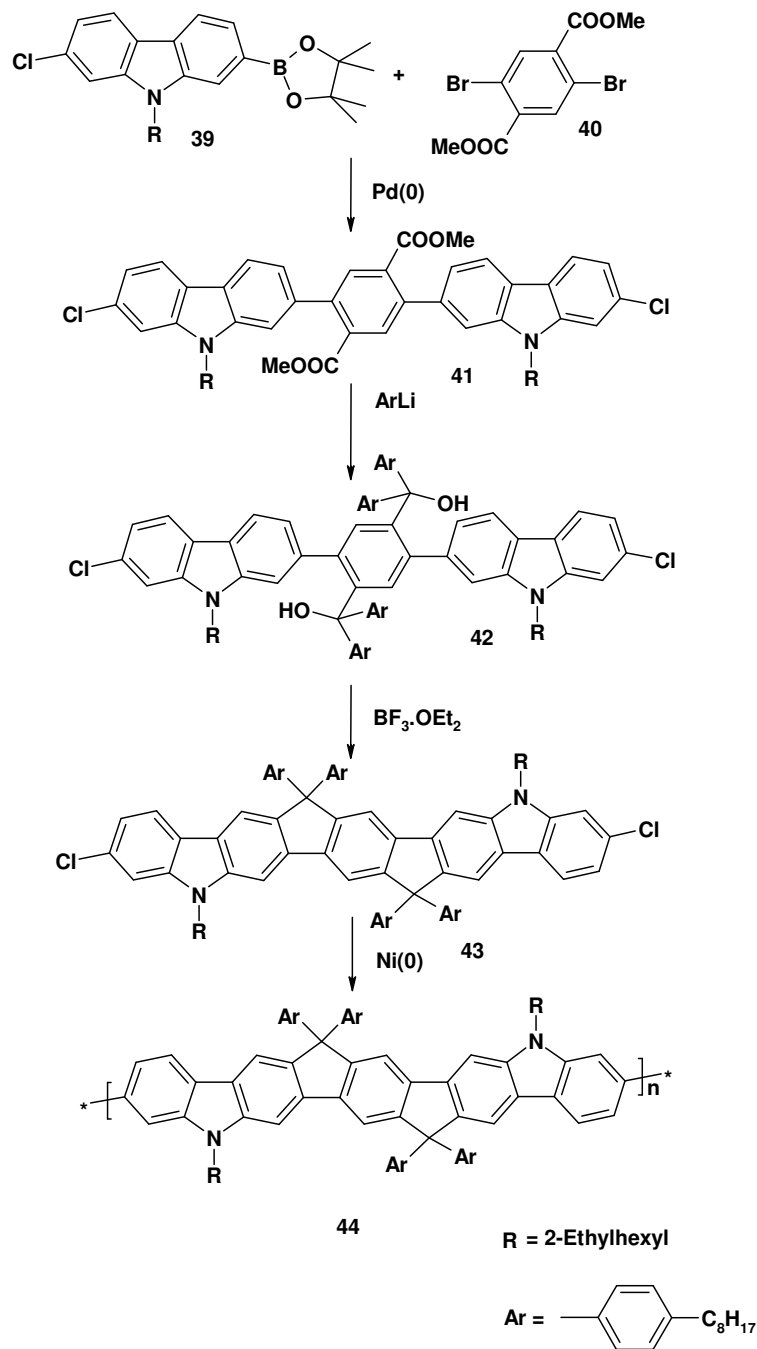
The synthesis starts from the coupling of 2-bromo-5-chloro-nitrobenzene and 4-iodo-anisole by Ullmann coupling reaction to give the 4-chloro-4'-methoxy-2-nitro-biphenyl (**34**) in 52 % yield. Cadogan reaction was performed on molecule **34** and ring closed product 2-chloro-7-methoxy-carbazole (**35**) was obtained in 40 % yield. Thereafter, carbazole **35** was alkylated by using sodium hydride as a base and 2-ethylhexylbromide as alkylating agent to give 2-chloro-9-(2-ethylhexyl)-7-

methoxy-carbazole in 91 % yield. This method of alkylation is better than that by using NaOH as base and THF as solvent where the yield is low and the reaction time is longer. Then methoxycarbazole **36** was hydrolyzed to 7-chloro-9-(2-ethylhexyl)carbazole-2-ol (**37**) by using BBr<sub>3</sub> as a hydrolyzing reagent. Again compound **37** was treated with triflic anhydride in the presence of dimethylamino pyridine as a base which gave trifluoro-methanesulfonic acid 7-chloro-9-(2-ethylhexyl)-carbazole-2-yl ester (**38**) in 90 % yield. Finally, molecule **38** was converted to 2-chloro-9-(2-ethylhexyl)-7-(4,4,5,5-tetramethyl-[1,3,2]dioxaborolan-2-yl)carbazole (**39**) by using pinacol diborane in the presence of palladium(0) as catalyst in 73 % yield. This intermediate **39** would be used in the synthesis of both nitrogen-bridged poly(ladder-type pentaphenylene) as well as nitrogen-bridged poly(ladder-type hexaphenylene).

#### 2.2.2.2 Synthesis of nitrogen-bridged poly(ladder-type pentaphenylene)

The synthesis towards poly(ladder-type pentaphenylene) is depicted in Scheme 2.17. First the 2,5-bis-[7-chloro-9-(2-ethylhexyl)-carbazole-2-yl]-terephthalic acid dimethyl ester (**41**) was made by Suzuki coupling of 2-chloro-9-(2-ethylhexyl)-7-(4,4,5,5-tetramethyl-[1,3,2]dioxaborolan-2-yl)carbazole (**39**) and 2,5-dibromo-terephthalic acid dimethyl ester (**40**) in 96 % yield. The diester **40** was synthesized by the esterification of commercially available 2, 5-dibromo-terephthalic acid by refluxing in methanol with few drops of sulfuric acid in almost quantitative yield. Then, pentaphenylene diester **41** was treated with four equivalent of 4-octylphenyllithium to generate pentaphenylene diol **42** in 92 % yield. The 4-octylphenyllithium was obtained by lithiation of 4-octylbromobenzene with n-BuLi at -78 °C. Pentaphenylene diol **42** was treated with Lewis acid BF<sub>3</sub>·OEt<sub>2</sub> in 1,2-dichloroethane which gave ring closed product **43** nearly in quantitative yield. The pentaphenylene monomer **43** was precipitated from reaction mixture by addition of excess of methanol and then purified by column chromatography followed by recrystallization from THF/Ethanol mixture prior to polymerization. The nitrogen-

bridged poly(ladder-type pentaphenylene) **44** was synthesized by nickel mediated Yamamoto polycondensation of pentaphenylene monomer **43**



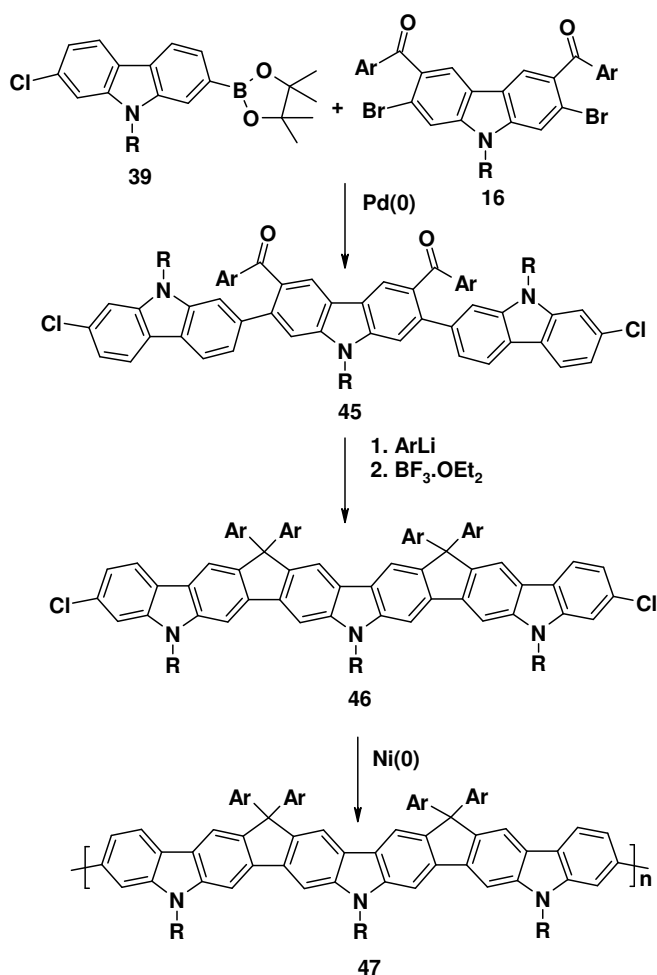
**Scheme 2.17** Synthesis of nitrogen-bridged poly(ladder-type pentaphenylene)



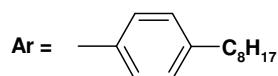
GPC analysis of polymer **44** showed a  $M_n$  of  $4.6 \times 10^4 \text{ gmol}^{-1}$ ,  $M_w$  of  $1.1 \times 10^5 \text{ gmol}^{-1}$ , and a polydispersity index (D) of 2.5 against PPP standard, and a  $M_n$  of  $7.59 \times 10^4 \text{ gmol}^{-1}$ ,  $M_w$  of  $2.47 \times 10^5 \text{ gmol}^{-1}$ , and a polydispersity index of 3.3 against PS standard. This corresponds to a degree of polymerisation of 32 monomer units by taking PPP as reference. The polymer had good solubility in common organic solvents like dichloromethane and tetrahydrofuran.

## 2.2.3 Synthesis of poly(ladder-type hexaphenylene)

### 2.2.3.1 Synthesis of poly(ladder-type hexaphenylene) with three nitrogen bridges in the monomer



R = 2-Ethylhexyl

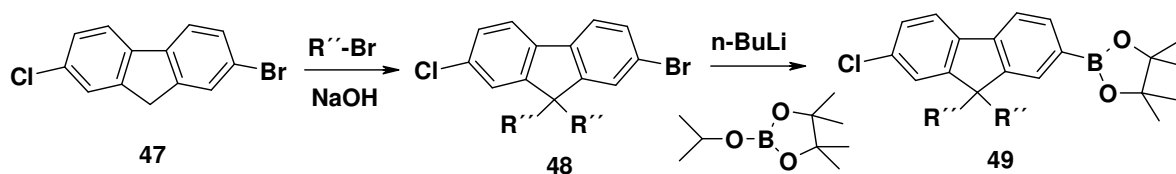


**Scheme 2.18** Synthesis of nitrogen-bridged poly(ladder-type hexaphenylene)

The synthetic approach towards nitrogen-bridged poly(ladder-type hexaphenylene) is shown in Scheme 2.18. The carbazole boronic ester **39** was coupled with dibromocarbazole **16** in the presence of  $\text{Pd}(\text{PPh}_3)_4$  to generate diketone **45** in 71 % yield. Treatment of **45** with a slight excess of 4-octylphenyllithium produced the corresponding diol, which upon ring closure with  $\text{BF}_3$ -etherate gave the nitrogen-bridged ladder-type hexaphenylene monomer **46** in 85 % overall yield. The polymer **47** was synthesized using nickel (0) mediated Yamamoto-type polymerization of monomer **46** in 83 % yield. GPC analysis against PPP standard showed a  $M_n$  value of  $2.3 \times 10^4 \text{ gmol}^{-1}$ , with a polydispersity index of 2.4. This corresponds to a degree of polymerization of about 15 and the resulting polymer had very good solubility in common organic solvents like dichloromethane and tetrahydrofuran.

### 2.2.3.2 Synthesis of poly(ladder-type hexaphenylene) with one nitrogen bridge in the monomer

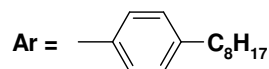
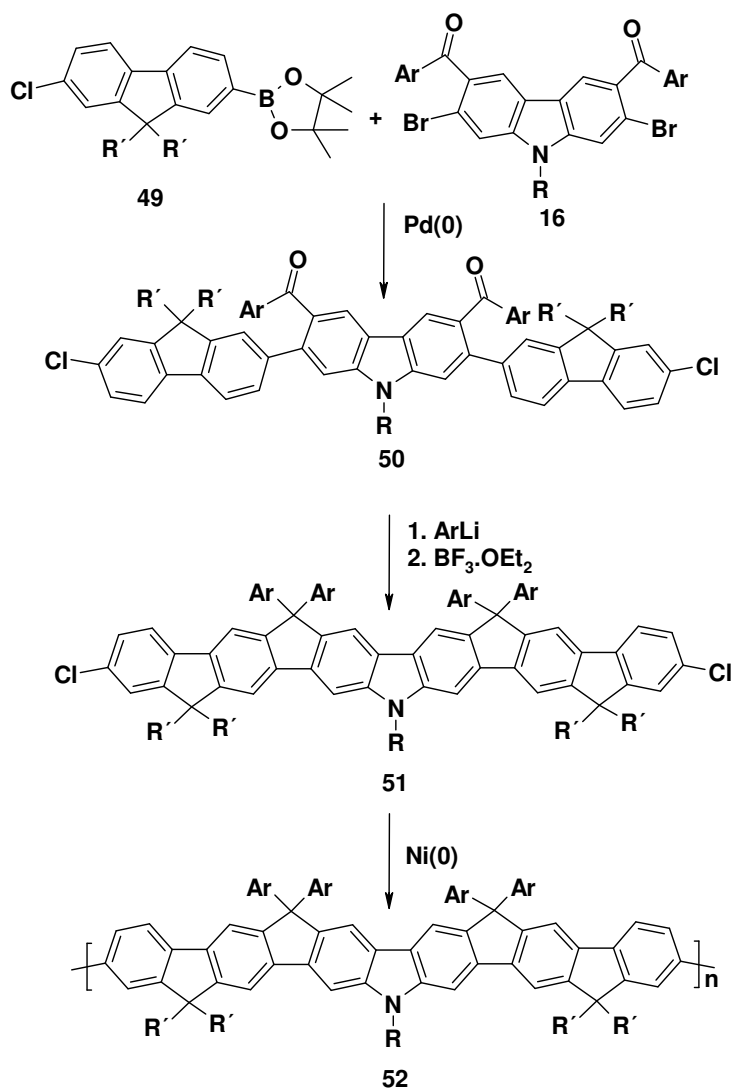
For comparison, polymer **52** was also synthesized which was expected to absorb between the poly(ladder-type tetraphenylene) **19** and poly(ladder-type hexaphenylene) **47** with three nitrogen bridges. The synthetic scheme is outlined in Scheme 1.20. Compound **47** was synthesized according to literature (Scheme 2.19).<sup>37</sup>



$R'' = n\text{-Octyl}$

**Scheme 2.19** Synthesis of 2-chloro-9,9'-dioctyl-7-(4,4,5,5-tetramethyl-[1,3,2]dioxaborolan-2-yl)fluorene **49**

Alkylation of 2-bromo-7-chloro-fluorene (**47**) with 1-bromooctane in the presence of tetrabutylammoniumchloride as a phase transfer catalyst afforded compound **48** in a 78 % yield. Then compound **48** was converted to boronic ester **49** by lithiation in THF at  $-78^{\circ}\text{C}$ , followed by reaction with 2-isopropoxy-4,4,5,5-tetramethyl-1,3,2-dioxaborolane in 65 % yield. The monoboronic ester **49** was used to synthesize the polymer **52** as depicted in Scheme 2.20.



$\text{R} = \text{n-Ethylhexyl}$

$\text{R}' = \text{n-Octyl}$

**Scheme 2.20** Synthetic route for nitrogen-bridged poly(ladder-type hexaphenylene)

52

The diketone **50** was synthesized in 73 % yield by standard Suzuki coupling of fluorene boronic ester **49** and dibromocarbazole **16**. Addition of four equivalents of 4-octylphenyllithium generated the corresponding diol which was ring closed with  $\text{BF}_3 \cdot \text{etherate}$  to give the ladder-type hexaphenylene **51** in 69 % overall yield. This was polymerized by Yamamoto-type polycondensation to generate polymer **52** in 77 % yield. GPC analysis using PPP standard showed a  $M_n$  value of  $2.3 \times 10^4 \text{ g mol}^{-1}$  with a polydispersity index of 1.7. This corresponds to a degree of polymerization of about 13 and the material had good solubility in common organic solvents. Table 2.1 summarizes the GPC results of all six ladder-type polymers.

**Table 2.1** Physical properties of ladder polymers(19, 23, 28, 44, 47, and 52)<sup>a</sup>

Polymer	$M_n \times 10^{-4}(\text{g/mol})$	$M_w \times 10^{-4}(\text{g/mol})$	PDI
<b>19</b>	<b>4.6</b>	<b>12.8</b>	<b>2.8</b>
<b>23</b>	<b>3.5</b>	<b>8.0</b>	<b>2.3</b>
<b>28</b>	<b>7.0</b>	<b>19.6</b>	<b>2.8</b>
<b>44</b>	<b>4.6</b>	<b>10.6</b>	<b>3.3</b>
<b>47</b>	<b>2.3</b>	<b>5.5</b>	<b>2.4</b>
<b>52</b>	<b>2.3</b>	<b>3.9</b>	<b>1.7</b>

<sup>a</sup>Estimated from GPC (THF as eluent and PPP as standard)

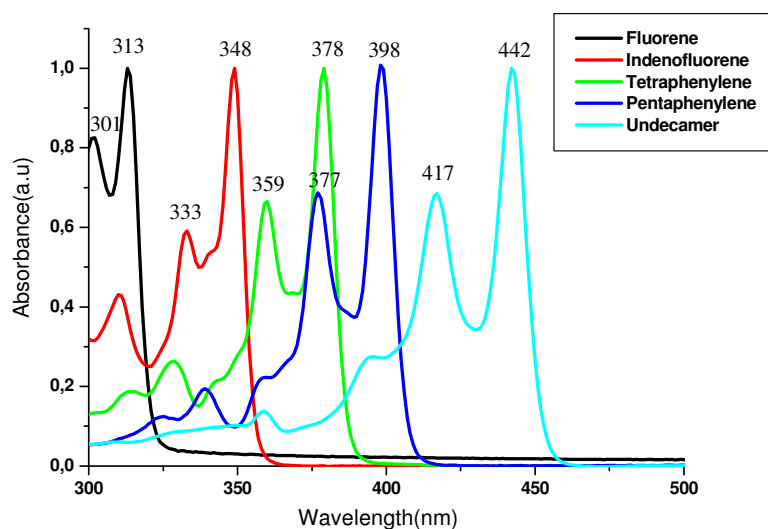
## 2.3 Photophysical properties of ladder-type monomers and ladder-type polymers

### 2.3.1 Photophysical properties of ladder-type monomers

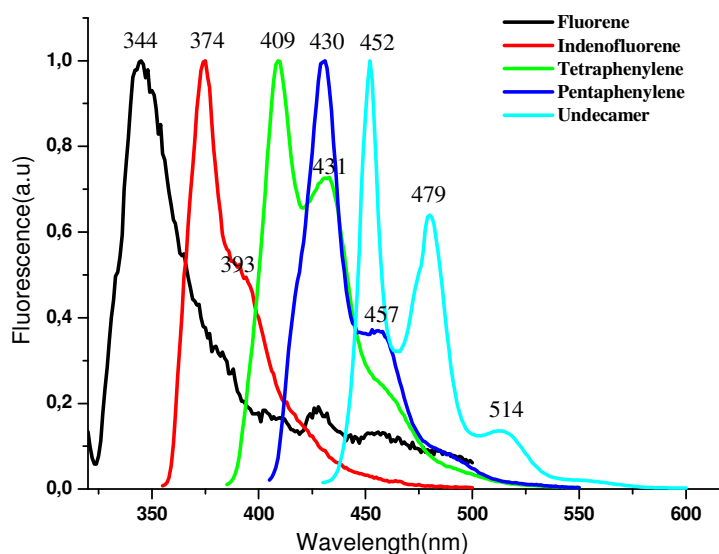
#### 2.3.1.1 All carbon-bridged ladder-type monomers

Figure 2.1 depicts the absorption spectra of all carbon-bridged ladderized monomers such as fluorene, indenofluorene<sup>38</sup>, tetraphenylene, pentaphenylene<sup>36</sup> and undecamer<sup>39</sup>. All the absorption spectra were similar in shape with well resolved

absorption maximum and high energy shoulder. As expected, with every addition of extra benzene ring, the absorption spectra displayed a bathochromic shift in the absorption maximum which was very pronounced for fluorene and indenofluorene but less so for the higher monomers. Similarly, Figure 2.2 presents the photoluminescence (PL) spectra of the all carbon-bridged ladder-type monomers. Here again, with every extra benzene ring in the monomer, the PL spectrum displayed a red shift in the emission maximum.



**Figure 2.1** Absorption spectra of all-carbon bridged ladder-type monomer in THF



**Figure 2.2** PL spectra of all-carbon bridged ladder-type monomer in THF

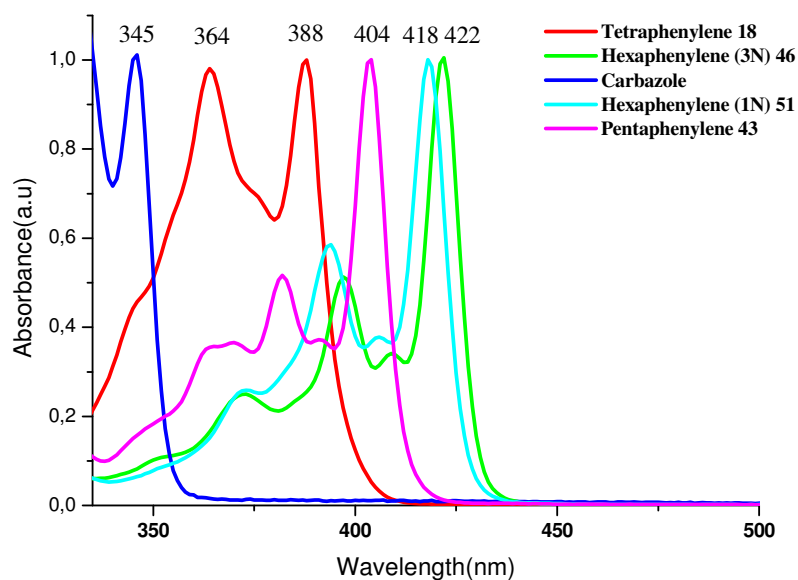
One structural feature which distinguishes the PL spectra from absorption spectra was the well resolved vibrational band which was not significant in the case of fluorene and indenofluorene but became pronounced with tetraphenylene and higher analogues, pentaphenylene and undecamer which is a characteristic of higher order of rigidity by process of further ladderization. Table 2.2 outlines the photophysical properties of all carbon-bridged monomers. The Stokes shift for all the ladder-type monomers were around 30 nm except for the undecamer which exhibited very low Stokes shift of 10 nm may be due to the very low degree of structural freedom or high degree of rigidity.

**Table 2.2** Optical properties of all-carbon bridged ladder-monomers in THF solution

Monomer	Absorption maximum(nm)	Emission maximum (nm)	Stokes shift (nm)
<b>Fluorene</b>	313	344	31
<b>Indenofluorene</b>	348	374	26
<b>Tetraphenylene</b>	378	409	31
<b>Pentaphenylene</b>	398	430	32
<b>Undecamer</b>	442	452	10

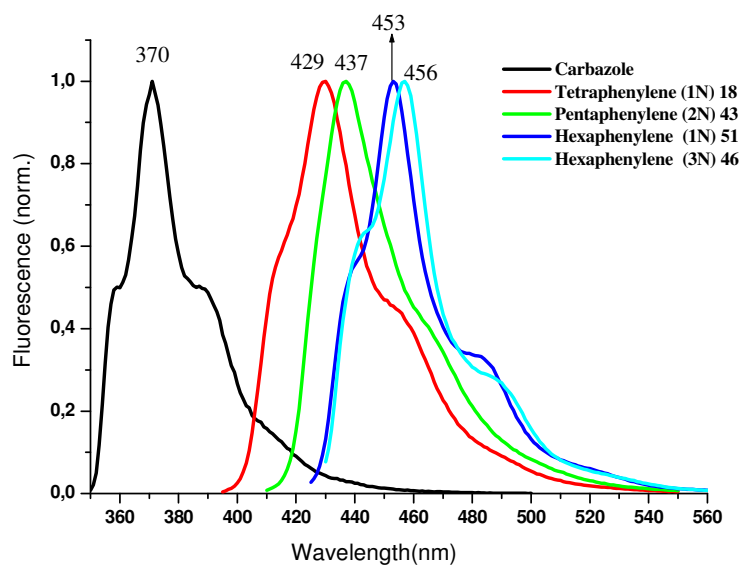
### 2.3.1.2 Nitrogen-bridged ladder-type monomers (dichloro)

Figure 2.3 displays the absorption spectra of nitrogen-bridged ladder-type monomers such as dichlorocarbazole, nitrogen-bridged tetraphenylene **18**, nitrogen-bridged pentaphenylene **43**, nitrogen-bridged hexaphenylene (3N) **46**, and nitrogen-bridged hexaphenylene (1N) **51**. It was clearly observed that both by increasing the extra benzene ring or replacing the carbon bridge by a nitrogen bridge resulted in a bathochromic shift in the absorption maximum. However, later has a less significant effect on the absorption maximum where each nitrogen contributed around 2 nm red shift in the absorption maximum.



**Figure 2.3** Absorption spectra of nitrogen-bridged ladder-type monomers in THF

Figure 2.4 presents the PL spectra of nitrogen-bridged ladder-type monomer. Similar to absorption maximum, both replacing the carbon bridge with nitrogen as well as the introduction of extra benzene ring resulted in a red shift in the PL maximum due to increase in the conjugation along the backbone.



**Figure 2.4** PL spectra of nitrogen-bridged ladder-type monomers in THF

Table 2.3 summarizes the optical properties of the various nitrogen-bridged monomers.

**Table 2.3** Optical properties of nitrogen- bridged ladder monomer in THF solution

Monomers (Dichloro)	Absorption maximum(nm)	Emission maximum (nm)	Stokes shift (nm)
<b>Carbazole</b>	345	370	25
<b>Tetraphenylene 18</b>	388	429	41
<b>Pentaphenylene 43</b>	404	437	33
<b>Hexaphenylene 46</b>	422	456	34
<b>Hexaphenylene 51</b>	418	453	35

### 2.3.2 Photophysical properties of ladder-type polymers

In the following sections optical properties of the nitrogen-bridged ladder-type polymer will be discussed as well as compared with the corresponding all carbon-bridged ladder-type polymers and fully ladder-type polymers reported in the literature.

#### 2.3.2.1 Poly(ladder-type tetraphenylene)

Figure 2.5 depicts the absorption spectra of nitrogen-bridged polymers as well as their carbon analogues in THF solution. The polymer **19** showed the  $\pi$ - $\pi^*$  transition at 433 nm and the analogous all carbon-bridged polymer **23** displayed the same transition at 427 nm. The red shift in the absorption maximum of polymer **19** can be explained by the presence of nitrogen in the backbone. Nitrogen has a free electron pair which it can easily contribute to the electron density of the polymer backbone hence accounts for the slight red shift in absorption maximum.<sup>31, 40</sup> Yang et al. reported the higher HOMO value for the polycarbazole compared to the polyfluorene by theoretical calculations and hence predicted red shift in the absorption maximum.<sup>41</sup>



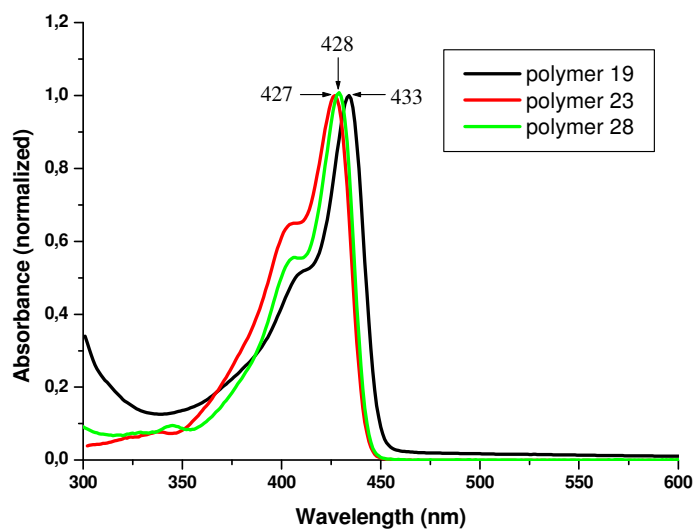


**Figure 2.5** Absorption spectra of ladder-type poly(tetraphenylene) in THF

Polymer **28** which was the fully arylated poly(ladder-type teraphenylene) exhibited almost same absorption maximum at 428 nm which suggested that the arylation at the carbon-bridge has no significant effect on the absorption maximum of the polymers.

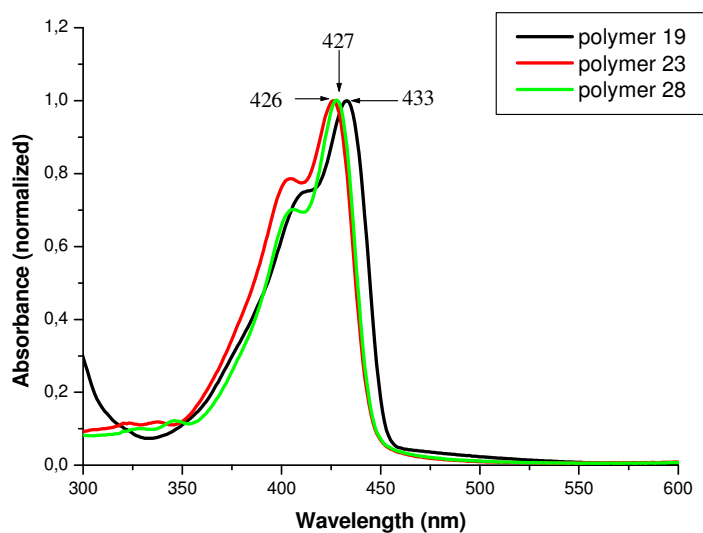


**Figure 2.6** Absorption spectra of ladder-type poly(tetraphenylene) in thin film

Figure 2.6 presents the absorption spectra of polymer **19**, **23** and **28** in thin film. The thin film spectra of all three polymers were similar to their solution spectra suggesting that undesirable solid-state interactions do not exist in the three polymers. The absorption maximum of all carbon-bridged polymers **23** and **28** were intermediate between poly(indenofluorene) (416 nm)<sup>38</sup> and ladder-type poly(pentaphenylene) (434 nm)<sup>36</sup> as expected. Figure 2.7 depicts the photoluminescence (PL) spectra of polymers **19**, **23** and **28** in THF solution. All polymers showed the well resolved PL spectra with very small Stokes shift, characteristics of ladder-type structure. Polymer **19** exhibited the primary emission maximum at 446 nm with secondary maximum at 473 nm. The emission maximum for poly(ladder-type tetraphenylene) **19** was the same as for ladder-type poly(pentaphenylene) which also emits at 446 nm and shoulder at 473 nm. This observation suggested that the increase in conjugation by one extra benzene ring in the monomer has the same effect as keeping the monomer length same but replacing one carbon bridge by nitrogen bridge in case of poly(ladder-type tetraphenylene).

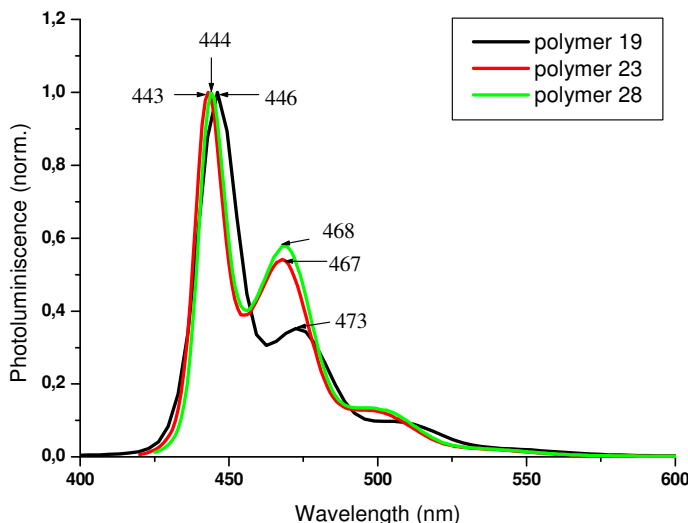


**Figure 2.7** Photoluminescence spectra of ladder-type poly(tetraphenylene) in THF

Polymer **23** and **28** had emission maximum at 443 and 444 nm with a secondary maximum at 467 and 468 nm respectively. Again, polymer **23** and **28** did not show any significant difference in their optical properties. Polymer **19** displayed a

red shift in both primary and secondary absorption maximum compared to the all carbon-bridged polymers **23** and **28** because of the presence of nitrogen in the backbone.<sup>31, 41</sup> The Stokes shift for polymers **19**, **23** and **28** were 13, 16 and 16 nm respectively. The small Stokes shift in nitrogen-bridged polymer **19** compared to the all carbon-bridged polymer suggested that the introduction of nitrogen instead of carbon bridge enhance the rigidity of polymer backbone. Figure 2.8 shows the photoluminescence spectra of polymers **19**, **23** and **28** in thin film. Unlike the absorption spectra which did not reveal any significant solid-state broadening, the PL spectra displayed significant solid-state broadening resulted from interchain interactions in the solid-state which is common for ladder-type polymers.<sup>32, 42</sup> The polymer **19**, **23** and **28** showed primary PL emission at 445, 445, 452 nm along with secondary bands at 472, 472 and 481 nm, and 508, 508 and 516 nm respectively.

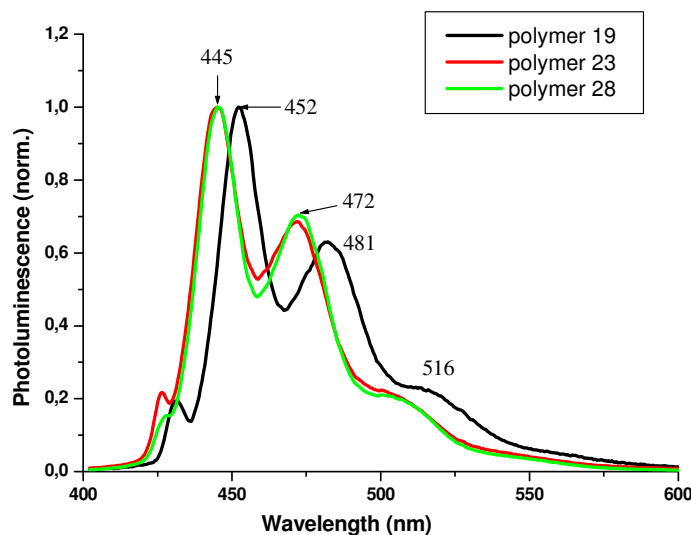


**Figure 2.8** PL spectra of ladder-type poly(tetraphenylene) in thin film

The solid-state broadening effect was more prominent in the nitrogen-bridged polymer which was 6 nm red shifted compared to the solution spectra. Dierschke et al. reported the similar broadening in the carbazole-based ladder-type polymers.<sup>32</sup> Optical data of all the poly(ladder-type tetraphenylene)s are depicted in Table 2.4 and Table 2.5.

**Table 2.4** Optical properties of polymers **19**, **23** and **28** in THF solution

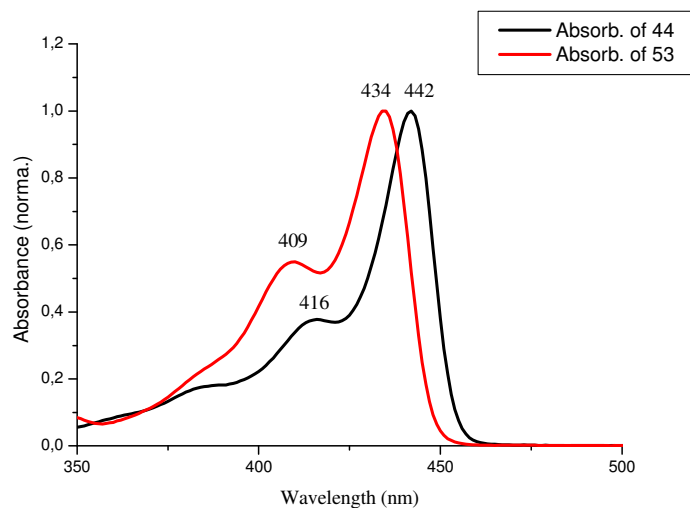
Polymer	Absorption maximum(nm)	Emission maximum (nm)	Stokes shift (nm)
<b>19</b>	433	446	13
<b>23</b>	427	443	16
<b>28</b>	428	444	16

**Table 2.5** Optical properties of polymers **19**, **23** and **28** in thin film

Polymer	Absorption maximum(nm)	Emission maximum (nm)	Stokes shift (nm)
<b>19</b>	433	452	19
<b>23</b>	426	445	19
<b>28</b>	427	445	18

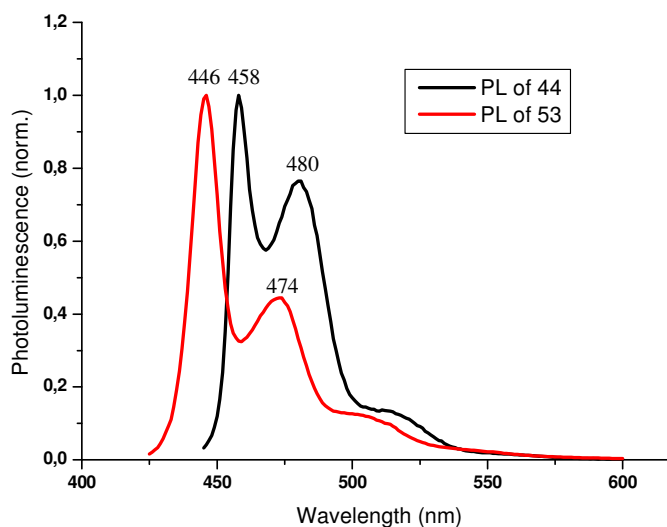
### 2.3.2.2 Nitrogen-bridged poly(ladder-type pentaphenylene)

Figure 2.9 depicts the absorption spectrum of nitrogen-bridged poly(ladder-type pentaphenylene) **44** and all carbon-bridged ladder-type poly(pentaphenylene)<sup>36</sup> **53** in THF solution.



**Figure 2.9** Absorption spectra of ladder-type poly(pentaphenylene)s **44** and **53** in THF

Polymer **44** exhibited the absorption maximum at 442 nm with a secondary high energy band at 416 nm. The corresponding all carbon-bridged polymer **53** displayed absorption maximum at 434 nm with a secondary band at 409 nm.<sup>42</sup> The red-shift of 8 nm in case of polymer **44** was because of the presence of two nitrogen atoms in each repeat unit of polymer which contribute more electron density to the polymer backbone than polymer **53**. Patil et al. also observed the similar trend in the optical properties for carbazole-based ladder-type polymer in comparison to MeLPPP.<sup>31</sup> Figure 2.10 shows the photoluminescence spectra of polymers **44** and **53** in THF solution. Polymer **44** exhibited the well resolved photoluminescence spectra with an emission maximum at 458 nm and secondary band at 480 nm which revealed the absence of any aggregation in solution.<sup>32</sup> The corresponding all carbon-bridged polymer **53** displayed an absorption maximum at 446 nm with secondary low energy band at 474 nm. However, the secondary band in nitrogen-bridged polymer was more prominent than in the carbon-bridged polymer **53**.



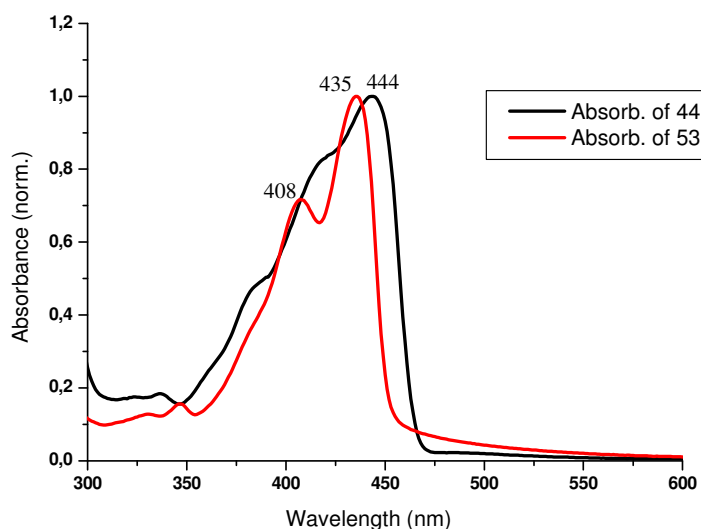
**Figure 2.10** PL of poly(ladder-type pentaphenylene) **44** and **53** in THF

The Stokes shift in the case of polymers **44** and **53** in solution were 16 nm and 12 nm respectively. In this case the Stokes shift in the carbon analogue was 4 nm less than the nitrogen-bridged polymer. Optical data of polymers **44** and **53** in solution are depicted in Table 2.6.

**Table 2.6.** Optical properties of polymers **44** and **53** in THF solution

Polymer	Absorption maximum(nm)	Emission maximum (nm)	Stokes shift (nm)
<b>44</b>	442 (416)	458 (480)	16
<b>53</b>	434 (409)	446 (474)	12

Figure 2.11 and 2.12 presents the absorption and photoluminescence spectra of polymers **44** and **53** in thin film. Polymer **53** showed well resolved absorption spectra similar to the solution, however, polymer **44** revealed broad absorption spectra indicating that solid-state aggregation was more significant in the case of the nitrogen containing polymer than the all carbon-bridged poly(ladder-type pentaphenylene).<sup>32</sup> This effect was clearly observed in the photoluminescence spectra of both polymers **44** and **53**.

**Figure 2.11** Absorption spectra of polymers **44** and **53** in thin film

Polymer **44** exhibited the emission maximum at 463 nm with low band secondary emissions at 491 and 530 nm. In comparison, the all carbon-bridged polymer **53** displayed the photoluminescence maximum at 449 nm and secondary low energy peak at 475 and 511 nm. Both polymers demonstrated a higher red-shift in emission maximum in the solid-state than in solution.

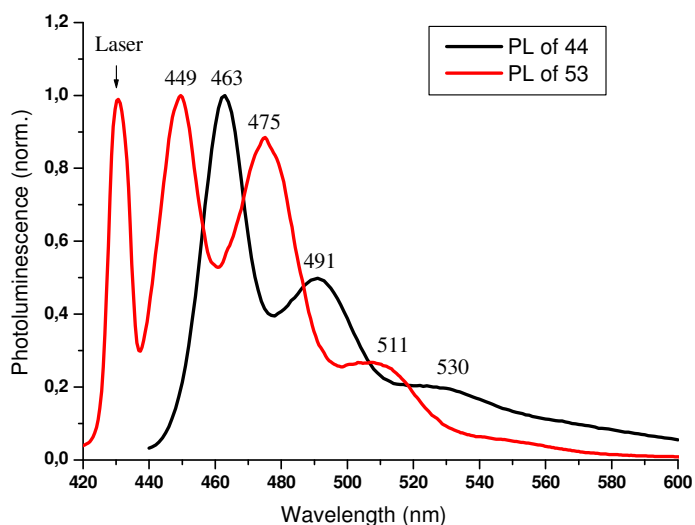


**Figure 2.12** PL spectra of polymers **44** and **53** in thin film

However, the effect was more prominent in polymer **44** which showed a 5 nm bathochromic shift for the maximum and 11 nm for the secondary band with a significant low energy band at 530 nm having a long tail. This result again demonstrated that the nitrogen in polymer backbone was more likely to be responsible for enhancement in the aggregation effect in the solid-state (also discussed in section 2.6 where 2D-WAX supported this result).<sup>32</sup> Optical data of polymers **44** and **53** in thin film are depicted in Table 2.7.

**Table 2.7** Optical properties of polymers **44** and **53** in thin film

Polymer	Absorption maximum(nm)	Emission maximum (nm)	Stokes shift (nm)
<b>44</b>	444	463 (491, 530)	19
<b>53</b>	435 (408)	449 (475, 511)	14

### 2.3.2.3 Nitrogen-bridged poly(ladder-type hexaphenylene)

Figure 2.13 and 2.14 depicts the absorption and the photoluminescence spectra of nitrogen-bridged poly(ladder-type hexaphenylene) **47** and **52**. Polymer **47**

has three nitrogen atoms at the bridges in each repeat unit compared to polymer **53** which has only one.

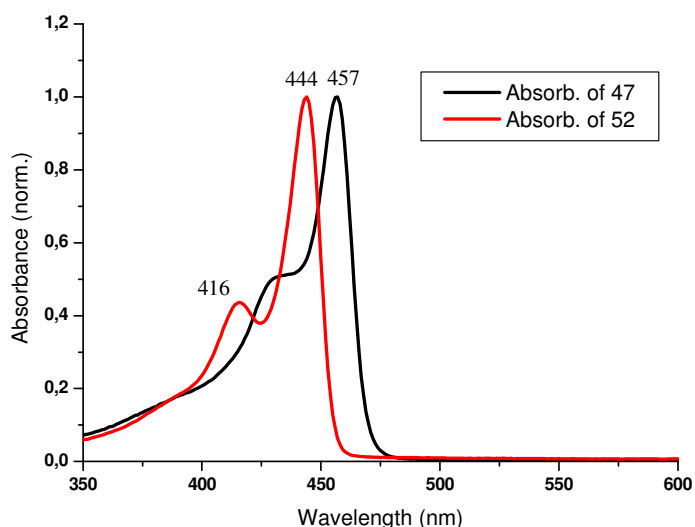


**Figure 2.13** Absorption spectra of polymers **47** and **52** in THF

Polymer **47** displayed an absorption maximum at 457 nm with a secondary high energy band at 433 nm. As expected, the absorption maximum of polymer **47** was more red-shifted compared to polymer **52** which exhibited absorption maximum at 444 nm with a secondary high energy emission peak at 416 nm.

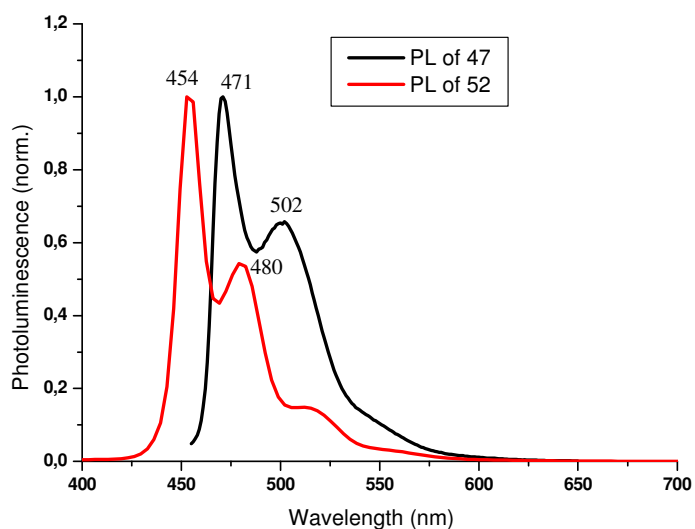




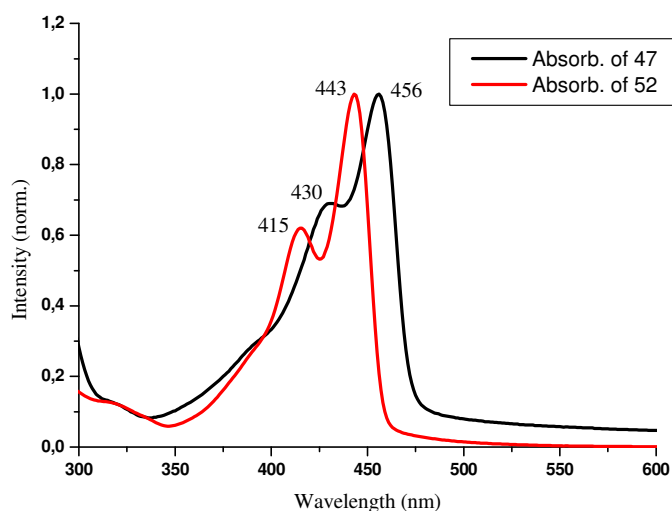
**Figure 2.14** PL spectra of polymers **47** and **52** in THF

Here again, the red-shift in absorption maximum was because of the ability of nitrogen lone pairs to enter into conjugation with the main chain.<sup>31</sup> It was also observed in the photoluminescence spectrum where polymer **47** displayed emission maximum at 471 nm in comparison to the emission of polymer **52** at 454 nm which showed the red- shift of 17 nm for the polymer **47**.<sup>31</sup> The Stokes shift in case of polymer **52** was larger (14 nm) than the polymer **52** (10 nm), which showed the same trend as observed in the case of poly(ladder-type pentaphenylene). Table 2.8 depicts the optical properties of polymer **47** and **52**.

**Table 2.8** Optical properties of polymers **47** and **52** in THF solution

Polymer	Absorption maximum(nm)	Emission maximum (nm)	Stokes shift (nm)
<b>47</b>	457(433)	471 (502)	14
<b>52</b>	444 (416)	454 (480)	10

Figure 2.15 and 2.16 presents the absorption and emission spectra of polymers **47** and **52** in thin film.

**Figure 2.15** Absorption spectra of polymers **47** and **52** in thin film

Polymer **47** showed the absorption maximum at 456 nm and a shoulder at 430 nm and polymer **52** displayed the absorption maximum at 443 nm with a secondary high energy band at 415 nm. There was no significant change in the absorption spectra in comparison to solution suggesting absence of solid-state interaction.<sup>31, 32</sup>

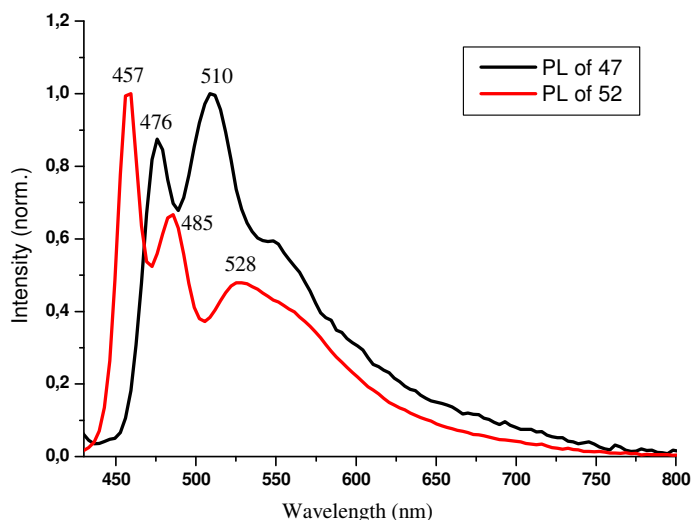


**Figure 2.16** Photoluminescence spectra of polymers **47** and **52** in thin film

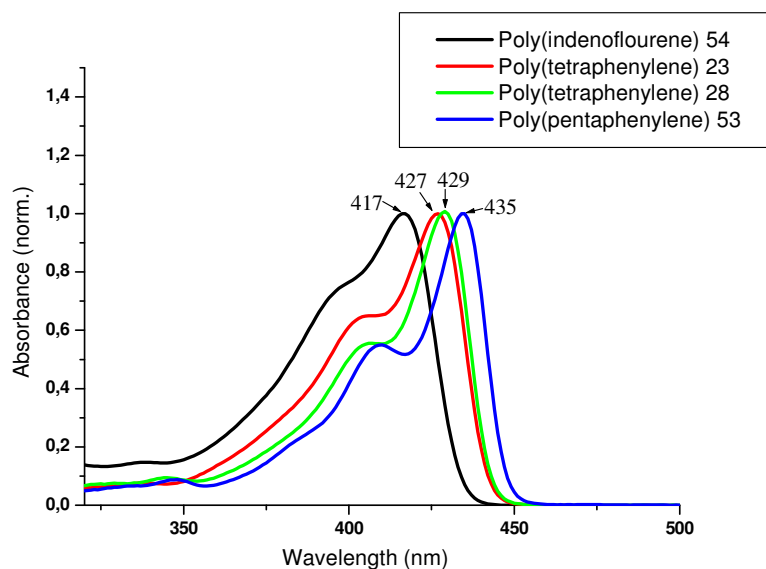
However, the photoluminescence spectrum displayed strong solid-state interactions for polymer **47** which exhibited a strong secondary peak at 510 nm and was even more intense than the primary peak at 476 nm.<sup>43</sup> Both the peaks were significantly red-shifted in film in comparison to solution suggesting strong aggregation in the case of polymer **47**. Polymer **52** also showed a similar effect but not so pronounced as in polymer **47**. The appearance of a maximum at 528 nm was either because of aggregation of polymer chains in the solid-state or due to keto defect. In this case keto defect was more likely because of the presence of dialkylated carbon bridge in the repeat unit of the polymer (discussed in section 2.5).<sup>44</sup> Again, this result suggests that the presence of more nitrogen atoms in the repeat unit of a polymer lead to increase in inter-chain interactions.<sup>32</sup> Both polymers were blue-green emitters. The optical properties of polymer **47** and **52** in thin film are summarized in the Table 2.9.

**Table 2.9** Optical properties of polymers **47** and **52** in thin film

Polymer	Absorption maximum(nm)	Emission maximum (nm)	Stokes shift (nm)
<b>47</b>	456 (430)	476 (510)	20
<b>52</b>	443 (415)	457 (485, 528 )	14

### 2.3.2.4 Comparison of all carbon-bridged ladder-type polymers

Figure 2.17 and 2.18 depict the absorption and photoluminescence spectra, respectively, for fully arylated poly(indenofluorene),<sup>38</sup> poly( ladder-type tetraphenylene) **23**, poly( ladder-type tetraphenylene) **28** and fully arylated poly(ladder-type pentaphenylene)<sup>36</sup> **53** in THF solution. The absorption maximum varied from 417 nm for poly(indenofluorene) to 435 nm for fully arylated poly(ladder-type pentaphenylene). The red shift was more significant from poly(indenofluorene) to polymers **23** or **28** which was 10 nm than polymer **28** to polymer **53** which was calculated to be 8 nm indicating that increasing the number of benzene rings contributes less to conjugation for the higher analogues.<sup>45</sup>

**Figure 2.17** Absorption spectra of all carbon-bridged polymers in THF

In the case of emission maximum which varied from 428 nm for poly(indenofluorene) to 446 nm for polymer **53**, the red shift was very significant from poly(indenofluorene) to poly(ladder-type tetraphenylene) (15 nm) but less so from polymer **23** to **53** (3 nm).<sup>38, 42, 46</sup>

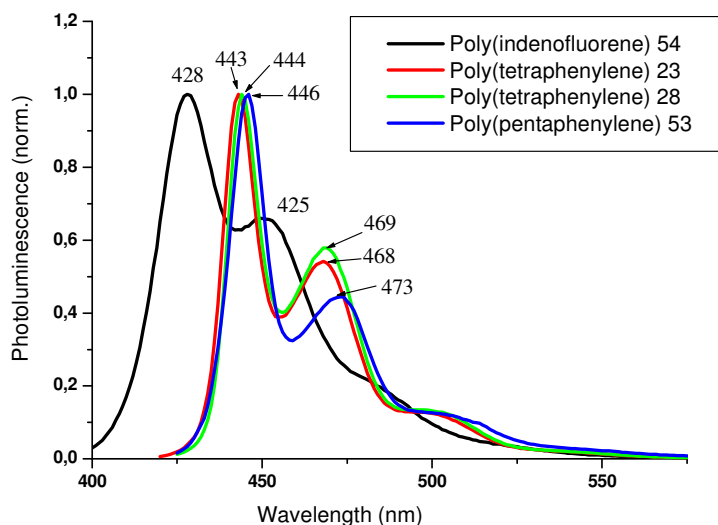


**Figure 2.18** PL spectra of all carbon-bridged polymers in THF solution

Figure 2.19 depicts the emission spectra of poly(indenofluorene), polymer **23**, polymer **28**, polymer **53** and MeLPPP<sup>26</sup> in toluene. Again the emission maximum showed a similar trend which vary from 433 nm for poly(indenofluorene) to 461 nm for MeLPPP which is the fully ladderized polymer and this was found to be the upper limit of emission maximum.<sup>45</sup> Unlike THF, in the case of toluene, there was no effect of substituents on the polymer emission maximum as both alkyl-aryl poly(ladder-type tetraphenylene) **23** and fully arylated poly(ladder-type tetraphenylene) **28** emitted at 441 nm. It may be because of the better ability of aryl groups to donate electron than the alkyl group which made polymer **28** more electron rich than polymer **23**. THF is more polar than toluene and so it stabilizes the LUMO much better than the HOMO (solvatochromic shifts) which resulted in red-shift in emission for polymer **28** in THF but no effect in toluene which is a non polar solvent.<sup>47-49</sup>

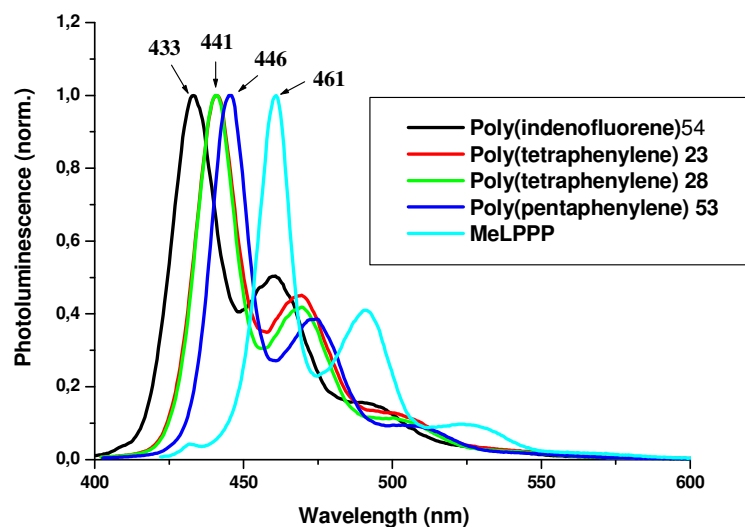


**Figure 2.19** PL spectra of all carbon-bridged polymers in toluene solution

The optical properties of poly(indenofluorene) **54**, polymer **23**, **28** and **53** in THF are summarized in the Table 2.10.

**Table 2.10** Optical properties of polymers **54**, **23**, **28** and **53** in THF solution

Polymer	Absorption maximum(nm)	Emission maximum (nm)	Stokes shift (nm)
<b>54</b>	417	428 (425)	11
<b>23</b>	427	443 (468)	15
<b>28</b>	429	444(469)	15
<b>53</b>	435	446 (473)	11

Figure 2.20 and 2.21 display the absorption and photoluminescence spectra, respectively, for fully arylated poly(indenofluorene), poly( ladder-type tetraphenylene) **23**, poly( ladder-type tetraphenylene) **28** and fully arylated poly(arylated pentaphenylene) **53** in thin film.

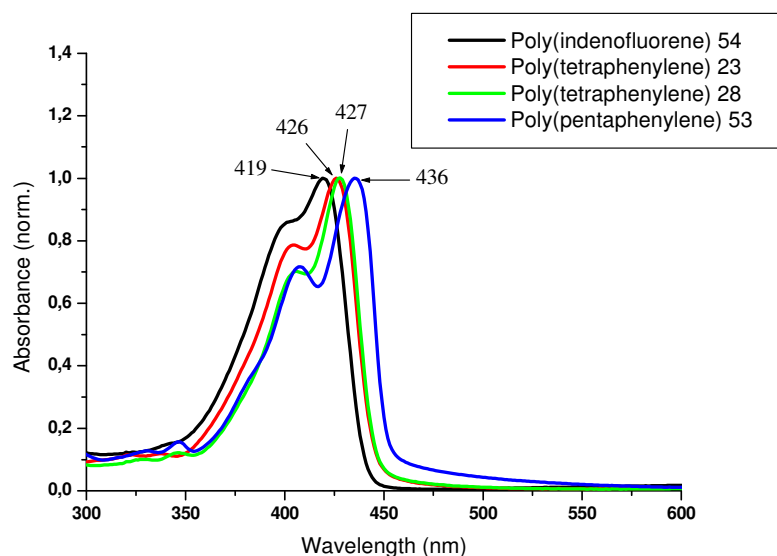


**Figure 2.20** Absorption spectra of all carbon-bridged polymers in thin film

The optical properties of poly(indenofluorene) **54**, polymer **23**, **28** and **53** in thin film are outlined in the Table 2.11.

**Table 2.11** Optical properties of polymers **54**, **23**, **28** and **53** in thin film

Polymer	Absorption maximum(nm)	Emission maximum (nm)	Stokes shift (nm)
<b>54</b>	419	434 (460)	15
<b>23</b>	426	445 (472)	19
<b>28</b>	427	445 (472)	18
<b>53</b>	436	449(475)	13

The absorption spectra did not show much difference in solution however the solid-state broadening was very significant in the case of the photoluminescence spectra (Figure 2.21) of all polymers. It may be because of the planar, rod like structure of these polymers which can easily aggregate to give intense low band emission.<sup>43</sup>

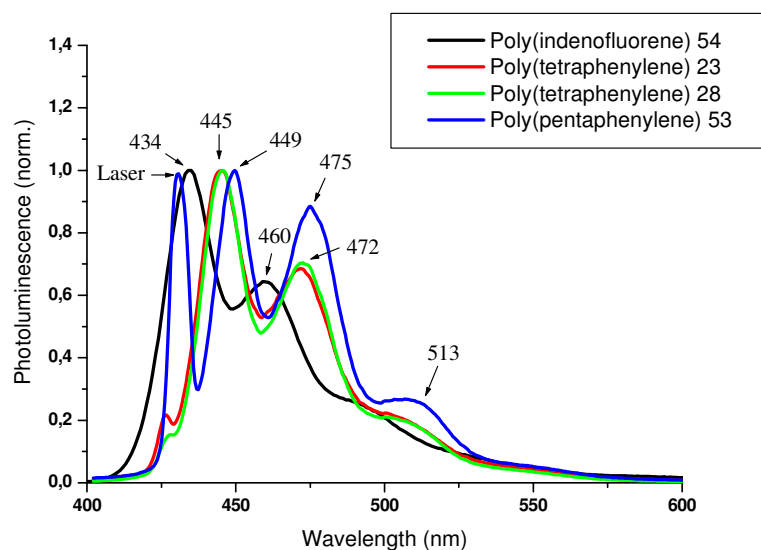


**Figure 2.21** PL spectra of all carbon-bridged polymers in thin film

### 2.3.2.5 Comparison of nitrogen-bridged ladder-type polymers

In this section the optical properties of the nitrogen-bridged polymers synthesized [poly(ladder-type tetraphenylene), poly(ladder-type pentaphenylene) and poly(ladder-type hexaphenylene)] will be compared with the fully ladder-type nitrogen-bridged polymer **9** reported by Müllen and coworkers.<sup>32</sup>

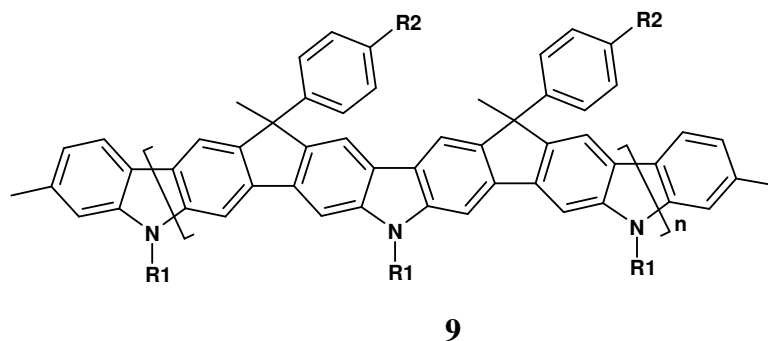


**Figure 2.22** Fully ladder-type carbazole based polymer **9** reported by Dierschke et. al.<sup>32</sup>

Figure 2.23 and 2.24 display the absorption spectra and photoluminescence spectra of polymers **19**, **44**, **47**, **52** and fully ladder-type polymer **9**. The absorption maximum varied from 434 nm for nitrogen-bridged polymer **19** to 476 nm for fully ladder-type polymer **9** with other polymers falling in between. In a similar way, emission maximum varied from 446 nm for polymer **19** to 481 nm for fully ladder polymer **9**.

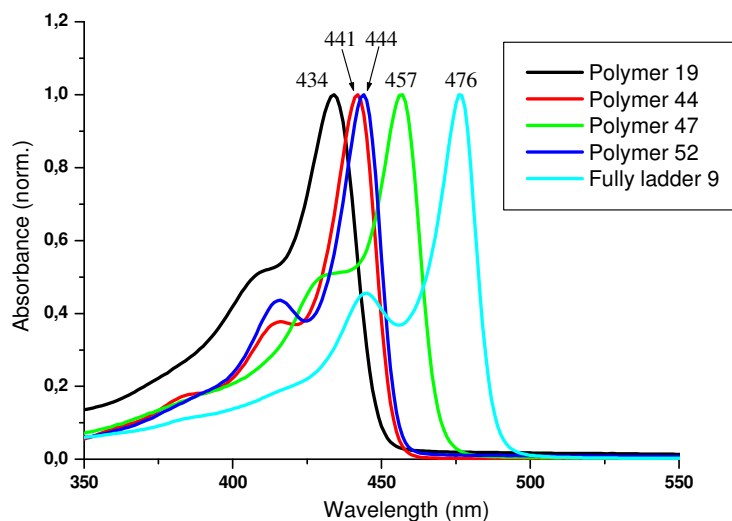


**Figure 2.23** Absorption spectra of nitrogen-bridged polymers in THF solution

So, it is possible to tune the emission color from a pure blue emitter to blue-green and finally green by increasing the conjugation length. The conjugation within the polymer can be tuned by increasing the benzene unit in the ladderized monomer as shown in the last section or by introducing heteroatoms such as nitrogen.<sup>31, 46</sup> For example, polymer **19** emitted at 446 nm and has one nitrogen and four benzene ring in the each repeat unit whereas polymer **52** emitted at 454 nm with the same number of nitrogen atoms per monomer but six benzene units in the repeat unit. This increase of 8 nm resulted from the two extra benzene rings. In the same way, the emission maximum depends upon the number of nitrogens in the repeat unit such as polymer **47** and polymer **52** where both have the same number of benzene units but the former has three nitrogen atoms and the latter has one nitrogen atom in each repeat unit. Hence polymer **47** demonstrated a red-shift in both the absorption and emission maximum by 13 and 17 nm respectively. Polymer **44**, which has two nitrogens in



each repeat unit with five benzene unit showed a blue shift of 3 nm compared to polymer **52** which has one nitrogen and six benzene rings in the repeat unit. However, the photoluminescence spectrum showed the reverse trend where polymer **44** displayed emission maximum at 458 nm compared to polymer **52** which demonstrated primary emission at 454 nm.

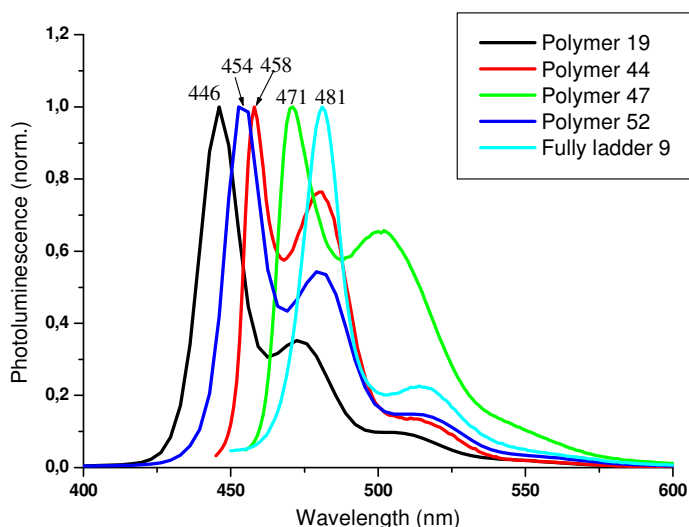


**Figure 2.24** PL spectra of nitrogen-bridged polymers in THF solution

This suggested that the presence of nitrogen bridges have more impact on the emission maximum than the absorption maximum. Fully ladder-type polymer **9** showed surprisingly less intense secondary band emission (Figure 2.24) compared to all other nitrogen-bridged ladder-type polymers. Table 2.12 summarizes the optical properties of nitrogen-bridged polymers in THF solution.

**Table 2.12.** Optical properties of polymers **19**, **44**, **47**, **52** and **9** in THF solution

Polymer	Absorption maximum(nm)	Emission maximum (nm)	Stokes shift (nm)
<b>19</b>	434	446 (473)	12
<b>44</b>	441	458 (480)	17
<b>47</b>	457	471(502)	14

<b>52</b>	444	454 (480)	10
<b>9</b>	476	481(515)	5

Figure 2.25 showed the emission spectrum of the all the nitrogen-bridged polymer in the thin film. All polymers displayed a solid-state broadening in the emission spectra but the broadening was very significant in poly(ladder-type hexaphenylene) **47** and **52** and less and less prominent in poly(ladder-type pentaphenylene) and poly( ladder-type tetraphenylene).

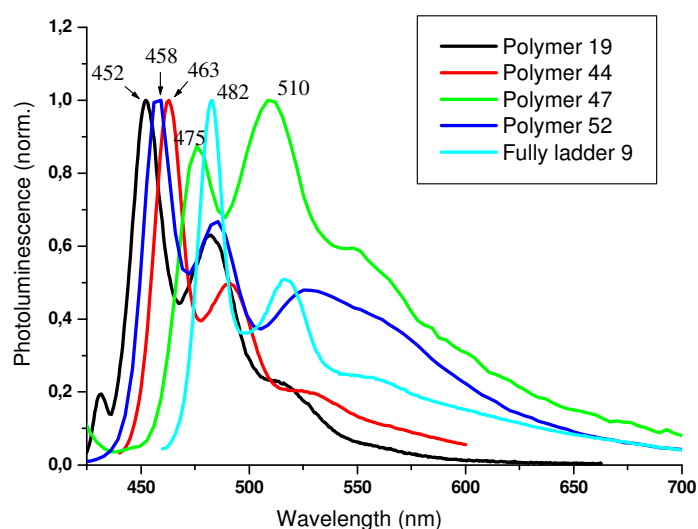


**Figure 2.25** PL spectra of nitrogen-bridged polymers in thin film

This could be because of the long rigid planar like structure of [poly(ladder-type hexaphenylene)] which is more likely to form strong aggregates than the short [poly(ladder-type tetraphenylene)].

## 2.4 Electrochemical properties of ladder-type polymers

### 2.4.1 Poly(ladder-type tetraphenylene)s

The redox behavior of thin films of polymer **19**, **23** and **28** were investigated by cyclic voltammetry (CV) against  $\text{Ag}/\text{Ag}^+$ . As shown in Figure 2.26, polymer **19**

and **28** demonstrated an irreversible oxidation but polymer **23** exhibited partially reversible oxidation, with oxidation onset values of 1.20 V Vs Ag/Ag<sup>+</sup> for polymer **19**, 1.23 V for polymer **23** and 1.29 V for polymer **28**.

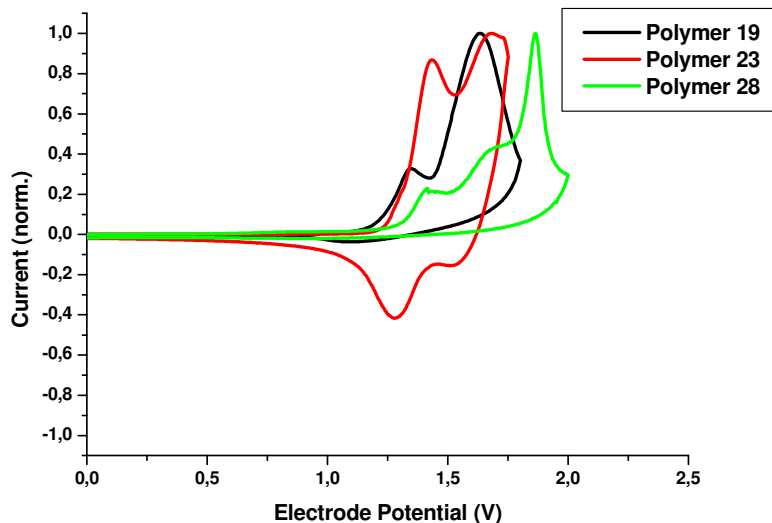


**Figure 2.26** Cyclic voltammograms of the polymer films coated on platinum electrodes measured in acetonitrile containing 0.1 M Bu<sub>4</sub>NClO<sub>4</sub> solution at a scan rate of 100 mV/s at room temperature.

The voltammograms listed in Figure 2.26 exhibited a slight increase in the oxidation onset for the all carbon-bridged polymer **28**. Calculating the energy level of Ag/AgCl to be -4.4 eV from the ferrocene/ferrocenium standard<sup>50</sup>, and determining the band gap from the absorption onset, the HOMO and LUMO values for nitrogen-bridged poly(ladder-type tetraphenylene) were estimated to be -5.53 and -2.81 respectively.

**Table 2.13** Electrochemical data for polymer **19**, **23** and **28**

Polymer	$E_{ox}$ (Onset, V)	HOMO (eV)	LUMO (eV)	$E_g$ (Optical, eV)
<b>19</b>	1.20	- 5.53	- 2.81	2.72
<b>23</b>	1.23	- 5.62	- 2.87	2.75
<b>28</b>	1.29	- 5.65	- 2.88	2.77

The corresponding HOMO and LUMO values are -5.62 and -2.87 for polymer **23** and 5.65 and -2.88 for polymer **28**, respectively. The lone pairs on nitrogen pushed up the HOMO by 0.09 eV in polymer **19** in comparison with the carbon bridged polymer **23**.

### 2.4.2 Nitrogen-bridged Poly(ladder-type pentaphenylene)

The redox behaviour of thin films of nitrogen-bridged poly(ladder-type pentaphenylene) **44** was investigated by cyclic voltamogram and results were compared with the all carbon-bridged poly(ladder-type pentaphenylene) **53** synthesized by Jacob et. al.<sup>42</sup>

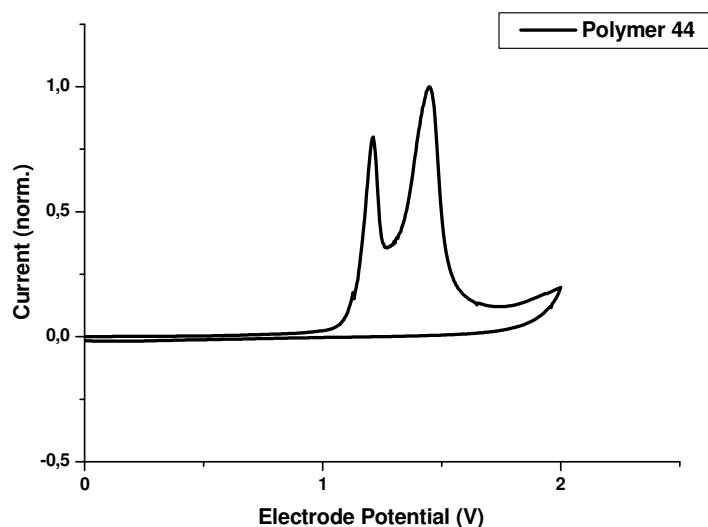


**Figure 2.27** Cyclic voltammograms of the polymer **44** [same experimental conditions as poly(ladder-type tetraphenylene)]

Polymer **44** showed irreversible oxidation with two oxidation peak at 1.20 V and 1.44 V and oxidation onset at 1.13 V (Figure 2.27). The band gap, calculated from the absorption onset, was found to be 2.60 eV from which the HOMO-LUMO energy levels were estimated to be - 5.4 eV and - 2.8 eV for poly(ladder-type pentaphenylene) **44** given an energy level of 4.4 eV for Ag/AgCl. Table 2.14 outlines the electrochemical properties of polymer **44** and **53**.

**Table 2.14** Electrochemical data for polymer **44** and **53**

Polymer	$E_{ox}$ (Onset, V)	HOMO (eV)	LUMO (eV)	$E_g$ (Optical, eV)
<b>44</b>	1.13	- 5.4	- 2.8	2.6
<b>53</b>	--	-5.5	-2.7	2.8

When the optical band gap of polymer **44** was compared with the analogous polymer **53**, it was observed that the optical band gap of **44** decreased by 0.2 eV compared to polymer **53**. The lone pair on nitrogen pushed up the HOMO value by 0.1 eV and LUMO pushed down by 0.1 eV.

### 2.4.3 Nitrogen-bridged poly(ladder-type hexaphenylene)

Cyclic voltammograms were recorded for polymers **47** and **52** against Ag/AgCl with a ferrocene/ferrocenium internal standard (Figure 2.28). Both polymers showed only p-doping (anodic) peaks. However, polymer **52** exhibited a partially reversible anodic peak in contrast to polymer **47** which underwent irreversible oxidation. The band gap, calculated from the absorption onset, was estimated to be 2.62 eV for polymer **47** and 2.71 eV for polymer **52**.

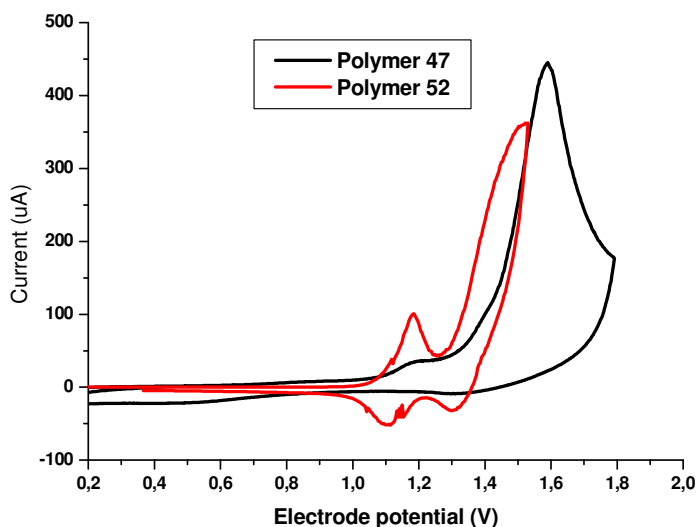


**Figure 2.28** Cyclic voltammograms of the polymer films coated on platinum electrodes measured in acetonitrile containing 0.1 M  $\text{Bu}_4\text{NClO}_4$  solution at scan rate of 100 mV/s at room temperature.

The onset of oxidation occurred at 1.07 and 1.09 V for polymer **47** and **52** respectively, from which the HOMO-LUMO energy levels were estimated to be -5.40 eV and -2.78 eV for polymer **47** and -5.46 eV and -2.76 eV for polymer **52** given an energy level of 4.4 eV for Ag/AgCl. The higher electron density contributed by the three nitrogen atoms pushed the HOMO up by 0.06 eV and the LUMO down by 0.02 eV in polymer **47** in comparison with the one nitrogen-bridged polymer **52**. Table 2.15 depicts the electrochemical properties of polymers **47** and **52**.

**Table 2.15** Electrochemical data for polymer **47** and **52**.

Polymer	$E_{ox}$ (Onset, V)	HOMO (eV)	LUMO (eV)	$E_g$ (Optical, eV)
<b>47</b>	1.07	-5.40	-2.78	2.62
<b>52</b>	1.09	-5.46	-2.76	2.71

#### 2.4.4 Comparison of nitrogen-bridged ladder-type polymers

Figure 2.29 compares the electrochemical properties of all the nitrogen-bridged ladder-type polymers synthesized with the fully ladder-polymer reported by Dierschke et. al.<sup>32</sup>

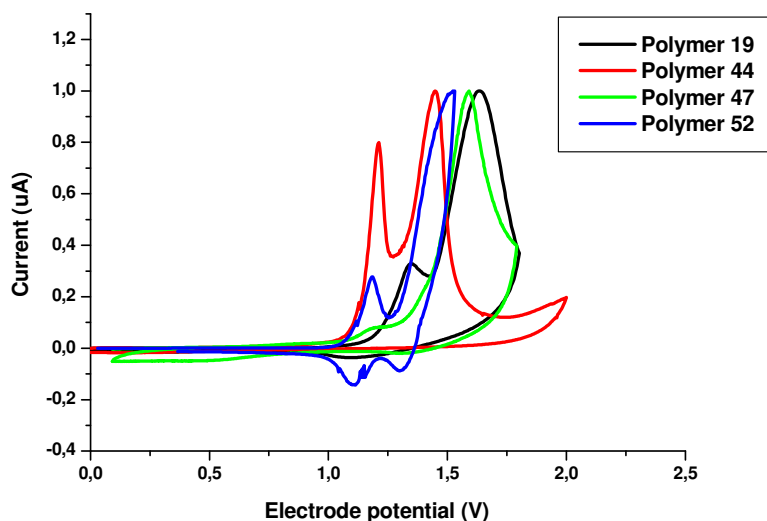


**Figure 2.29** Cyclic voltammograms of the polymers **19**, **44**, **47** and **52**

This comparison clearly showed the influence of nitrogen on the electrochemical properties of ladder-polymers. The HOMO level of the polymers exhibited a dependence on both the number of nitrogen bridges as well as on the number of benzene units in each repeat unit or in other words on the extent of conjugation. For example, polymer **19** and polymer **52** both had one nitrogen bridge in each repeat unit but they varied in the number of benzene rings. So, polymer **52** which had six benzene units showed its HOMO level at -5.46, while polymer **19** with four benzene units at -5.53 V. Similarly, the number of nitrogen bridges also influenced the HOMO level, the more the number of nitrogen bridges, the better the conjugation and hence higher the HOMO level<sup>41</sup> which can be clearly seen by comparing polymers **47** and **52**. Both polymers had the same number of benzene units in the repeat unit but polymer **47** had three nitrogen bridges as compared to polymer **52** which had only one (the HOMO level of polymer **47** was higher by 0.06 than polymer **52**). The fully ladder type polymer demonstrated the highest HOMO level, which is not surprising because it was the most conjugated polymer among all. Table 2.16 summarizes the electrochemical properties of all ladder-type nitrogen-bridged polymers.

**Table 2.16** Electrochemical data for polymers **19**, **44**, **47**, **52** and **54**

Polymer	HOMO (eV)	LUMO (eV)	$E_g$ (Optical, eV)
<b>19</b>	- 5.53	- 2.81	2.72
<b>44</b>	- 5.49	- 2.83	2.66
<b>47</b>	-5.40	-2.78	2.62
<b>52</b>	-5.46	-2.76	2.71
<b>Fully ladder 9</b>	-5.30	-2.80	2.50

## 2.5 Stability of ladder-type polymers under oxidative environment

### 2.5.1 Poly(ladder-type tetraphenylene)

#### 2.5.1.1 Nitrogen-bridged poly(ladder-type tetraphenylene) **19**

This experiment was done by Michael Graf and Florian Grasse from the group of Dr. Emil J. W. List. The polymer was dissolved in chloroform and a film was prepared by spincoating a 4 g/L solution on to a quartz substrate.

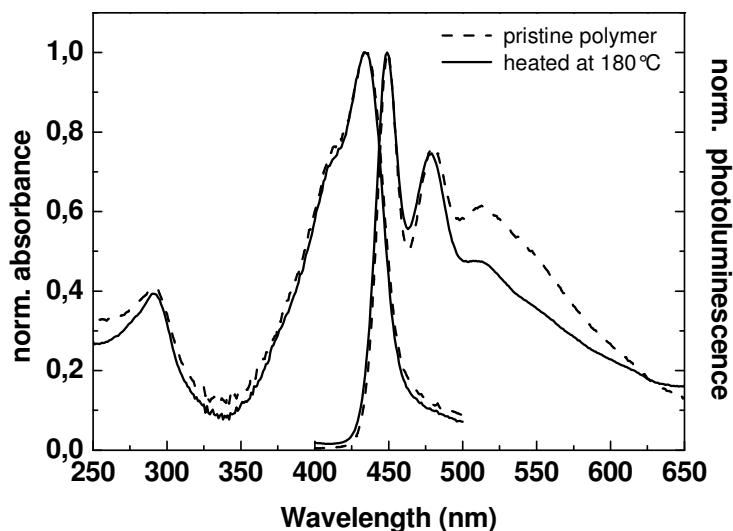


**Figure 2.30** Absorption and photoluminescence spectra of polymer **19** for pristine and annealed film in air at 180 °C.

On heating the polymer **19** in air at 180 °C for 30 minutes, the emission spectrum was almost unaltered and no oxidative degradation was observed. Note that the oxidative degradation at the 9-position of the carbon-bridged positions was hindered by the aryl substitution as reported earlier,<sup>36</sup> so that upon heating only the nitrogen bridge position could be affected, which was not observed. This result suggests that the nitrogen bridges are stable under oxidative degradation conditions.

### 2.5.1.2 Carbon-bridged poly(ladder-type tetraphenylene) **23**

In contrast to polymer **19**, polymer **23** showed a strong alteration of the photoluminescence upon thermal stress in air. Heating the polymer **23** for 30 minutes in air, led to the well known formation of oxidative products in the form of ketonic defects with an emission centered at 575 nm, which increased with ongoing degradation. The fact that the position of the ketonic defect emission was



bathochromically shifted compared to polyfluorene, where the same emission was found at 530 nm, is due to the more extended conjugation of the tetraphenylene unit as compared to the fluorene unit leading also to a shift in the oxygen related on chain defect emission.

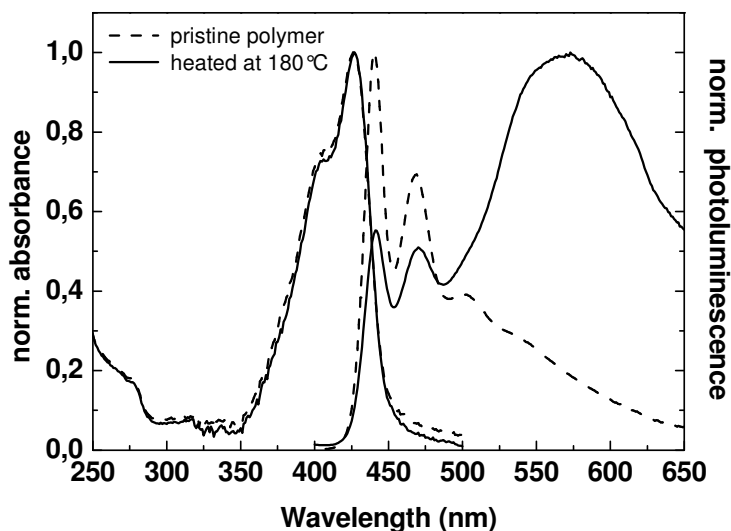


**Figure 2.31** Absorption and photoluminescence spectra of polymer **23** for pristine and annealed film in air at 180 °C.

For comparison under inert conditions, i.e. a dynamic vacuum of  $10^{-6}$  mbar, no degradation of the polymer was detected. From a previous study, it is known that the degradation was taking place at the dialkyl bridgeheads in polymer **23**, which are susceptible towards oxidation. Thus polymer **19**, the nitrogen bridge poly(ladder-type tetraphenylene) showed a clear advantage over the poly(ladder-type tetraphenylene) with all carbon bridges, when it comes to oxidative degradation under ambient atmosphere.

### 2.5.2 Nitrogen-bridged poly(ladder-type hexaphenylene)

Figure 2.32 depicts the thermal degradation of poly(ladder-type hexaphenylene) polymer **52** in vacuum (This experiment was conducted by Sabrina Eder from group of Dr. Emil J. W. List). The polymer exhibited good stability even after heating upto

200 °C for several hours in vacuum as no new peaks appeared during the heating process both in absorption and photoluminescence spectra.

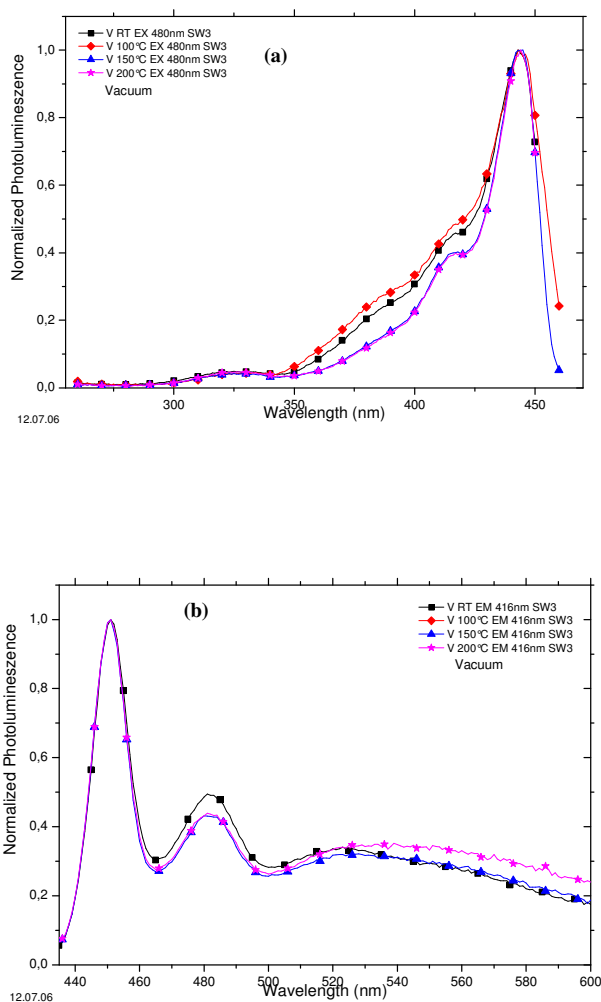


**Figure 2.32** Absorption and photoluminescence spectra of polymer **52** for pristine and annealed film in vacuum at 100, 150, and 200 °C

However, when the same polymer was heated under air at 100 °C (shown in Figure 2.33), it exhibited the appearance of a new peak both in absorption as well as in the PL spectrum. The new peak in emission spectrum around 570 nm was most likely from the formation of ketone defects at the dialkyl bridge because the dialkyl bridge was relatively more prone to oxidative degradation compared to the diaryl or nitrogen bridge. The intensity of the peak increased with further heating at 150 and 200 °C.

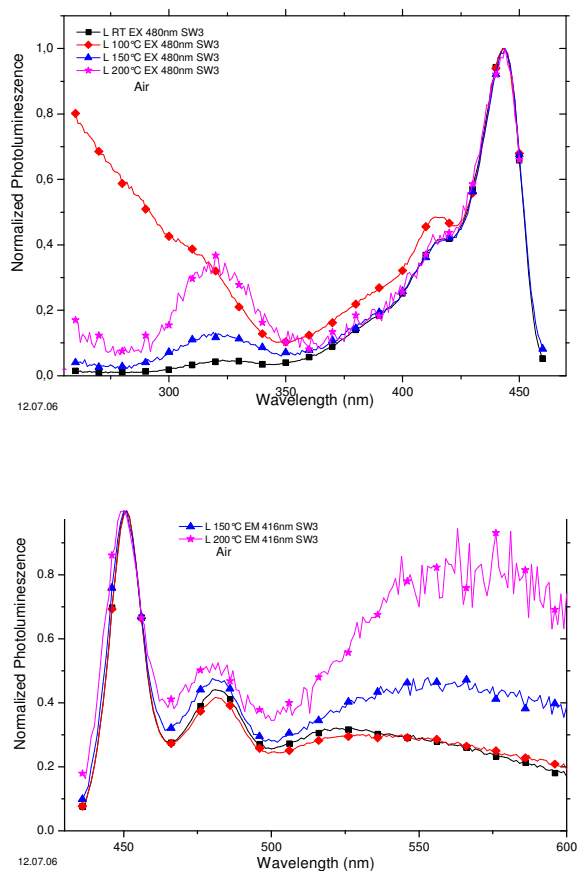


**Figure 2.33** Absorption and photoluminescence spectra of polymer **52** for pristine and annealed film in air at 100, 150, and 200 °C

Figure 2.34 depicts a comparison of thermal degradation tests under vacuum and air at 200 °C for **52** which clearly showed that the new peak at 570 nm appeared only in the presence of air and that it was very stable under vacuum. Furthermore, this new peak which appeared in the presence of air, was more likely to be a ketone defect generated at the dialkyl bridge of polymer **52**.

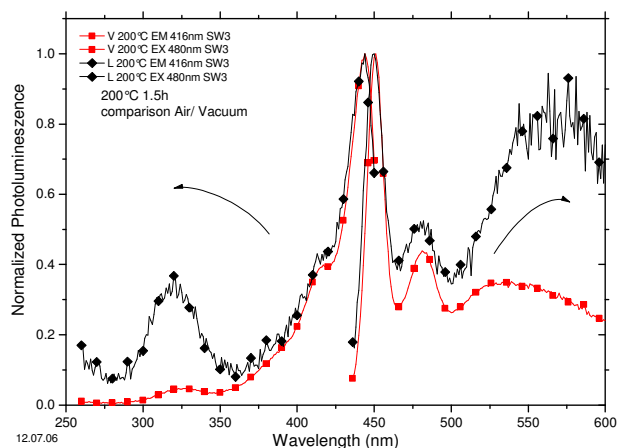


**Figure 2.34** Absorption and photoluminescence spectra of polymer **52** for pristine and annealed film in vacuum and air at 200 °C.

## 2.6 Supramolecular organization of ladder-type polymers

In this section the supramolecular organization of polymers **19**, **44**, **47** and **52** in solid-state was studied by using 2D wide angle X-ray scattering. This investigation was done together with Dr. Wojciech Pisula at Max-Planck Institute for Polymer Research.

The DSC measurements did not reveal any phase transitions for all the investigated polymers within a temperature range of –100 °C to 220 °C. Therefore, for the structural investigation, all polymer samples were extruded under the same conditions for comparison of their supramolecular organization. The sample preparation was carried out by using a home-built mini-extruder as illustrated in Figure 2.35 at a temperature of 200 °C at which the materials show little plasticity. The X-ray scattering experiments were performed at room temperature. For all investigated polymers, the organization did not change with temperature and annealing procedures. The extruded filament was positioned vertical toward the 2D-WAXS detector. The distribution of the reflections over the scattering pattern allowed the conclusion about the relative arrangement of the building units within the supramolecular organization.

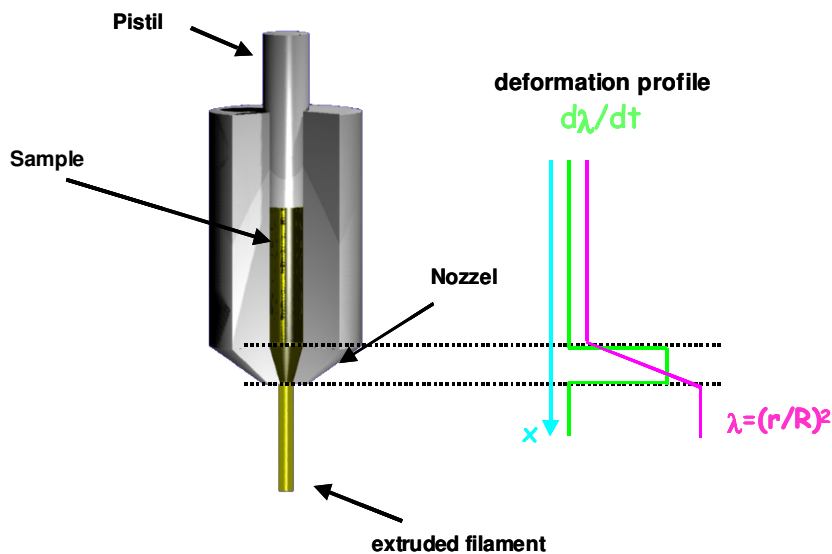


**Figure 2.35** Schematic illustration of the alignment by mechanical extrusion.

Figure 2.36a shows a typical 2D-WAXS pattern of polymer **47**. The high intensity and distinct reflections indicate a pronounced organization of the polymer with a strong alignment of the chains along the shearing direction and thus along the filament. The position and location of the reflection within the pattern gives information about the corresponding periodicities and orientation of the polymer chains in the sample. The small-angle reflections attributed to a distance of 1.51 nm, as derived from the position in the plot in Figure 2.36a, can be related to the lateral distance of the polymer chains to each other and indicated once again the alignment of the macromolecules. On the other hand, the strong wide-angle reflection at a correlation distance of 0.45 nm implied the  $\pi$ -stacking distance between the polymer units. The meridional reflections correspond to the repeating distance between monomers along the polymer chain. The theoretical distance between single units was 2.3 nm could not be derived since the reflection position was slightly superimposed by the equatorial reflection corresponding to 1.51 nm. However, multiple higher order reflections, which correlated with the distance between monomer units, were obvious in the pattern. For instance, the second higher order reflection was related to 1.15 nm which is the half value of 2.3 nm. Reflection up to the sixth order appeared indicating the pronounced order of the polymer chains towards each other.

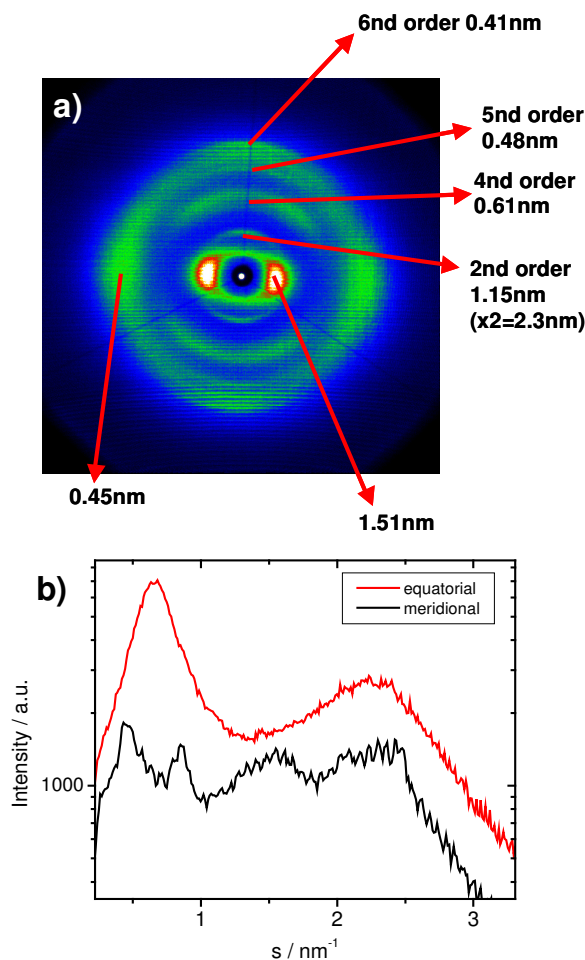


**Figure 2.36** a) 2D-WAXS pattern of polymer **47** with the corresponding distances of the reflections and b) the scattering intensity distribution as a function of the scattering vector  $s$ .

This was also in a good accordance with  $\pi$ -stacking reflection, which was characteristic for single building blocks effectively interacting with each other. The organization of the conjugated polymer chains is illustrated schematically in Figure 2.37. All essential periodicities are indicated in the drawing. Due to simplifications, the alkyl side chains are shown as stiff. In reality the alkyl substituents are flexible and rather disordered filling the periphery of the rigid conjugated polymer macromolecules which are stacked on top of each other. The aryl groups play an important role not only for the solubility of the material, but also influence the packing. Since these groups possess a rather high steric requirement due to the out-of-plane rotation towards the backbone, one can assume that for the stacking the conjugated polymer has to flip leading to the most favored arrangement as illustrated

in the inset in Figure 2.37. In consequence, the high steric requirement does not necessarily decrease the  $\pi$ -orbital overlap, which is so important for an unhindered interchain charge carrier transport.

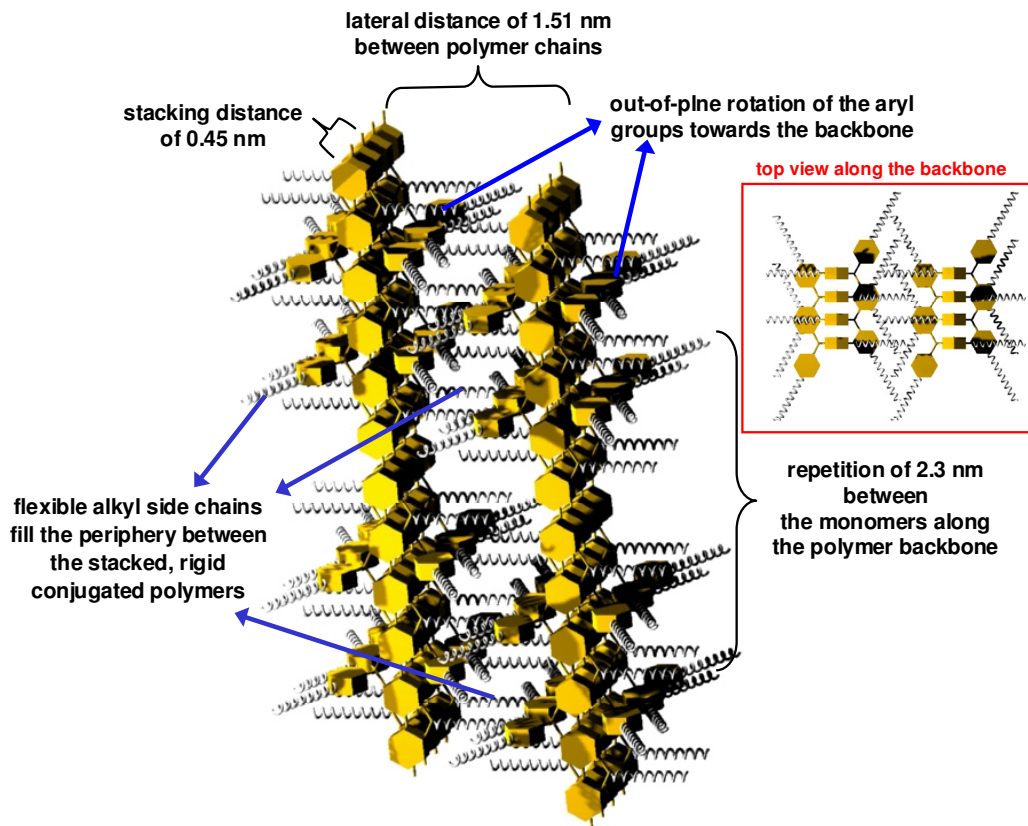


**Figure 2.37** Schematic illustration of the packing of polymer 47. The alkyl side chains are simplified. The inset shows the top view of the polymer packing.

To relate the macromolecular architecture with the packing, the organization of other conjugated polymers were investigated. Polymer **19** revealed a similar X-ray pattern as polymer **47**, however, with weaker reflections corresponding to the stacking and the sequence repetition (Figure 2.38). The packing parameters changed slightly due to different polymer architectures. The well pronounced small-angle equatorial reflections corresponding to the lateral chain distance of 1.77 nm indicated an alignment of the conjugated polymer chains in the shearing direction. The characteristic stacking distance of also 0.48 nm was implied by the wide-angle reflections (Figure 2.38) which were much weaker in comparison to polymer **47** indicating therefore a lower interaction between the polymer blocks.

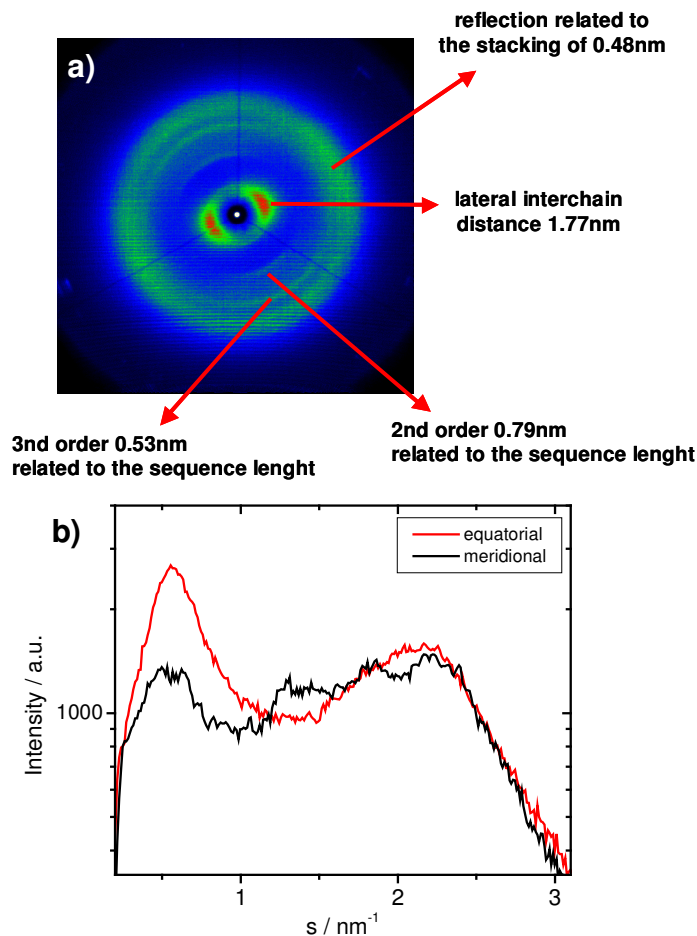


**Figure 2.38** a) 2D-WAXS pattern of polymer **19** with the corresponding distances of the reflections and b) the scattering intensity distribution as a function of the scattering vector  $s$ .

This was also confirmed by the low intensity meridional second order reflection related to a period of 0.79 nm between the monomer units along the conjugated chain. Due to the lower interaction, the order of the polymer blocks to each other was probably also significantly decreased leading to a lowering of the intrachain correlation. The poor amorphous halo was also observed for polymer **47** and was typical for the disordered alkyl side chains filling the periphery of the conjugated polymers.



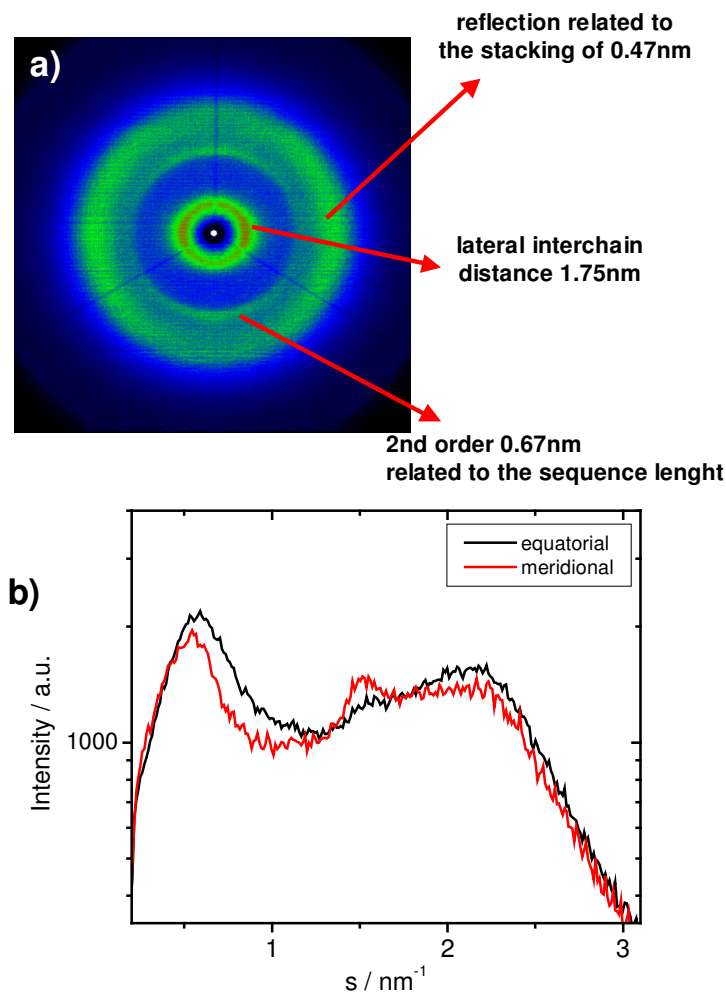


**Figure 2.39** a) 2D-WAXS pattern of polymer **44** with the corresponding distances of the reflections and b) the scattering intensity distribution as a function of the scattering vectors.

Figure 2.39 presents the X-ray pattern of polymer **44** indicating an identical supramolecular organization as described for the two previous polymers. The wide-angle equatorial reflection was related to 1.75 nm to the lateral distance of polymers, whereas the wide-angle equatorial one was typical for the stacking distance of 0.47 nm which was in the same range as for polymer **47** and polymer **19**. However, the weak anisotropy of the reflections, and especially of the equatorial small-angle, suggested a significant difference in the extent of order in the samples. This order diversity between the compounds was obvious from the shape difference between the meridional and equatorial integrations of the 2D patterns of the compounds. The more identical the plot shape is, the lower the degree of supramolecular order. Although,

one can clearly observe the reflections for polymer **44**, there is a clear difference to polymer **47** and polymer **19**. However, it should be noted once again that the stacking distance between the conjugated chains did not change, only the macroscopic organization.

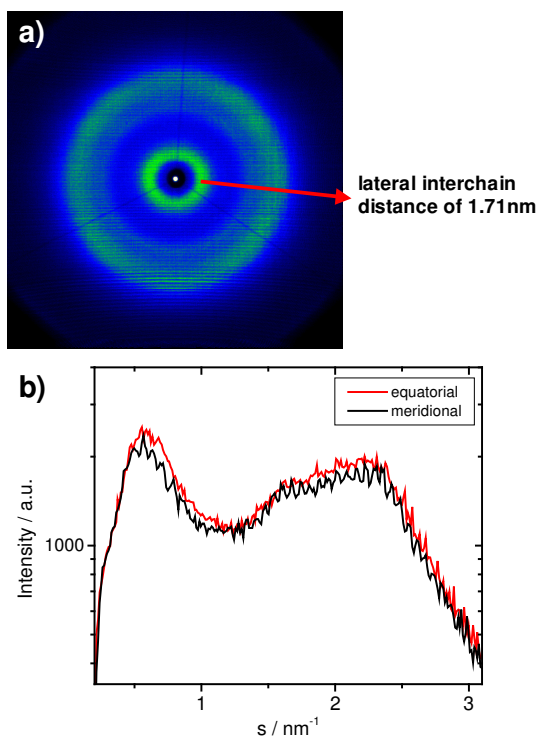


**Figure 2.40** a) 2D-WAXS pattern of polymer **52** with the corresponding distances of the reflections and b) the scattering intensity distribution as a function of the scattering vectors.

The change of macroscopic order with the variation of the polymer design is strongly visible in Figure 2.40. The 2D pattern of polymer **52** revealed only isotropic reflections indicating no order of the extruded sample. The small-angle reflection was correlated with the lateral interchain distance of 1.71 nm. The larger distance in comparison to polymer **47** was also in very good accordance with the longer attached alkyl chains. The  $2\theta$  integration along this small-angle reflection displayed a low degree of anisotropy and thus poor alignment of the conjugated chains of polymer **52**. As a result of the poor macroscopic order, no reflections related to the stacking and the intrachain correlation along the polymers appeared implying once again the weak orientation of the polymer blocks. In Figure 2.40a, the equatorial and meridional plots verified the poor reflection anisotropy.

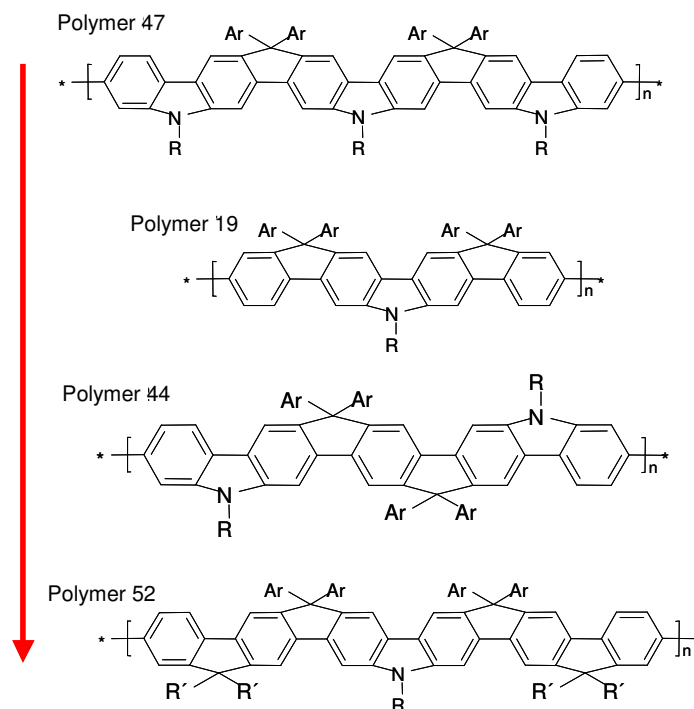


**Figure 2.41** Relation between the macroscopic order and polymer architecture of the investigated polymers. Arrow direction shows the direction of decreasing order.

To understand the relation between polymer architecture and macroscopic order indicated by the structural results, one has to take a more detailed look at the differences in the chemical structure between the investigated polymers which are listed in Figure 2.41. The most significant difference in the macroscopic order was observed between polymer **47** and polymer **52**, whereby polymer **47** revealed the highest degree of order and polymer **52** showed only anisotropic reflections in the X-ray pattern. This was even more interesting, since both polymers possess an almost identical polymer design. Polymer **47** bore only carbazole units within the polymer backbone which were substituted by short branched alkyl side chains. On the other hand, polymer **52** consisted of only one carbazole and two fluorene unit per monomer unit. Each of the fluorene units was substituted by two octyl side chains at the carbon bridge position increasing their steric requirement. It has been shown for small molecular weight species like discotic hexa-*peri*-hexabenzocoronene that longer alkyl side chains, which were branched close to the rigid conjugated building block, decreased the  $\pi$ -interaction and thus increased the macroscopic disorder.<sup>51</sup> Therefore,

the two octyl side chains at the two fluorene units decreased the interaction between the rigid polymer blocks of polymer **52** and led to higher disorder in comparison to polymer **47**. An additional reason might be the enhanced interaction between carbazole units than between fluorene units. Since polymer **47** consisted only of carbazoles, it possessed the most pronounced macroscopic organization among all the investigated polymers. On the other hand, the slight order decrease of polymer **19** could be explained by the larger “density” of aryl groups along the conjugated backbone. Since the aryl groups rotate out-of-plane towards the polymer, they endure high steric hindrance which decreases the  $\pi$ -interaction. Polymer **19** showed the highest aryl fraction (or density) in relation to the molecular weight of each monomer unit. However, the X-ray results indicated a well-defined structure of polymer **19** in the extruded filaments, since, on the other hand, the polymer backbone was substituted by less flexible side chains than the other investigated polymers. The structural investigation of polymer **44** indicated the packing of the polymers into a supramolecular organization, but having a lower degree of order than polymer **47** and polymer **19**. In contrast to the other polymers, polymer **44** was attached by the aryl groups on both sides of the conjugated backbone. This increased the steric requirement significantly since the macromolecule cannot flip to find the most favorite packing, as in the case of polymer **47** and polymer **19**. It can be assumed that the chains of polymer **44** are shifted towards each other to be able to interact.

The control of the processability and pronounced order for conjugated polymers is a challenging subject for the synthetic chemist. On the one hand, bulky aryl groups and long, branched alkyl side chains are required to ensure solubility of the polymers. However, on the other hand these substituents decrease the  $\pi$ -interaction due to sterics and thus the macroscopic order which is essential for the charge carrier transport. In this investigation, we were able to indicate important elements in the polymer architecture which affect the organization. Long alkyl side chains, which were branched close at the rigid conjugated building block, and a too high “concentration” of aryl groups along the backbone and the attachment of these units on different backbone sides diminish the macroscopic order. It has been revealed that carbazole units can enhance the packing of conjugated polymers, whereby the

material's processibility is maintained being a significant advantage for device fabrication.

## 2.6 Application of ladder-type polymers in Field-effect transistor

This work was performed together with Nok Tsao at Max-Planck Institute for polymer research. The nitrogen-bridged ladder-type polymers were used as an organic semiconductor layer in a field-effect transistor. In general, a transistor is a current modulating device schematically shown in Figure 2.42, consisting of a gate electrode covered by a dielectric insulator on top of which resides the organic semiconductor (OSC) film. This film is in contact with source and drain electrodes (Figure 2.42).

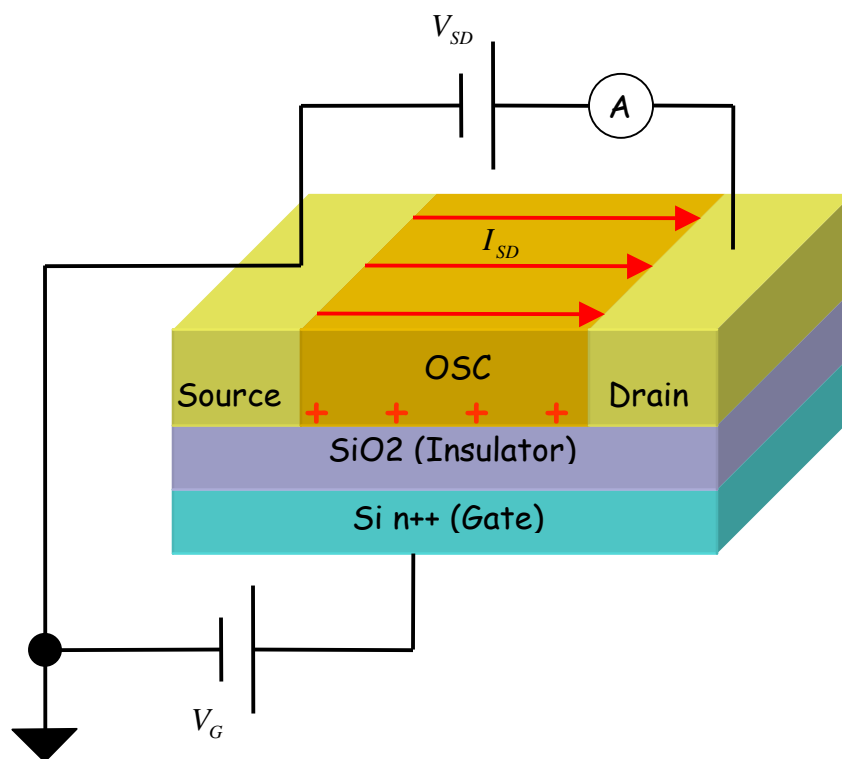


**Figure 2.42** Schematic of an organic field-effect transistor (OFET)

The current  $I_{SD}$  which flows through the organic semiconductor can be controlled by a gate voltage  $V_G$  and a source drain voltage  $V_{SD}$ . Application of a nonzero gate voltage triggers the accumulation of charge carriers at the OSC/insulator interface. The presence of a nonzero  $V_{SD}$  would in addition cause these accumulated charge carriers to flow between source and drain, and hence generates and control the  $I_{SD}$ . Such a transistor was fabricated as follows: A highly n-type doped silicon wafer (acting as the gate electrode) with a 150 nm thermally grown silicon dioxide layer (acting as the insulator) serves as a transistor substrate. On top of the silicon dioxide, gold electrodes were patterned via optical lithography and evaporated in vacuum. To avoid charge carrier trapping by the polar silanol groups on the silicon dioxide surface, it was treated with 1,1,1,3,3,3-hexamethyldisilazane (HMDS) via vapor phase deposition. HMDS is known for capping these silanol groups. Then polymer **47** was dissolved in toluene at a concentration of 10 mg/ml and spin coated on the transistor substrate at 1500 rpm to form the organic semiconductor film. Right after sample preparation, the devices exhibited no transistor action. However, after annealing the sample at 140 °C for 1h, transistor performance was observed, shown in Figure 2.43 and Figure 2.44.

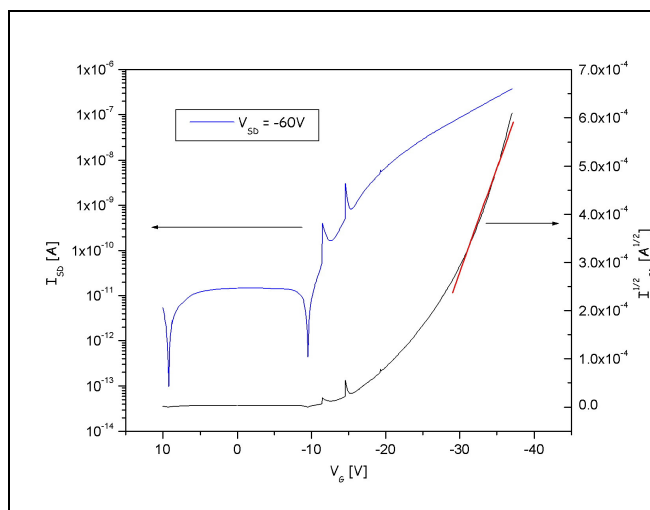


**Figure 2.43** Transfer characteristic of spin-coated polymer 47 after annealing at 140 °C for 1 h

Sample preparation and measurements were all done in a glove box in a nitrogen atmosphere to prevent any possible oxidation of the polymers. Figure 2.43 is a semi logarithmic plot of  $I_{SD}$  Vs.  $V_G$  at a fixed  $V_{SD} = -60V$  (blue curve). Such curve is called the transfer characteristic of the transistor. The most important parameter to judge the quality of a transistor is the charge carrier mobility  $\mu_{sat}$  in the saturation regime where the current  $I_{SD}$  does not increase anymore but remains constant.  $I_{SD}$  in saturation regime ( $I_{sat}$ ) can be given by

$$I_{sat} = \frac{W}{2L} \mu_{sat} C_I (V_G - V_T)^2$$

where  $C_I$  is the capacitance per unit area of the insulator ( $2.6 \times 10^{-8} \frac{F}{cm^2}$ ),  $W$  is the channel width (1.5 cm),  $L$  the channel length (10  $\mu m$ ), and  $V_T$  the threshold voltage.

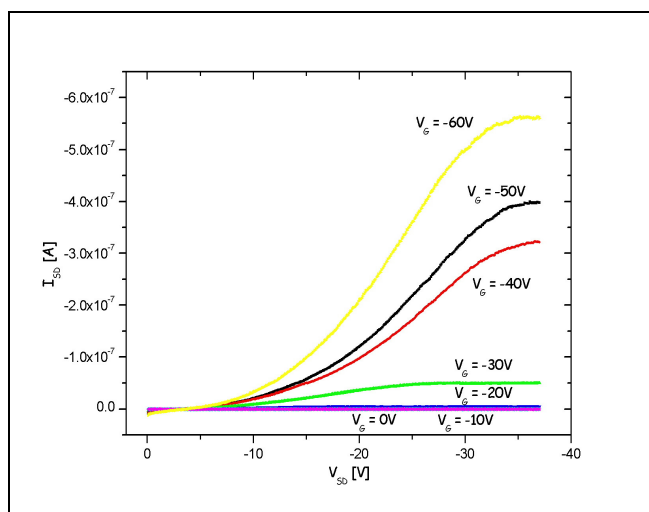


**Figure 2.44** Output characteristics of spin-coated polymer **47** after annealing at 140 °C for 1 h

From this equation, it is evident that in order to calculate the mobility, one has to plot  $\sqrt{I_{SD}}$  Vs.  $V_G$ , followed by a linear fit of this curve. The square of the slope of this fit is equal to  $\frac{W}{2L} \mu_{sat} C_I$  from which the mobility  $\mu_{sat}$  can be calculated. The red line in

Figure 2.43 is such a linear fit from which a mobility of  $\mu_{sat} = 1 \times 10^{-4} \frac{cm^2}{Vs}$  was deduced.

## Chapter 2

Another transistor parameter is the above mentioned threshold voltage given by the intersection of the linear fit with the  $V_G$  axis. Physically,  $V_T$  is the gate voltage at which the free charge carrier density equals the trap density at the insulator interface. In this sense,  $V_T$  is the gate voltage needed to fill all interface traps and so to turn on the transistor. For this transistor, a threshold voltage of  $-25$  V was obtained.

Finally, to estimate the switching ability of a transistor, the on/off current ratio  $\frac{I_{on}}{I_{off}}$  is a very important parameter. The higher this ratio, the bigger the difference in current between the on and off states, and hence the better one can distinguish these two switching states. A ratio of  $\frac{I_{on}}{I_{off}} = 3 \times 10^5$  was observed for this transistor.

Annealing the same sample for a longer time (16 h) at the same temperature (140 °C) resulted in a slightly increased maximum saturated mobility of  $\mu_{sat} = 3 \times 10^{-4} \frac{cm^2}{Vs}$ . The corresponding transistor curves are highlighted in Figure 2.45 and 2.46. However, the threshold voltage  $V_T$  for the film annealed for 1 h was  $V_T = -25V$ , whereas  $V_T = -15V$  for the film annealed for 16h, a significant decrease in threshold voltage with increased annealing time was observed.

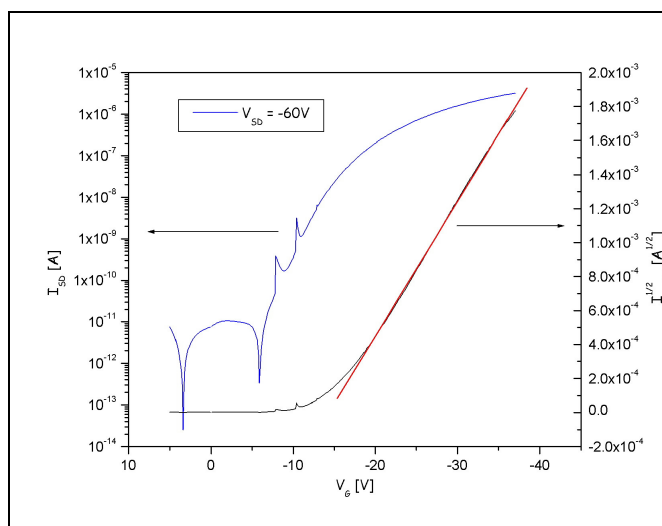


**Figure 2.45** Transfer characteristic of spin-coated polymer **47**, annealed at 140 °C for 16 h.



Since the threshold voltage is associated with the gate voltage needed to fill in all traps in an organic semiconductor film in order to guarantee a smooth flow of saturation current, the lower the threshold voltage, the less traps are present and the better the molecular ordering. So in this case the film annealed for 16 h apparently showed better ordering than the film annealed for 1h only. The output characteristics ( $I_{SD}$  vs.  $V_{SD}$  for various  $V_G$ ) illustrated in

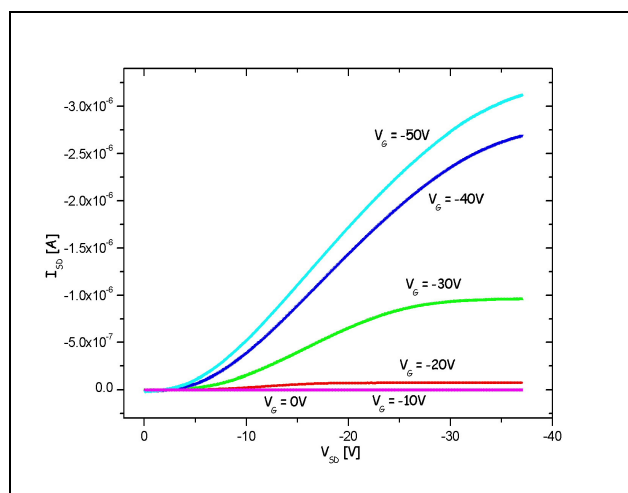


**Figure 2.46** Output characteristics of spin-coated polymer **47** after annealing at 140 °C for 16 h

Figure 2.50 showed typical transistor behavior, where the current rose with increasing  $V_{SD}$  and  $V_G$ . In addition, the transistor reached saturation at  $V_G = -30V$  (green curve in Figure 2.46), alluding to good device performance.

Further optimizations were carried out with a higher concentration of the polymer **47**. This time, 20 mg/ml of the polymer solution was spin-coated (twice as much material as before), followed by an annealing step at 120 °C for 12 h. The resulting transistor behavior is illustrated in Figure 2.47 and 2.48, with a maximum saturation mobility of

$$\mu_{sat} = 5 \times 10^{-4} \frac{cm^2}{Vs} \text{ and a threshold voltage of } V_T = -15V .$$

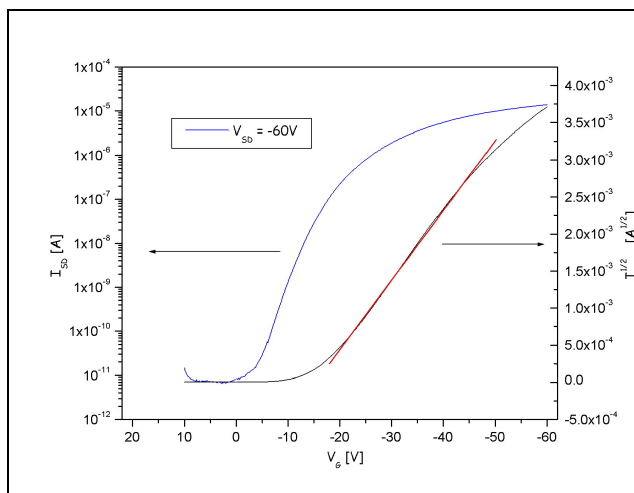


**Figure 2.47** Transfer characteristic of spin-coated polymer **47** (20 mg/ ml), annealed at 120 °C for 12 h.

Apparently, with twice as much material present, the mobility did not increase significantly. Also, the threshold voltage remained unchanged. Based on these findings, FET behavior of other nitrogen-bridged ladder-type polymers was also investigated, using the same processing steps as just mentioned (spin-coating a 20 mg/ml polymer/toluene concentration at 1500 rpm with a successive sample annealing at 120 °C for 12h).

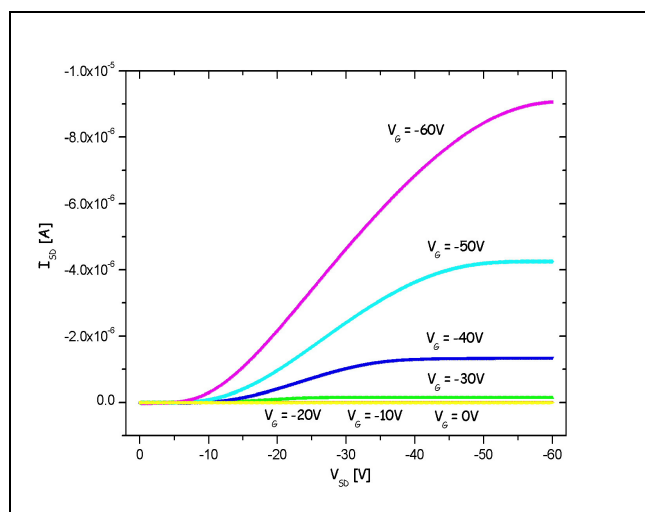


**Figure 2.48** Output characteristics of spin coated polymer **47** (20 mg/ ml), annealed at 120 °C for 12 h.

Figure 2.49 and 2.50 depict the transistor behavior for polymer **44**, resulting in

$$\mu_{sat} = 6 \times 10^{-3} \frac{cm^2}{Vs}, \quad \frac{I_{on}}{I_{off}} = 9 \times 10^4, \quad \text{and } V_T = -31V.$$

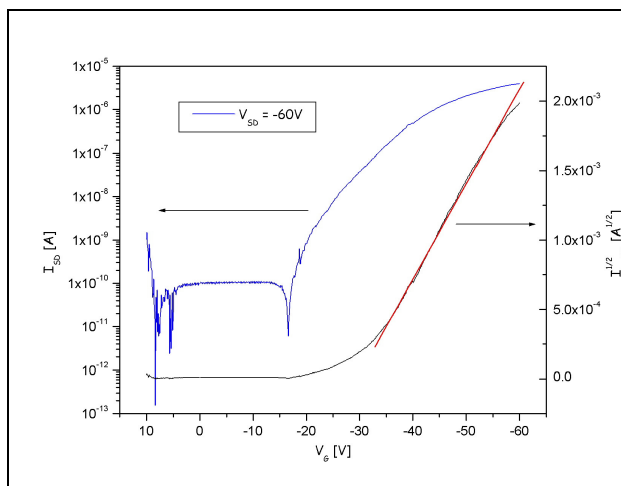


**Figure 2.49** Transfer characteristic of spin-coated polymer **44**, annealed at 120 °C for 12 h.

Even though the mobility for this material was quite decent,  $\mu_{sat} = 6 \times 10^{-3} \frac{cm^2}{Vs}$ , the transistor did not show ideal FET behavior, particularly, in the output characteristics (Figure 2.50) where a gate voltage higher than  $-30V$  was needed for the onset of significant  $I_{SD}$  (red and green curves). This may be because of high threshold voltage of  $-31V$ , alluding to the presence of traps.

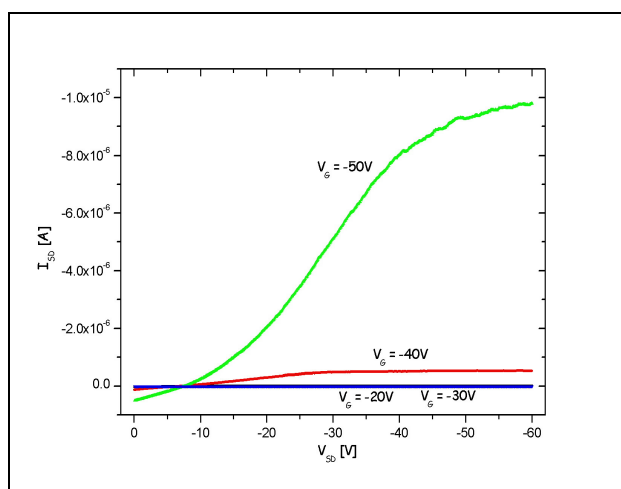


**Figure 2.50** Output characteristics of spin-coated polymer **44**, annealed at 120 °C for 12 h.

## Chapter 2

Polymer **19** was also studied, with the corresponding transistor performance illustrated in Figure 2.51 and 2.52, resulting in  $\mu_{sat} = 5 \times 10^{-4} \frac{cm^2}{Vs}$ ,  $\frac{I_{on}}{I_{off}} = 4 \times 10^4$ , and  $V_T = -32V$ .

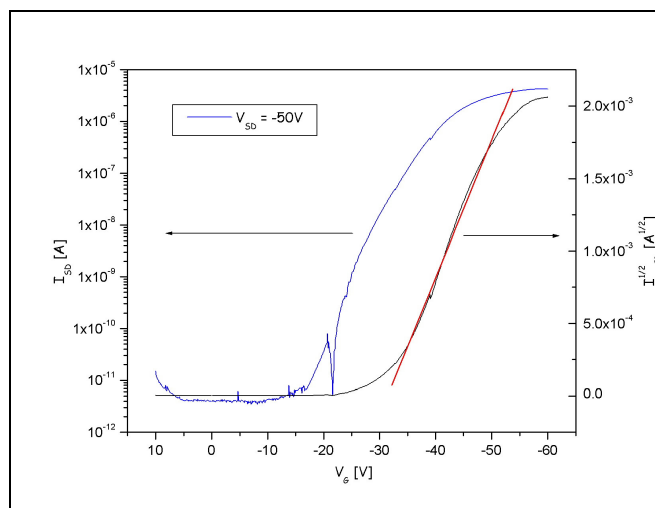


**Figure 2.51** Transfer characteristic of spin-coated polymer **19**, annealed at 120 °C for 12 h.

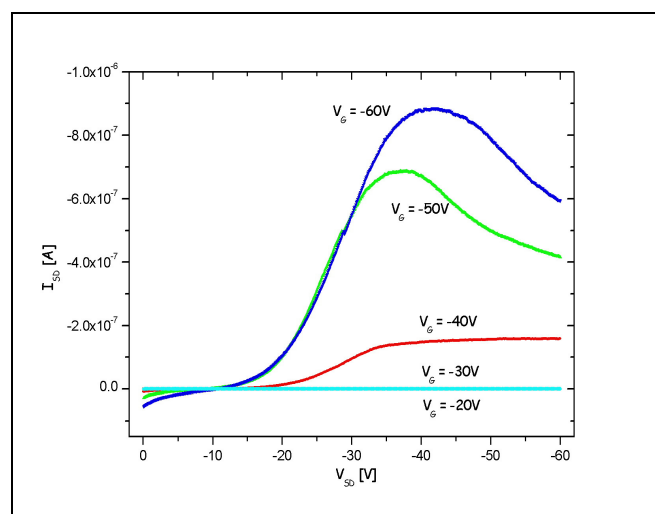


**Figure 2.52** Output characteristic of spin-coated polymer **19**, annealed at 120 °C for 12 h.

However, here the material did not show clean transistor performance, particularly for the output characteristics (Figure 2.52) at high  $V_G$ , for example the green

## Chapter 2

and blue curves, where the current was decreasing with  $V_{SD}$  higher than  $-40V$ . This was unexpected since the current should saturate at high  $V_{SD}$  and not suddenly drop. One explanation for these poor FET characteristics is the weak order at the contacts, possibly leading to current drop at high gate voltages when the charge carrier density is high.

Finally, polymer **52** was also examined with the transistor performance shown in Figure 2.53 and 2.54, resulting in  $\mu_{sat} = 3 \times 10^{-4} \frac{cm^2}{Vs}$ ,  $\frac{I_{on}}{I_{off}} = 3 \times 10^3$ , and  $V_T = -29V$ .

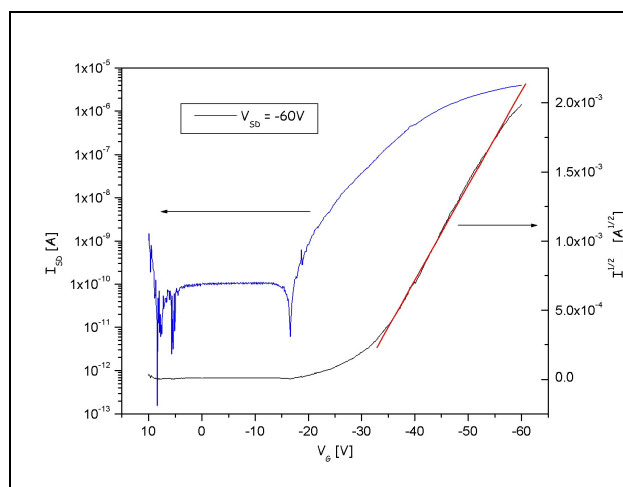


**Figure 2.53** Transfer characteristic of spin-coated polymer **52**, annealed at  $120^\circ C$  for 12 h.

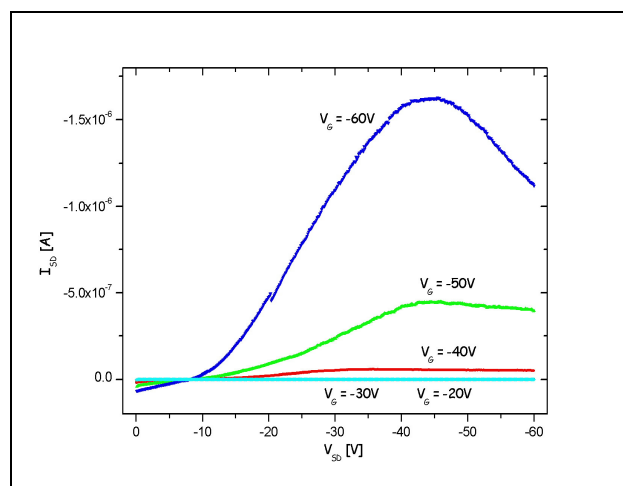


**Figure 2.54** Output characteristic of spin-coated polymer **52**, annealed at  $120^\circ C$  for 12 h.

Here again we see the current decrease for the output characteristics (Figure 2.58) for high gate voltage ( $V_G = -60V$ ).

Table 2.17 summarizes the important transistor parameter of all polymers investigated.

**Table 2.17** The FET parameter of polymers **19**, **44**, **47** and **52**.

Polymer	$\mu_{\text{sat}}$ (cm <sup>2</sup> /Vs)	$V_T$ (V)	$I_{\text{on}} / I_{\text{off}}$
<b>19</b>	$5 \times 10^{-4}$	-32	$4 \times 10^4$
<b>44</b>	$6 \times 10^{-3}$	-31	$9 \times 10^4$
<b>47</b>	$5 \times 10^{-4}$	-15	$3 \times 10^5$
<b>52</b>	$3 \times 10^{-4}$	-29	$3 \times 10^3$

In summary, all polymers displayed a charge carrier mobility between  $10^{-3}$  to  $10^{-4}$ , and among all nitrogen-bridged ladder-type polymers, polymer **44** demonstrated the best hole mobility of  $6 \times 10^{-3}$  cm<sup>2</sup>/Vs with on and off ratio  $10^5$ . The drop of current at higher voltages for polymer **19** and **52** are still unclear and under investigation. Furthermore, the mobility can still be improved by further device optimization such as selection of appropriate dielectric, better solvent and probably by zone casting to orientate the polymers.<sup>52</sup>

### 2.7 Performance of ladder-type polymers in light emitting diodes

These studies were performed by Michael Graf, Florian Grasse, Sabrina Eder and Horst Scheiber from the group of Emil J. W. List at University of Graz, Austria. The electroluminescent properties of materials were tested by incorporating the polymer into a device, similar in structure to the one shown in Figure 2.55. The ITO covered substrate was etched using oxygen plasma, then the PEDOT/PSS layer was subsequently applied by spin-coating then heated at 150 °C for 2 h in a vacuum.

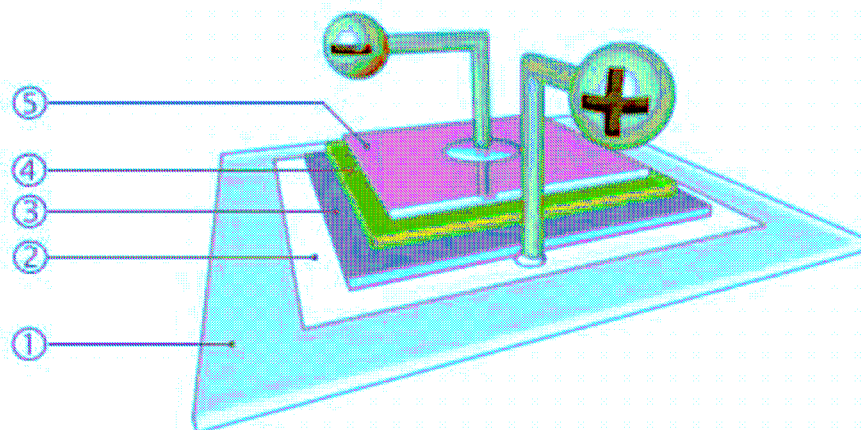


**Figure 2.55** Device architecture used in the EL experiments. 1. Transparent substrate 2. Hole injecting anode (ITO) 3. Hole transporting layer 4. light emitting layer 5. Electron injecting cathode (Ca/Al).

Polymer was deposited by spin-coating in an argon box to prevent oxidation and heated at 150 °C for 2 h in vacuum. The cathode (Ca) was vacuum deposited to give a 10 nm thick layer covered with a 100 nm thick aluminum layer.

## 2.8.1 Poly(ladder-type tetraphenylene)s

### 2.8.1.1 Nitrogen-bridged poly(ladder-type tetraphenylene) **19**

As depicted in Figure 2.56, polymer light emitting diode (PLEDs) prepared from polymer **19** showed a deep blue electroluminescence emission spectrum with very high luminance values of typically over 700-900 cd/m<sup>2</sup> at a bias of 10 V which was rather stable during several tens of minutes of operation under glove box conditions. The color coordinates of the emission were  $x = 0.19$ ,  $y = 0.19$  according to the CIE standard 1931.

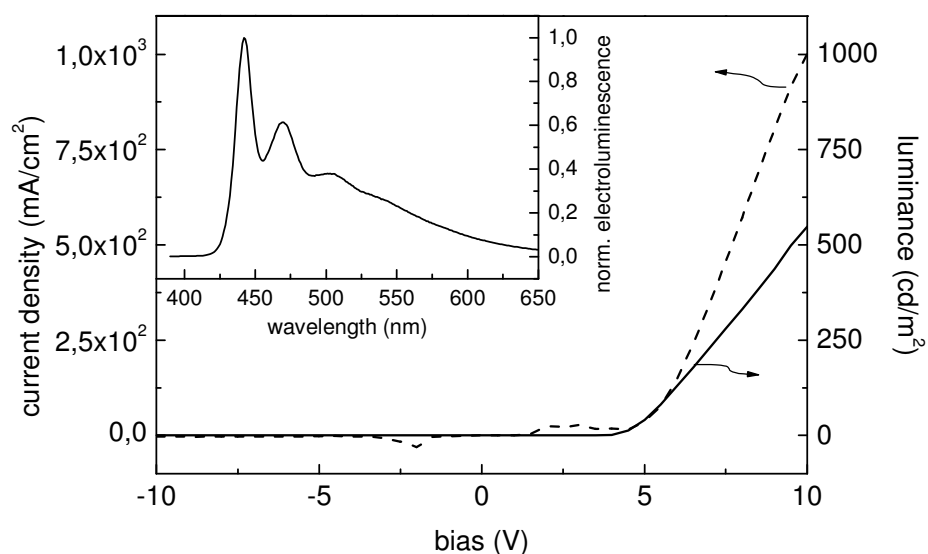


**Figure 2.56.** Bias/current and Bias/electroluminescence characteristics and normalized electroluminescence of an ITO/PEDOT/Polymer **19**/Ca/Al device.

The electroluminescence maximum was found to be at 445 nm. The devices showed the electroluminescence onset at ca 4 V in forward bias direction and exhibited moderate efficiencies of 0.1 cd/A.

### 2.8.1.2 All carbon-bridged ladder-type poly(tetraphenylene) **23**

In comparison, PLEDs prepared from polymer **23** showed green-blue electroluminescence emission spectrum with typical luminance values of 600 cd/m<sup>2</sup> at a bias of 15 V (Figure 2.57). The emission was composed of the blue emission of the polymer at 450 nm and of an additional band peaking at 510 nm with a shoulder at 540 nm.



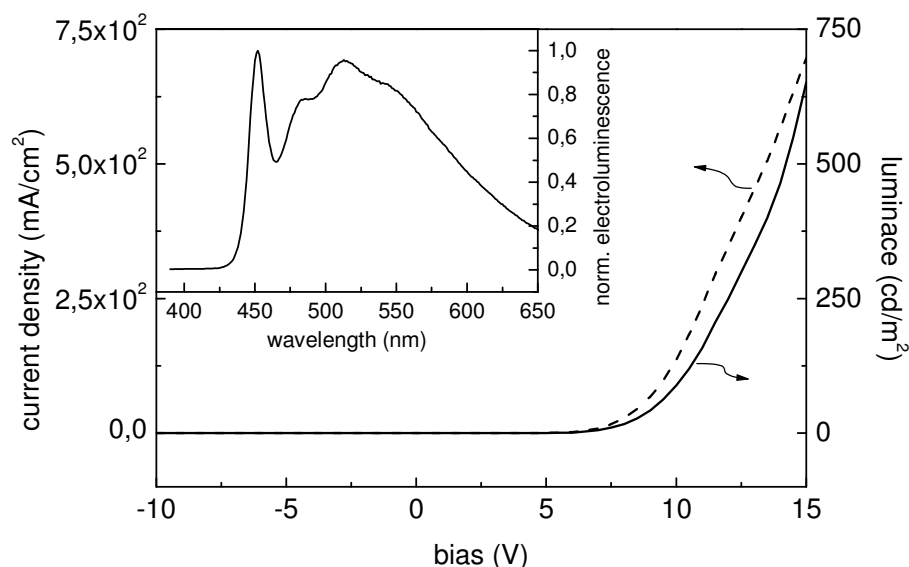


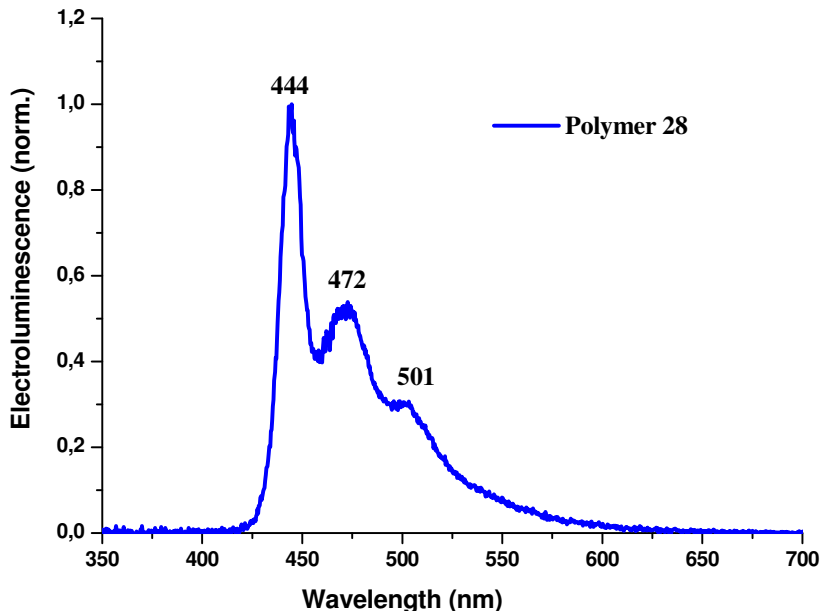
**Figure 2.57** Bias/current and Bias/electroluminescence characteristics and normalized electroluminescence of an ITO/PEDOT/Polymer **23**/Ca/Al device.

The color coordinates of this emission were  $x = 0.29$ ,  $y = 0.41$  according to the CIE standard 1931. The devices exhibited an electroluminescence onset at ca 5.5 V in the forward direction and demonstrated only moderate efficiencies of less than 0.1 cd/A. The observation of the additional broad electroluminescence peak at 510 nm was unexpected. A comparison of the results from the degradation experiments obtained for the two polymers showed that the peak at 510 nm, which was observed in polymer **23** cannot be related to an emission, which has its origin in a product from an oxidative degradation. In such a case, the additional low energy band in electroluminescence should be located at ca. 570 nm as it was found for polymer **23** in photoluminescence upon degradation. In order to explain one must, however, not only focus on bulk polymer defects but also the observation of additional distinct spectral features in electroluminescence of PLEDs emerging from the interaction of the polymer with the (Ca)/Al-electrode or the PEDOT/PSS interface have to be taken into account. Such emission bands in the spectral region of 480-510 nm and their relation to the interface have been clearly identified for polyphenylene type polymers in literatures.<sup>53-55</sup> Such features only emerged upon coverage of the polymer with

metals such as Al or Ca and they were attributed to the formation of chemical defects in the polymer in a chemical degradation reaction caused by the low work function metal electrodes.

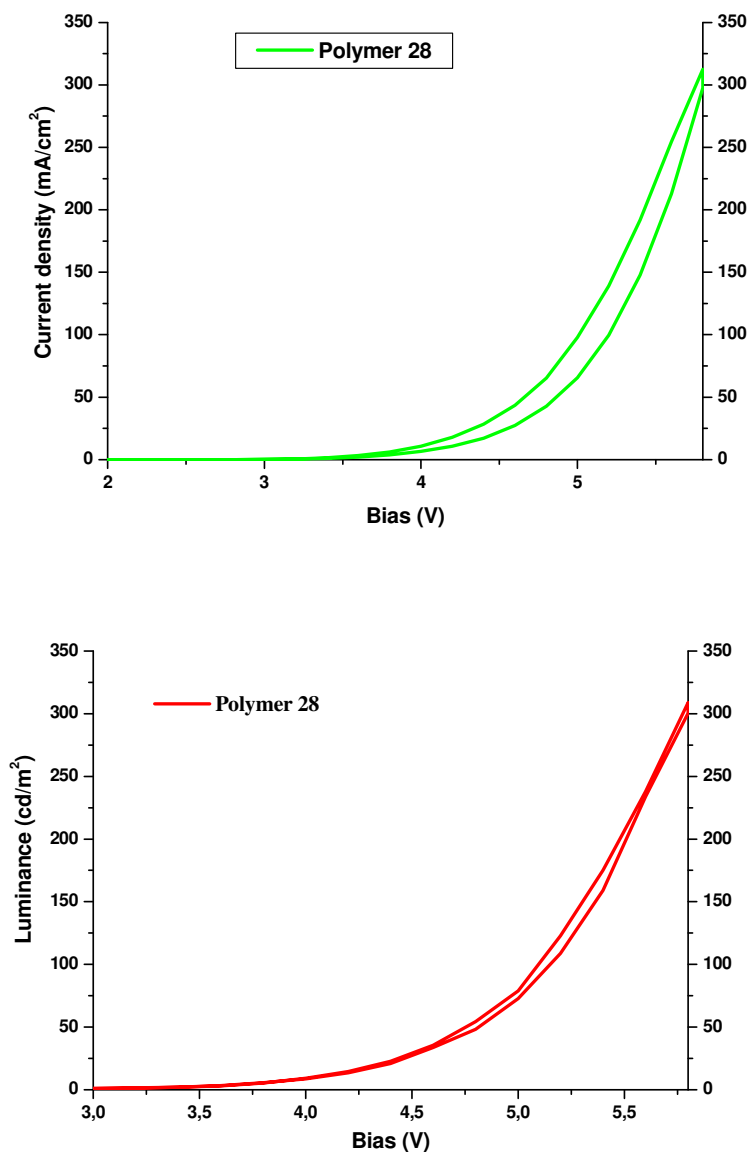
### 2.8.1.3 Fully arylated carbon-bridged poly(ladder-type tetraphenylene) 28

Figure 2.58 presents the electroluminescence spectrum of polymer **28**. The devices had a maximum emission at 444 nm with shoulders at 472 nm and 501 nm. In this case, Ca was replaced with CsF due to the better electron injection property of the latter.



**Figure 2.58** Normalized electroluminescence of an ITO/PEDOT/Polymer **28**/CsF (1 nm)/Al (20 nm) device.

Figure 2.59 displays the current density-voltage and intensity-voltage characteristics of the PLEDs with polymer **28** as the active layer.



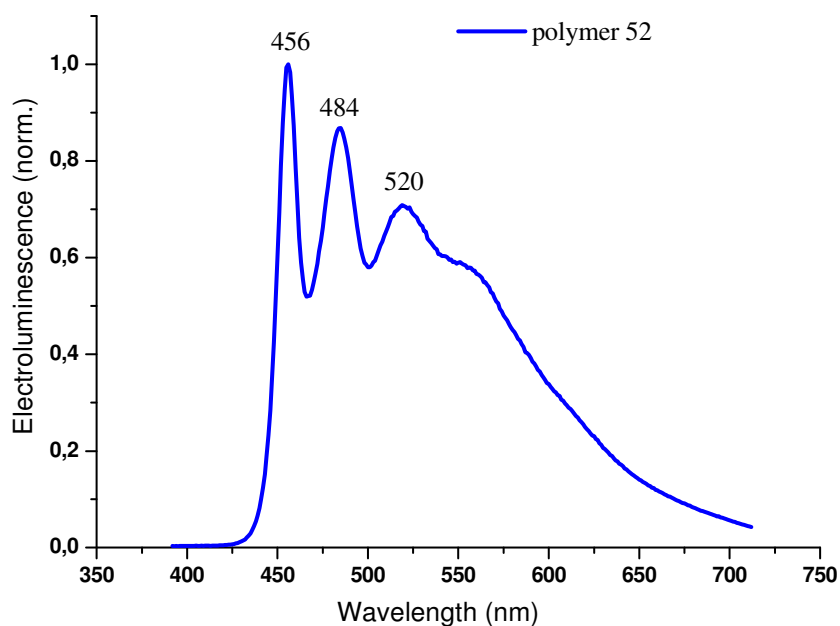
**Figure 2.59** a. Current density-Voltage characteristics b. Luminance-Voltage characteristics of OLED of polymer **28**.

The devices showed the electroluminescence onset at ca 3.2 V in forward bias direction and exhibited moderate efficiencies of 0.1 cd/A. A maximum luminance of 300 cd/m<sup>2</sup> was obtained at 5.8 V which was stable during several tens of minutes of operation under glove box conditions. Polymer **28** demonstrated better stability than

polymer **23** in electroluminescent devices which may be due to complete arylation of the bridge heads in polymer **28**.

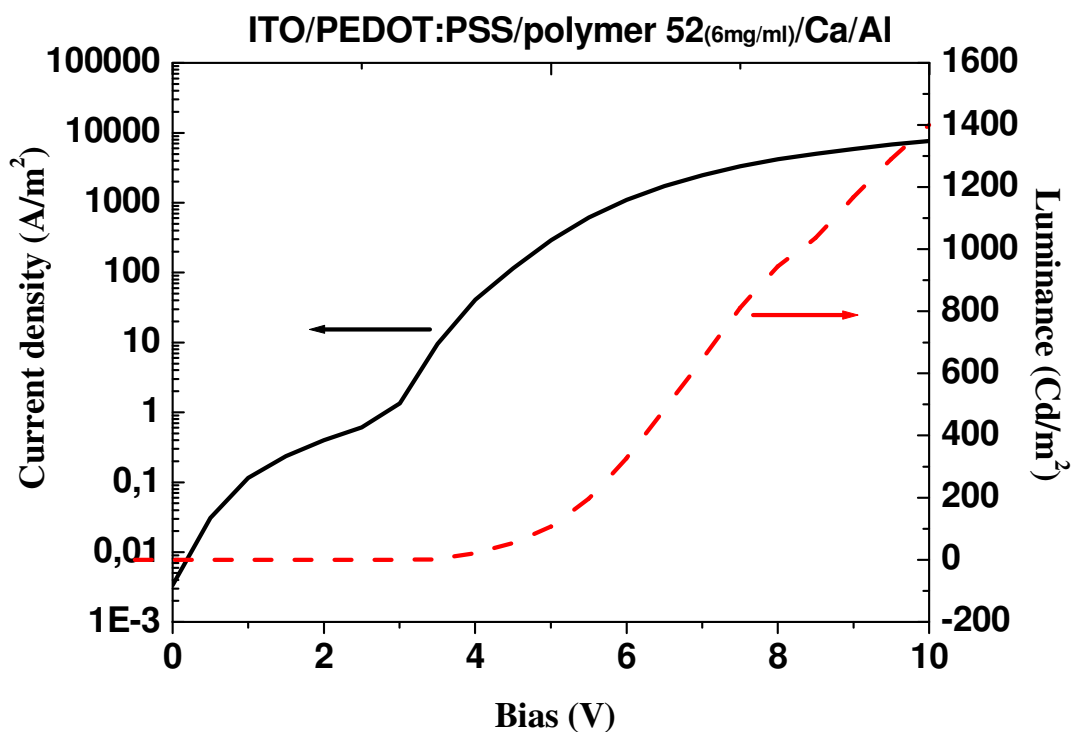
### 2.8.2 Poly(ladder-type hexaphenylene) **52**

Figure 2.60 depicts the electroluminescence spectrum of polymer **52**. The devices had a maximum emission at 456 nm with shoulders at 484 nm and 520 nm and displayed blue-green electroluminescence.



**Figure 2.60** Normalized electroluminescence of an ITO/PEDOT/Polymer **52**/Ca/Al device.

Figure 2.61 depicts the current density-voltage and luminescence-voltage characteristics of the PLEDs with polymer **52** as an active layer. The devices showed the electroluminescence onset at ca 3.5 V in forward bias direction and exhibited moderate efficiencies of 0.1 cd/A. A maximum luminescence of 1400 cd/m<sup>2</sup> was obtained at 10 V under glove box conditions.



**Figure 2.61** Current density-voltage and luminance-voltage characteristics of PLED of polymer 52.

The electroluminescence data derived from all polymers studied are summarized in the Table 2.18.

**Table 2.18** Electroluminescence properties of polymers 19, 23, 28, and 52

Polymers	Turn on voltage(V)	Emission maximum (nm)	Maximum luminescence Cd/m <sup>2</sup> (corresponding voltage)
19	4	445	900 (10 V)
23	5.5	450	600 (15 V)
28	3.2	444	300 (5.8 V)
52	3.5	456	1400 (10 V)

An analysis of the data on Table 2.19 reveals that polymer **19** which has nitrogen bridge in the repeat unit exhibited higher value of luminescence compared to the all carbon-bridged analogues **23** and **28** and the turn on voltage of polymer **19** was also lower than that of polymer **23**, probably due to the high HOMO value of **19** compared to **23** which makes easy hole injection inside the active polymer layer. Polymer **19** showed higher turn on voltage and low luminescence value compared to **52**, both has one nitrogen in the repeat unit, but **52** has six benzene ring in the repeat unit as compared to **19** which has four. This suggests that a more extended conjugation makes easier charge injection into the active layer and also result in high luminescence.

### 2.9 Performance of nitrogen-bridged ladder-type polymers in solar cell devices

The solar cell devices were fabricated together with Jiaoli Li from our group at Max-Planck Institute for Polymer Research.

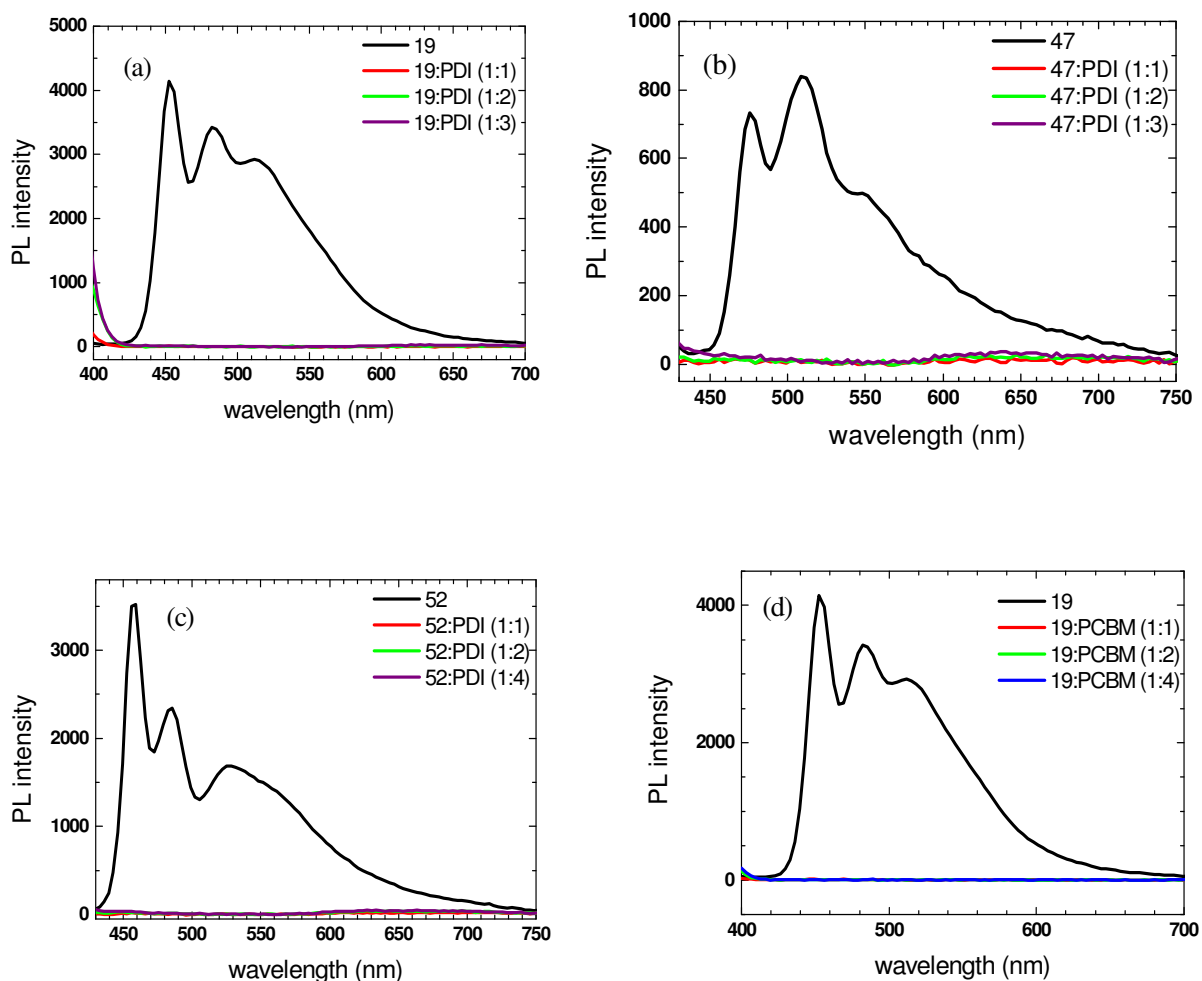
Polycarbazole (PCz) is shown to be a novel promising donor material for solar cell, but it absorbs mainly in the violet or ultraviolet region, which limits its application as a good light-harvesting component in photovoltaic cells.<sup>56</sup> The incorporation of a long branched alkyl chain in polycarbazole increases its solubility but reduces the amount of light absorbing chromophores in the active layer. The large density of alkyl chain also increases the insulating effects,<sup>57-59</sup> which prevents the intermolecular contact of semiconducting material and hampers the facile photoinduced electron transfer from donor to acceptor material as well as the charge transport.

In order to overcome these problems, the nitrogen-bridged ladder-type polymers **19**, **47** and **52** were designed, which absorbs in the visible region where the solar spectrum is prominent due to their extended conjugation and also has shorter alkyl chains. The absorption of the polymers **19**, **47**, and **52** were close to the strongest emission of solar light at 480 nm, so they would be expected to absorb photons more efficiently than PCz. Polymer/PCBM is one of the best known donor and acceptor pairs because of good electron accepting property of PCBM from most

conjugated polymers as well as its good electron carrier mobility.<sup>60-64</sup> Therefore, PCBM, was used as acceptor materials for the polymer **19**, **47** and **52**.

### 2.9.1 Photoquenching in the film made by blending of donor and acceptor materials:- A first indication of efficient photo-induced charge transfer

The quenching of photoluminescence of a donor material by an acceptor material gives a first indication of an effective D/A charge transfer as described by Sariciftci for p-conducting polymers and fullerene derivatives.<sup>60</sup> The fluorescence of the ladder-type polymers **19**, **47** and **52** and their blends with PCBM or PDI at the ratios of 1:1 to 1:3 were recorded in thin films as shown in Figure 2.62.



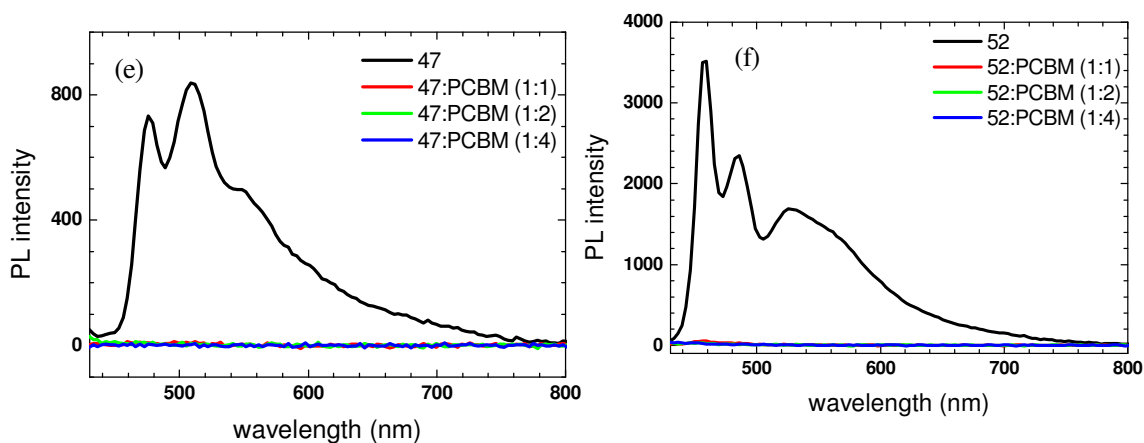


**Figure 2.62** PL spectra of the polymers **19** (a, d), **47** (b, e), **52** (c, f) and their blends with PDI (a, b, c) or PCBM (d, e, f) in thin films, excited at 380 nm

It was demonstrated that the fluorescence of the polymers were effectively quenched by the addition of even low amounts of acceptor molecules such as PCBM or PDI, which indicated an efficient charge transfer from nitrogen-bridged ladder-type polymers **19**, **47**, and **52** to PCBM or PDI.

### 2.9.2 Photovoltaic devices of polymer **19**, **47** and **52** as donor and PCBM as acceptor

The UV absorption of the polymers **19**, **47** and **52** displayed at least a 40 nm bathochromic shift compared with PCz, which suggested PCBM as possible acceptor material in solar cell. The orbital energy values of these polymers allow their pairing with both PDI and PCBM. The photovoltaic devices based on these two acceptor materials are presented here.

In order to investigate the effect of the chemical structure on device performance, photovoltaic devices based on polymers **19**, **47** and **52** were fabricated in the same ratio of polymer/PCBM = 1:4. Figure 2.63 depicts the EQE curve as well as current density vs. voltage curve under solar light AM1.5 G with light intensity of 150-160 W/m<sup>2</sup> for polymer **19**, **47** and **52**.



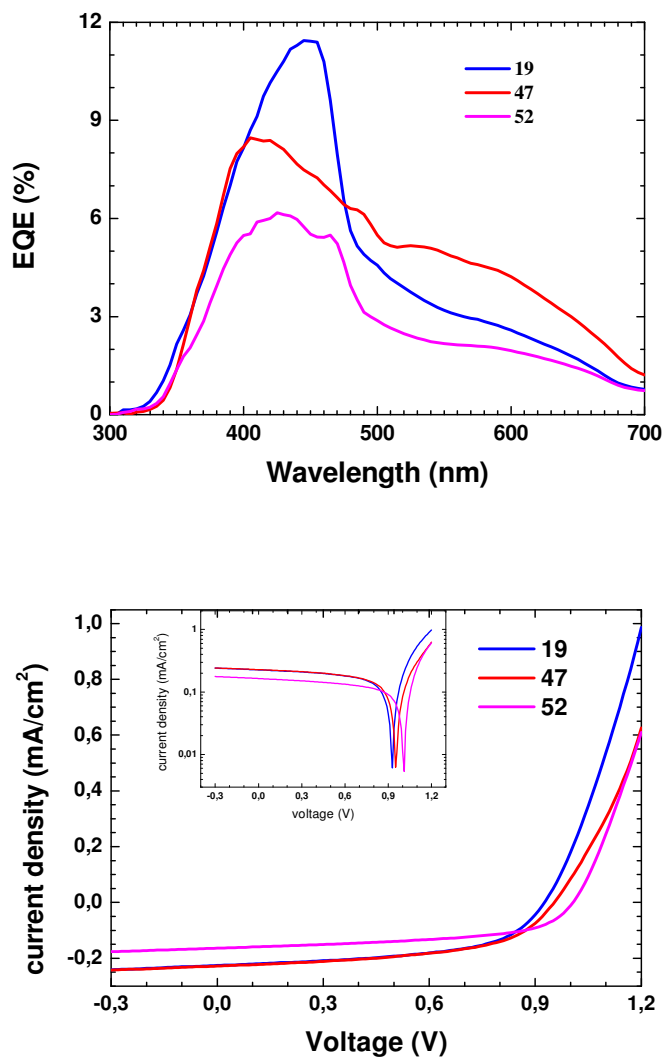


**Figure 2.63** Photovoltaic performance of device ITO/polymer **19**, **47** and **52**:PCBM (1:4)/Ag. The active layer was about 100 nm. I-V curves were recorded under solar light AM1.5 G with light intensity of 150-160 W/m<sup>2</sup>. The inset is I-V curve with logarithm ordinate.

As shown in Figure 2.63, the EQE curves showed only one peak near the absorption maximum of the donor material. For **19**, **47** and **52**, a shoulder peak appeared with an extended tail to 650 nm, which was attributed to the absorption of PCBM. The device characteristics are listed in Table 2.19. The typical  $V_{oc}$  of the

nitrogen-bridged ladder- polymers/PCBM devices were greater than 0.9 V, which was higher than the  $V_{oc}$  (0.6 V) of the most successful P3HT/PCBM devices. This was in accordance with the HOMO of P3HT (-5.2 eV)<sup>65</sup> being higher than the HOMO of polymers **19**, **47** and **52** (-5.4~-5.7 eV). However, for these devices, the  $I_{sc}$  was much lower than that for the P3HT device, which might arise from the high charge carrier mobility of P3HT,<sup>21</sup> thus decreasing the overall efficiency.

**Table 2.19** Photovoltaic device parameters for polycarbazole, polymer **19**, **47** and **52**

Polymer/PCBM (1:4)	$I_{sc}$ (mA/cm <sup>2</sup> )	$V_{oc}$ (V)	FF	Efficiency (%)	EQEmax (%)
<b>19</b>	0.23	0.93	0.55	0.72	11
<b>47</b>	0.23	0.95	0.54	0.74	9
<b>52</b>	0.16	1.01	0.55	0.56	6
<b>Polycarbazole</b>	0.02	0.90	0.37	0.07	4

### 2.9.3 Relation between the polymer design, supramolecular order and photovoltaic performance

The very low efficiency of polycarbazole is due to its most blue-shifted absorption as well as largest lateral inter-chain distance (Figure 2.64). Polymers **19**, **47**, and **52** have absorption spectra more attuned to the solar spectrum. If the red-shift of the absorption maximum were the only dominant factor in determining the relevant efficiencies then polymer **52** should have displayed a better efficiency value than polymer **19**. It is noteworthy that the efficiency values seem to correlate in a linear fashion with the  $I_{sc}$  values, suggesting that the ability of the charges to move within the donor material was the key element in determining the overall device efficiency. This in turn would depend upon the supramolecular order of the chains.

In comparing the device performance to the supramolecular organization in the extruded samples, it became apparent that the performance was mainly dependent

upon the lateral distance between the conjugated polymer chains and their long-range order. This lateral distance depends only on the length of the substituted alkyl side chains, which filled the periphery between the conjugated backbones.

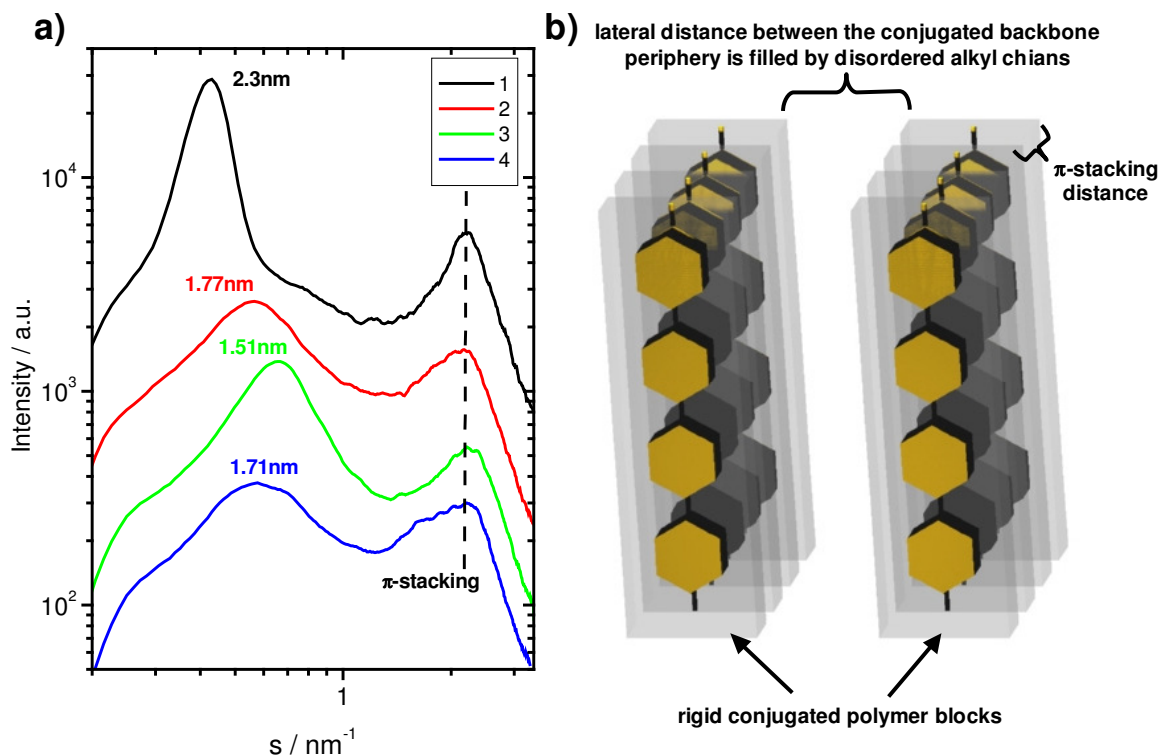


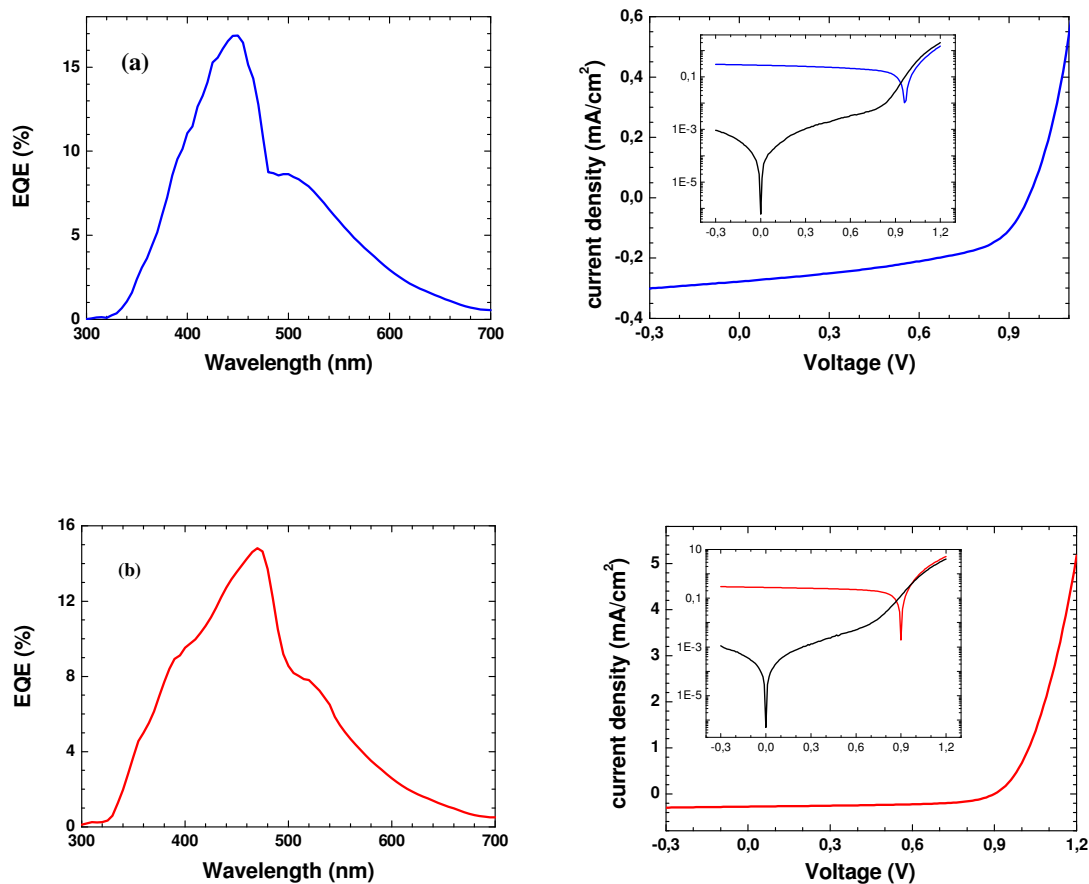
**Figure 2.64** The lateral distance between conjugated polycarbazole, polymers **19**, **47**, and **52** depending on the alkyl side chain length which also determine the photovoltaic performance: a) equatorial scattering intensity distribution as a function of the scattering vector, and b) schematic illustration of the periodicities observed in the plot.

Therefore, the longer the disordered, insulating side chains are, the larger is the lateral distance and the more hindered the inter-chain charge carrier transport and the shorter the exciton diffusion length between conjugated units. Additionally, the long alkyl substituents dilute the concentration of the chromophore, decreasing in this way the light absorption and also the semiconducting fraction. In our study, this relation was quite obvious, since polycarbazole showed the highest supramolecular order, but the largest lateral distance between chains and the blue shift of the

absorption maximum, thus the lowest photovoltaic performance. By contrast, compounds **19** and **47** revealed a significantly lower lateral distance and consequently a higher photovoltaic outcome. As a secondary parameter for the device, the macroscopic order seems to play an additional role. Polymer **52** showed a comparable lateral chain distance to **47**, but a lower device performance, which can be explained by the poorer long-range organization observed by X-ray scattering.

### 2.9.4 Optimization of devices

The optimized D/A ratios were confirmed to be 1:4 for devices using PCBM as acceptor material, and 1:2 for devices using PDI as acceptor material. Based on this, the devices were further optimized by film thickness (Figure 2.65).



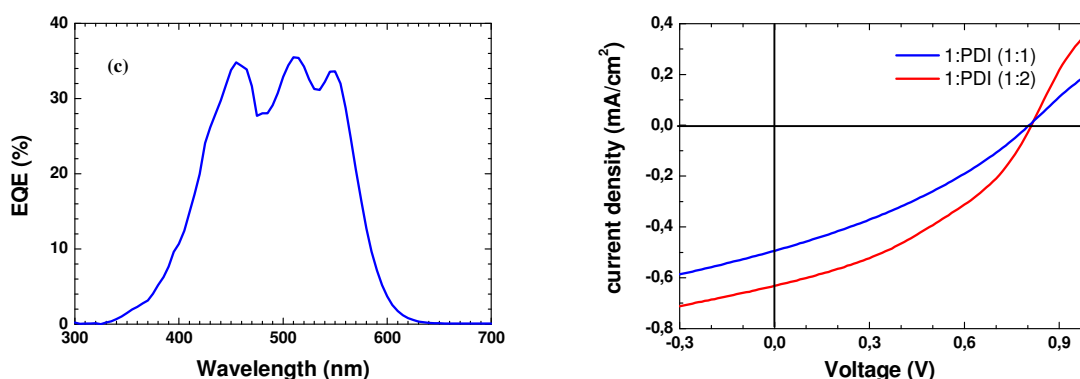


**Figure 2.65** Optimized device ITO/active layer/Ag of a) **19**:PCBM (1:4) with thickness of 70 nm, and b) **47**:PCBM (1:4) with thickness of 60 nm, and c) **19**:PDI (1:2) with thickness of 50 nm. The I-V curves were tested under solar light AM1.5 G with light intensity of 150-160 W/m<sup>2</sup>.

In comparison to PCBM, PDI can absorb photons more efficiently near the strongest emission of the sun. So in the devices of polymer/PDI, both of the components have the potential to harvest the solar energy in the visible optical range.

An overall efficiency as high as 0.9 % under solar light was recorded for PCBM based devices. For PDI containing devices, the highest efficiency of 1.32 % was achieved using polymer **19** as donor material. For polymer **19**/PDI, Voc was calculated to be about 0.8 V, slightly larger than that of PCz/PDI device (0.71 V). The Isc was found to be 0.63 mA/cm<sup>2</sup>, which was much higher than the corresponding value for the PCz based device (0.18 mA/cm<sup>2</sup>). The combined effects of short circuit current and open circuit voltage resulted in a great improvement of power conversion efficiency for the ladder-type polymer based device (1.32 % for polymer **19** and 0.48 % for PCz). It was also shown that the thinner device had higher photocurrent and EQE values than the 100 nm-thick devices. Since the thinner device can benefit from better charge collection at the electrode because of reduced distance between the charge separation at polymer/PCBM interface and electrode. The experimental result also indicated that the charge carrier mobility of the ladder-type polymer **19**, **47**, and

**52** was one of the limiting factors for the low photocurrent comparing with P3HT based device, except for the overlap with solar spectrum.

**Table 2.20** The photovoltaic performance of polymers **19** and **47**

Active layer	Isc (mA/cm <sup>2</sup> )	Voc (V)	FF	Efficiency (%)	EQEmax (%)
<b>19</b> /PCBM (1:4)	0.28	0.96	0.51	0.89	17
<b>47</b> /PCBM (1:4)	0.28	0.90	0.58	0.90	17
<b>19</b> /PDI (1:2)	0.63	0.81	0.38	1.32	35

This study shows the successful application of the new ladder-type carbazole based polymers as donor materials in photovoltaic devices, and suggests ways to improve device performance by molecular design, *viz.* maintaining the HOMO level while bathochromically shifting the absorption by adopting a more rigid ladder like structure. Here a high ratio of nitrogen bridges with small alkyl substituents seems to be a desirable feature both in terms of adjusting the absorption and of maintaining a low lateral inter-chain separation which is necessary for obtaining high current and efficiency values.

## 2.10 Application of ladder-type polymers as a gain medium in the amplification of blue light by amplified spontaneous emission

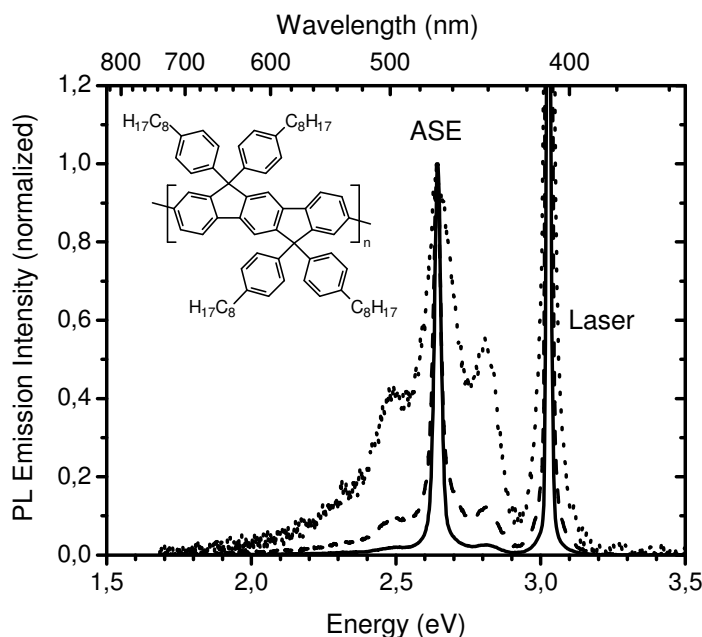
This work was carried out together with Dr. Frederic Laquai at Max-Planck Institute for Polymer Research.

Amplification of blue light by amplified spontaneous emission (ASE) in thin polymer film waveguides applying the ladder-type polymers as gain medium was demonstrated.

Recently, ASE has been demonstrated for thin film polymer slab waveguides of poly(tetraaryllindenofluorene)<sup>66</sup> and the photophysical properties of the polymer in solution and solid-state have been reported by Keivanidis et al.<sup>67</sup> In the present study the influence of increasing monomer length (indenofluorene → tetraphenylene → pentaphenylene), side-group substitution (alkyl vs. aryl), and presence of heteroatoms

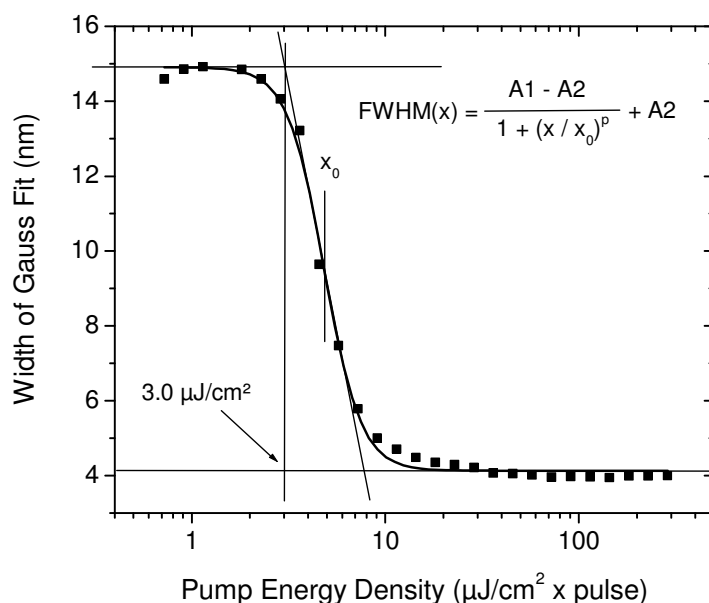
(carbazole moieties) on the ASE parameters, especially the threshold value for the occurrence of ASE, have been investigated.

Figure 2.66 shows the emission spectra of a polyindenofluorene thin film ( $d \sim 146$  nm) detected from the sample edge at three different pump energy densities.



**Figure 2.66** Edge detected PL-spectra of a poly(tetraaryindenofluorene) thin film ( $d \sim 120$  nm) upon pumping the sample with a stripe shape beam of  $8 \times 1$  mm<sup>2</sup> at 3.0 eV (410 nm). Spectra were normalized to the 0-1 vibronic. Pump energy densities were: 3.6  $\mu\text{J}/\text{cm}^2$  (dashed line), 9.1  $\mu\text{J}/\text{cm}^2$  (dashed dotted line) and 28.8  $\mu\text{J}/\text{cm}^2$  (solid line). The sharp peak at 3.02 eV (410 nm) corresponds to reflection of the pump laser beam.

At the lowest pump energy density shown here (3.6  $\mu\text{J}/\text{cm}^2$  corresponding to 450 W/cm<sup>2</sup>) the emission resembled the typical vibronic splitting of a fluorescence spectrum. Upon further increasing the pump energy density, the 0-1 vibronic band became much more pronounced compared to the other vibronics. Furthermore the fluorescence spectrum collapsed into one single peak at 469 nm (2.64 eV) with a full width at half maximum of 4 nm.



**Figure 2.67** The width of the ASE peak as a function of the pump energy density for poly(indenofluorene) waveguides. The inset shows the sigmoidal function that was used to fit the data and to extract the threshold value of ASE onset.

The reason for the observed gain narrowing was waveguiding along the stripe shape excitation region leading to the amplification of light at the spectral position of the highest gain with most of the light being emitted from the ends of the stripe.<sup>68</sup> The coincidence of the ASE peak with the 0-1 transition of the fluorescence has frequently been observed in such experiments and can be explained by a quasi-four level vibronic system with the highest net gain and lowest threshold value at the position of the 0-1 vibronic.<sup>69, 70</sup>

To determine the threshold value for ASE, the width of the ASE band at 2.64 eV (469 nm) was extracted from a Gaussian fit to the ASE bands and plotted against the pump energy density in semilogarithmic fashion. Finally, the data was fitted to a sigmoidal relation (Figure 2.67) as described earlier by Salbeck et al. and the threshold value was extracted from the intersection of the upper line width limit with the tangent at the turning point of the sigmoidal curve.<sup>71</sup>

The value extracted by this method corresponds to a threshold value of 3  $\mu\text{J}/\text{cm}^2$  ( $\sim 375 \text{ W}/\text{cm}^2$ ) for the onset of ASE in polyindenofluorene thin films. The low threshold value was confirmed for several samples at different thickness.



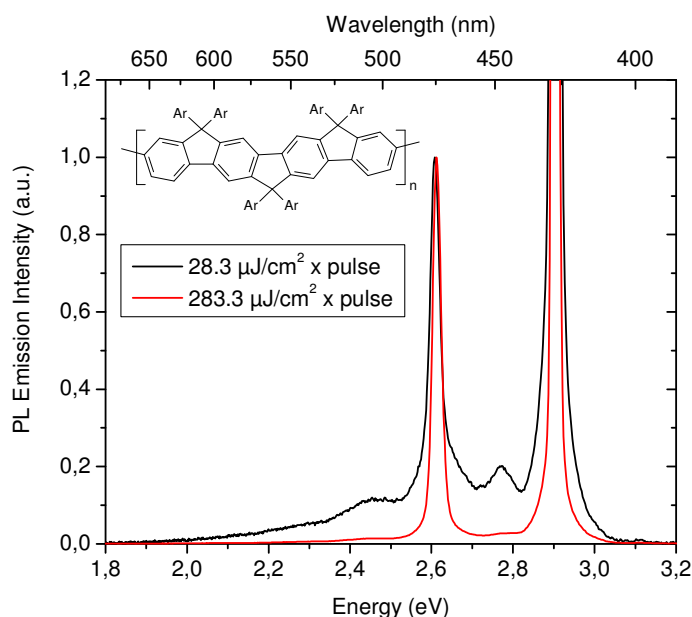


**Figure 2.68** Edge-detected PL-spectra of fully-arylated poly(tetraphenylene) at different pump energy densities. Inset shows polymer structure.

Applying the same method to the other polymer film waveguides, the influence of the monomer length (number of phenyl units), sidegroups (aryl-alkyl) and the presence of heteroatoms (carbazole moieties) on the ASE threshold value was studied. Figure 2.68 shows edge-detected PL-spectra of a thin film polymer waveguide of fully-arylated poly(tetraphenylene) at two different pump energy densities.

At relatively low pump energy densities the PL-spectrum resembles the shape of a typical fluorescence spectrum with a 0-0 transition and vibronic progressions. As the pump energy density was increased the PL-spectrum collapsed into one single peak at the position of the 0-1 transition, as observed for the poly(indenofluorene) waveguides.

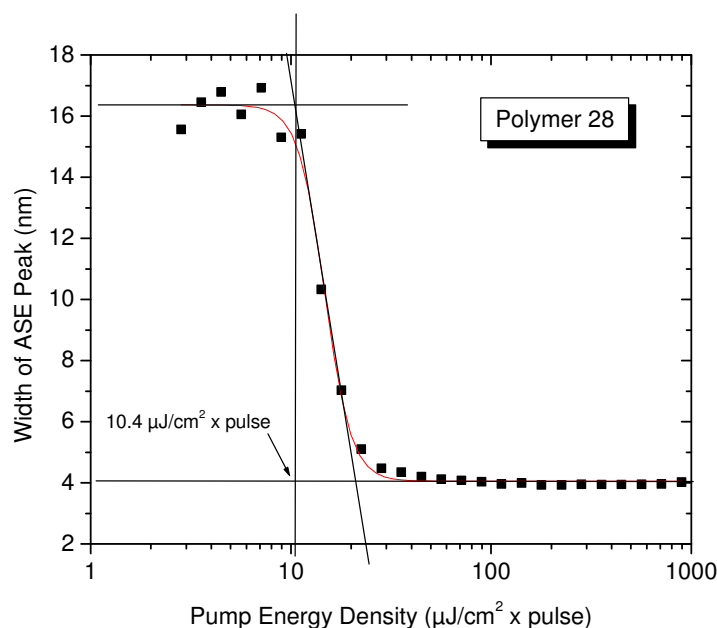


**Figure 2.69** The width of the ASE peak as a function of the pump energy density for fully-arylated poly(tetraphenylene) waveguides. A threshold value of  $10 \mu\text{J}/\text{cm}^2 \times \text{pulse}$  was extracted from the sigmoidal fit of the data.

Analysing the ASE peak width as a function of the pump energy density (Figure 2.69) showed a threshold value for the onset of ASE of  $10 \mu\text{J}/\text{cm}^2 \times \text{pulse}$ . This was around three times as high as observed in the case of poly(indenofluorene). Changing the substitution from aryl to alkyl at the middle carbon atom resulted in similar PL-spectra and ASE onset threshold values (Figure 2.70 and 2.71).

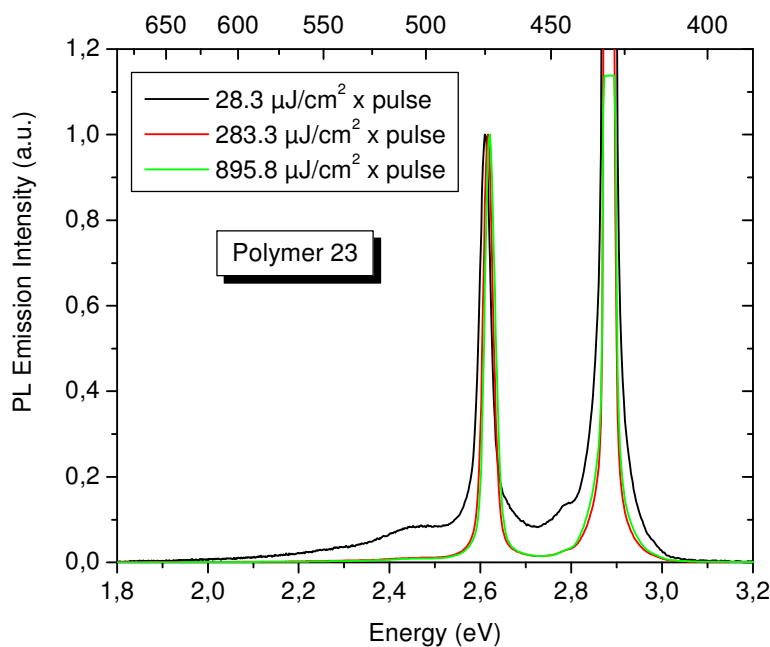


**Figure 2.70** Edge-detected PL-spectra of partially-arylated poly(ladder-type tetraphenylene) substituted with alkyl chains at the middle carbon atom at different pump energy densities.

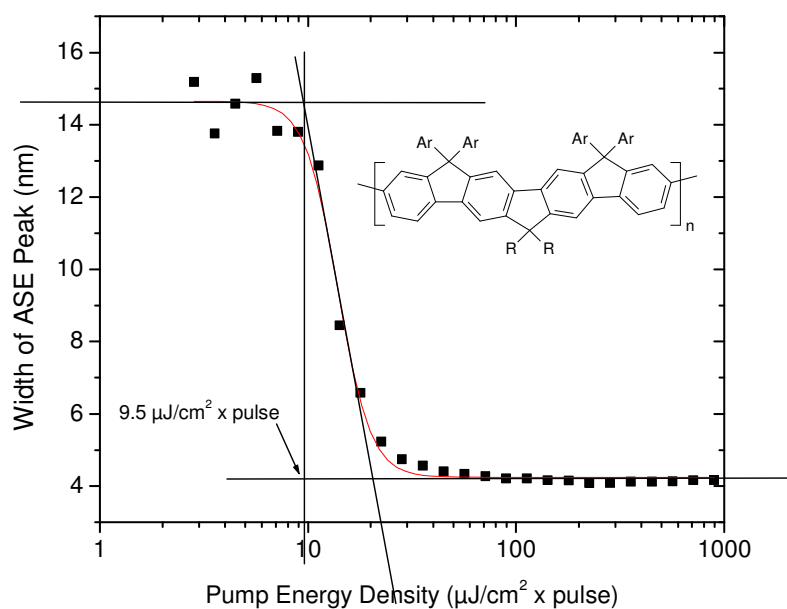


**Figure 2.71** The width of the ASE peak as a function of the pump energy density for partially alkyl-substituted poly(ladder-type tetraphenylene) thin film waveguides. A threshold value of  $9.5 \mu\text{J}/\text{cm}^2 \times \text{pulse}$  was extracted from the sigmoidal fit to the data.

Interestingly, the ASE onset threshold value increased by an order of magnitude when heteroatoms (carbazole moieties) were present in the monomeric unit. Figure 2.72 shows the edge-detected PL-spectra of carbazole-containing poly(ladder-type tetraphenylene) at different pump energy densities, whereas Figure 2.73 shows the ASE peak width as a function of the pump energy density.

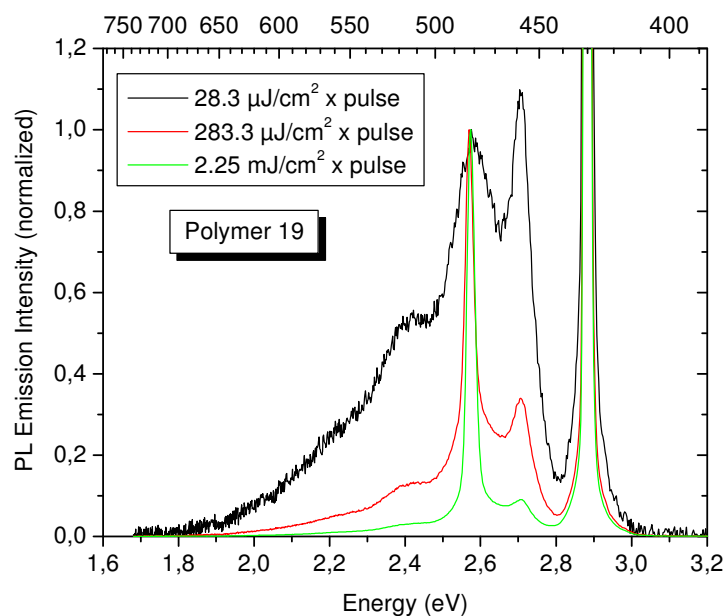


**Figure 2.72** Edge-detected PL-spectra of carbazole-containing poly(tetraphenylene) at different pump energy densities.

Clearly, the PL spectrum did not collapse entirely into one single peak even at high pump energy densities unlike the other materials.

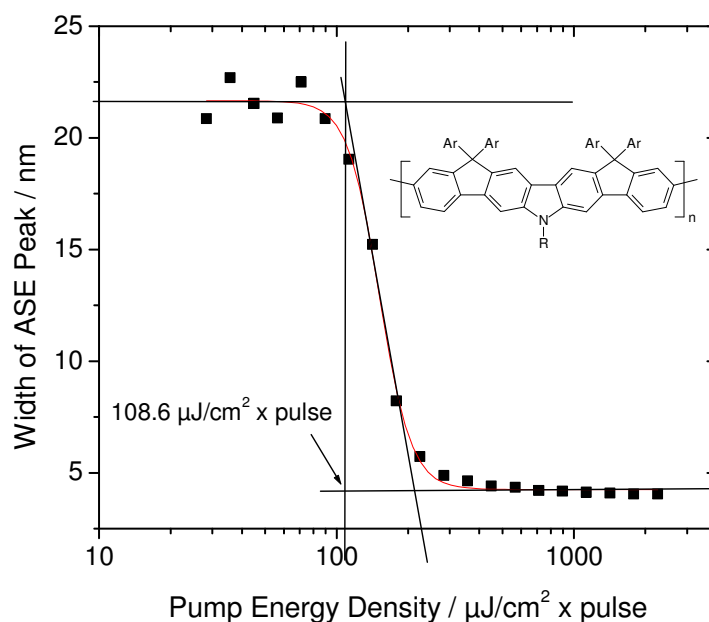


**Figure 2.73** The width of the ASE peak as a function of the pump energy density for carbazole-containing poly(tetraphenylene) thin film waveguides. A threshold value of  $108 \mu\text{J}/\text{cm}^2 \times \text{pulse}$  was extracted from the sigmoidal fit to the data.

Further increase of the monomer length by one phenyl ring going to the fully-arylated poly(pentaphenylene) resulted in a dramatic increase of the ASE spectra and onset threshold value. Figure 2.74 and 2.75 show the edge-emitted PL-spectra already at high pump energy densities.

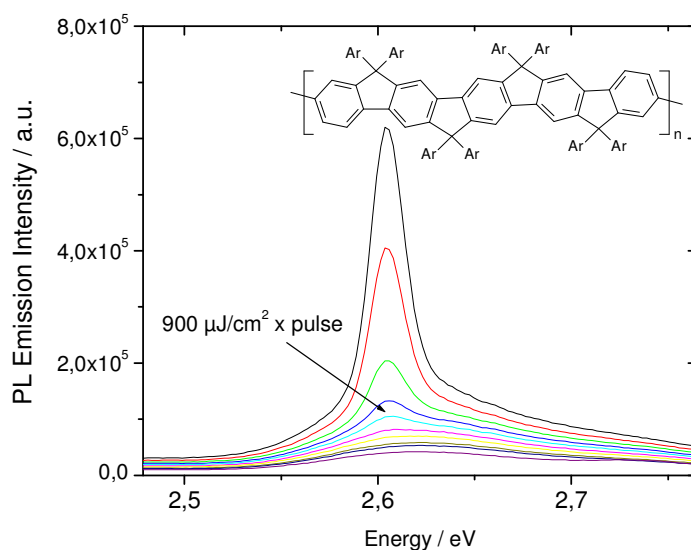


**Figure 2.74** Edge-emitted PL-spectra (region of the 0-1 transition) of fully-arylated poly(ladder-type pentaphenylene) at high pump energy densities.

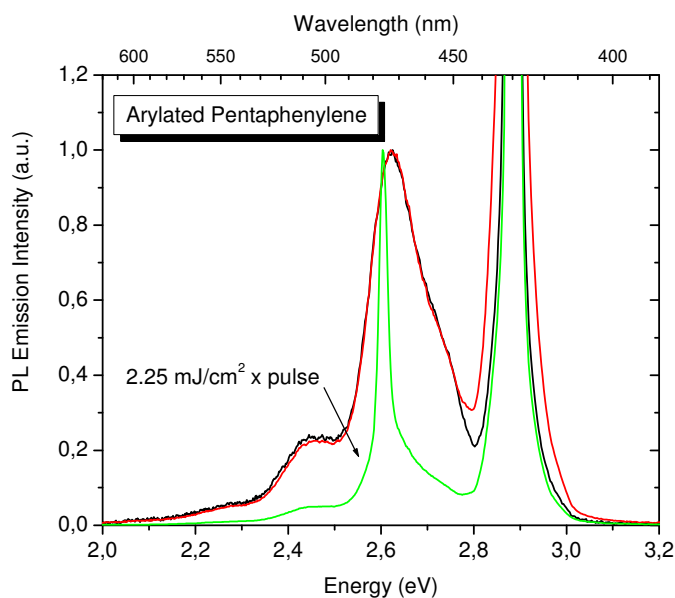


**Figure 2.75** Edge-emitted PL-spectra of fully-arylated poly(ladder-type pentaphenylene) thin film polymer waveguides at different pump energy density. Note that a high pump energy density has to be applied to see stimulated emission.

In conclusion it was shown that increasing the monomer length from three (indenofluorene) over four (tetraphenylene) to five (pentaphenylene) phenyl rings increases significantly the onset threshold value for the occurrence of amplified

spontaneous emission in thin film polymer waveguides. The reason for the dramatic increase of the ASE threshold value is not yet entirely understood since many parameters influence the ASE properties of a certain polymer. It may be, for instance, that excited state absorption caused by the excited singlet state itself, limits the applicability of a polymer as gain medium in slab waveguides.

The present results further demonstrate that not only the length of the monomer unit has an impact on the ASE properties of the polymer but also that the presence of heteroatoms changes dramatically the ASE threshold value by an order of magnitude as shown for polymer **19**. On the other hand the sidegroup substitution has only little effect on the ASE threshold value as was shown for poly(ladder-type tetraphenylene) by changing from aryl to alkyl substitution. In total, the investigated ladder-type materials are promising candidates for organic lasing due to their good oxidative stability and relatively low ASE onset threshold values.<sup>72-74</sup> Further experiments have to be conducted to unravel the influence of the chemical and electronic structure of the monomer on the ASE properties by studying excited state absorption, for instance, on thin film polymer waveguides.

### 2.11 Conclusions

A series of carbazole based semi-ladder-type polymers have been synthesized such as poly(ladder-type tetraphenylene), poly(ladder-type pentaphenylene) and poly(ladder-type hexaphenylene) and also for comparison all carbon-bridged poly(ladder-type tetraphenylene) were prepared. Photophysical studies were performed on all polymers which demonstrated a red-shift in the absorption and photoluminescence maximum with increasing benzene unit as well as on introduction of nitrogen bridge in the repeat unit. Nitrogen bridges in the polymer also enhance the aggregation effect particularly in solid-state. Electrochemical data recorded on thin films of these polymers revealed a decrease in the band gap with increasing number of nitrogen bridges and benzene unit. The nitrogen-bridged poly(ladder-type tetraphenylene) showed remarkable stability against oxidation. However, the all carbon-bridged poly(ladder-type tetraphenylene) showed only limited stability

towards oxidation. The 2D-WAXS studies on extruded fibres of nitrogen-bridged polymers demonstrated the effect of substituents as well as the nitrogen bridge in the repeat unit on the supramolecular organization of these polymers. Long alkyl side chains, which are branched close to the rigid conjugated building blocks, and too high “concentration” of aryl groups along the backbone and the attachment of these units on different backbone sides diminish the macroscopic order. Additionally, it revealed that the carbazole units can enhance the packing of conjugated polymers. Finally, these polymers were tested in various electronic devices such as polymer light emitting diodes, field effect transistor, solar cell and blue laser.

- (1) Polymer light emitting diode:** Polymer **19**, **23**, **28** and **52** were incorporated into PLED devices. All the polymers were blue emitters except polymer **23** which was found to be a blue-green emitter due to an emission maximum at 510 nm which probably originates from either an interface defect caused by low work function of the metal cathode or aggregation in the solid-state. Fully arylated poly(ladder-type tetraphenylene) **28** demonstrated good stability in PLED device compared to the aryl, alkyl poly(ladder-type tetraphenylene) **23** due to the fact that fully arylation at carbon bridges suppress the ketone defect as well as aggregation in solid-state. Polymer **23** and **52** displayed a peak around 570 nm upon heating the polymer film at 200 °C which was attributed to the ketone defect because of the presence of dialkyl-bridges in the polymer backbone. The Nitrogen-bridged polymer showed a lower electroluminescence onset voltage as compared to the all carbon-bridged polymer
- (2) Field effect Transistor:** Polymers **19**, **44**, **47**, and **52** were tested in FET devices. All polymers exhibited a charge carrier mobility between  $10^{-3}$  to  $10^{-4}$   $\text{cm}^2/\text{Vs}$ , among all, polymer **44** demonstrated the best hole mobility of  $6 \times 10^{-3}$   $\text{cm}^2/\text{Vs}$  with an on/off ratio of  $10^5$ . Polymer **47** showed good FET performance with moderate charge carrier mobility ( $5 \times 10^{-4}$   $\text{cm}^2/\text{Vs}$ ). The



drop of current at higher voltage for polymer **19** and **52**, are still unclear and under investigation.

- (3) **Solar cell:** Polymers **19**, **47** and **52** were incorporated in to solar cells as donor materials and PCBM or PDI was used as the acceptor material. These polymers demonstrated a good performance in solar cell with power conversion efficiency of 0.9 % wit PCBM and 1.32 % with PDI. Performance of polymer 47/PCBM was best among all polymers and it was correlated with the short lateral distance between chain also the long range order found in 2D-WAX studies.
- (4) **ASE experiment:** Polymer **19**, **23**, **28** were tested in ASE experiment. The results obtained from these experiments were compared with poly(indenofluorene) as well as with poly(ladder-type pentaphenylene). It was shown that increasing the monomer length from three (indenofluorene) over four (tetraphenylene) to five (pentaphenylene) phenyl rings increased significantly the onset threshold value for the occurrence of amplified spontaneous emission in thin film polymer waveguides. Side group substitution had only little effect on the ASE threshold value as shown for the poly(ladder-type tetraphenylene) by changing from aryl to alkyl substitution. Presence of heteroatoms such as nitrogen changed dramatically the ASE threshold value by an order of magnitude as shown for polymer **19**.

**2.12 References**

1. Scherf, U.; Müllen, K., The synthesis of ladder polymers. *Adv. Polym. Sci.* **1995**, 123, 1.
2. Wang, C.-S., *Trends Polym. Sci.(TRIP)* **1997**, 5, 138.
3. Scherf, U., *J. Mater. Chem.* **1999**, 9, (9), 1853.
4. Löffler, M.; Schlüter, A.-D.; Gessner, K.; Saenger, W.; Toussaint, J.-M.; Bredas, J.-L., *Angew. Chem., Int. Ed. Engl.* **1994**, 33 2209.
5. Overberger, C. G.; Moore, J. A., Ladder Polymer. *Adv. Polym. Sci.* **1970**, 7, 113.
6. Marvel, C. S.; Levesque, C. L., *J. Am. Chem. Soc.* **1938**, 60, 280.
7. Marvel, C. S.; corner, J. O.; Riddle, E. H., *J. Am. Chem. Soc.* **1942**, 64, 92.
8. vanDeussen, R. L., *J. Polym. Sci. B* **1966**, 4, 211.
9. vanDeussen, R. L.; Goins, O. K.; Sicree, A. J., *J. Polym. Sci. AI* **1968**, 6, 1777.
10. Arnold, F. E.; vanDdeussen, R. L., *Macromolecules* **1969**, 2, 479.
11. Arnold, F. E.; vanDeussen, R. L., *J. Appl. Polym. Sci.* **1971**, 15, 2035.
12. Agrawal, A. K.; Wang, C.-S.; Song, H. H., *Mater. Res. Soc. Symp. Proc.* **1994**, 328, 279.
13. Leopold, D. J.; Brown, I. M.; Sandreczki, T. C., *Synth. Met.* **1996**, 78, 67.
14. Jenekhe, S. A.; Tibbets, S. J., *J. Polym. Sci., Polym. Phys.* **1988**, 26, 201.
15. Stille, J. K.; Mainen, E. L.; Freeburger, M. E.; Harris, F. W., *Polym. Prep.* **1967**, 8, 244.
16. Stille, J. K.; Freeburger, M. E., *J. Polym. Sci. AI* **1968**, 6, 161.
17. Stille, J. K.; Mainen, E. L., *Macromolecules* **1968**, 1, 36.
18. Stille, J. K.; Mainen, E. L., *J. Polym. Sci. B* **1966**, 5, (39), 665.
19. Okada, M.; Marvel, C. S., *J. Polym. Sci. AI* **1968**, 6, 1259.
20. Wolf, R.; Okada, M.; Marvel, C. S., *J. Polym. Sci. AI* **1968**, 6, 1503.
21. Jadamus, H.; DeSchryver, F.; Dewinter, W.; Marvel, C. S., *J. Polym. Sci. AI* **1966**, 4, 2831.
22. Yu, L. P.; Dalton, L. R., *Synth. Met.* **1989**, 29, (1), E463.
23. Yu, L. P.; Dalton, L. R., *Macromolecules* **1990**, 23, (14), 3439.
24. McCullough, R. D., *Adv. Mater.* **1998**, 10, 93.
25. Schlüter, A.-D., *Acta Polym.* **1993**, 44, 59.
26. Scherf, U.; Müllen, K., *Makromol. Chem. Rapid Commun.* **1991**, 12, 489.
27. Lemmer, U.; Heun, S.; Mahrt, R. F.; Scherf, U.; Hopmeier, M.; Siegner, U.; Göbel, E. O.; Müllen, K.; Bässler, H., *Chem. Phys. Lett.* **1995**, 240, 373.
28. Graupner, W.; Eder, S.; Tasch, S.; Leising, G.; Lanzani, G.; Nisoli, M.; Silvestri, S. d.; Scherf, U., *J. Fluorescence* **1995**, 7, 195.
29. Stampfl, J.; Graupner, W.; Leising, G.; Scherf, U., *J. Lumin.* **1995**, 63, 117.
30. Tasch, S.; Niko, A.; Leising, G.; Scherf, U., *Appl. Phys. Lett.* **1996**, 68, 1090.
31. Patil, S.; Scherf, U.; Kadashchuk, A., *Adv. Funct. Mater.* **2003**, 13, 609.
32. Dierschke, F.; Grimsdale, A. C.; Müllen, K., *Macromol. Chem. Phys.* **2004**, 205, 1147.

33. Smith, K.; James, D. M.; Mistry, A. G.; Bye, M. R.; Faulkner, D. J., *Tetrahedron* **1992**, 48, (36), 7479-7488.
34. Carpino, L. A., *J. Org. Chem.* **1980**, 45, (21), 4250-4252.
35. Dierschke, F.; Grimsdale, A. C.; Müllen, K., *Synthesis-Stuttgart* **2003**, (16), 2470.
36. Jacob, J.; Sax, S.; Gaal, M.; List, E. J. W.; Grimsdale, A. C.; Müllen, K., *Macromolecules* **2005**, 38, (24), 9933.
37. Wang, H.; Uckert, F. P.; Kim, S. WO 2004072123, 26. Aug. 2004.
38. Jacob, J.; Zhang, J. Y.; Grimsdale, A. C.; Müllen, K.; Gaal, M.; List, E. J. W., *Macromolecules* **2003**, 36, (22), 8240.
39. Schindler, F.; Jacob, J.; Grimsdale, A. C.; Scherf, U.; Müllen, K.; Lupton, J. M.; Feldmann, J., *Angew. Chem., Int. Ed. Engl.* **2005**, 44, (10), 1520.
40. Xu, T.; Lu, R.; Jin, M.; Qiu, X.; Xue, P.; Bao, C.; Zhao, Y., *Tetrahedron Lett.* **2005**, 46, 6883.
41. Yang, L.; Feng, J.-K.; Ren, A.-M.; Sun, J.-Z., *Polymer* **2006**, 47, 1397.
42. Jacob, J.; Sax, S.; Piok, T.; List, E. J. W.; Grimsdale, A. C.; Müllen, K., *J. Am. Chem. Soc.* **2004**, 126, (22), 6987.
43. Keivanidis, P. E.; Jacob, J.; Oldridge, L.; Sonar, P.; Carbonnier, B.; Balushev, S.; Grimsdale, A. C.; Müllen, K.; Wegner, G., *Chem. Phys. Chem.* **2005**, 6, (8), 1650.
44. List, E. J. W.; Guentner, R.; de Freitas, P. S.; Scherf, U., *Adv. Mater.* **2002**, 14, 374.
45. Grimme, J.; Kreyenschmidt, M.; Uckert, F.; Müllen, K.; Scherf, U., *Adv. Mater.* **1995**, 7, (3), 292.
46. Wong, K.-T.; Chi, L.-C.; Huang, S.-C.; Liao, Y.-L.; Liu, Y.-H.; Wang, Y., *Org. Lett.* **2006**, 8, (22), 5029-5032.
47. Köhler, G.; Rechthaler, *Pure & Appl. Chem.* **1993**, 65, (8), 1647.
48. Suppan, P., *J. Photochem. Photobiol. Chem.* **1990**, 50, (293).
49. Köhler, G.; Wolschann, P.; Rotkiewicz, K., *Proc. Indian Acad. Sci. (Chem. Sci.)* **1992**, 104, 197.
50. Janietz, S.; Bradley, D.; Grell, M.; Giebeler, C.; Inbasekaran, M.; Woo, E., *Appl. Phys. Lett.* **1998**, 73, 2453.
51. Pisula, W.; Kastler, M.; Wasserfallen, D.; Mondeshki, M.; Piris, J.; Schnell, I.; Müllen, K., *Chem. Mater.* **2006**, 18, (16), 3634.
52. Piris, J.; Debije, M. G.; Stutzmann, N.; Laursen, B. W.; Pisula, W.; Watson, M. D.; Bjornholm, T.; Müllen, K.; Warman, J. M., *Adv. Funct. Mater.* **2004**, 14, (11), 1053.
53. Mauthner, G.; Collon, M.; List, E. J. W.; Wenzl, F. P.; Bouguettaya, M.; Reynolds, J. R., *J. Appl. Phys.* **2005**, 97, 635081.
54. Gamerith, S.; Nothofer, H.-G.; Scherf, U.; List, E. J. W., **2004**, 43, L891.
55. Omhori, Y.; Uchida, M.; Muro, K.; Yoshino, K., *J. Appl. Phys.* **1991**, 11B, L1941.
56. Li, J. L.; Dierschke, F.; Wu, J. S.; Grimsdale, A. C.; Müllen, K., *J. Mater. Chem.* **2006**, 16, (1), 96.
57. Chen, Z. K.; Huang, W.; Wang, L. H.; Kang, E. T.; Chen, B. J.; Lee, C. S.; Lee, S. T., *Macromolecules* **2000**, 33, (24), 9015.

58. Yamamoto, T.; Lee, B. L., *Macromolecules* **2002**, 35, 2993.
59. Egbe, D. A. M.; Nguyen, L. H.; Hoppe, H.; Mühlbacher, D.; Sariciftci, N. S., *Macromol. Rapid Commun.* **2005**, 26, 1389.
60. Sariciftci, N. S.; Smilowitz, L.; Heeger, A. J.; Wudl, F., *Science* **1992**, 258, (5087), 1474.
61. Frankevich, E.; Maruyama, Y.; Ogata, H., *Chem. Phys. Lett.* **1993**, 214, (1), 39-44.
62. Lee, C. H.; Yu, G.; Moses, D.; Pakbaz, K.; Zhang, C.; Sariciftci, N. S.; Heeger, A. J.; Wudl, F., *Phys. Rev. B* **1993**, 48, (20), 15425-15433.
63. Brabec, C. J.; Zerza, G.; Cerullo, G.; De Silvestri, S.; Luzzati, S.; Hummelen, J. C.; Sariciftci, S., *Chem. Phys. Lett.* **2001**, 340, (3-4), 232.
64. Wienk, M. M.; Kroon, J. M.; Verhees, W. J. H.; Knol, J.; Hummelen, J. C.; van Hal, P. A.; Janssen, R. A. J., *Angewandte Chemie-International Edition* **2003**, 42, (29), 3371-3375.
65. Chirvase, D.; Chiguvare, Z.; Knipper, A.; Parisi, J.; Dyakonov, V.; Hummelen, J. C., *Synth. Met.* **2003**, 138, (1-2), 299-304.
66. Laquai, F.; Keivanidis, P. E.; Balushev, S.; Jacob, J.; Müllen, K.; Wegner, G., *Appl. Phys. Lett.* **2005**, 87, (26), *In press*.
67. Keivanidis, P. E.; Jacob, J.; Oldridge, L.; Sonar, P.; Carbonnier, B.; Balushev, S.; Grimsdale, A. C.; Müllen, K.; Wegner, G., *Chemphyschem* **2005**, 6, (8), 1650.
68. McGehee, M. D.; Gupta, R.; Veenstra, S.; Miller, E. K.; Diaz-Garcia, M. A.; Heeger, A. J., *Physical Review B* **1998**, 58, (11), 7035.
69. Schweitzer, B.; Wegmann, G.; Giessen, H.; Hertel, D.; Bassler, H.; Mahrt, R. F.; Scherf, U.; Müllen, K., *Appl. Phys. Lett.* **1998**, 72, (23), 2933.
70. Wegmann, G.; Schweitzer, B.; Hopmeier, M.; Oestreich, M.; Giessen, H.; Mahrt, R. F., *Phys. Chem. Chem. Phys.* **1999**, 1, (8), 1795.
71. Salbeck, J.; Schörner, M.; Fuhrmann, T., *Thin Solid Films* **2002**, 417, (1-2), 20-25.
72. Wegmann, G.; Schweitzer, B.; Hertel, D.; Giessen, H.; Oestreich, M.; Scherf, U.; Müllen, K.; Mahrt, R. F., *Chem. Phys. Lett.* **1999**, 312, (5-6), 376-384.
73. Wegmann, G.; Schweitzer, B.; Hopmeier, M.; Oestreich, M.; Giessen, H.; Mahrt, R. F., *Phys. Chem. Chem. Phys.* **1999**, 1, (8), 1795-1800.
74. Schweitzer, B.; Wegmann, G.; Hertel, D.; Mahrt, R. F.; Bassler, H.; Uckert, F.; Scherf, U.; Müllen, K., *Phys. Rev. B* **1999**, 59, (6), 4112-4118.

## Chapter 3

### Carbazole and thiophene fused oligomers

In this chapter, synthesis and characterization of solution as well as melt processable carbazole-thiophene fused oligomers are presented. 2D-WAXS was performed on extruded samples of oligomers to study the supramolecular organization in the solid-state. The polarized optical microscopy was also done on the film obtained from the melt to study the molecular organization in film. The oligomers were incorporated in the FET devices and their performances are discussed.

#### 3.1 Introduction

A promising trend which has emerged in recent years is the use of well defined oligomers as model compounds for their corresponding polymers. Soluble conjugated polymers are prepared using bifunctional monomers and are typically polydisperse and may have unreacted functional groups at the chain ends unless suitable end capping reagents are used during synthesis. The problems of variable molecular weight and molecular weight distributions (polydispersity) between different polymers, or even between two samples of the same polymer, make systematic comparisons of different polymers difficult. As a result, a study of well-defined oligomers offers the best route to determine the relationship between structural features and electronic properties. Conjugated oligomers have precisely defined chemical structures, they are monodisperse and can be obtained in high purity. Currently, high performances OFETs can be fabricated based on pentacene and fused oligomers. The mobility can be about  $1 \text{ cm}^2\text{V}^{-1}\text{s}^{-1}$  with an ON/OFF ratio of  $10^8$ .<sup>1</sup> For most practical purposes, this value is sufficient. However, these molecules are not soluble in any solvent so cannot be solution processed and one has to use vapor deposition techniques which require high vacuum and temperature and cannot be used for large area applications. One solution to this problem is the synthesis of small molecules having enough alkyl chain on the backbone so that they can be solution or melt processed and has the ability to form thin films like polymers

as well as retain the high ordered structure characteristics of small molecules. Both carbazole and thiophene are well known p-type materials suitable for use in electronic devices such as solar cell and organic field effect transistors (OFETs).<sup>2,3</sup> The introduction of planarity in the molecule facilitates  $\pi$ - $\pi$  stacking between the molecules, and could result in the formation of materials that exhibit high field effect mobility since the macroscopic charge transport properties of organic semiconducting materials depend mainly on the efficiency of the inter-chain charge hopping mechanism. Hence a control of inter-chain packing is thus vital in optimizing charge carrier mobilities.<sup>4-6</sup> The best way to introduce planarity is the ladderization of molecules using Friedal Craft type reactions to produce five membered bridges or McMurry type of reaction to obtain six membered bridges.<sup>7,8</sup> Therefore, in the present work soluble ladderized oligomers based on thiophene and carbazole with different end group were made (shown in Figure 3.1) and tested in OFET devices.

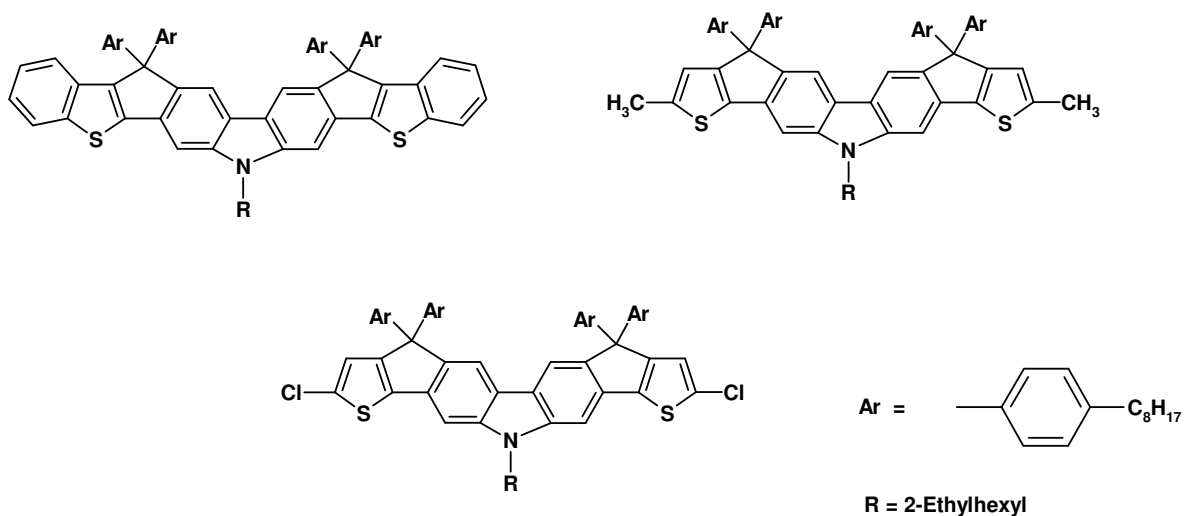
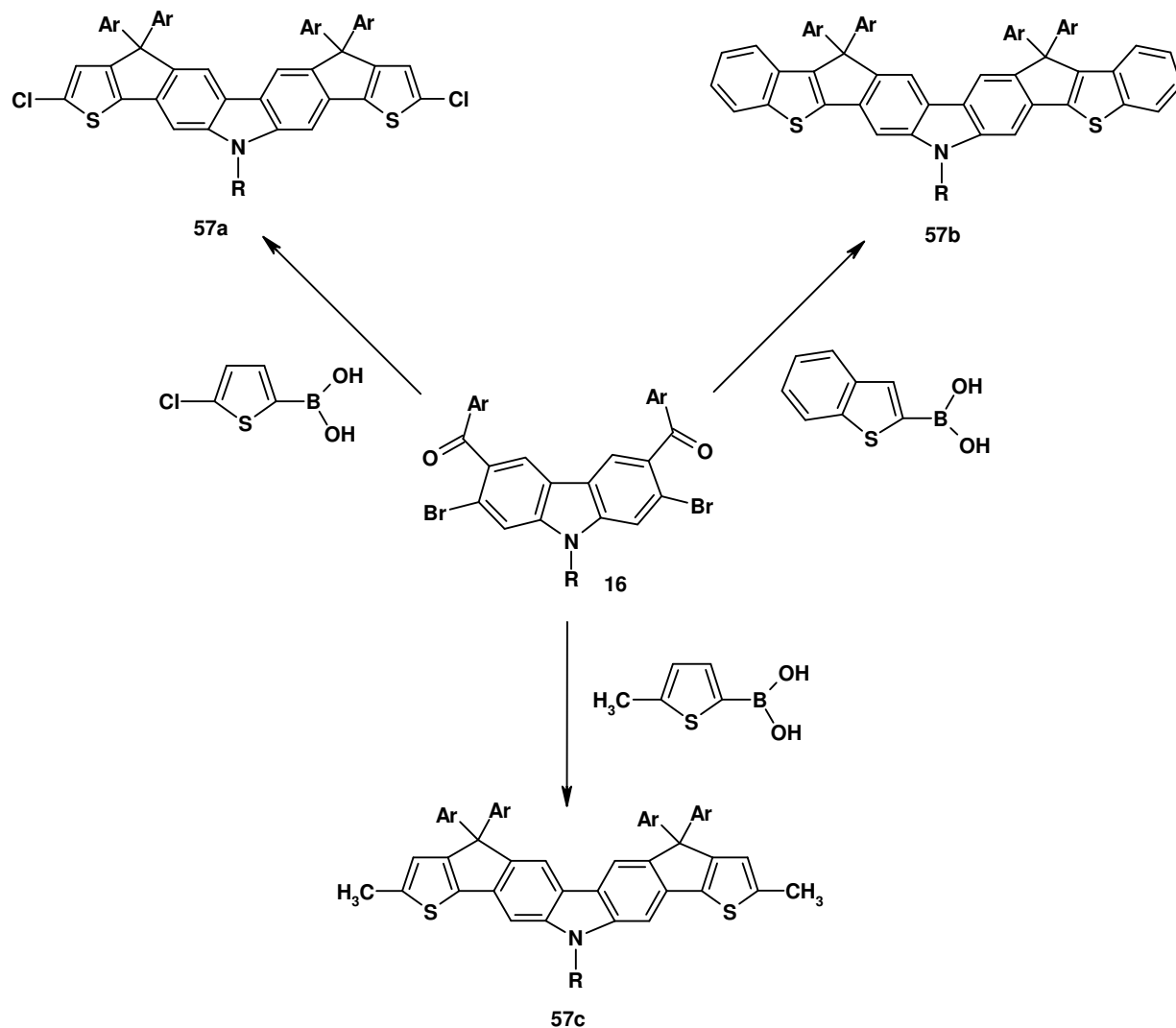


**Figure 3.1.** Fused carbazole-thiophene molecules

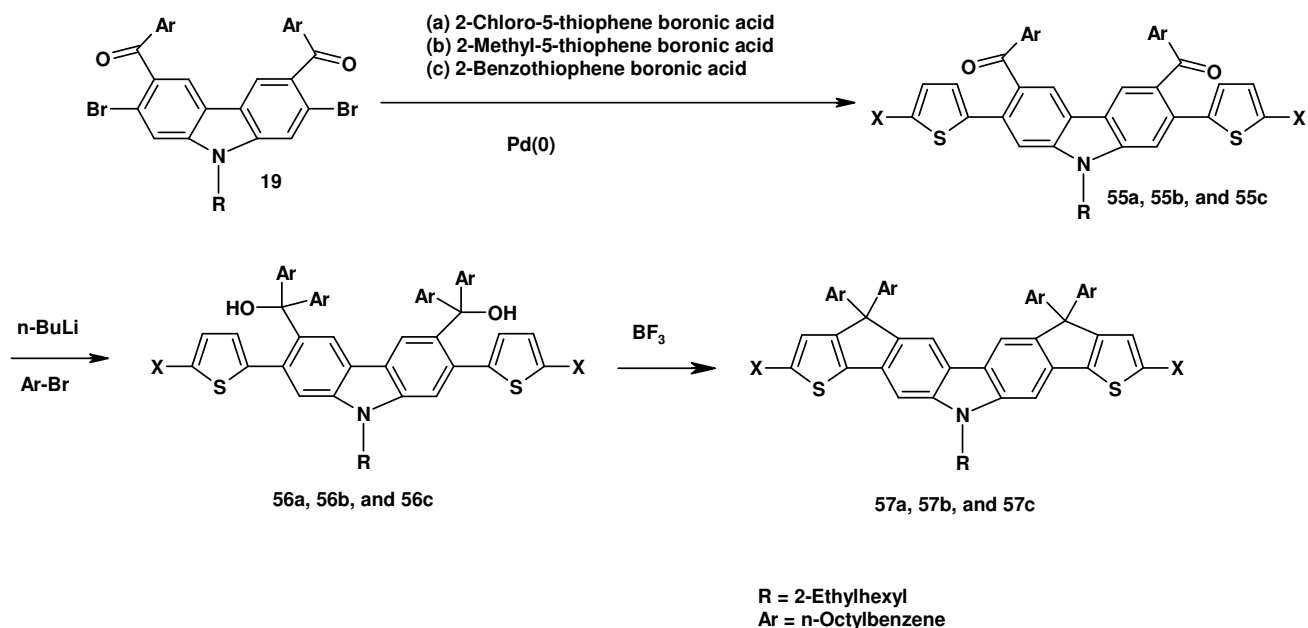
### 3.2 Synthesis and optical properties

Synthesis of carbazole-thiophene fused oligomers with different end groups starting from the Suzuki coupling of the common intermediate 2,7-Dibromo-N-(2-ethylhexyl)-3,6-bis(4-octylbenzoyl)carbazole (**16**) with different thiophene derivatives are depicted in Scheme 3.1.



**Scheme 3.1** Synthetic route to carbazole-thiophene oligomers

Scheme 3.2 presents the synthesis of oligomers **57a**, **57b**, and **57c** with different end groups. Dibromocarbazole **16** was coupled with two equivalents of 2-chloro-5-thiophene boronic acid, 2-methyl-5-thiophene boronic acid, and 2-benzothiophene boronic acid in the presence of  $\text{Pd}(\text{PPh}_3)_4$  as catalyst to generate the diketones **55a**, **55b**, and **55c** in 94 %, 88 % and 81 % yield respectively. Treatment with a slight excess of 4-octylphenyl lithium produced the corresponding diols **56a**, **56b**, and **56c** which upon ring closure with  $\text{BF}_3$ -etherate gave the carbazole-thiophene fused oligomers **57a**, **57b**, and **57c** in 55 % , 64 %, and 79 % combined yield.



**Scheme 3.2** Synthesis of oligomers **57a**, **57b** and **57c**

Figure 3.2 depicts the absorption spectra of oligomers **57a**, **57b**, and **57c**. Compound **57a** with a methyl group at both the end exhibited an absorption maximum at 400 nm with a shoulder at 377 nm.

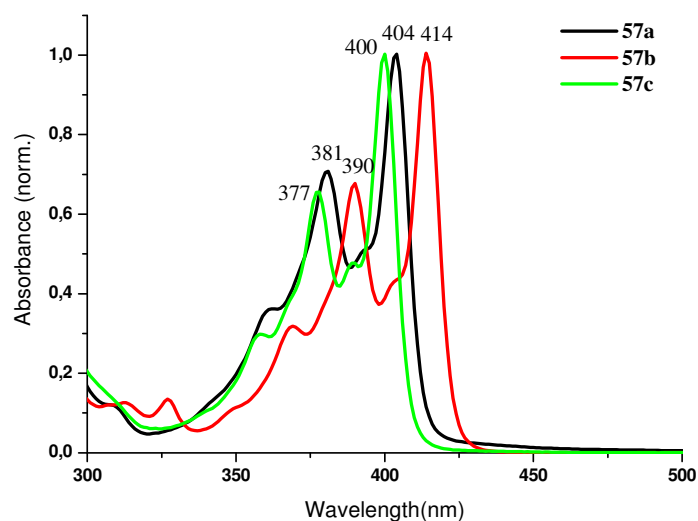


**Figure 3.2** Absorption spectra of carbazole-thiophene oligomers **57a**, **57b** and **57c**



Similarly, oligomer **57b** displayed an absorption maximum at 404 nm with a high energy band at 381 nm. This was anticipated since the chloro group is a better electron donating group than methyl group. Oligomer **57c** showed the most red-shift in absorption maximum at 414 nm with a shoulder at 390 nm due to the additional extension of conjugation by fused benzene ring at both sides. All oligomers exhibited well resolved absorption spectra, which is a characteristic of ladder-type molecules. Figure 3.3 presents the photoluminescence spectra of oligomers **57a**, **57b**, and **57c**. PL spectra demonstrated similar pattern as absorption maximum for emission maximum which is at 429 nm for **57c**, 433 nm for **57a** and 445 nm for **57b**.

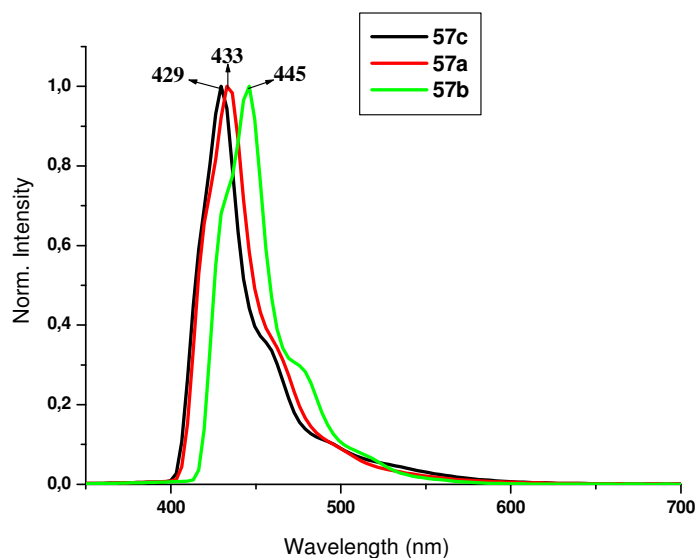


**Figure 3.3** Photoluminescence spectra of oligomers **57a**, **57b** and **57c**

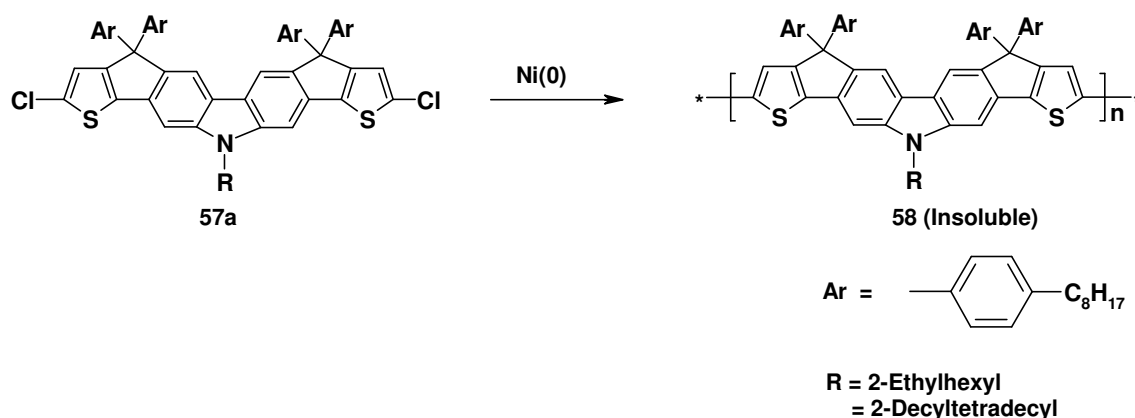
However, unlike the absorption spectra, only small vibronic splitting was observed in the photoluminescence spectra. The Stokes shift for both oligomers **57a** and **57c** was 29 nm which revealed that the end group had no effect but in case of **57b**, the Stokes shift was 31 nm which was 2 nm higher than the other two.

Table 3.1 outlines the photophysical properties of compounds **57a**, **57b** and **57c**.

**Table 3.1** Photophysical properties of oligomers **57a**, **57b** and **57c**.

Carbazole-thiophene oligomers	Absorption maximum(nm)	Emission maximum (nm)	Stokes shift (nm)
<b>57a</b>	404	433	29
<b>57b</b>	414	445	31
<b>57c</b>	400	429	29

In a further attempt, the monomer **57a** with a chloro group at the end was polymerized by Yamamoto-type polycondensation as depicted in Scheme 3.3.

**Scheme 3.3** Attempt to synthesize polymer **58**

However, all attempts to make polymer **58** failed even with the dove tail alkyl chain (2-decyltetradecyl) at nitrogen. After polymerization, only a mixture of dimer and trimer were obtained. This may be because of the very strong inter molecular packing between the oligomers (dimer and trimer) formed during the polymerization which precipitated out of the solution and did not react further to give polymers. Even the dove alkyl was not successful in keeping these oligomers inside the solution. Increasing the reaction temperature to 100 °C or dilution of the reactants did not help either.

### 3.3 Two-dimensional wide-angle X-ray scattering (2D-WAXS) and polarized optical microscopic (POM) studies on oligomers.

This study was performed together with Dr. Wojciech Pisula at Max-Planck Institute for Polymer Research.

To correlate the supramolecular organization of the oligomers **57a**, **57b**, **57c**, and **19** (nitrogen-bridged ladder-type hexaphenylene was also studied together with carbazole-thiophene fused oligomers) at different temperatures, first the thermal behavior was determined by using differential scanning calorimetry (DSC). All compounds **57a**, **57b**, **57c**, and **19** demonstrated only one endothermic transition upon heating, indicating a transition from the solid to the isotropic phase, at temperatures depending on the chemical structure of the molecules. The isotropization temperature shifted from 200 °C for **57a** to 250 °C for **19** suggesting an influence of the substitution and mainly the length of the rigid core. Figure 3.4 shows the DSC traces at a scanning rate of 10 °C/min for all

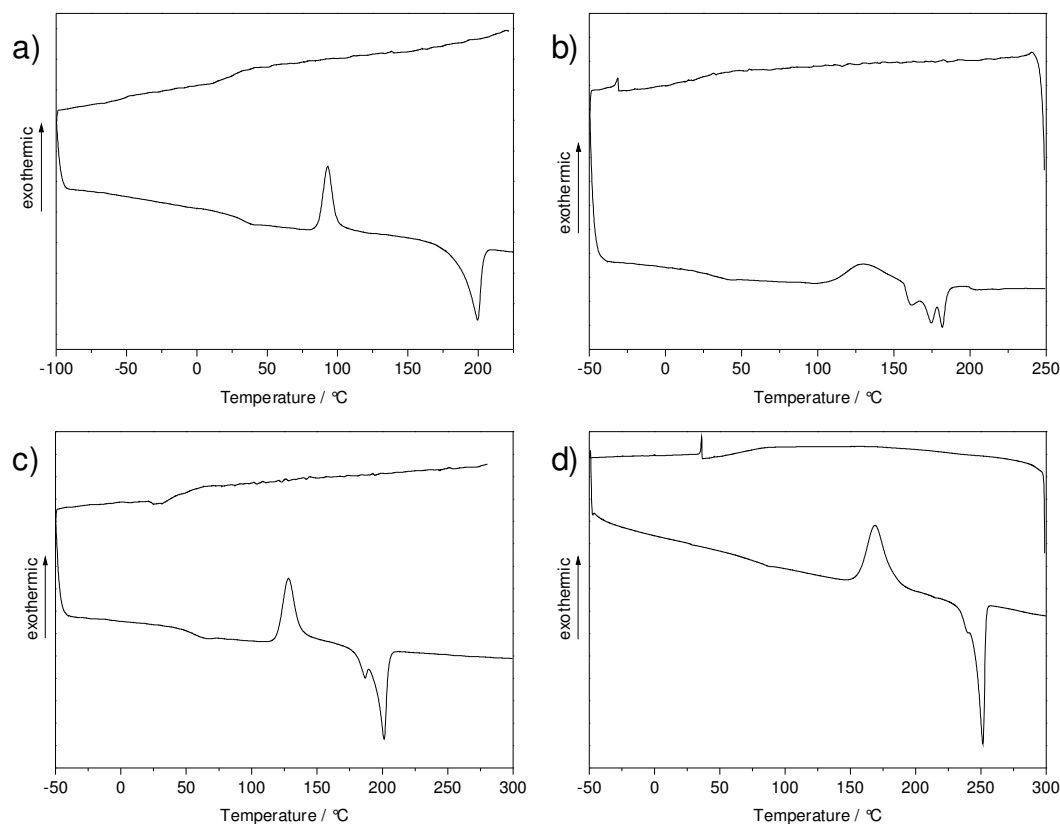


**Figure 3.4** DSC traces at 10 °C/min of a) **57a**, b) **57c**, c) **57b** and d) **19**

the four oligomers. Surprisingly, during cooling at the same rate no phase transition was observed, whereas at the second heating run prior to the endothermic peak, which was related to the isotropization temperature, an exothermic transition appeared with an

identical enthalpy value as the melting point. The phase transition temperatures and the corresponding enthalpy values of the four oligomers are given in Table 3.2. This endothermic peak was attributed to a supercooling of the sample during a too rapid cooling during which the crystallization was suppressed as confirmed by the absence of the crystallization peak. This phenomenon is well discussed for thermoplastic polymers.<sup>9</sup>  
<sup>10</sup> During the second heating run, the sample coldcrystallized, during which partial melting, reorganization and remelting occurred, leading to the endothermic and exothermic peaks.

**Table 3.2** Temperatures and enthalpy of the endothermic melting point and the exothermic coldcrystallization

<b>Compound</b>	<b>Endothermic Ti</b>	<b>Exothermic transition</b>
<b>57a</b>	199 °C (18.80 J/g )	93 °C (11.65 J/g )
<b>57b</b>	201 °C (25.33 J/g)	128 °C (25.20 J/g)
<b>57c</b>	182 °C (15.31 J/g)	130 °C (15.71 J/g)
<b>19</b>	252 °C (30.61 J/g)	169 °C (30.84 J/g)

The supramolecular organization on the macroscopic level was investigated on a filament extruded sample by using two-dimensional wide-angle X-ray scattering (2D-WAXS). The method for the sample preparation is explained in detail in chapter 2 (Section 6). All compounds **57a**, **57b**, **57c**, and **19** were extruded at temperatures approximately 20 °C below their isotropization temperature, at which the material became deformable enough to achieve a suitable macroscopic alignment by the shear forces during extrusion. The filaments were positioned vertically towards the 2D detector. Figure 3.5 shows the X-ray pattern of **57a** at different temperatures to verify no change of the structure within the solid-state at different temperatures. It was possible to

clearly distinguish between equatorial and meridional reflections. In both cases, the high intensity and sharpness evidently indicated a well-aligned supramolecular organization. At room temperature, the small-angle equatorial scattering intensities implied a uniaxial orientation of the **57a** oligomers with their longer molecular axis along the shearing direction and therefore along the filament axis (Figure 3.5a).

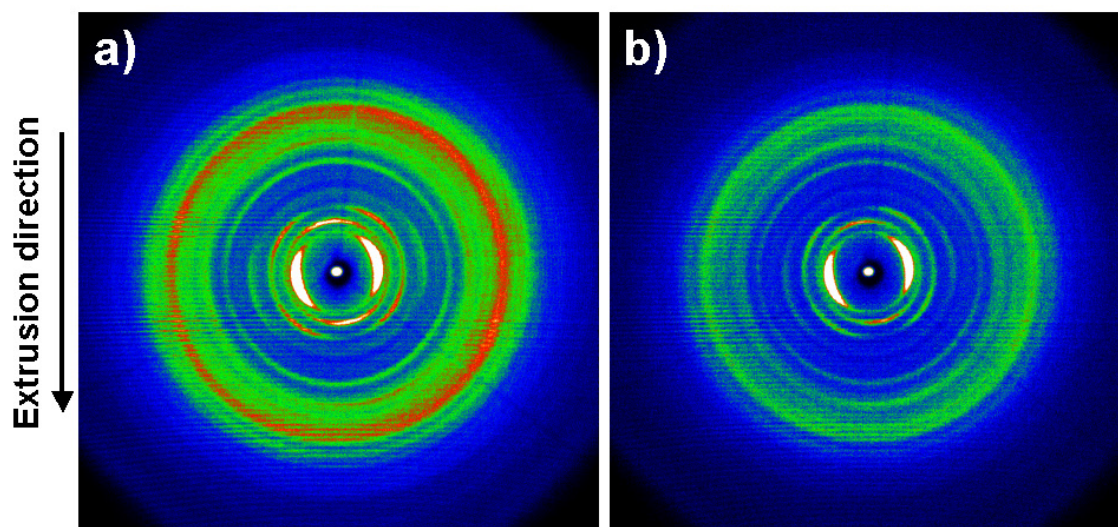


**Figure 3.5** 2D-WAXS patterns of an extruded filament of **57a** at a) room temperature and b) 150 °C.

Furthermore, these reflections corresponded at a period of 1.7 nm, which was attributed to the lateral distance between the oligomer molecules and therefore also between lamellae. This distance was determined by the length, bulkiness and density of the substituents. The meridional reflections at a distance of 1.4 nm were related to the repetition of the molecules and were in a good agreement with their length along the longer molecular axis. Further meridional reflections were assigned to higher order intensities which indicated once again the pronounced macroscopic order in the extruded sample. The strong anisotropic reflection corresponding to a distance of 0.45 nm of the alkyl side chains suggested high crystallinity for the compound. A higher crystallinity can be achieved by strong flexibility of the single building blocks which allow the aliphatic substituents to crystallize in the molecular periphery contributing to the overall

crystallinity of the compound. Crystalline and well ordered alkyl side chains were recently proven in well aligned HBC films.<sup>11, 12</sup> In this case, the crystalline side chains were rather disordered resulting in the anisotropic reflections. Heating the sample to 150 °C did not lead to a change in the X-ray scattering pattern (Figure 3.5b). The reflections remained at identical positions, however, slight change in the scattering intensity is observed probably due to a slight increase in the molecular dynamics at higher temperatures. After cooling back to room temperature, no annealing effect as well as no improvement in the order was observed. This confirms the DSC results which showed only one phase transition to the isotropic phase, and no additional solid-state phases. Identical results were obtained for the other oligomers, **57b**, **57c**, and **19**.

The influence of the endcapping group by changing the chloro to a methyl group was investigated in the next step. The compound **57c** was prepared in the same way as **57a** and was studied only at room temperature. The 2D X-ray pattern indicated also a pronounced order and a well-aligned structure for **57c** (Figure 3.6). The equatorial reflections revealed a lamellar distance of 1.8 nm which was slightly larger than observed for **57a**. Since both compounds had a similar chemical design, the meridional reflections, which were related to the length of the oligomers of 1.4 nm, were at the same positions. However, in contrast to **57a**, the compound **57c** revealed a distinct reflection in the equatorial wide-angle range corresponding to the  $\pi$ -stacking distance of 0.4 nm, which could not be observed for **57a**. Furthermore, the reflections attributed to the alkyl side chains were less anisotropic indicating preferential orientation of the substituents in the case of **57c**. This was additionally confirmed by the strong meridional wide-angle reflections which were positioned in the alkyl correlation range of 0.45 nm. A structural comparison between **57a** and **57c** obviously indicates an influence of a slight change of the substitution pattern not only on the supramolecular organization, but on the order and crystallinity.

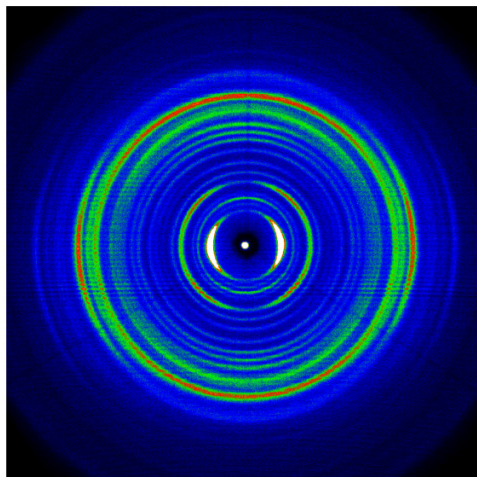


**Figure 3.6** 2D-WAXS pattern of an extruded filament of **57c** at room temperature.

Compound **57b** is the only example in this study showed an effect of the annealing at higher temperatures on the supramolecular order. Oligomer **57b** was extruded under the same conditions as the oligomers described above. Figure 3.7a shows the 2D X-ray pattern at room temperature directly after the extrusion. The appearing reflections were of weak intensity and broad suggesting a poor order on the macroscopic level. Despite the poor order, the supramolecular structures were well-aligned as implied by the distinct equatorial small-angle reflections. After annealing at 150 °C, the X-ray pattern was taken again at room temperature, which changed significantly. Reflections with a much higher intensity emerged suggesting a considerable improvement in the order (Figure 3.7b). The equatorial small-angle reflections were assigned to a lateral oligomer distance as well as a distance between lamellae of 2.64 nm. Surprisingly, the positions of the equatorial reflections could be only fitted to a hexagonal arrangement as shown in the plot in Figure 3.7c, which was in contrast to the other investigated oligomers. The meridional reflection corresponding to the repeating distance of 1.3 nm between oligomers was in good agreement with the molecular architecture of **57b**. Identical to **57a** and **57c**, also for compound **57b**, a broad and strong reflection attributed to the alkyl side chains was observed. The intensity of this reflection indicated a favored orientation of the substituents in the periphery between the lamellae consisting of the rigid aromatic rods. A correlation between the chemical structure and the supramolecular

organization in relation to the other oligomers was difficult in this case. Following the conclusions from the last paragraph, one might expect a much better order in comparison to **57c**. However, the supramolecular order was even decreased and only a post-treatment by annealing resulted in a comparable order to **57a**.

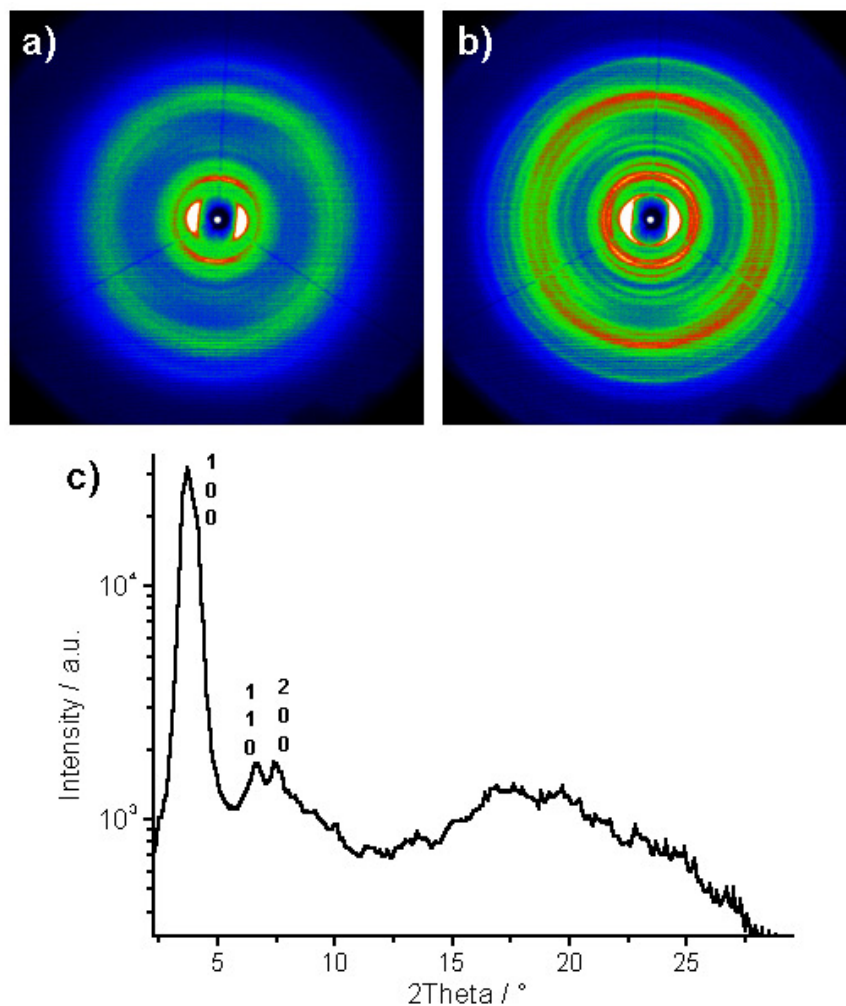


**Figure 3.7** 2D-WAXS patterns of an extruded filament of **57b** at room temperature a) before and b) after annealing. Figure c) shows the equatorial scattering intensity as a function of the scattering angle. The Miller's indexes indicate a hexagonal fit of the positions of the reflections.

As another example, a longer oligomer consisting of only carbazole units **19** and endcapped by chloro atoms was investigated. The 2D X-ray pattern suggested a well-aligned and highly ordered supramolecular structure (Figure 3.8). The distance of 1.44



nm between lamellae, indicated by the small-angle equatorial reflections, was independent of the oligomer length. On the other hand, only the meridional reflection was now positioned at smaller angles, and related to a period of 2.3 nm which was in good accordance with the chemical structure of the molecule. As already observed for **57c**, the equatorial wide-angle reflections were characteristic for a  $\pi$ -stacking distance of 0.36 nm between stacked oligomers. The maximum intensity of the alkyl correlation wide-angle reflection at the meridional axis of the pattern suggested once again in this case a probable preferred orientation of the side chains.

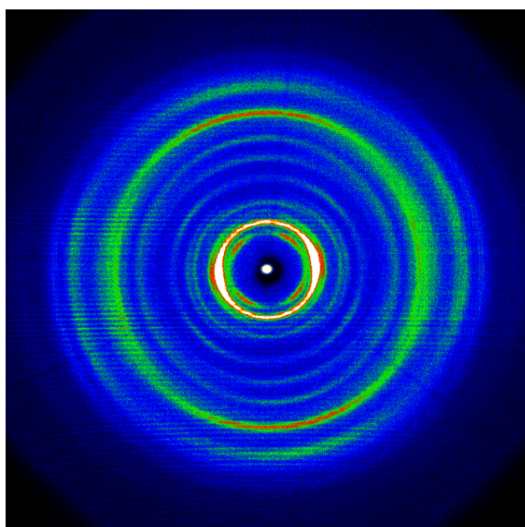


**Figure 3.8** 2D-WAXS pattern of an extruded filament of **19** at room temperature.

It is important to raise the question how all oligomers can pack, despite substituted by the bulky aryl groups. Figure 3.9a schematically illustrate the configuration and packing in oligomer **19**. It is most probable that the aryl groups rotated out-of-plane towards the rigid oligomer rod increasing their steric demand. Therefore, the only possibility for the molecules to interact and to stack is by flipping of the oligomers, so that the aryl groups of neighboring molecules point to opposite directions and fill together with the alkyl side chains in the lamellae periphery. One can conclude that the aryl groups, being attached at one side of an aromatic rigid molecule, influence the solubility and the thermal behavior, but do not hinder the stacking of molecules. Figure 3.9b shows the arrangement of the molecules into the lamellae organization provoked by

a nanophase separation between the alkyl chains and the aromatic rods. The distance between lamellae was simply determined by the length of the side chains. In all investigated cases, the oligomers oriented along their molecules axis as well as in the alignment direction.

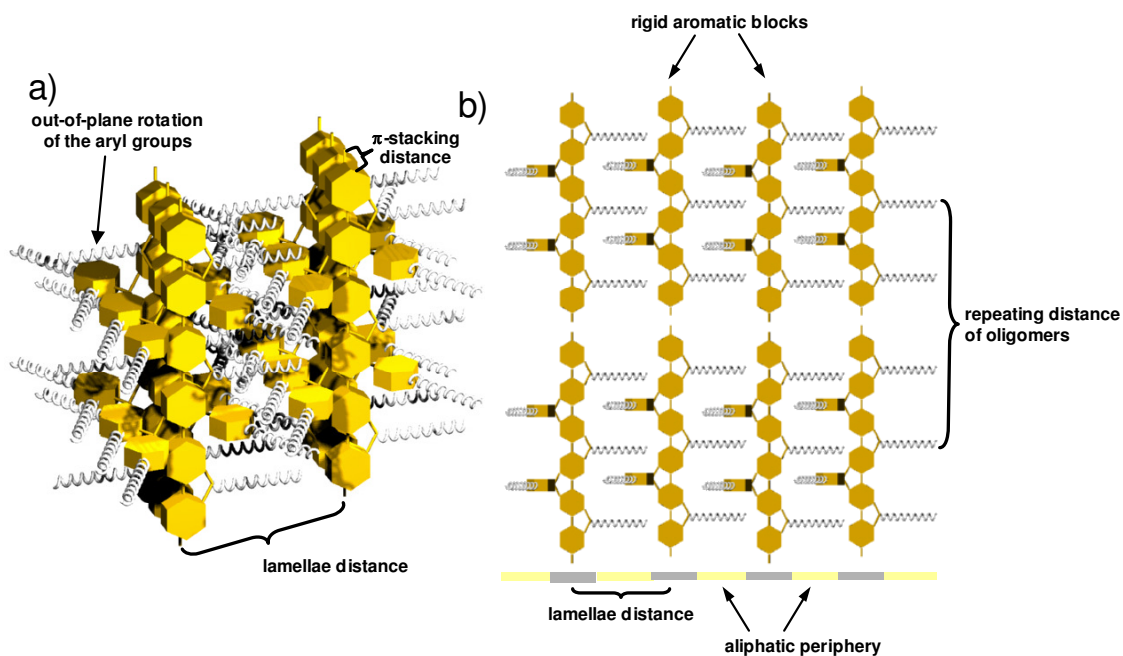


**Figure 3.9** Schematic illustrations of a) the oligomer conformation and packing and b) one layer of the organization into lamellae.

Since the isotropization phase transition of all four oligomers was at accessible temperatures, it was possible to melt process the compounds. Therefore, the powder was sandwiched between two glass slides, heated above the melting temperature and slowly cooled down at a controlled rate. The formed film morphology was investigated by polarized optical microscopy (POM) and X-ray scattering in reflection mode.

Figure 3.10 displays POM images of **57a** taken at room temperature of films cooled from the melt at cooling rates of 10 °C/min and 1 °C/min. When the film was processed by 10 °C/min, only a small number of randomly distributed crystallites appeared giving rise to birefringence between cross-polarizers, whereas the rest of the sample remained

amorphous and therefore black in the polarized light (Figure 3.10a). By decreasing the cooling rate to 1 °C/min, it was possible to observe large uniform domains, which exceeded sizes of several hundreds of micrometers (Figure 3.10b). Their high optical anisotropy during rotation of the films towards the cross-polarizers indicated a uniaxial alignment of the supramolecular structures in each of the domains. Furthermore, the strong regular birefringence was characteristic for an edge-on arrangement of the molecules on the glass surface. Slightly thicker films cooled with the same rate of 1 °C/min revealed an identical pronounced order as in thinner samples (Figure 3.10c)

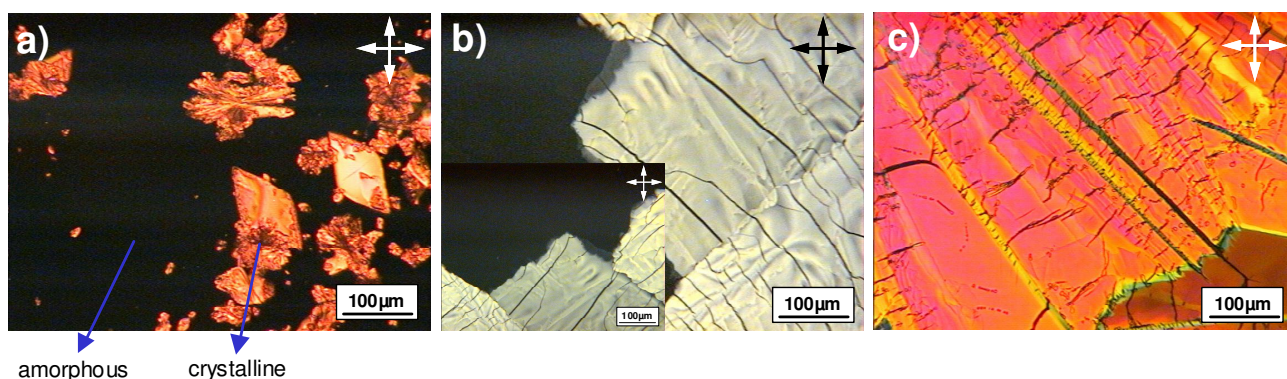


**Figure 3.10** POM images of **57a** taken after cooling by a) 10 °C/min and b) and c) 1 °C/min [(sample in b) is thinner than in c)].

Compound **57c** showed similar highly ordered films when it was processed from the melt. However, in this case, a much lower cooling rate was necessary to achieve a comparable result as observed for **57a**. Figure 3.11a presents thin films of **57c** cooled

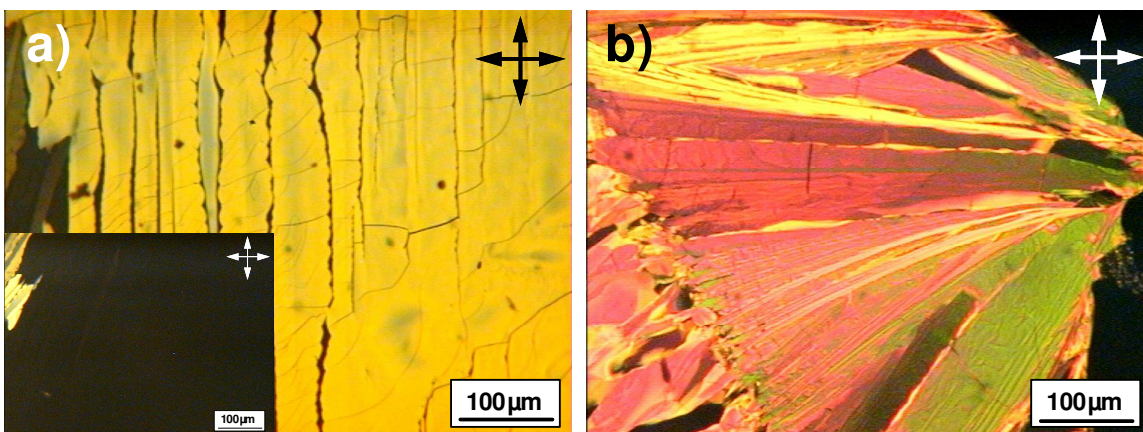


**Figure 3.11** POM images of **57c** taken after cooling by a) 0.05 °C/min and b) 1 °C/min. down with 0.05 °C/min consisting of large domains which exhibited high optical anisotropy and strong birefringence indicating a uniaxial orientation. Cooling of **57c** by 1 °C/min resulted in less uniform and smaller domains as suggested by the absence of a homogenous optical behavior when the sample was rotated towards the cross-polarizers. Finally, only amorphous films without any birefringence were obtained when the sample was cooled by 10 °C/min.

Figure 3.12 displays impressively the establishment of the morphology of **57b** dependent on the cooling rate. It is obvious that, by lowering the cooling rate, larger domains as well as higher crystallinity can be achieved. Processing at 10 °C/min resulted in the emergence of small nucleation sites which did not continue to crystallize (Figure 3.12a), whereas the cooling with 1 °C/min allowed a further structure formation shown in Figure 3.12b. After nucleation, large spherulites maintained their growth, but stopped the solidification process reaching a certain domain size. It is well known that molecules are edge-on arranged and radially oriented in such spherulitic domains. Similar to **57a** and **57c**, at low cooling rate of 0.05 °C/min in **57b**, again large and highly ordered areas were observed (Figure 3.12c). X-ray scattering was used to investigate the structure of a well-ordered crystalline film. Sharp (h00) reflections up to the sixth order confirmed the pronounced organization within the slowly crystallized film (Figure 3.13). The well-indexed reflection indicated an edge-on arrangement of the oligomers on the glass substrate as schematically illustrated in the inset in Figure 3.13.

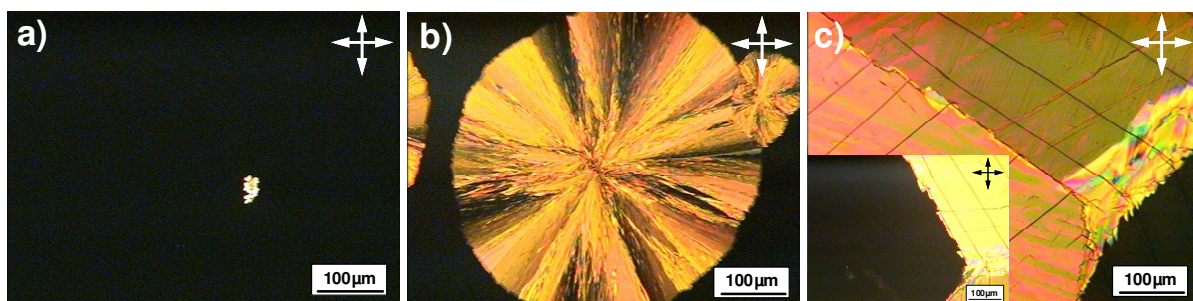


**Figure 3.12** POM images of **57b** taken after cooling by a) 10 °C/min and b) 1 °C/min and c) 0.05 °C/min.

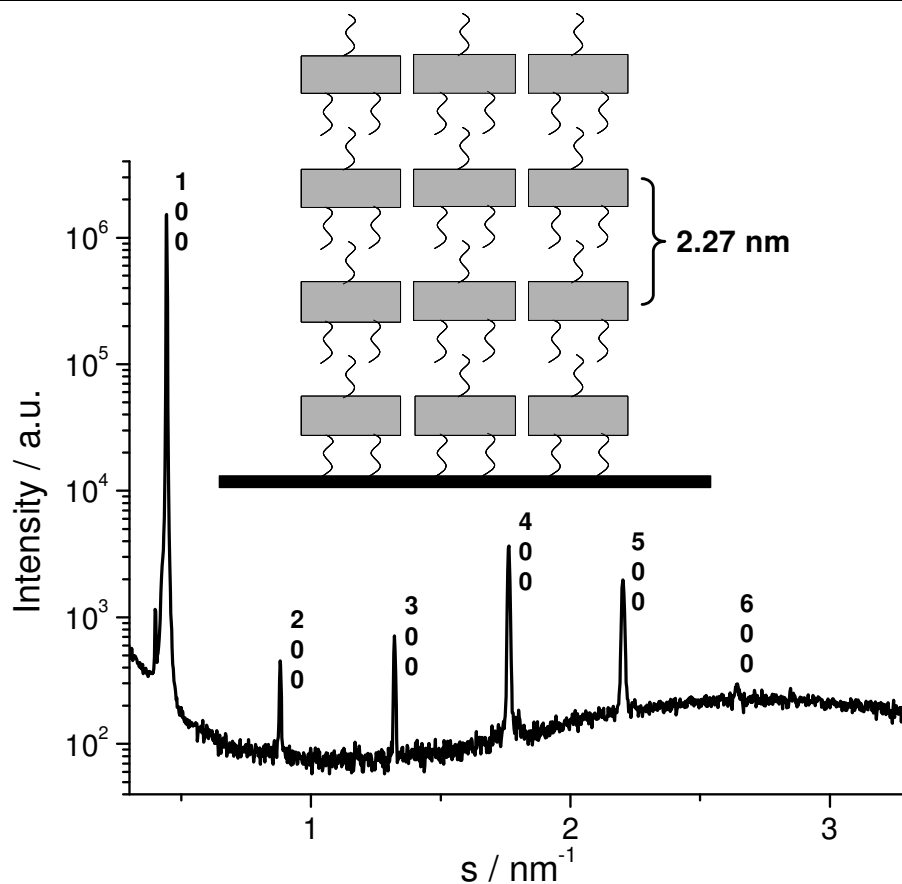


**Figure 3.13** X-ray diffractogram of **57b** as a film presented in Figure 3.12c prepared by 0.05 °C/min. The scattering intensity is plotted as a function of the scattering vector  $s$ . The Miller's indexes are used to assign the reflections. The inset illustrates schematically the supramolecular organization of the oligomers on the surface as derived from the X-ray results.

The determined periodicity of 2.27 nm was an out-of-plane correlation and was assigned to the inter-lamellar distance, as already found in the extruded filaments. Additionally, the appearance of only this characteristic distance indicated that the oligomers were preferentially lying with their longer axis on the surface. It might be assumed that the alkyl side chains played thereby an important role leading to this molecular organization. The rigid rod shape of the molecules was an additional reason for the edge-on order. This phenomenon was also observed in other small-weight molecular systems with a rod-like shape, as for instance in perylene tetracarboxydiimides.<sup>13</sup>

Finally, oligomer **19** as the longer model molecule was processed in the same manner as described above. Compound **19** revealed an identical behavior as observed for

**57a, 57b, and 57c.** Relatively fast cooling rates of 1 °C/min led to only partly crystallized films, where the ordered areas showed birefringence and the amorphous parts remained black between cross-polarizers (Figure 3.14a). Large and well-ordered domains were formed when the sample was slowly processed from the melt independent from the sample thickness (Figures 3.14b and 3.14c).

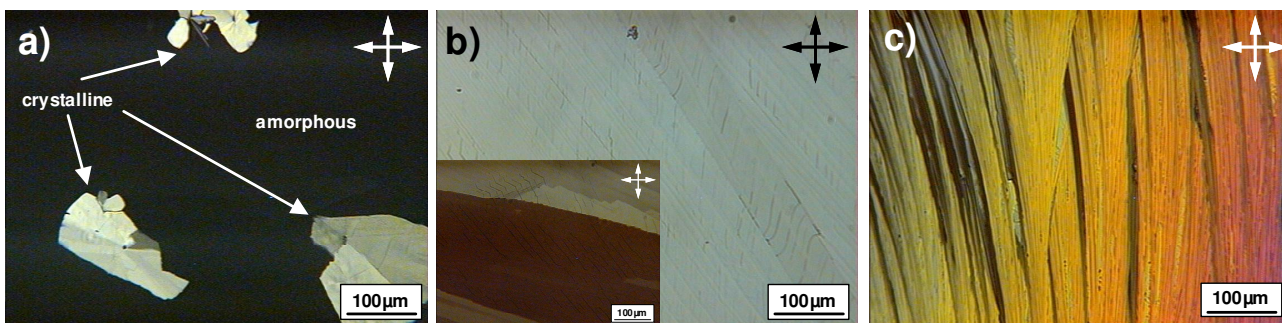


**Figure 3.14** POM images of **19** taken after cooling by a) 1 °C/min and b) and c) 0.05 °C/min [(sample in b) is thinner than in c)].

The DSC results and the morphology investigation of melt processed thin films were in good agreement. In both cases, it was possible to observe a supercooling of the compounds at cooling rates of 10 °C/min and 1 °C/min, respectively. In the DSC scans the supercooling was indicated by the absence of the crystallization peak during cooling and the cold crystallization peak during heating prior to the melting temperature. In the POM, the supercooled samples showed only partly crystallized areas, whereas the rest of the samples remained black suggesting amorphous regions. On the other hand, slow processing led to extraordinary large domains which were highly crystalline, implied by the strong birefringence, and consisted of uniaxially oriented structures with a macroscopic homogenous edge-on arrangement of the molecules. The super cooling of the compounds during relatively moderate cooling rates can be attributed to the bulky aryl groups which decrease the  $\pi$ -stacking interaction between the single building blocks and hamper the self-assembly. However, during slow structure formation the molecules have enough time to find the most favorite packing lead to the observed high order. Identical behavior has been reported for discotic molecules, where substituents with a high steric demand hindered the self-organization, but on a long time scale, the structure formation occurred macroscopically large and well-ordered domains were formed.<sup>14</sup>

Therefore, the more bulky the substituents, the slower the self-assembly process, however, higher order can be achieved by slow rates of cooling. The additional edge-on arrangement of the oligomers in this case, made the films more promising for application in field-effect transistors.<sup>15</sup> However, until now it is not possible to measure any field-effect mobility, even with source-drain gaps of 10  $\mu\text{m}$  where the crystalline domains, with sizes over several hundreds of micrometers, definitely span the distance between the electrodes. This puzzle is still under investigation. One reason for the lack of performance might be a contact problem between the gold electrodes and the organic semiconductor. There is only one example of a FET based melt processed organic thin film of thiophenes.<sup>16</sup> The authors reported a significant performance decrease between a vacuum deposited film and a thin layer obtained from the melt. Their explanation was the high crystallinity and the formation of domain boundaries which hinder an efficient charge carrier transport. Similar results were also obtained during time-of-flight experiments of homeotropically aligned discotics.<sup>17</sup> Up to now, it was not possible to determine the charge carrier mobility in the crystalline phase of a discotic compound due to the appearance of polycrystallinity and large grain boundaries. This problem was overcome by heating the samples to the liquid crystalline phases, at which high and non-disperse charge transience plot were measured. Nevertheless, the domains observed in this case indicated a uniform structure far above 10  $\mu\text{m}$ .

### 3.4 Performance of oligomers in field-effect transistors

FET performance of the oligomers **57a**, **57b**, and **57c** were investigated together with Nok Tsao at Max-Planck Institute for Polymer research. The monomer **19** (nitrogen-bridged ladder-type hexaphenylene) was also investigated along with carbazole-thiophene fused oligomers to compare the FET results. The transistor substrates were fabricated in the same way as described in the polymer section 2.7. Here, the source and drain electrodes have a width of 5  $\mu\text{m}$  and a separation between each other (channel length) of 10  $\mu\text{m}$ . As discussed above, no charge carrier mobility was observed in the film obtained from the melt, therefore, the oligomers were drop-casted from a 30 mg/ml toluene solution on substrates heated at 60  $^{\circ}\text{C}$ . Afterwards, the resulting film was

annealed in vacuum at 100 °C for 18 h. For **57a**, the film is shown in Figure 3.15. This oligomer did not exhibit FET behavior.

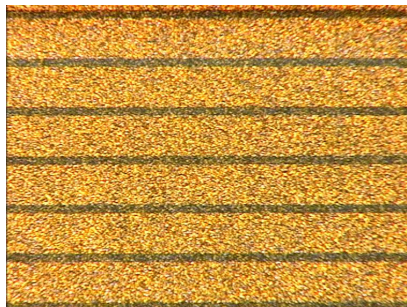


**Figure 3.15** Drop-cast film of **57a**.

The film of **57c** is illustrated in Figure 3.16. In contrast to **57a**, it demonstrated a field-effect behavior, as depicted in Figure 3.17, though the performance was weak, which led to a maximum saturated mobility of  $\mu_{sat} = 1.3 \times 10^{-7} \frac{cm^2}{Vs}$ , an on/off ratio of

$$\frac{I_{on}}{I_{off}} = 70, \text{ and a threshold voltage of } V_T = -16V .$$

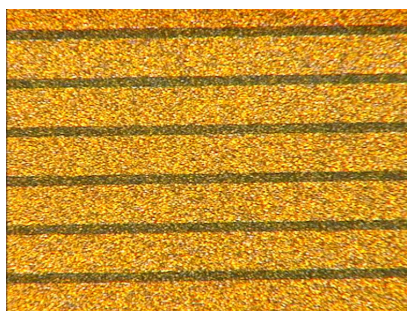


**Figure 3.16** Drop-cast film of **57c**.



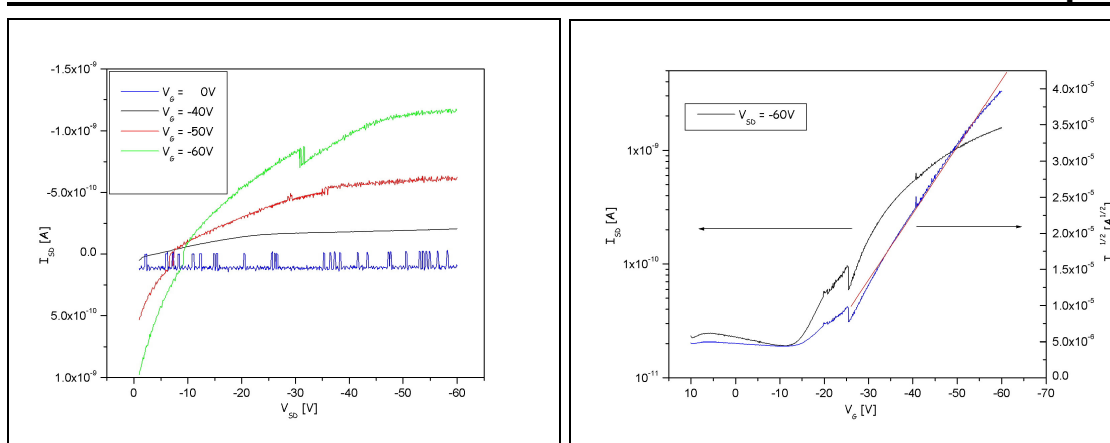


**Figure 3.17** Output and transfer characteristics of **57c**.

Compared to **57a** and **57c**, oligomer **57b** has one benzene ring fused at both sides, and the film (Figure 3.18) of this compound showed much better FET behavior than **57a** and **57c**, as outlined in Figure 3.19, with a maximum saturated mobility of  $\mu_{sat} = 5.6 \times 10^{-5} \frac{cm^2}{Vs}$ , an on/off ratio of  $\frac{I_{on}}{I_{off}} = 2 \times 10^2$ , and a threshold voltage of  $V_T = -11V$ . The mobility was two orders of magnitude higher than for **57c**.

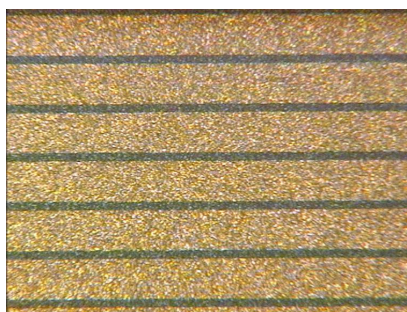


**Figure 3.18** Drop-cast film of **57b**.

Finally, monomer **19** was also tested in a field-effect transistor. The drop-cast film is illustrated in Figure 3.20. FET performance can be observed, as depicted in Figure 3.21,

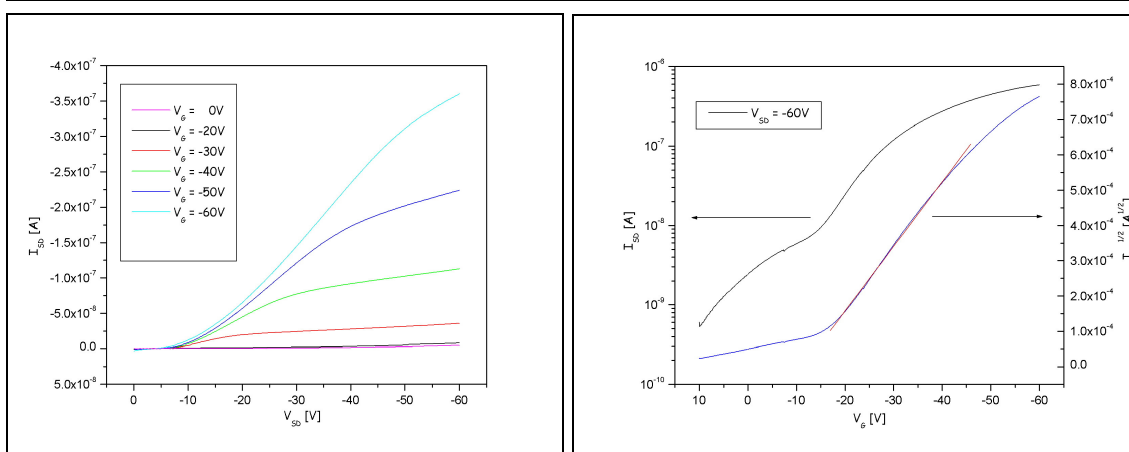


**Figure 3.19** Output and transfer characteristics of **57b**.

with a maximum saturated mobility of  $\mu_{sat} = 2.6 \times 10^{-5} \frac{cm^2}{Vs}$ , an on/off ratio of

$$\frac{I_{on}}{I_{off}} = 9 \times 10^3, \text{ and a threshold voltage of } V_T = -19V.$$



**Figure 3.20** Drop-cast film of **19**.

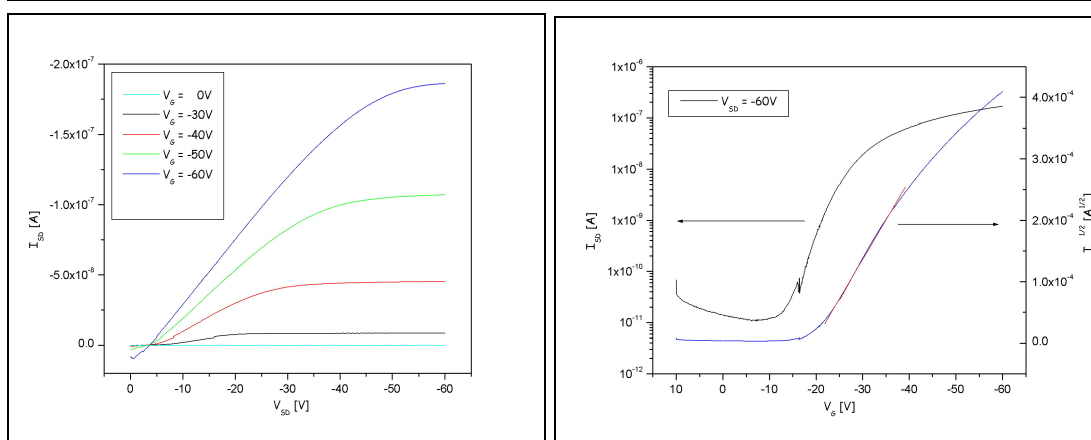


**Figure 3.21** Output and transfer characteristics of **19**

The FET performance for these oligomers are outlined in Table 3.3.

**Table 3.3** FET parameter for oligomers **57a**, **57b**, **57c** and **19**.

Oligomers	$\mu_{\text{sat}}$ (cm <sup>2</sup> /Vs)	V <sub>T</sub> (V)	I <sub>on</sub> / I <sub>off</sub>
<b>57a</b>	-	-	-
<b>57b</b>	$5.6 \times 10^{-5}$	-11	$2 \times 10^2$
<b>57c</b>	$1.3 \times 10^{-7}$	-16	70
<b>19</b>	$2.6 \times 10^{-5}$	-19	$9 \times 10^3$

### 3.5 Conclusions

In conclusion, the carbazole-thiophene fused molecules with different end group were synthesized, which can be processed both from melt and solution. The 2D-WAXs studies on oligomers demonstrated a long range order in the solid-state as well as POM studies showed a formation of big domains of more than 100  $\mu\text{m}$  sizes in the film obtained by melt processing. However, no charge carrier mobility was obtained from the film obtained by melt processing probably due to the appearance of polycrystallinity and large grain boundaries which hindered the charge carrier mobility between the electrode and organic semiconducting material. The FET devices were investigated on the film made by drop-cast method. It was observed that endcapping groups influenced the charge

carrier mobility dramatically, even though the drop-casted films of all three oligomers appeared very similar. However, from these FET data, it can be concluded that the chloro group resulted in no FET performance, the methyl group showed poor FET performance, and benzene ring as the endcapping unit demonstrated good transistor behavior. The nitrogen-bridged ladder-type hexaphenylene displayed best FETs mobility among all oligomers.

### 3.6 References

1. Klauk, H.; Halik, M.; Zschieschang, U.; Schmid, G.; Radlik, W.; Weber, W., High-mobility polymer gate dielectric pentacene thin film transistors. *J. App. Phys.* **2002**, 92, (9), 5259-5263.
2. Li, J. L.; Dierschke, F.; Wu, J. S.; Grimsdale, A. C.; Müllen, K., *J. Mater. Chem.* **2006**, 16, (1), 96-100.
3. Halik, M.; Klauk, H.; Zschieschang, U.; Schmid, G.; Ponomarenko, S.; Kirchmeyer, S.; Weber, W., *Adv. Mater.* **2003**, 15, (11), 917.
4. Roncali, J., Synthetic principles for bandgap control in linear pi-conjugated systems. *Chem. Rev.* **1997**, 97, (1), 173-205.
5. Meng, H.; Bao, Z. N.; Lovinger, A. J.; Wang, B. C.; Mujsce, A. M., High field-effect mobility oligofluorene derivatives with high environmental stability. *J. Amer. Chem. Soc.* **2001**, 123, (37), 9214-9215.
6. Katz, H. E.; Bao, Z. N.; Gilat, S. L., Synthetic chemistry for ultrapure, processable, and high-mobility organic transistor semiconductors. *Acc. Chem. Reser.* **2001**, 34, (5), 359-369.
7. Dierschke, F.; Grimsdale, A. C.; Müllen, K., Novel carbazole-based ladder-type polymers for electronic applications. *Macromol. Chem. and Phy.* **2004**, 205, (9), 1147-1154.
8. Scherf, U.; Müllen, K., Polyarylenes and Poly(Arylenevinylens) .7. a Soluble Ladder Polymer Via Bridging of Functionalized Poly(Para-Phenylene)-Precursors. *Makromol. Chem.-Rapid Commu.* **1991**, 12, (8), 489-497.
9. Bashir, Z.; Khan, N., Correlation of observations made by DSC and hot-stage optical microscopy of the thermal properties of a monotropic liquid-crystal polyester. *Thermochim. Acta* **1996**, 276, 145.
10. Tsuji, H.; Miyase, T.; Tezuka, Y.; Saha, S. K., Physical properties, crystallization, and spherulite growth of linear and 3-arm poly(L-lactide)s. *Biomacromolecules* **2005**, 6, (1), 244-254.
11. Kastler, M.; Pisula, W.; Wasserfallen, D.; Pakula, T.; Müllen, K., *J. Amer. Chem. Soc.* **2005**, 127, (12), 4286-4296.
12. Pisula, W.; Kastler, M.; Wasserfallen, D.; Mondeshki, M.; Piris, J.; Schnell, I.; Müllen, K., *Chem. Mater.* **2006**, 18, (16), 3634-3640.

13. Nolde, F.; Pisula, W.; Müller, S.; Kohl, C.; Müllen, K., Synthesis and self-organization of core-extended perylene tetracarboxdiimides with branched alkyl substituents. *Chem. Mater.* **2006**, 18, (16), 3715-3725.
14. Pisula, W.; Dierschke, F.; Müllen, K., *J. Mater. Chem.* **In Press**.
15. Sirringhaus, H., Device physics of Solution-processed organic field-effect transistors. *Adv. Mater.* **2005**, 17, (20), 2411-2425.
16. Torsi, L.; Dodabalapur, A.; Lovinger, A. J.; Katz, H. E.; Ruel, R.; Davis, D. D.; Baldwin, K. W., *Chem. Mater.* **1995**, 7, (12), 2247.
17. Adam, D.; Schuhmacher, P.; Simmerer, J.; Haussling, L.; Siemensmeyer, K.; Etzbach, K. H.; Ringsdorf, H.; Haarer, D., Fast Photoconduction in the Highly Ordered Columnar Phase of a Discotic Liquid-Crystal. *Nature* **1994**, 371, (6493), 141-143.

## Chapter 4

### Aminocarbazole-anthraquinone fused dyes and polymers

In this chapter, the synthesis and characterization of a new series of dyes by Buchwald-type coupling of 3-aminocarbazole with various isomers of chloroanthraquinone are presented. The absorption maxima of the resulting dyes were found to vary from 542 nm (violet) to 777 nm (green) depending on the extent of conjugation. Also, three different polymers have been synthesized by coupling of 3,6-diaminocarbazole with isomers of dichloroanthraquinone under palladium-catalyzed conditions. We demonstrated that the conjugation length in these polymers was largely confined to their monomer repeat units.

#### 4.1 Introduction

Synthetic dyes and their intermediates were the first organic chemicals whose commercial production started in the industrialized countries in Europe as early as the second part of 19<sup>th</sup> century.<sup>1</sup> A rapid development of efficient processes for the manufacture of synthetic dyestuffs was responsible for the fact that these products virtually replaced natural dyes on world market.<sup>2</sup> The development of dye chemistry and technology has resulted in an implementation on a commercial scale of a vast number of products that meet all the quality requirements expected from good dyes, especially their hues, light and wash fastness, as well as color fastness of dyed fibers. A high demand for synthetic dyes on the world market and, in consequence, their high price, however, account for the fact that dye industry has a high economic efficiency and a full profitability, even in the case of low-volume production.<sup>3,4</sup>

A substantial raw-material for dyestuff industry is the coal tar whose world production is 14 million ton per annum. Anthracene, acenaphthene, naphthalene, pyrene and carbazole derived from coal tar are important starting materials for the manufacture of synthetic dyes.<sup>5</sup>

Carbazole is a tricyclic coplanar heterocyclic molecule with properties of an aromatic compound. At room temperature, carbazole is a white solid, which melts at 245-246 °C turning into a colorless liquid.<sup>6, 7</sup> Numerous methods of synthesis of carbazole and its simple derivatives have been known to proceed via pyrrole ring closure.<sup>8</sup> The major source of carbazole is, however, the high-carbonization temperature coal tar obtained by coking of bituminous coals. During the primary distillation of the feedstock, carbazole is collected in the anthracene oil together with anthracene and phenanthrene, from which it is isolated together with anthracene as the so-called “crude anthracene”. Carbazole is purified from crude anthracene by either crystallization or solid-liquid extraction methods.<sup>5</sup>

There were two major applications of carbazole in the past viz. production of (i) poly (vinyl carbazole) and (ii) carbazole based dyes and pigments. The first application of carbazole has recently lost its industrial importance due to the brittle nature of the polymer, however, dyes and pigments have increasing commercial significance on the market. It is also useful as a biological and physiologically active compound useful for agriculture (herbicides, fungicides) and pharmaceutical industries.<sup>6</sup>

Carbazole shows a chemical reactivity typical of an aromatic polycyclic compound. It easily undergoes alkylation and acylation at 9- position due to the acidic proton as well as electrophilic substitution reaction at 3, 6- positions.

Carbazole gives a number of colored reactions typical of a condensed aromatic system. For example, by heating carbazole in concentrated sulfuric acid with formaldehyde, a blue-green color is produced; with p-chloroanil in ether the color is red; and with antimony pentachloride in carbon tetrachloride results in green color.<sup>7</sup>

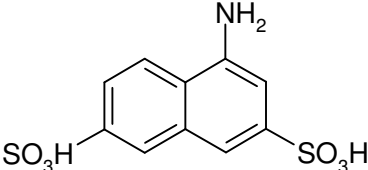
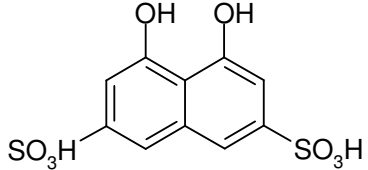
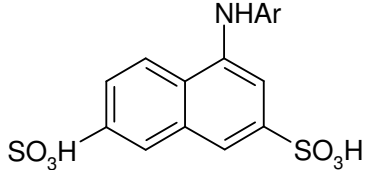
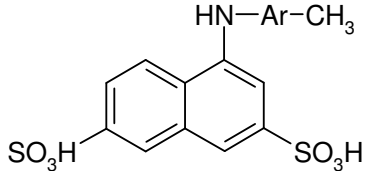
The dyes and pigments based on carbazole can be divided into three major categories: (1) Carbazole azo dyes, (2) Carbazole dyes with quinone groups, and (3) Dioxazine dyes.

**4.1.1 Carbazole azo dyes :** Azo dyes are by far the most important class of dyes, comprising over 50 % of total world dye production.<sup>9</sup> They are tinctorially strong, usually easy to prepare from cheap, readily available starting materials, cover the whole shade range and, cost effective compared to other classes of dyes. However, azo dyes do have

some deficiencies. Compared to their main rivals, the anthraquinone dyes, they tend to be duller in shade and generally cannot equal in the excellent light fastness particularly in the blue shade area.

The carbazole diazonium salts are known since Morgan and Read produced carbazole-3-diazonium chloride by treating of 3-amino carbazole with sodium nitrite solution in hydrochloric acid.<sup>10</sup> The azo dyes are obtained by the coupling of diazonium salts with aromatic amine, phenol or naphthole type of compounds (coupler component). Depending upon the nature of the coupler component it is possible to tune the color of the final compounds, for instance, when carbazole-3-diazonium chloride is coupled with sulfonated naphthalene derivative, it gives different colors as shown in Table 4.1.

**Table 4.1** Coupling products of carbazole-3-diazonium chloride with sulfonaphthalenes<sup>11</sup>

Sulfonaphthalene	Color of resulting dye
	Light red blue
	Blue
	Tan with golden hue
	Orange

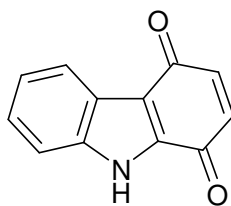


Other amino derivatives such as 3,6-diamino, 2-monoamino, 2,7-diamino carbazoles are also used for azo dye synthesis with a wide range of colors.<sup>12</sup>

**4.1.2 Carbazole dyes with quinone groups :** The quinone-group carbazole dyes, which are not necessarily made from carbazole itself, represent a large group of dyes used in dyeing cellulose fibers (rayon, cotton, linen etc.). The hues produced on the fiber range from yellow to red, brown to gray and black. The dyes are water-insoluble and are deposited on the fabrics from alkaline baths containing the leuco forms of the dyes. Subsequently, the leuco compound adsorbed on the fiber, is oxidized in the air to fast colors. During the oxidation process the water-soluble leuco compound turns into a water-insoluble dye, with good wash fastness for the resultant dye. An added advantage of carbazole vat dyes as compared to other vat dyes is their enhanced affinity to fibers due to an almost planar structure which makes penetration of the dye molecule easier into the bulk of fiber so that the dye is not easily washed out from the fiber.<sup>5</sup>

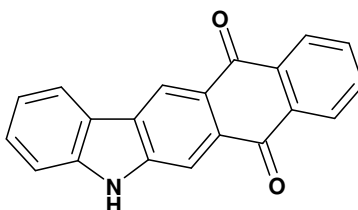
Depending on the location of the quinone grouping in the structure of the compound, the dye can be subdivided into three major groups:

- (i) Quinonocarbazoles in which the quinoid group occurs directly in one or both benzene rings of the carbazole molecules as shown below (Figure 4.1).<sup>13</sup>



**Figure 4.1** 1,4-Quinonocarbazole

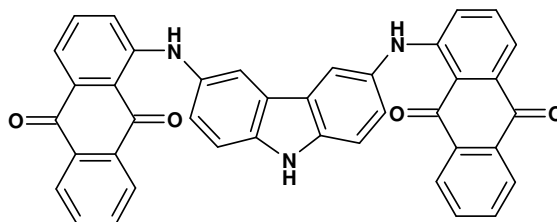
- (ii) Phthaloylcarbazole in which the quinoid group is in the close vicinity of carbazole such as 2,3-phthaloylcarbazole (Figure 4.2).<sup>14</sup>



**Figure 4.2** 2,3-Phthaloylcarbazole

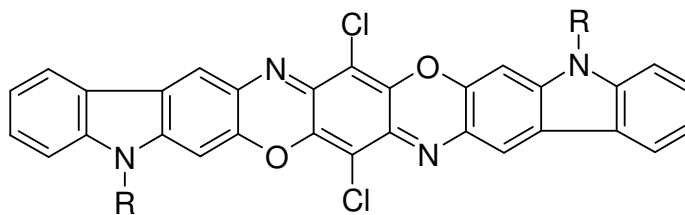
Commercially, the majority of these dyes are obtained from aminoanthraquinones or from the products of their condensation with halogenoanthraquinones known as anthrimides via an oxidative cyclization to form carbazole rings. The dyes of this kind, as compared with the parent anthrimides, give faster dyeing, with higher light and wash fastness, greater affinity to fibers and superior color purity. Due to these characteristics they have found multiple uses in textile, printing and plastic industries.

- (iii) The dyes containing quinoid group linked to the carbazole ring by single bond such as 3,6-di(1-antraquinonylamino)carbazole (Figure 4.3).<sup>15</sup>

**Figure 4.3** 3,6-di(1-antraquinonylamino)carbazole

This dye is prepared by the condensation of 3,6-diaminocarbazole with 1-chloroanthraquinone. Analogous dyes are also made by condensation of some more readily available dihalogenocarbazoles with 1-amino anthraquinone.<sup>16</sup>

**4.1.3 Dioxazine dyes :** An important group of carbazole-derived dyes are the carbazoledioxazines with the general structure shown below (Figure 4.4)

**Figure 4.4** Carbazoledioxazines

It is synthesized from 3-aminocarbazole by initial condensation with *p*-chloroanil to generate dicarbazolylaminochlorobenzoquinone and subsequent cyclization of the

quinone gives carbazodioxazine. A commonly recognized representative of the carbazodioxazine pigments which contains an ethyl group attached to nitrogen is called Violet 23 (Figure 4.5).<sup>17</sup> Recently, Ikeda *et al.* have confirmed the structure spectroscopically by attaching a long alkyl chain at the nitrogen center of carbazole.<sup>18-20</sup> This pigment is used in printing, in paint and varnish industry, as well as for coloration of plastics especially poly(vinyl chloride).<sup>5</sup> Because of its good properties it ranks in the valuable pigment group, as it has a high coloring power and a considerable light fastness.

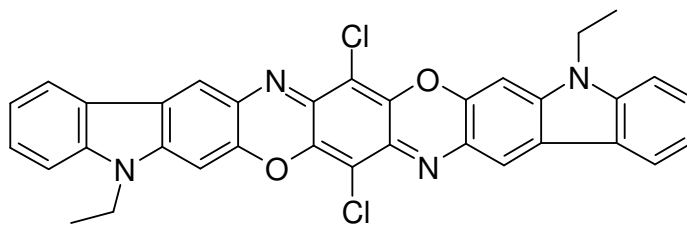
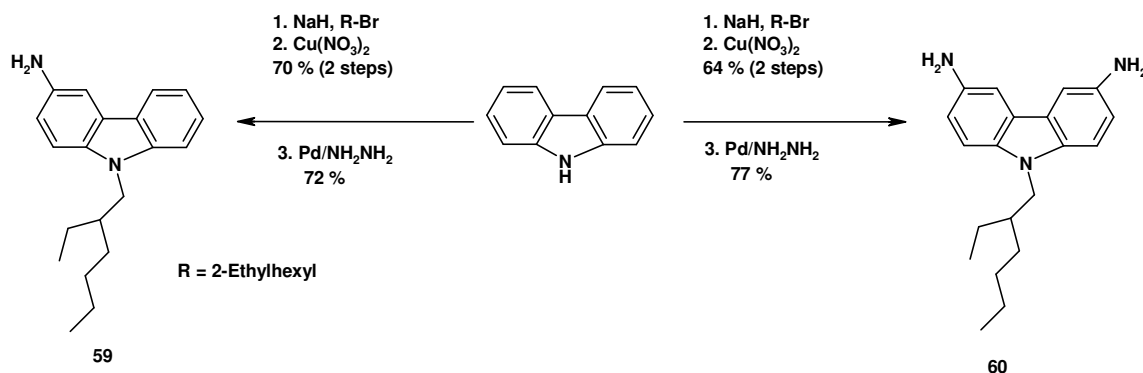


Figure 4.5 Violet 23

However, Violet 23 requires multistep synthesis and environmentally unfriendly because of the presence of the chloro group in the molecule. As part of our efforts into developing cheap alternatives for violet 23, we have focussed on the coupling of two readily available substrates, 3-aminocarbazole and chloroanthraquinones. Both 3-aminocarbazole and 3,6-diaminocarbazole are easy to synthesize and dichloroanthraquinones are readily available in various isomeric forms. The synthesis of 3,6-bis(1-anthraquinonylamino)carbazole has been reported either by the condensation of 3,6-diaminocarbazole with 1-chloroanthraquinone or by condensation of the more readily available dihalocarbazoles with 1-aminoanthraquinone.<sup>16</sup> The resulting pigment was violet in color ( $\lambda_{\max} = 513$  nm) but the absorbance maximum was too hypsochromic compared to violet 23 ( $\lambda_{\max} = 602$  nm). In the present study, we report on the synthesis and characterization of dyes and pigments based on the coupling of 3-aminocarbazole **2** with 1,4-, 1,5- and 1,8-dichloroanthraquinones, under palladium catalyzed Buchwald-Hartwig type amination conditions.<sup>21</sup> This yielded materials ranging in color from violet to greenish blue. The synthesis and characterization of a series of soluble polymers by coupling of diaminocarbazole with 1,4-, 1,5- and 1,8-dichloroanthraquinones are also presented.

## 4.2 Synthesis and optical properties

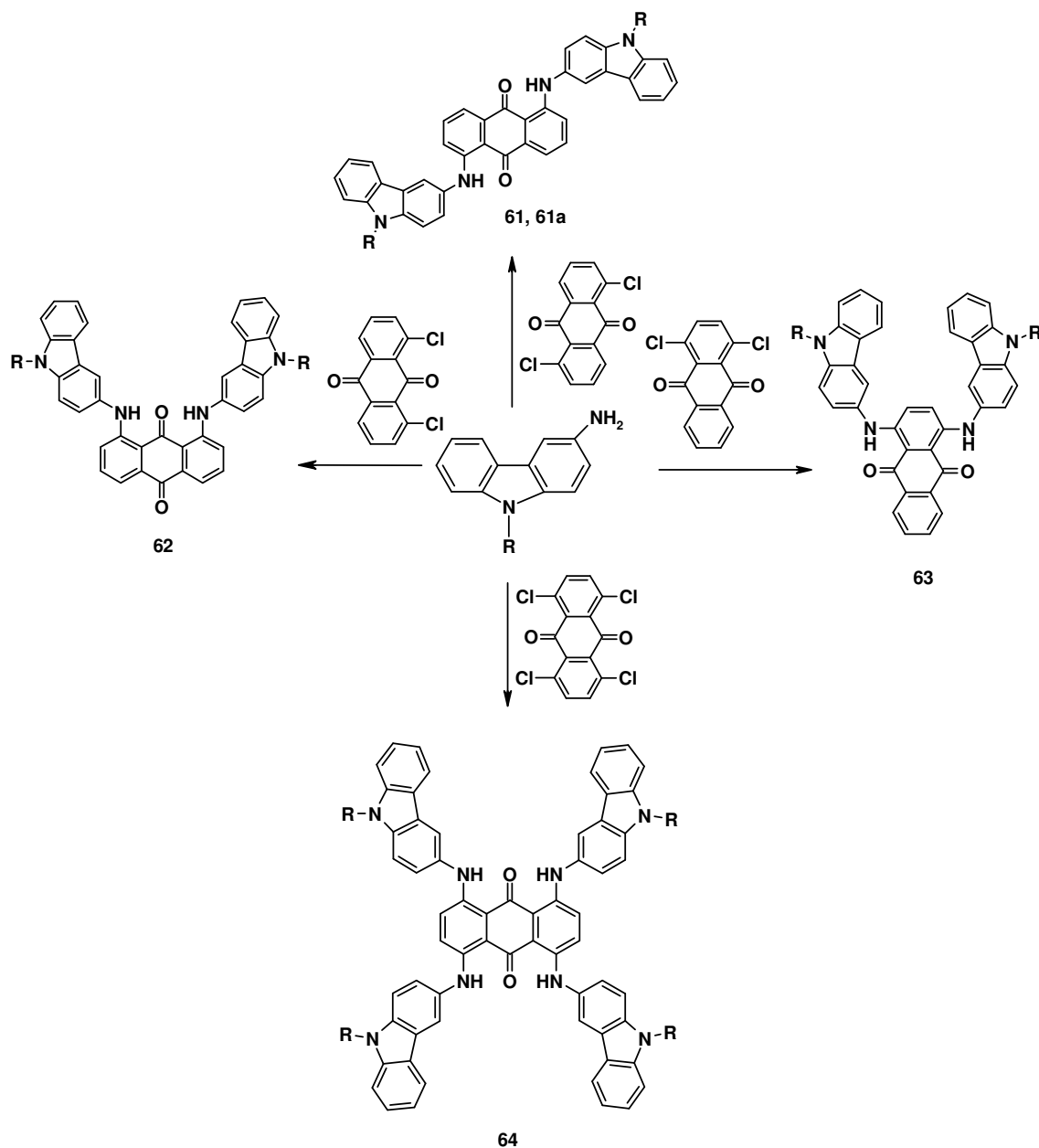
Starting from widely available carbazole, various dyes were synthesized, the structures and synthesis of which are presented below. The synthesis of 3-amino-9-(2-ethylhexyl)carbazole (**59**) and 3,6-diamino-9-(2-ethylhexyl)carbazole (**60**), two of the key intermediates in all the syntheses, are shown in Scheme 4.1. Carbazole was first alkylated with 2-ethylhexyl bromide under argon using sodium hydride as a base in dry DMF in near quantitative yield. This was then selectively converted to either 3-nitro-9-(2-ethylhexyl)carbazole or 3,6-dinitro-9-(2-ethylhexyl)carbazole by varying the amount of the copper nitrate reagent. Finally the reduction of the nitro group with hydrazine in the presence of palladium on charcoal gave the desired 3-aminocarbazole **59** and 3,6-diaminocarbazole **60** in 50 % and 49 % overall yield respectively.



**Scheme 4.1** Synthesis of 3-amino- and 3,6-diaminocarbazole

The coupling of **59** with 1,5-dichloroanthraquinone under standard Buchwald-type conditions, using Pd<sub>2</sub>(dba)<sub>3</sub> as catalyst and BINAP as a ligand in the presence of cesium carbonate, gave the dicoupled product **61** in 72 % isolated yield (Scheme 4.2). Use of

$P(t\text{-Bu})_3$  as a ligand was equally successful.



**61, 62, 63, 64:** R = 2-Ethylhexyl

**61a:** R = Ethyl

**Scheme 4.2** Coupling of 3-aminocarbazole with chloroanthraquinones

However, when the same reaction was carried out with sodium *tert*-butoxide as a base, only a trace amount of the product was observed. It was found that shorter alkyl chains on the nitrogen of carbazole gave lower yields. The temperature required for

completion of the reaction was higher with the ethyl than with the 2-ethylhexyl substituent. This can be attributed to the lower solubility of the precursor molecule with the ethyl moiety. Compound **61** was soluble in common organic solvents such as DCM and THF. The solubility was drastically decreased when the ethylhexyl alkyl chain was replaced with the ethyl group. Compound **61** gave a violet solution. The UV-vis absorption spectrum of **61** (Figure 4.6) exhibited an absorbance maximum at 542 nm and the extinction coefficient was calculated to be  $1.40 \times 10^4 \text{ Lmol}^{-1}\text{cm}^{-1}$ .

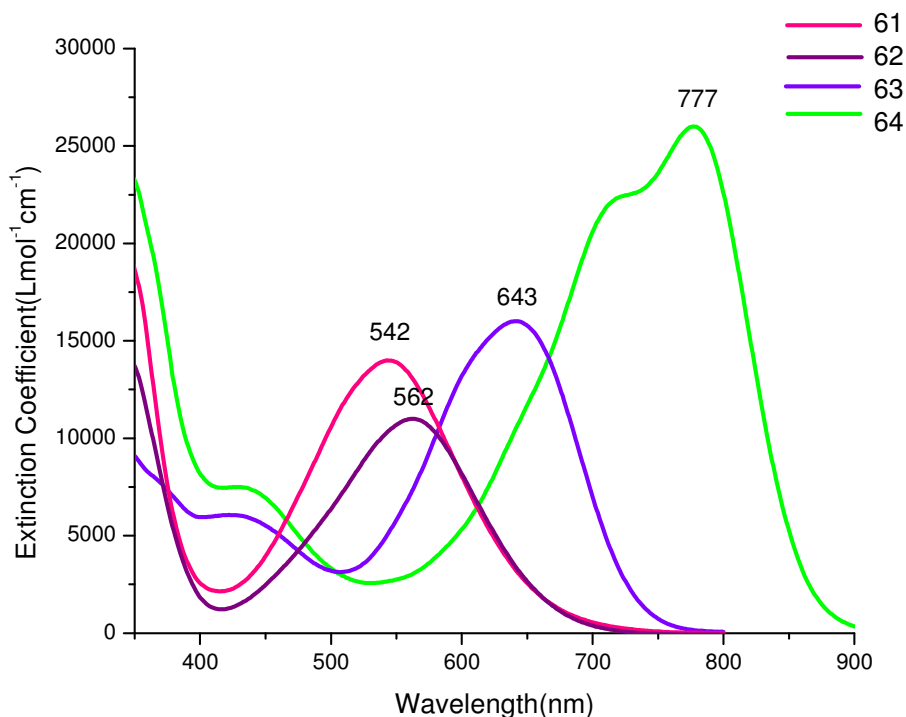


**Figure 4.6** Absorption spectra for compounds **61**, **62**, **63** and **64** (THF solution)

The UV-vis spectrum of the ethyl substituted **61a** demonstrated that the absorbance maximum was the same, while the extinction coefficient was found to be  $2.05 \times 10^4 \text{ Lmol}^{-1}\text{cm}^{-1}$ . The IR spectrum of **61** showed only one carbonyl stretch at  $1617 \text{ cm}^{-1}$ , which revealed that the imine of carbazole was interacting with the respective carbonyl group of anthraquinone and that the two carbonyl moieties were equivalent. However, the absorbance maximum was blue-shifted compared to violet 23 (602 nm) and the extinction coefficient was five times lower (violet 23,  $\lambda = 1.01 \times 10^5 \text{ Lmol}^{-1}\text{cm}^{-1}$ ). To improve the

conjugation within the molecule and to induce a red shift in the absorbance maximum, an analogous coupling of **59** with 1,8-dichloroanthraquinone was performed, which gave the product **62** in 56 % isolated yield (Scheme 2). Compound **62** was soluble in common organic solvents like DCM and THF to give a violet solution. The UV-vis spectrum of **62** (Figure 4.6) exhibited an absorption maximum at 562 nm, red-shifted by 20 nm compared to **61**. This suggested that the 1,8-isomer **62** was better conjugated than the 1,5-isomer **61**. The extinction coefficient of **62** was found to be  $1.1 \times 10^4 \text{ Lmol}^{-1}\text{cm}^{-1}$ , less than the value obtained for **61**. The IR spectrum of **62** revealed two bands in the carbonyl region at  $1660 \text{ cm}^{-1}$  and  $1613 \text{ cm}^{-1}$ , which suggested that the two carbonyl groups were different and that one was interacting more with the amine of carbazole as compared to the other. The absorption maximum and extinction coefficient of **62** were too hypsochromic and low, respectively, for use as a pure violet pigment. To further improve the conjugation between the two aminocarbazoles through anthraquinone, 1,4-dichloroanthraquinone was coupled with 3-amino-(9-ethylhexyl)carbazole to generate the product **63** in 80 % isolated yield (Scheme 4.2). Compound **63** was soluble in common organic solvents such as DCM and THF, to give a greenish-blue solution. The UV-vis absorption spectrum (Figure 1) of **63** exhibited an absorbance maximum at 643 nm and an extinction coefficient of  $1.60 \times 10^4 \text{ Lmol}^{-1}\text{cm}^{-1}$ . The 1,4-isomer showed the highest bathochromic shift in absorption maximum among the three isomeric coupling products, **61**, **62** and **63**. The same was true with extinction coefficients, which was highest for the 1,4-isomer. The IR spectrum of **63** revealed a single peak at  $1599 \text{ cm}^{-1}$  in the carbonyl region suggesting that the secondary amine was interacting with the carbonyl group of anthraquinone stronger than the 1,5- and 1,8-isomers.

The above results suggested that the substitution pattern at the anthraquinone has a significant impact on the absorbance maximum of the resulting dye. To extend the concept, 1,4,5,8-tetrachloroanthraquinone was treated with an excess of 3-amino-9-(2-ethylhexyl)carbazole under standard Buchwald conditions to give the tetracoupled product **64** in 42 % isolated yield (Scheme 2). In this case, the reaction took longer (72 h) time and required a higher temperature ( $100 \text{ }^\circ\text{C}$ ) for the coupling to reach completion. Compound **64** was soluble in DCM and THF to yield a green solution. The UV-vis spectrum (Figure 1) of **64** exhibited an absorbance maximum at 777 nm and an

extinction coefficient of  $2.60 \times 10^4 \text{ Lmol}^{-1}\text{cm}^{-1}$ . This was the highest amongst the molecules synthesized in this investigation. The IR spectrum of **64** displayed a single peak at  $1590 \text{ cm}^{-1}$ , which was consistent with the four electron donating amino groups in conjugation with the two carbonyl moieties. This dye has potential for near infrared absorption applications.

All the results for dyes derived from 3-aminocarbazole and different isomers of dichloroanthraquinone and 1,4,5,8-tetrachloroanthraquinone are summarized in Table 4.2.

**Table 4.2** Optical and physical data for Dyes (**61**, **61a**, **62**, **63**, and **64**)

Compound	Chloroanthraquinone	Substituent on nitrogen	$\lambda_{\text{max}}$ (nm)	Extinction coefficient ( $\text{Lmol}^{-1}\text{cm}^{-1}$ ) $\times 10^{-4}$	Color
<b>61</b>	1,5-	2-Ethylhexyl	542	1.40	Violet
<b>61a</b>	1,5-	Ethyl	542	2.05	Violet
<b>62</b>	1,8-	2-Ethylhexyl	562	1.10	Violet
<b>63</b>	1,4-	2-Ethylhexyl	643	1.60	Greenish-blue
<b>64</b>	1,4,5,8-	2-Ethylhexyl	777	2.60	Green

### 4.3 Explanation of observed optical properties by resonance structures

The observed shift in the absorption maximum can be explained by the resonance structures as discussed here. In 1,5 substituted anthraquinones the excited state may be crudely represented by the charge separated structures **61b** and **61c** (Figure 4.7). There is no interaction between the two halves of the chromogen (separated by solid line).



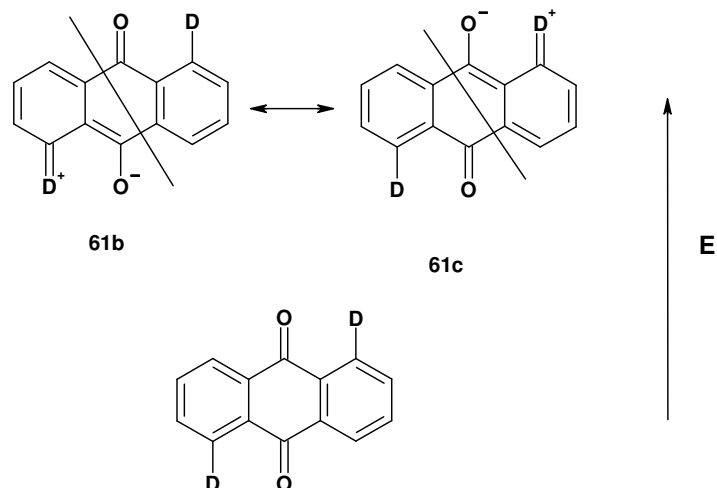


**Figure 4.7** Resonance structure of compound **61**

In contrast, the corresponding charge separated structures for 1,4-disubstituted anthraquinone **63b** are predicted to be exceptionally stable since they contain a fully aromatic naphthalene nucleus (Figure 4.8).

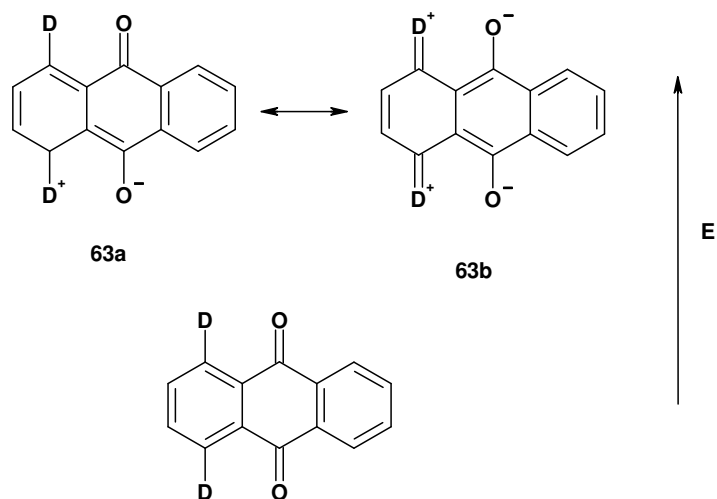


**Figure 4.8** Resonance structure of compound **63**

Hence, the energy gap between the ground and first excited state of 1,4-disubstituted anthraquinones is much smaller than that for the 1,5-isomers and therefore it is expected to absorb at longer wavelengths.

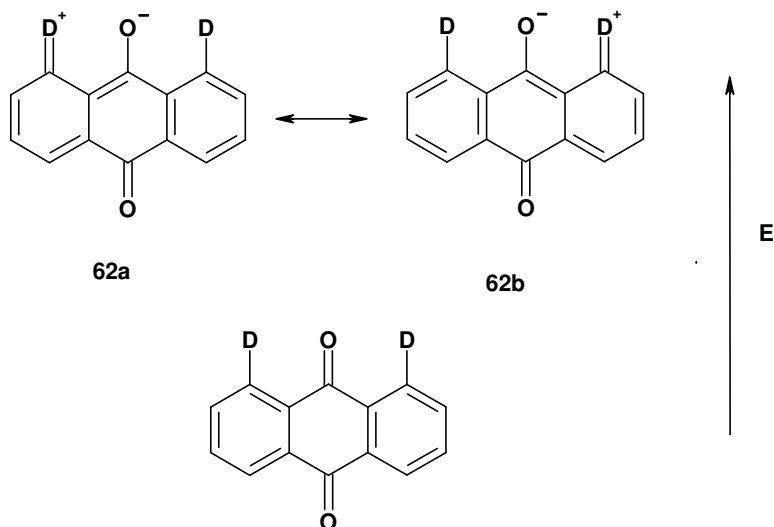


**Figure 4.9** Resonance structures of compound **62**

There is more conjugation in 1,8-disubstituted anthraquinones than in the 1,5-isomer but less than in the 1,4-isomer. Thus, although the donor groups can interact with each other, they are only conjugated to one carbonyl group (Figure 4.9). None of the structures contributing to the excited state contain a naphthalene nucleus.

1,4,5,8-Tetrasubstituted anthraquinones are the most red-shifted among the anthraquinone dyes because the major contributing structures to the excited state each contain a naphthalene ring (Figure 4.10).

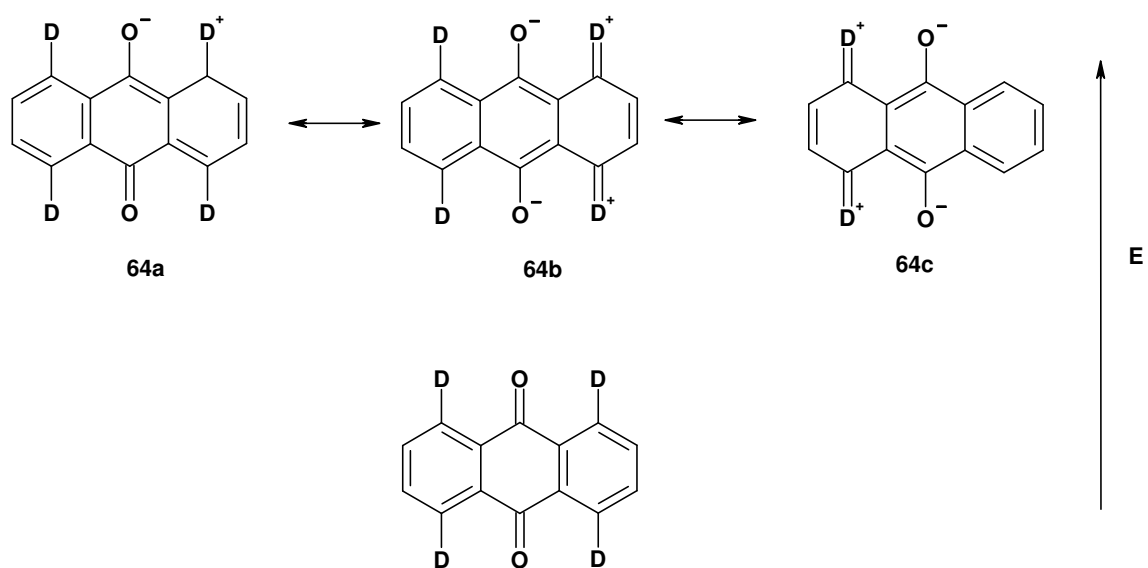
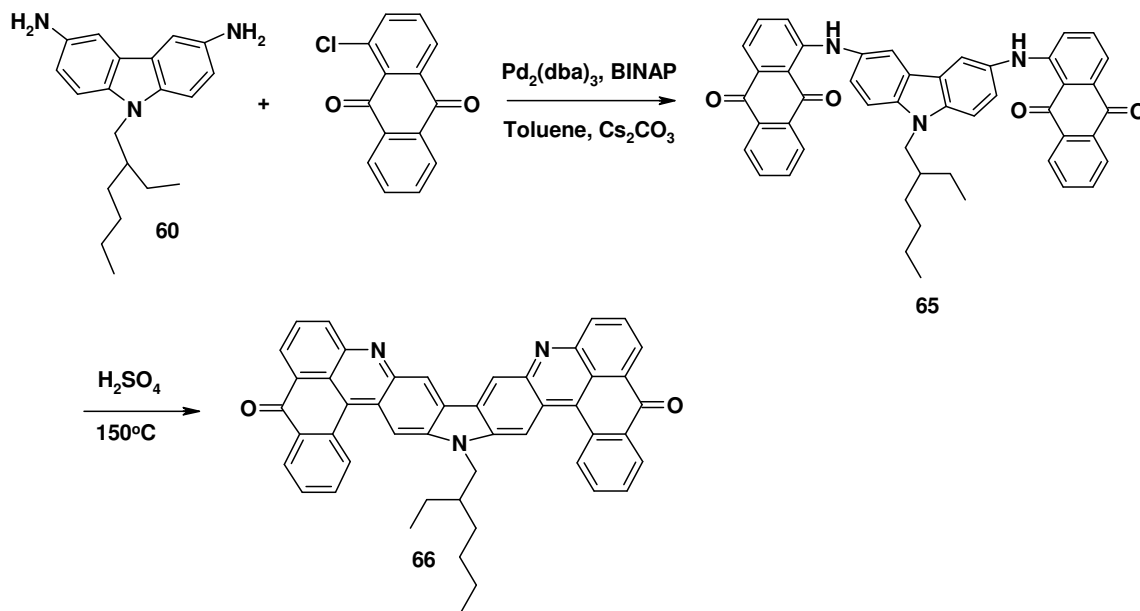


**Figure 4.10** Resonance structure of compound **64**

Therefore, valence bond (VB) theory predicts the following order of bathochromicity for donor substitution at anthraquinones. 1,4,5,8 > 1,4 > 1,8 > 1,5.

#### 4.4 Synthesis of a novel red-emitting material by double dehydration of **65**

3,6-Diaminocarbazole **60** was coupled with 1-chloroanthraquinone under standard Buchwald-type conditions to generate **65** in 80% yield (Scheme 4.3). Compound **65** was soluble in common organic solvents like THF and DCM. The UV-vis (Figure 4.11) spectrum of **65** showed an absorbance maximum at 513 nm, with an extinction coefficient of  $1.35 \times 10^4 \text{ Lmol}^{-1}\text{cm}^{-1}$ , and gave a pink-violet solution. In comparison with molecule **61**, the absorption maximum for molecule **65** was blue-shifted by 28 nm, which suggested that the increase in anthraquinone content led to a blue-shift in the absorption maximum.



**Scheme 4.3** Synthesis of red-emitting molecule **66**

The IR spectrum exhibited two bands in the carbonyl region at  $1669 \text{ cm}^{-1}$  and  $1627 \text{ cm}^{-1}$  revealing that the secondary amine of **65** was in poor conjugation with the carbonyl of the anthraquinone when compared with **61** ( $1617 \text{ cm}^{-1}$ ). In order to narrow

the absorption band width, compound **65** was treated with sulfuric acid at 150 °C to generate the ring closed product **66** in 24 % yield (Scheme 4.3).

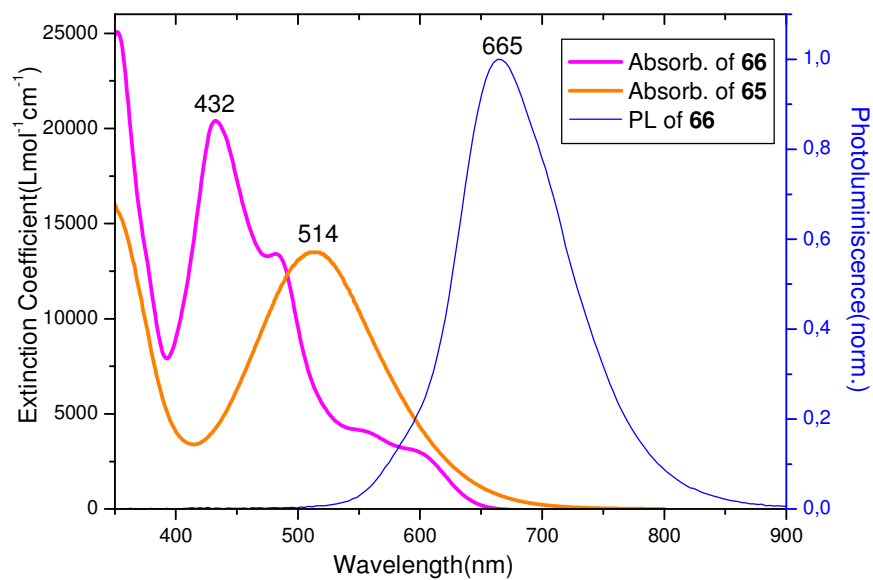


Figure 4.11 Optical properties of **65** and **66**

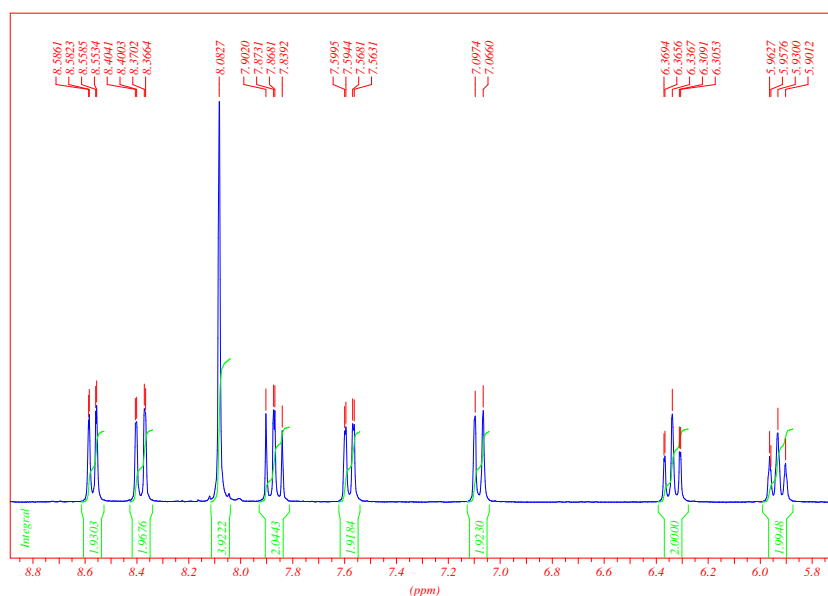
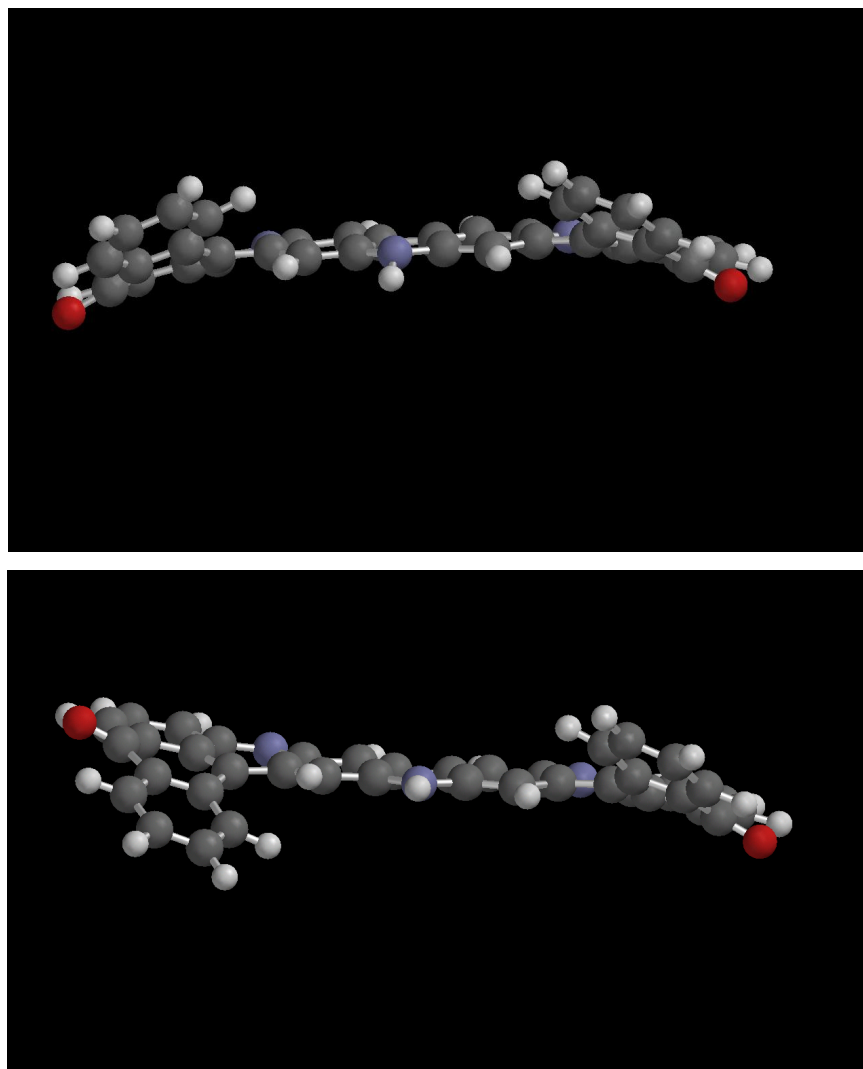


Figure 4.12 Aromatic region of compound **66** in  $^1\text{H-NMR}$

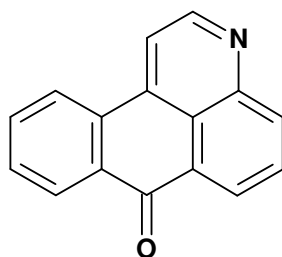
Compound **66** yielded a pale yellow solution and exhibited a fluorescence maximum at 665 nm, compared to the pink-violet color and absence of fluorescence for the precursor molecule **65**. Compound **66** was characterized by  $^1\text{H-NMR}$ ,  $^{13}\text{C-NMR}$ , mass spectrometry, UV-vis and IR spectroscopy. Interestingly, two of the aromatic protons of **66** appeared at 6.38 and 5.99 ppm (Figure 4.12), which was more upfield than expected, and the aliphatic region in the  $^{13}\text{C-NMR}$  spectrum showed two signals for each alkyl carbon.



**Figure 4.13** Cis and trans isomers of compound **66** as calculated with RHF/AM1 method”.

To understand this abnormality, theoretical calculations of **66** were undertaken to find out the different conformations possible for this molecule. The results revealed

(Figure 4.13) that the molecule was not planar and existed in two different conformations, viz. a cis and trans form. These calculations also explained the anomalies in  $^1\text{H-NMR}$  spectrum where the aromatic protons that appeared at high field were not in the plane of the carbazole ring, but instead were shielded by the aromatic  $\pi$ -system. This also accounted for certain anomalies in the  $^{13}\text{C-NMR}$  signals for the alkyl carbons, as two conformational isomers were possible. The UV-vis spectrum of **66** (Figure 4.11) exhibited a strong absorption band at 432 nm with shoulder at a 482 nm and the extinction coefficient at 432 nm was found to be  $2.04 \times 10^4 \text{ Lmol}^{-1}\text{cm}^{-1}$ . The absorbance maximum of **66** was blue-shifted by 82 nm in comparison with precursor molecule **65**, suggesting that the conjugation was hindered as a result of the dehydration reaction. The observed carbonyl stretch in the IR spectrum of **66** at  $1658 \text{ cm}^{-1}$ , corresponding to the carbonyl group, implied weak conjugation with the rest of the molecule. The absorption maximum and the measured carbonyl stretch was consistent with the model compound **67** (Figure 4.14) which absorbed at 356 nm ( $\epsilon_{\text{max}}=1.54 \times 10^4 \text{ Lmol}^{-1}\text{cm}^{-1}$ ) and had its carbonyl stretch at  $1664 \text{ cm}^{-1}$ .<sup>22</sup>

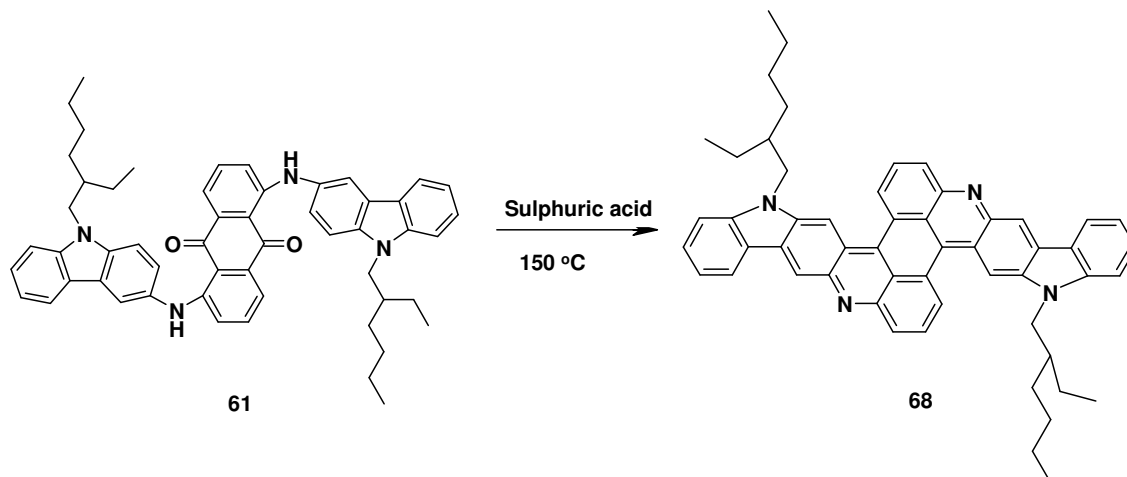


67

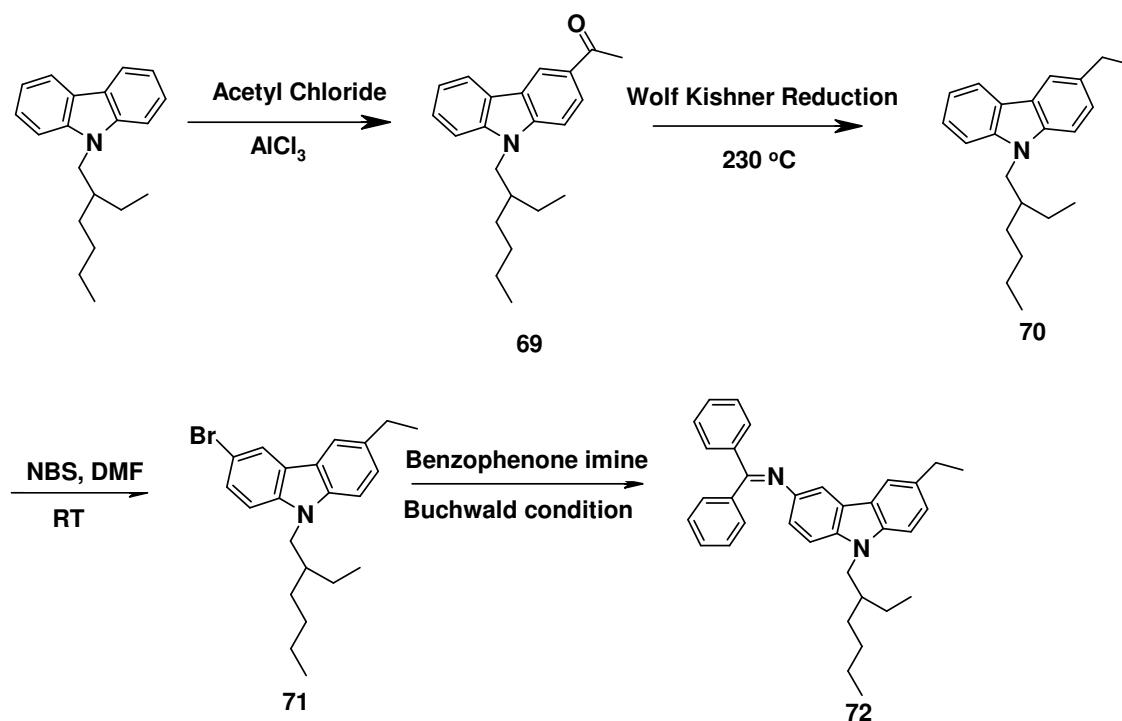
Figure 4.14 Model compound 67

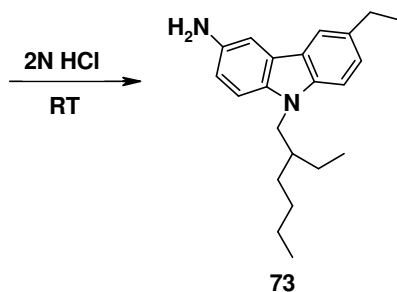
#### 4.5 Unsuccessful attempt of double dehydration on compound 61

Further attempts were made to synthesize **68** from **61** following the same synthetic procedure as in compound **65**. However, no product was formed.



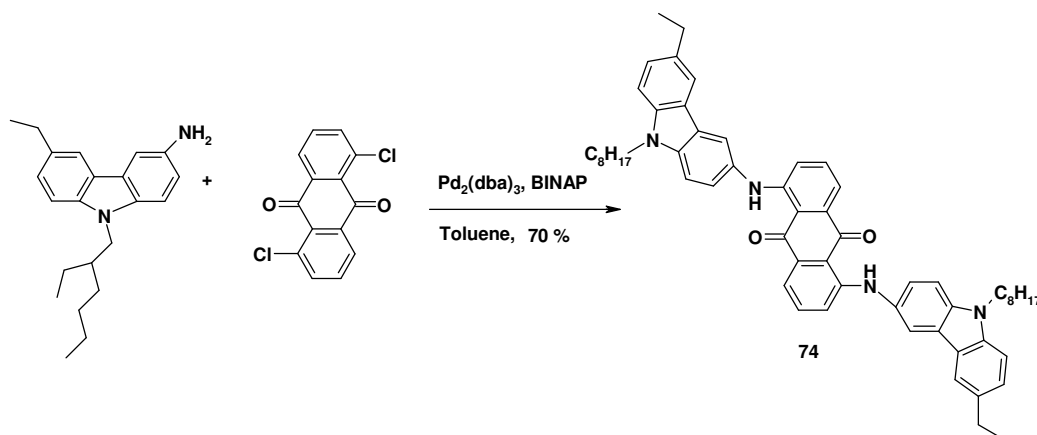
Then it was assumed that the failure of dehydration in this case may be due to the free 3- position of carbazole which is highly reactive towards electrophilic substitution reaction. This position was therefore blocked with an ethyl group and the ring closure was attempted again. The synthetic procedure to make 3-amino-6-ethyl-9-(2-ethylhexyl) carbazole (**73**) is shown in Scheme 4.4.





**Scheme 4.4** Synthetic route to 3-amino-6-ethyl-9-(2-ethylhexyl) carbazole (**73**)

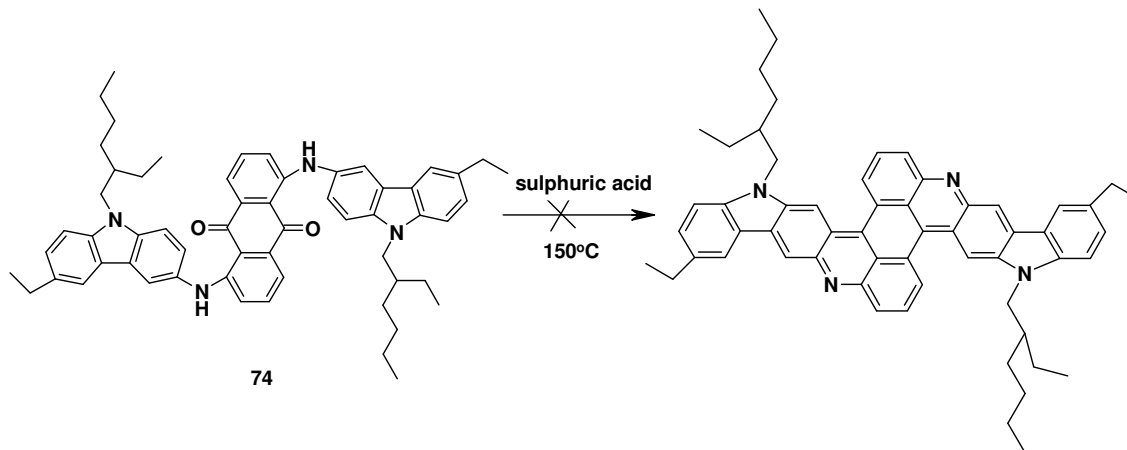
First, N-alkyl carbazole was monoacetylated by taking exactly one equivalent of acetyl chloride and aluminum chloride in 1,2-dichloroethane. It resulted in a mixture of carbazole, 3-acetylcabazole **69** and 3,6-diacetyl carbazole. However, the mixture was easily separable by column chromatography. Then, ketone **69** was reduced to **70** by treating with hydrazine and potassium hydroxide at 220 °C in 82 % yield. This step required high temperature and longer time than usual to break the imino adduct formed by nucleophilic attack of hydrazine on the carbonyl group of **69**. Further, the 3-ethyl-9-(2-ethylhexyl)carbazole (**70**) was mono brominated by N-bromosuccinimide in dimethylsulfoxide at room temperature to give 3-bromo-6-ethyl-9-(2-ethylhexyl)-carbazole (**71**) in 92 % yield. Compound **71** was treated with 1.2 equivalents of benzophenone imine by using  $\text{Pd}_2(\text{dba})_3$  and BINAP as a metal-ligand system in presence of sodium tertiary butoxide as a base at 100 °C to give **72** in 95 % crude yield. Then the hydrolysis of **72** in the mixture of 2N hydrochloric acid and tetrahydrofuran gave 3-amino-6-ethyl-9-(2-ethylhexyl)carbazole (**73**) in quantitative yield.





## Scheme 4.4 Synthetic route to compound 74

The resulting compound **73** was treated with 1,5-dichloroanthraquinone following standard Buchwald coupling as discussed before to give **74** in 70 % yield. Once again the ring closure was tried on molecule **74** following the same procedure as for **65**. However, no product was obtained (Scheme 4.5).



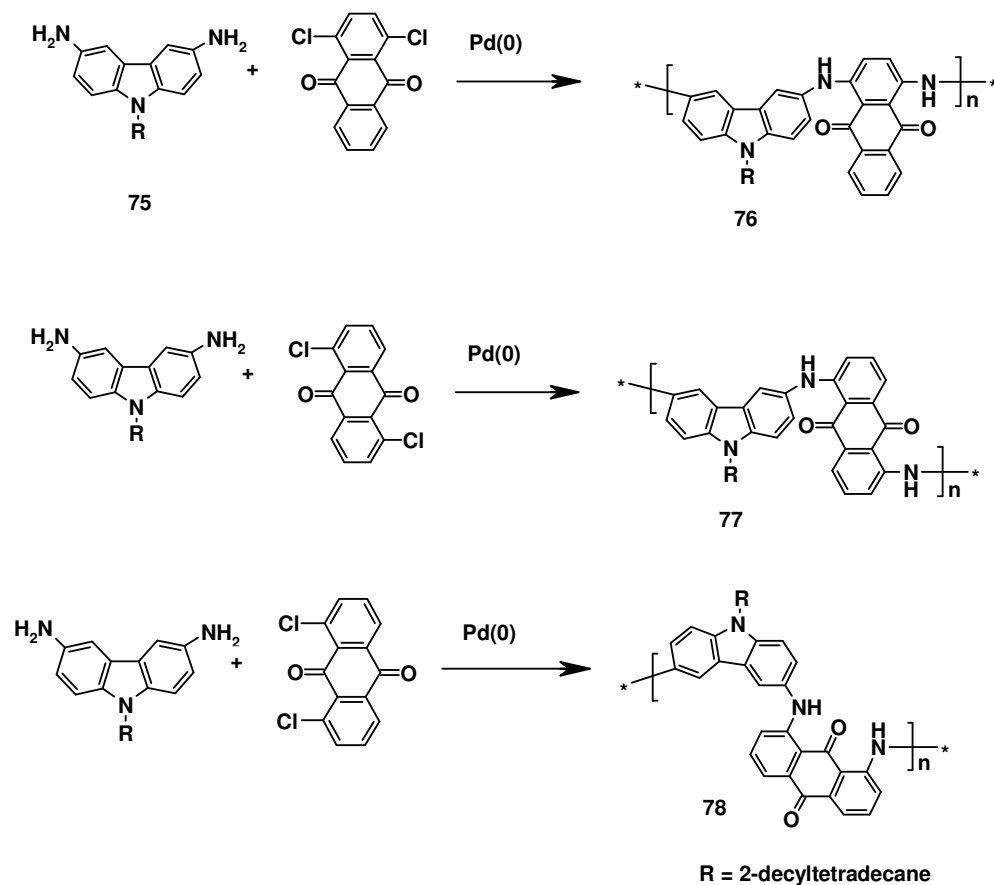
Scheme 4.5 Dehydration reaction on molecule 74

So, it was concluded that the reason for failure of dehydration on compound **74** is not because of the side reaction at highly reactive 3-position of carbazole. However, the actual reason is not known to us at this moment.

#### 4.6 Polymers based on diaminocarbazole and dichloroanthraquinone

Polymers based on diaminocarbazole and dichloroanthraquinone were also synthesized to achieve the maximum possible conjugation length and thereby the maximum red-shift in absorbance spectrum. The conditions for polymerization were optimized by varying the choice of catalyst and ligand, temperature and solvent. The best results were obtained when Pd<sub>2</sub>(dba)<sub>3</sub> was used as a catalyst and BINAP as the ligand, at 100 °C in toluene. First, the polymerization was carried out with 3,6-diamino-9-(2-ethylhexyl)carbazole (**60**) with 1,5-dichloroanthraquinone. This resulted in an insoluble polymer, due to strong inter- and intrachain hydrogen bonding. However when the polymerization was done with 3,6-diamino-9-(2-decyltetradecyl)carbazole (**75**), a

polymeric material **77** soluble in common organic solvents like DCM and THF was obtained. The longer, branched alkyl chain was sufficient to overcome the inter- and intrachain hydrogen bonding by giving enough entropy to the polymer chain. The 3,6-diaminocarbazole **75** was synthesized by the same procedure as shown in Scheme 4.1.



**Scheme 4.6** Synthesis of polymers **76**, **77**, and **78**

Three additional polymers were synthesized by copolymerization of **75** with 1,4-dichloroanthraquinone, 1,5-dichloroanthraquinone and 1,8-dichloroanthraquinone to generate **76**, **77**, and **78** respectively as shown in Scheme 4.6. Diaminocarbazole **75** was coupled with 1,4-dichloroanthraquinone in stoichiometric ratio with  $\text{Pd}_2(\text{dba})_3$  as the catalyst and BINAP as the ligand at 100 °C in toluene to give polymer **76** (71 % yield), which was soluble in common organic solvents like DCM and THF. GPC analysis

displayed a number average molecular weight ( $M_n$ ) of  $7.0 \times 10^3$   $\text{gmol}^{-1}$  with a polydispersity index (PDI) of 3.0. This corresponds to a degree of polymerization of about 19. Further attempts to increase the molecular weight of the polymer by varying the monomer concentration, temperature and the catalyst ligand systems were not successful. The UV-vis absorption spectrum of **78** (Figure 4.15) exhibited an absorbance maximum at 645 nm with an extinction coefficient of  $2.25 \times 10^4$   $\text{Lmol}^{-1}\text{cm}^{-1}$ . When compared to model compound **63**, the polymer showed no change in the absorption maximum suggesting that the chromophore was confined to the monomer unit.

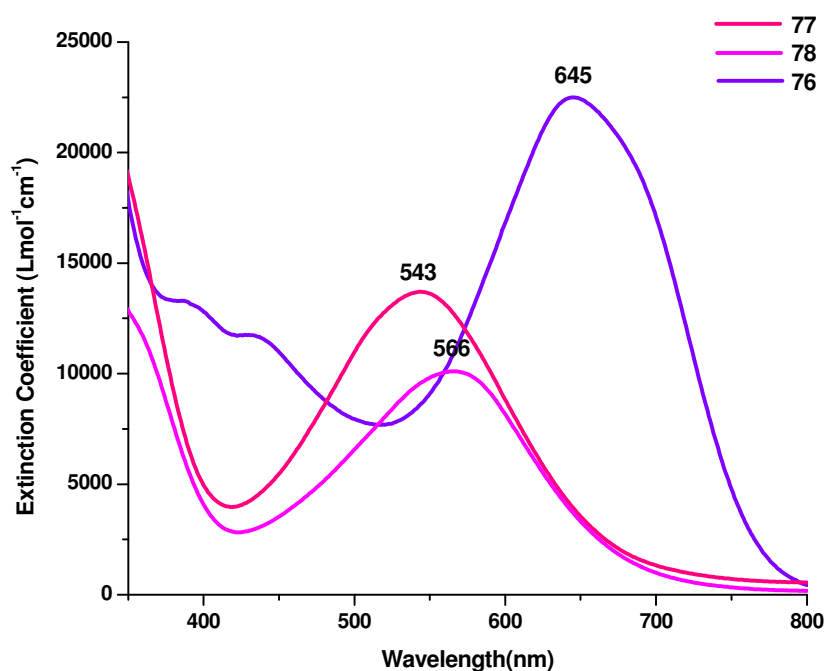


**Figure 4.15** Absorption spectra of compounds **76**, **77** and **78**.

An analogous polymerization of **75** with 1,5-dichloroanthraquinone under the same conditions resulted in polymer **77** in 62 % yield. GPC analysis demonstrated an  $M_n$  value of  $5.6 \times 10^3$   $\text{gmol}^{-1}$  with a PDI of 2.6, which corresponds to a degree of polymerization of about 15. The UV-vis (Figure 4.15) spectrum of **77** exhibited an absorbance maximum at 543 nm, with an extinction coefficient of  $1.4 \times 10^4$   $\text{Lmol}^{-1}\text{cm}^{-1}$ , and gave a violet solution. Again, in comparison with model compound **61**, polymer **77** displayed no change in the absorption maximum or the extinction coefficient. Similar

results were observed when **75** was polymerized with 1,8-dichloroanthraquinone. GPC analysis showed a  $M_n$  value of  $5.60 \times 10^3 \text{ gmol}^{-1}$  with a PDI of 2.3, which corresponds to a degree of polymerization of about 14. The results obtained for all three copolymers are summarized in Table 4.3.

**Table 4.3** Optical and physical data for Polymers **76**, **77**, and **78**.

Polymer	$^aM_n \times 10^{-3}$	PDI	$\lambda_{\text{max}}$ (nm)	Extinction coefficient ( $\text{Lmol}^{-1}\text{cm}^{-1}$ ) $\times 10^{-4}$	Color
<b>76</b>	7.0	3.0	645	2.25	Greenish-blue
<b>77</b>	5.6	2.5	543	1.37	Violet
<b>78</b>	5.0	2.3	566	1.01	Violet

<sup>a</sup>calibrated against PS standard

## 4.7 Conclusions

In conclusion, a series of carbazole-based dyes have been synthesized by Buchwald-type coupling of 3-amino and 3,6-diamino carbazole with various isomers of chloro and dichloroanthraquinone. With increasing carbazole content, the absorption maxima of the resulting dye was found to vary from 513 nm (pinkish violet) to 777 nm (green). When diaminocarbazole was coupled with 1-chloroanthraquinone, the resulting product underwent double dehydration upon treatment with sulfuric acid to generate a red-emitting material. Also, a series of soluble polymers were synthesized by coupling of diaminocarbazole with 1,4-, 1,5- and 1,8-dichloroanthraquinone. The resulting polymers showed absorption maxima similar to their model compounds suggesting that the conjugation in these materials were largely confined to their monomer units.

**4.8 References**

1. Kwiatkowski, E., *History of chemistry and chemical industry*. WNT: Warszawa, 1962.
2. Farris, R. E., *Kirk-Othmer's Encycl. Chem. Technol.* **1979**, 8, 351.
3. Bannister, D. W.; Olin, A. D.; Stingl, H. A., *Kirk-Othmer's Encycl. Chem. Technol.* **1979**, 8, 159.
4. sullivar, G., *Chemist and Colorist. Przem. Chem.* **1984**, 63, 554.
5. Pielichowski, J.; Polaczek, J.; Chrzaszcz, R.; Galka, S., *Carbazole dyes, pigments abd related products*. Cracow: Warsaw, 1996.
6. Collin, G., *Ullmann's Encycl. Techn. Chem.* . **1975**, 9, 120.
7. Freudenberg, W., *Heterocycl. Comp.* **1952**, 3, 291.
8. Ivanskii, V. I., *Chemistry of heterocyclic compounds*. Vysshaya Shkola: Moskva, 1978.
9. Chen, H. Z., *Curr. Prot. Pept. Sci.* **2006**, 7, (2), 101-111.
10. Morgan, G. T.; Read, H. M., *J. Chem. Soc.* **1922**, 121, 2709.
11. Shishkina, V. I.; Sprsheva, E. T.
12. Krasovitski, B. M.; Pereyastova, D. G., *Ukrain. Khim. Zh.*
13. ram, f.
14. Bien, H.; Wunderlich, K., *Ullm. Encycl. Techn. Chem.* **1974**, 7, 585.
15. 1940.
16. 1941
  
17. Nishi, H.; kubo, M., *Senryou To Yakuhin* **1976**, 21, 177.
18. Ikeda, M.; Kitahara, K.; Nishi, H., *J. Heterocycl. Chem.* **1991**, 28, 1165
  
19. Ikeda, M.; Kitahara, K.; Nishi, H., *J. Heterocycl. Chem.* **1992**, 29, 289.
20. Ikeda, M.; Kitahara, K.; Nishi, H.; Kozawa, K.; Uchida, T., *J. Heterocycl. Chem.* **1990**, 27, 1575.
21. Wolfe, J. P.; Tomori, H.; Sadighi, J. P.; Yin, J.; Buchwald, S. L., *J. Org. Chem.* **2000**, 65, 1158.
22. Zaitsev, B. E.; Gromov, D. N.; Ndongo, K. A.; Odinets, Z. K.; Sheban, V. G.; Krasnova, L. B., *Chem. Heterocycl. Compd. (Engl. Transl.)* **1991**, 27, (3), 321.

## Chapter 5

### Experimental Details

#### 5.1 Apparatus for analysis

All solvents were purified and freshly distilled prior to use according to literature procedures.  $^1\text{H}$  and  $^{13}\text{C}$ -NMR spectra were recorded on a Bruker DRX 250 (250 and 62.5 MHz respectively). UV-Vis data were recorded on a Perkin-Elmer Lambda 9 and the PL measurements in solution on a SPEX Fluorolog 2 type 212 steady state fluorometer. Gel-permeation chromatography (GPC) analysis was performed with PL gel columns ( $10^3$  and  $10^4$  Å pore widths) connected to a UV-Vis detector against poly-p-phenylene and polystyrene standards with narrow weight distributions.

Electrochemical measurements were performed on a Voltametric Analyzer (AutoLab PGSTAT-30, Potentiostat/Galvanostat) in a three-electrode cell with a working electrode of indium-tin-oxide (ITO) glass (sheet resistance of 20  $\Omega$ /square), a silver quasi-reference electrode (AgQRE, calibrated with the Fc/Fc<sup>+</sup> redox couple  $E^\circ = -4.8$  eV) and a Pt counter electrode. Films were spin-coated on the pre-treated ITO glass. Tetrabutylammonium perchlorate (TBAClO<sub>4</sub>, 0.1 M), and acetonitrile were used as electrolyte and solvent, respectively.

DSC was measured by Mettler DSC 30 with a heating rate of 10 °C/min. The 2D-WAXS experiments were performed by means of a rotating anode (Rigaku 18 kW) X-ray beam with a pinhole collimation and a two-dimensional Siemens detector. A double graphite monochromator for the Cu K $\alpha$  radiation ( $\lambda = 0.154$  nm) was used. The intensity distributions are plotted as a function of the scattering vector  $s$  (defined as  $s = 2\sin\theta/\lambda$ , where  $2\theta$  is the scattering angle).

---

## **5.2 General Procedures**

### **5.2.1 Electroluminescence devices**

The ITO covered glass substrates for the PLEDs were thoroughly cleaned in a variety of organic solvents and exposed to an oxygen plasma dry cleaning step. PEDOT:PSS (Baytron P from Bayer Inc.) layers were spin coated under ambient conditions and dried according to specifications by Bayer Inc. under inert atmosphere. The emissive polymer films were spin-cast from solution and dried at 80°C overnight in vacuum. Metal electrodes were thermally deposited in a vacuum coating mounted in a glove box at a base pressure of below  $2 \times 10^{-6}$  mbar.

EL spectra were recorded using an ORIEL spectrometer with an attached CCD camera. The current/luminance/voltage (ILV) characteristics were recorded in a customized setup using a Keithley 236 source measure unit for recording the current/voltage characteristics while recording the luminance using a calibrated photodiode attached to an integrating sphere (Ulbrich).

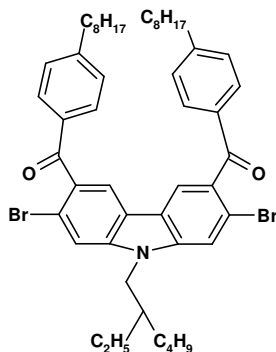
### **5.2.2 Solar cell devices**

The devices were fabricated by spin coating **1-4**:PCBM solutions (8-15 mg/ml) onto ITO substrates pre-treated with acetone and isopropanol in an ultrasonic bath followed by cleaning for 10 min with oxygen plasma. 100 nm thick silver was subsequently evaporated through a mask on the surface to form the cathode. The effective area of the device was approximately 6 mm<sup>2</sup> defined by overlap of etched ITO and the top electrode, which was accurately measured by an optical microscope for subsequent calculations.

### **5.2.3 FET Devices**

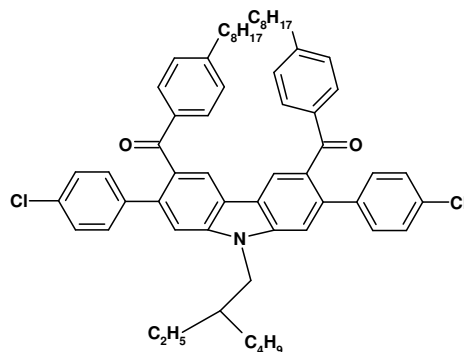
A highly n-type doped silicon wafer (acting as the gate electrode) with a 150 nm thermally grown silicon dioxide layer (acting as the insulator) serves as a transistor substrate. On top of the silicon dioxide, gold electrodes were patterned via optical lithography and evaporated in vacuum. To avoid charge carrier trapping by the polar silanol groups on the silicon dioxide surface it was treated with 1,1,1,3,3,3-Hexamethyldisilazane (HMDS) via vapor phase deposition.

## 5.3 Synthetic Procedures

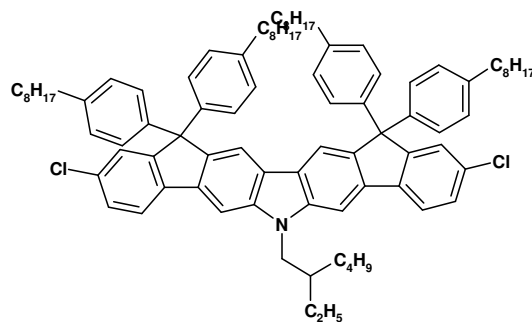
2,7-Dibromo-N-(2-ethylhexyl)-3,6-bis(4-octylbenzoyl)carbazole (**16**)

2,7-Dibromo-N-(2-ethylhexyl)carbazole (1.0 g, 2.28 mmol) and  $\text{AlCl}_3$  (0.73 g, 5.5 mmol) were dissolved in 1,2-dichloroethane (5 mL) and then 4-octylbenzoyl chloride (1.27 g, 4.8 mmol) was added slowly at room temperature. The mixture was stirred for 4 h at 50 °C and then quenched with ice. The inorganic precipitate was dissolved in 2M HCl and the product was extracted with dichloromethane. The organic fractions were dried over  $\text{MgSO}_4$  and the solvent was removed under reduced pressure. The product was purified by chromatography on silica gel with 0-10 % ethyl acetate in hexane as eluent to give compound **16** as a light yellow solid (1.8 g, 91 %).  $^1\text{H-NMR}$  (250 MHz,  $\text{CD}_2\text{Cl}_2$ ): ppm 8.01 (s, 2H), 7.74 (m, 6H), 7.28 (d, 4H,  $J = 8.2$  Hz), 4.22 (d, 2H,  $J = 7.7$  Hz), 2.67 (t, 4H,  $J = 7.75$  Hz), 2.13 (m, 1H), 1.70-1.15 (br m, 32H), 1.10-0.80 (br m, 12H).  $^{13}\text{C-NMR}$  (62.5 MHz,  $\text{CD}_2\text{Cl}_2$ ): ppm 196.09, 150.30, 143.51, 135.56, 132.94, 131.13, 129.38, 122.53, 121.77, 118.53, 115.15, 48.88, 40.02, 36.78, 32.61, 31.87, 31.49, 30.15, 30.05, 29.97, 29.33, 25.11, 23.80, 23.41, 14.61, 14.53, 11.42. FDMS:  $m/z$  870.0. Elemental analysis: Calculated C, 69.04; H, 7.30; N 1.61. Found C, 69.02; H, 7.28; N, 1.55.



**2,7-Bis(4-chlorophenyl)-9-(2-ethylhexyl)-3,6-(4-octylbenzoyl)carbazole (17)**

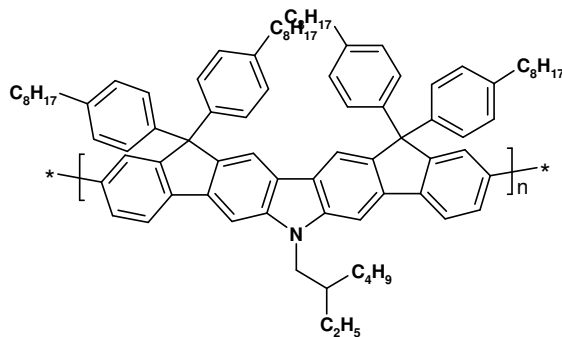
4-Chlorophenylboronic acid (0.96 g, 6.18 mmol), diketone **16** (2.44 g, 2.81 mmol), and  $\text{K}_2\text{CO}_3$  (775 mg, 5.62 mmol) were dissolved in THF (20 mL) and water (5 mL) in a 50 mL Schlenk flask. The solution was purged with argon for 20 min, and then tetrakis(triphenylphosphine)palladium (98 mg, 0.03 equiv) was added and the reaction was heated with stirring at 85 °C. The reaction was followed by TLC and was worked up after 24 h. The cooled mixture was extracted with dichloromethane, and the extract was washed with brine and then dried over  $\text{MgSO}_4$ . The crude product so obtained was purified by chromatography on silica gel with 0-20 % ethyl acetate in hexane as eluent. The product **17** was isolated as a colorless solid (2.15 g, 82 %).  $^1\text{H-NMR}$  (250 MHz,  $\text{CD}_2\text{Cl}_2$ ): ppm 8.24 (s, 2H), 7.64 (d, 4H,  $J = 8.1$  Hz), 7.49 (s, 2H), 7.29 (m, 8H), 7.16 (d, 4H,  $J = 8.1$  Hz), 4.33 (d, 2H,  $J = 7.3$  Hz), 2.62 (t, 4H,  $J = 7.6$  Hz), 2.17 (m, 1H), 1.68-1.20 (m, 32H), 1.0-0.80 (m, 12H).  $^{13}\text{C-NMR}$  (62.5 MHz,  $\text{CD}_2\text{Cl}_2$ ): ppm 197.84, 149.01, 143.19, 140.58, 139.81, 136.38, 133.49, 131.70, 131.01, 130.58, 128.67, 122.98, 121.46, 111.56, 48.21, 39.79, 36.31, 32.28, 31.54, 31.20, 29.80, 29.62, 29.02, 24.77, 23.44, 23.07, 14.27, 14.15, 11.08. FDMS:  $m/z$  931.1. Elemental analysis: Calculated C, 79.80; H, 7.67; N, 1.50. Found C, 79.72; H, 7.71; N, 1.46.

Ladder-type dichlorotetraphenylene **18**

(a) A solution of 4-octylbromobenzene (1.52 mL, 6.4 mmol) in dry THF (40 mL) in a 100 mL Schlenk flask was cooled to  $-78^{\circ}\text{C}$  in an acetone/dry ice bath. *n*-Butyllithium in hexane (4.21 mL, 1.6 M, 6.74 mmol) was then added and the mixture was stirred for 20 min. Then a solution of the diketone **17** (2.0 g, 2.14 mmol) in dry THF (10 mL) was added drop wise with stirring and the solution was slowly allowed to warm to room temperature. The mixture was stirred overnight and then quenched with brine. The product was extracted into diethyl ether, and the extract was washed with brine and dried over  $\text{MgSO}_4$ . The crude product was chromatographed on silica gel with 0-5 % ethyl acetate in hexane as eluent to give the diol as a thick viscous oil (2.53 g, 90 %).  $^1\text{H-NMR}$  (250 MHz,  $\text{CD}_2\text{Cl}_2$ ): ppm 7.35 (s, 2H), 7.04 (m, 22H), 6.78 (d, 4H,  $J = 8.4$  Hz), 4.07 (d, 2H,  $J = 7.4$  Hz), 2.74 (s, 2H), 2.62 (t, 8H,  $J = 7.4$  Hz), 2.02 (m, 1H), 1.72-1.54 (m, 8H), 1.44-1.10 (m, 48H), 0.95-0.70 (m, 18H).  $^{13}\text{C-NMR}$  (62.5 MHz,  $\text{CD}_2\text{Cl}_2$ ): ppm 145.61, 145.57, 142.38, 142.18, 140.41, 138.83, 137.30, 132.95, 131.77, 128.23, 127.94, 127.72, 121.61, 121.09, 83.42, 39.50, 35.90, 32.29, 32.02, 29.89, 29.81, 29.72, 28.57, 24.47, 23.36, 23.06, 15.75, 14.25, 14.12, 14.04, 11.86, 10.91. FDMS:  $m/z$  1315.5. Elemental analysis: Calculated C, 82.28; H, 8.82; N, 1.07. Found C, 82.39; H, 8.82; N 1.03. (b) The diol (1.2 g, 0.91 mmol) was dissolved in 1,2-dichloroethane (10 mL), and  $\text{BF}_3$ ·etherate (0.2 mL) was added with stirring at room temperature. The colorless solution turned deep blue immediately upon addition. The mixture was refluxed for 48 h, cooled and then quenched by adding 20 mL of methanol upon which the monomer **18** started precipitating as a light yellow solid. The mixture was further stirred for 2 h and then solid was collected by filtration, washed with methanol, and dried. The product was redissolved in dichloromethane and precipitated again by addition of methanol. Isolated yield of monomer **18** = 1.10 g (95 %).  $^1\text{H-NMR}$  (250 MHz,  $\text{CD}_2\text{Cl}_2$ ): ppm 7.88 (s, 2H), 7.80 (d,

2H,  $J = 8.7$  Hz), 7.70 (s, 2H), 7.37 (m, 4H), 7.06 (m, 16H), 4.30 (d, 2H,  $J = 7.4$  Hz), 2.52 (t, 8H,  $J = 7.7$  Hz), 2.21 (m, 1H), 1.64-1.15 (m, 56H), 1.04-0.78 (m, 18H):  $^{13}\text{C}$ -NMR (62.5 MHz,  $\text{CD}_2\text{Cl}_2$ ): ppm 154.64, 143.69, 143.45, 142.34, 141.96, 139.62, 137.63, 133.21, 128.68, 128.27, 128.07, 126.74, 123.81, 121.30, 117.91, 100.66, 64.77, 48.19, 39.76, 35.82, 32.26, 31.84, 31.34, 29.85, 29.81, 29.60, 29.19, 24.95, 24.90, 23.48, 23.04, 14.24, 11.20. FDMS:  $m/z$  1275.8. Elemental analysis: Calculated C, 84.60; H, 8.76; N, 1.10. Found C, 84.67; H, 8.73; N, 1.01.

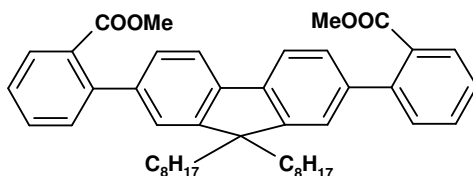
### Ladder-type nitrogen-bridged Poly(tetraphenylene) **19**



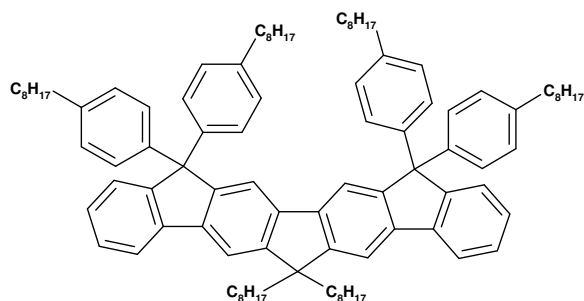
Bis(1,5-cyclooctadiene)nickel (152 mg, 2.4 equiv), cyclooctadiene (0.068 mL, 2.4 equiv), and 2,2'-bipyridine (88 mg, 2.4 equiv) were dissolved in dry toluene (2 mL) and dry N,N-dimethylformamide (2 mL) in a Schlenk tube within a glovebox. The mixture was heated at 60 °C with stirring under argon for 20 min to generate the catalyst, and then a solution of the monomer **18** (0.3 g, 0.23 mmol) in dry toluene (10 mL) was added. The reaction was heated at 80 °C for 2 days, where upon the solution became so viscous that it ceased to stir. Then a mixture of toluene (4 mL) and bromobenzene (0.1 mL) was added and the mixture was heated at 80 °C for an additional 12 h. The mixture was then poured into a mixture of methanol and concentrated hydrochloric acid (1:1, 200 mL) and stirred for 4 h. The precipitated yellow solid was redissolved in THF (10 mL) and added drop wise to methanol (100 mL). The resulting solid was filtered off and subjected to Soxhlet extraction for two days in acetone. The residue was then redissolved in THF and precipitated from mixture of methanol and ammonia (4:1, 200 mL), filtered, washed with methanol, and dried. Isolated yield of polymer **19** = 214 mg (77 %).  $^1\text{H}$ -NMR (250 MHz,  $\text{CD}_2\text{Cl}_2$ ): ppm 7.83 (br m, 10H), 7.17 (d, 8H,  $J = 7.2$  Hz), 7.04 (d, 8H,  $J = 7.5$  Hz), 4.96

(br m, 2H), 2.52(m, 8H), 2.24 (s, 1H), 1.70-1.10 (br m, 56H), 1.10-0.80 (br m, 18H)  
 GPC analysis:  $M_n = 4.6 \times 10^4 \text{ g mol}^{-1}$  and  $D = 2.8$  (against PPP standard). Elemental  
 analysis: Calculated C, 89.57; H, 9.27; N, 1.16. Found C, 89.38; H, 9.35; N, 1.05.

### Tetraphenylene diester **20**



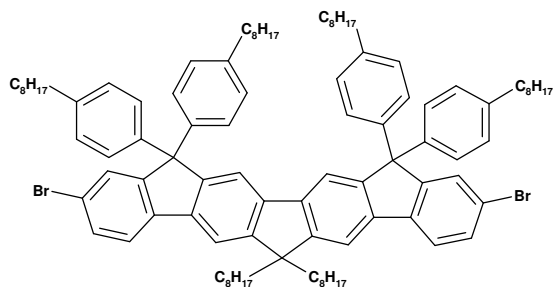
The methyl 2-bromobenzoate (0.64 mL, 4.60 mmol), 9,9'-dioctyl-2,7-fluorenediboric acid (1.00 g, 2.09 mmol), and K<sub>2</sub>CO<sub>3</sub> (634 mg, 4.60 mmol) were dissolved in THF (8 mL) and water (4 mL) in a 50 mL Schlenk flask. The solution was purged with argon for 20 min, and then tetrakis(triphenylphosphine)palladium (80 mg, 0.03 equiv) was added and the reaction was heated with stirring at 80 °C. The reaction was followed by TLC and was worked up after 24 h. The cooled mixture was extracted with dichloromethane, and the extract was washed with brine and then dried over MgSO<sub>4</sub>. The crude product so obtained was purified by chromatography on silica gel with 0-30 % ethyl acetate in hexane as eluent. The diester **20** was isolated as a white solid (0.98 g, 71 %). <sup>1</sup>H-NMR (250 MHz, CD<sub>2</sub>Cl<sub>2</sub>): ppm 7.80 (t, 4H, *J* = 6.7 Hz), 7.59 (m, 2H), 7.46 (m, 4H), 7.32 (m, 4H), 3.62 (s, 6H), 1.99 (m, 4H), 1.30-1.00 (m, 20H), 0.85-0.65 (m, 10H). <sup>13</sup>C-NMR (62.5 MHz, CD<sub>2</sub>Cl<sub>2</sub>): ppm 169.52, 151.28, 143.07, 140.71, 140.37, 131.79, 131.45, 131.12, 129.95, 127.52, 127.41, 123.50, 119.80, 55.62, 52.09, 40.87, 32.17, 30.46, 29.70, 29.63, 24.17, 22.97, 14.20. FDMS: *m/z* 660.0. Elemental analysis: Calculated C, 82.03; H, 8.26. Found C, 82.01; H, 8.25.

Tetraphenylene **21**

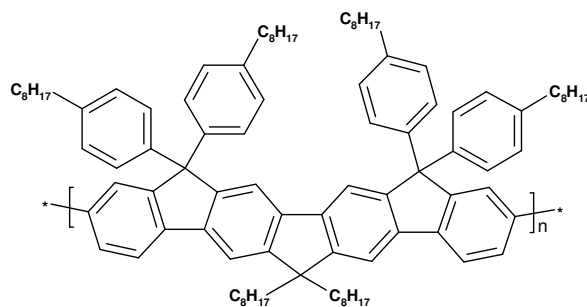
(a) A solution of 4-octylbromobenzene (0.96 mL, 4.06 mmol) in dry THF (40 mL) in a 100 mL Schlenk flask, was cooled to  $-78\text{ }^{\circ}\text{C}$  in an acetone/dry ice bath. *n*-Butyllithium in hexane (2.67 mL, 1.6 M, 4.27 mmol) was then added and the mixture was stirred for 20 min. Then a solution of the diester **20** (0.9 g, 1.36 mmol) in dry THF (10 mL) was added drop wise with stirring and the solution was slowly allowed to warm to room temperature. The mixture was stirred overnight and then quenched with brine. The product was extracted into diethyl ether, and the extract was washed with brine and dried over MgSO<sub>4</sub>. The crude product was chromatographed on silica gel with 0-5 % ethyl acetate in hexane as eluent to give the diol as a thick viscous oil (1.73 g, 94 %). <sup>1</sup>H-NMR (250 MHz, CD<sub>2</sub>Cl<sub>2</sub>): ppm 7.49 (d, 2H,  $J = 7.8$  Hz), 7.29 (d, 2H,  $J = 7.3$  Hz), 7.24-7.92 (m, 20H), 6.83 (m, 6H), 3.02 (s, 2H), 2.62 (t, 8H,  $J = 7.6$  Hz), 1.72-0.96 (m, 72H), 0.88 (t, 12H,  $J = 6.4$  Hz), 0.79 (t, 6H,  $J = 6.6$  Hz), 0.42 (s, 4H). <sup>13</sup>C-NMR (62.5 MHz, CD<sub>2</sub>Cl<sub>2</sub>): ppm 150.93, 146.00, 145.57, 142.27, 141.87, 141.52, 140.12, 133.25, 130.70, 129.02, 128.35, 128.15, 127.07, 126.55, 124.02, 119.77, 83.68, 55.51, 35.88, 32.31, 32.22, 31.99, 30.21, 29.89, 29.76, 29.70, 24.15, 23.08, 23.01, 14.26, 14.22. FDMS:  $m/z$  1356.3. (b) The diol (1.5 g, 1.10 mmol) was dissolved in dichloromethane (10 mL), and BF<sub>3</sub>·etherate (0.5 mL) was added with stirring at room temperature. The colorless solution turned deep blue immediately upon addition. The mixture was stirred overnight at room temperature, and then quenched by adding 30 mL of methanol. No precipitation of the product was observed. Then, the mixture was extracted with diethyl ether, and the extract was washed with brine and dried over MgSO<sub>4</sub>. The crude product was chromatographed on silica gel with 0-2 % ethyl acetate in hexane as eluent to give the tetraphenylene **21** as a thick viscous oil (1.27 g, 88 %). <sup>1</sup>H-NMR (250 MHz, CD<sub>2</sub>Cl<sub>2</sub>): ppm 7.81 (d, 2H,  $J = 7.4$  Hz), 7.75 (s, 2H), 7.58 (s, 2H), 7.30 (m, 6H), 7.06 (m, 16H),

2.54 (t, 8H,  $J = 7.4$  Hz), 2.12 (m, 4H), 1.65-1.00 (m, 72H), 0.86 (t, 12H,  $J = 5.8$  Hz), 0.77 (t, 6H,  $J = 6.6$  Hz).  $^{13}\text{C}$ -NMR (62.5 MHz,  $\text{CD}_2\text{Cl}_2$ ): ppm 152.50, 151.63, 151.12, 143.75, 141.79, 141.63, 140.64, 139.77, 128.60, 128.36, 127.69, 126.43, 120.87, 120.24, 117.45, 114.92, 65.02, 54.86, 41.15, 35.81, 32.25, 32.17, 31.96, 31.83, 30.45, 29.85, 29.81, 29.59, 23.03, 22.94, 14.24, 14.18. FDMS:  $m/z$  1319.7.

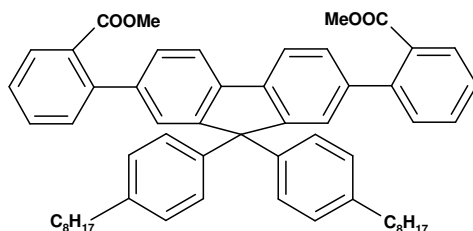
### Dibromotetraphenylene **22**



The tetraphenylene **21** (1.0 g, 0.75 mmol) was added to carbon tetrachloride (20 mL) in a 100 mL round bottom flask, followed by  $\text{CuBr}_2$  on alumina (3.18 g). The reaction was heated under reflux with stirring and monitored by FDMS, which showed nearly quantitative formation of the dibromide after 16 h. The reaction mixture was concentrated, the crude product so obtained was purified by chromatography on silica with hexane as eluent. The monomer **22** was isolated as a light yellow solid (0.95 g, 86 %).  $^1\text{H}$ -NMR (250 MHz,  $\text{CD}_2\text{Cl}_2$ ): ppm 7.72 (s, 2H), 7.69 (d, 2H,  $J = 8.0$  Hz), 7.55 (s, 2H), 7.49 (m, 4H), 7.06 (m, 16H), 2.53 (t, 8H,  $J = 7.4$  Hz), 2.08 (m, 4H), 1.64-1.00 (m, 72H), 0.87 (t, 12H,  $J = 6.5$  Hz), 0.77 (t, 6H,  $J = 6.6$  Hz).  $^{13}\text{C}$ -NMR (62.5 MHz,  $\text{CD}_2\text{Cl}_2$ ): ppm 154.64, 151.89, 151.08, 142.97, 142.12, 141.90, 139.76, 138.80, 130.91, 129.55, 128.79, 128.34, 121.73, 121.17, 117.59, 115.09, 65.16, 54.96, 41.10, 35.85, 32.29, 32.19, 31.83, 30.43, 29.87, 29.84, 29.63, 29.59, 24.33, 23.07, 22.98, 14.28, 14.22. FDMS:  $m/z$  1477.2. Elemental analysis: Calculated C, 80.46; H, 8.73. Found C, 80.36; H, 8.75.

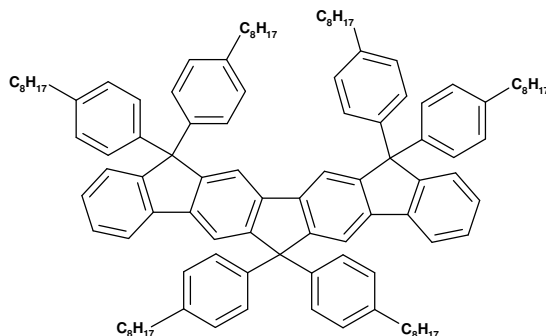
Poly(ladder-type tetraphenylene) **23**

Bis(1,5-cyclooctadiene)nickel (225 mg, 2.4 equiv), cyclooctadiene (0.163 mL, 2.4 equiv), and 2,2'-bipyridine (130 mg, 2.4 equiv) were dissolved in dry toluene (2 mL) and dry N,N-dimethylformamide (2 mL) in a Schlenk tube within a glovebox. The mixture was heated at 60 °C with stirring under argon for 20 min to generate the catalyst, and then a solution of the monomer **22** (0.50 g, 0.34 mmol) in dry toluene (12 mL) was added. The reaction was heated at 80 °C for 2 days, where upon the solution became so viscous that it ceased to stir. Then a mixture of toluene (5 mL) and bromobenzene (0.1 mL) was added and the mixture was heated at 80 °C for an additional 12 h. The mixture was then poured into a mixture of methanol and concentrated hydrochloric acid (1:1, 200 mL) and stirred for 4 h. The precipitated yellow solid was redissolved in THF (10 mL) and added drop wise to methanol (100 mL). The resulting solid was filtered off and subjected to Soxhlet extraction for two days in acetone. The residue was then redissolved in THF and then precipitated from methanol (100 mL), filtered, and dried. Isolated yield of polymer **23** = 313 mg (70 %). <sup>1</sup>H-NMR (250 MHz, CD<sub>2</sub>Cl<sub>2</sub>): ppm 7.80-7.45 (m, 10H), 7.30-6.90 (m, 16H), 2.70-1.95 (m, 12H), 1.65-0.95 (m, 72H), 0.86 (t, 12H, *J* = 6.6 Hz), 0.77 (t, 6H, *J* = 6.7 Hz). GPC analysis: Mn = 3.5 × 10<sup>4</sup> and D = 2.3 (against PPP standard). Elemental analysis: Calculated C, 90.21; H, 9.79. Found C, 90.22; H, 9.69.

Tetraphenylene diester **25**

The methyl 2-bromobenzoate (0.20 mL, 1.36 mmol), 9,9'-bis(4-octyl phenyl)-2,7-fluorenediboronic ester **24** (0.5 g, 0.62 mmol), and  $K_2CO_3$  (188 mg, 1.36 mmol) were dissolved in THF (6 mL) and water (3 mL) in a 50 mL Schlenk flask. The solution was purged with argon for 20 min, and then tetrakis(triphenylphosphine)palladium (27 mg, 0.03 equiv) was added and the reaction was heated with stirring at 80 °C. The reaction was followed by TLC and was worked up after 24 h. The cooled mixture was extracted with dichloromethane, and the extract was washed with brine and then dried over  $MgSO_4$ . The crude product so obtained was purified by chromatography on silica gel with 0-7 % ethyl acetate in hexane as eluent. The diester **25** was isolated as a white solid (0.38 g, 77 %).  $^1H$ -NMR (250 MHz,  $CD_2Cl_2$ ): ppm 7.89 (d, 2H,  $J = 7.82$  Hz), 7.77 (d, 2H,  $J = 7.72$  Hz), 7.59-7.48 (m, 2H), 7.47-7.35 (m, 6H), 7.33 (s, 2H), 7.14 (d, 4H,  $J = 8.24$  Hz), 7.07 (d, 4H,  $J = 8.31$  Hz), 3.40 (s, 6H), 2.55 (d, 4H,  $J = 7.72$  Hz), 1.67-1.45 (m, 4H), 1.40-1.20 (m, 20H), 0.89 (t, 6H,  $J = 6.40, 6.40$  Hz).  $^{13}C$ -NMR (62.5 MHz,  $CD_2Cl_2$ ): ppm 169.22, 152.03, 143.47, 142.58, 141.92, 141.16, 139.28, 131.64, 131.46, 131.04, 130.00, 128.64, 128.40, 128.07, 127.49, 126.80, 120.47, 65.36, 52.07, 35.80, 32.26, 31.92, 29.83, 29.80, 29.62, 23.04, 14.25. FDMS:  $m/z$  810.4. Elemental analysis: Calculated C, 84.41; H, 7.70. Found C, 84.38; H, 7.78.

### Fully arylated Tetraphenylene **26**

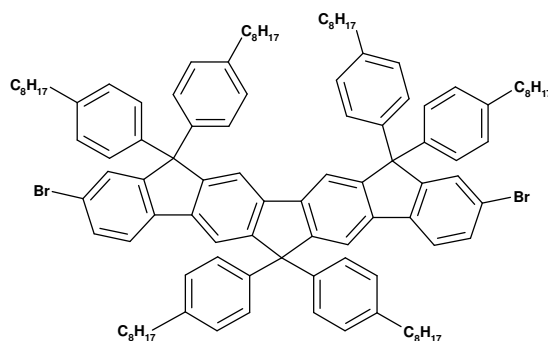


(a) A solution of 4-octylbromobenzene (0.26 mL, 1.10 mmol) in dry THF (30 mL) in a 100 mL Schlenk flask, was cooled to  $-78$  °C in an acetone/dry ice bath. *n*-Butyllithium in hexane (0.72 mL, 1.6 M, 1.16 mmol) was then added and the mixture was stirred for 20 min. Then a solution of the diester **25** (0.3 g, 0.37 mmol) in dry THF (10 mL) was added drop wise with stirring and the solution was slowly allowed to warm to room temperature. The mixture was stirred overnight and then quenched with brine. The



product was extracted into diethyl ether, and the extract was washed with brine and dried over  $\text{MgSO}_4$ . The crude product was chromatographed on silica gel with 0-2 % ethyl acetate in hexane as eluent to give the diol as thick viscous oil (0.49 g, 88 %) (**b**) The diol (0.40 g, 0.26 mmol) was dissolved in dichloromethane (5 mL), and  $\text{BF}_3 \cdot \text{etherate}$  (0.2 mL) was added with stirring at room temperature. The colorless solution turned deep blue immediately upon addition. The mixture was stirred overnight at room temperature, and then quenched by adding 30 mL of methanol. No precipitation of the product was observed. Then, the mixture was extracted with diethyl ether, and the extract was washed with brine and dried over  $\text{MgSO}_4$ . The crude product was chromatographed on silica gel with 0-3 % ethyl acetate in hexane as eluent to give the tetraphenylene **26** as a thick viscous oil (0.37 g, 98 %).  $^1\text{H-NMR}$  (250 MHz,  $\text{CD}_2\text{Cl}_2$ ): ppm 7.75 (s, 2H), 7.72-7.62 (m, 4H), 7.31 (t, 4H,  $J = 7.41, 7.41$  Hz), 7.23 (d, 6H,  $J = 7.96$  Hz), 7.15-7.06 (m, 12H), 7.04 (d, 8H,  $J = 8.26$  Hz), 2.61-2.47 (m, 12H), 1.66-1.46 (m, 12H), 1.40-1.18 (m, 60H), 0.91-0.81 (m, 18H).  $^{13}\text{C-NMR}$  (62.5 MHz,  $\text{CD}_2\text{Cl}_2$ ): ppm 152.46, 152.34, 151.84, 143.65, 143.48, 141.97, 141.90, 140.47, 140.38, 140.27, 128.73, 128.66, 128.52, 128.38, 127.84, 127.70, 126.39, 120.49, 118.10, 118.02, 65.10, 64.73, 35.84, 32.28, 31.87, 29.87, 29.84, 29.63, 23.06, 14.27. FDMS:  $m/z$  1471. Elemental analysis: Calculated C, 90.55; H, 9.45. Found C, 90.07; H, 9.19.

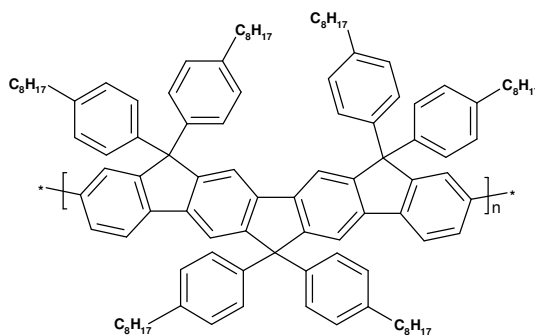
### Fully arylated Dibromotetraphenylene **27**



The tetraphenylene **26** (0.5 g, 0.34 mmol) was added to carbon tetrachloride (25 mL) in a 100 mL round bottom flask, followed by  $\text{CuBr}_2$  on alumina (1.44 g). The reaction was heated under reflux with stirring and monitored by FDMS, which showed nearly quantitative formation of the dibromide after 16 h. The reaction mixture was concentrated; the crude product so obtained was purified by chromatography on silica gel

with hexane as eluent. The monomer **27** was isolated as a light yellow solid (0.44 g, 79 %).  $^1\text{H-NMR}$  (250 MHz,  $\text{CD}_2\text{Cl}_2$ ): ppm 7.72 (s, 2H), 7.63 (s, 2H), 7.55 (d, 2H,  $J = 7.83$  Hz), 7.48-7.39 (m, 4H), 7.19 (d, 4H,  $J = 8.20$  Hz), 7.12-7.01 (m, 20H), 2.63-2.44 (m, 12H), 1.66-1.44 (m, 12H), 1.45-1.12 (m, 60H), 0.95-0.80 (m, 18H).  $^{13}\text{C-NMR}$  (62.5 MHz,  $\text{CD}_2\text{Cl}_2$ ): ppm 154.54, 152.56, 151.72, 143.40, 142.68, 142.21, 142.09, 140.71, 139.37, 130.90, 129.48, 128.81, 128.47, 128.31, 121.96, 121.45, 118.23, 118.11, 65.20, 64.75, 35.84, 32.28, 31.88, 31.84, 29.83, 29.62, 23.06, 14.27. FDMS:  $m/z$  1630.7. Elemental analysis: Calculated C, 81.79; H, 8.41. Found C, 81.65; H, 8.53.

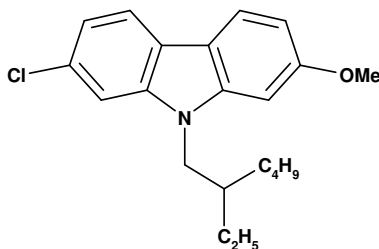
### Fully arylated Poly(tetraphenylene) **28**



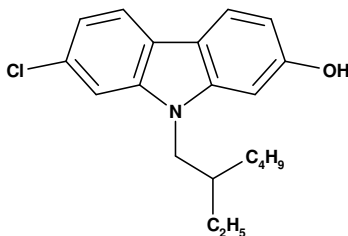
Bis(1,5-cyclooctadiene)nickel (103 mg, 2.4 equiv), cyclooctadiene (0.042 mL, 2.4 equiv), and 2,2'-bipyridine (58 mg, 2.4 equiv) were dissolved in dry toluene (3 mL) and dry *N,N*-dimethylformamide (3 mL) in a Schlenk tube within a glovebox. The mixture was heated at 60 °C with stirring under argon for 20 min to generate the catalyst, and then a solution of the monomer **27** (0.25 g, 0.34 mmol) in dry toluene (7 mL) was added. The reaction was heated at 80 °C for 2 days, where upon the solution became so viscous that it ceased to stir. Then a mixture of toluene (5 mL) and bromobenzene (0.1 mL) was added and the mixture was heated at 80 °C for an additional 12 h. The mixture was then poured into a mixture of methanol and concentrated hydrochloric acid (1:1, 200 mL) and stirred for 4 h. The precipitated yellow solid was redissolved in THF (10 mL) and added drop wise to methanol (100 mL). The resulting solid was filtered off and subjected to Soxhlet extraction for two days in acetone. The residue was then redissolved in THF and then precipitated from methanol (100 mL), filtered, and dried. Isolated yield of polymer **28** = 170 mg (75 %).  $^1\text{H-NMR}$  (250 MHz,  $\text{CD}_2\text{Cl}_2$ ): ppm 7.88-7.38 (m, 10H), 7.34-6.77 (m, 24H), 2.90-2.16 (m, 12H), 1.77-1.04 (m, 72H), 1.02-0.67 (m, 18H). GPC analysis:  $M_n$  =

$7.03 \times 10^4$  and  $D = 2.8$  (against PPP standard). Elemental analysis: Calculated C, 90.68; H, 9.32. Found C, 87.83; H, 8.89.

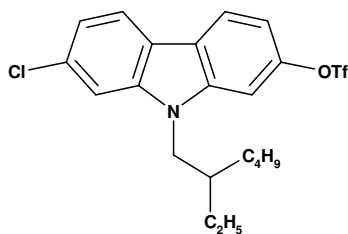
### 2-Chloro-7-methoxy-N-(2-ethylhexyl)carbazole (36)



A 250 mL Schlenk flask was charged with carbazole **35** (4.00 g, 17.2 mmol), NaH (0.96 g, 24.0 mmol) and 100 mL of DMF. The resulting mixture was stirred for 30 min. 2-Ethylhexylbromide (5.0 g, 25.9 mmol) was then added under argon and the mixture was stirred overnight at room temperature. The reaction was quenched with brine and extracted three times with diethyl ether (40 mL each). The combined organic fractions were washed with brine and dried over  $\text{MgSO}_4$ . The solvent was removed under reduced pressure and the residue was purified by column chromatography on silica gel with 0-5 % ethyl acetate in hexane as eluent to give the compound **36** as a colorless oil (5.4 g, 91 %).  $^1\text{H-NMR}$  (250 MHz,  $\text{CD}_2\text{Cl}_2$ ): ppm 7.94-7.84 (m, 2H), 7.34 (d, 1H,  $J = 1.7$  Hz), 7.14 (dd, 1H,  $J=1.8$  Hz,  $J = 8.2$  Hz), 6.88-6.81 (m, 2H), 4.08 (d, 2H,  $J = 7.8$  Hz), 3.91 (s, 3H), 2.04 (m, 1H), 1.45-1.20 (m, 8H), 0.96-0.81 (m, 6H).  $^{13}\text{C-NMR}$  (62.5 MHz,  $\text{CD}_2\text{Cl}_2$ ): ppm 159.69, 143.07, 142.04, 130.19, 122.00, 121.26, 120.45, 119.44, 116.37, 109.30, 108.10, 93.98, 55.93, 47.86, 39.49, 31.24, 29.10, 24.74, 23.43, 14.16, 11.07, FDMS:  $m/z$  343.1. Elemental analysis: Calculated C, 73.35; H, 7.62; N, 4.07. Found C, 73.26; H, 7.55; N, 4.01.

**2-Chloro-7-hydroxy-N-(2-ethylhexyl)carbazole (37)**

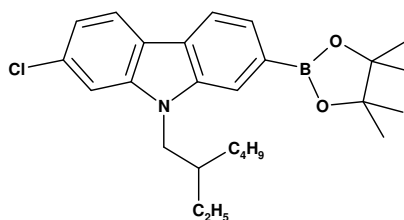
An oven dried flask was charged with chloromethoxycarbazole **36** (5 g, 14.5 mmol) and 100 mL of anhydrous methylene chloride. The solution was cooled to 0 °C and 43.6 mL of boron tribromide (1M in methylene chloride) was added over 30 min while stirring. The resulting mixture was slowly allowed to warm to room temperature. The mixture was stirred overnight and then quenched by 2M HCl to destroy excess of boron tribromide. The mixture was extracted with methylene chloride and the extract was washed with brine and then dried over MgSO<sub>4</sub>. The crude product so obtained was purified by chromatography on silica gel with 0-20 % ethyl acetate in hexane as eluent to give the compound **37** as a colorless viscous oil (4.24 g, 89 %). <sup>1</sup>H-NMR (250 MHz, CD<sub>2</sub>Cl<sub>2</sub>): ppm 7.87 (d, 2H, *J* = 8.3 Hz), 7.33 (d, 1H, *J* = 1.5 Hz), 7.15 (dd, 1H, *J* = 1.6 Hz, *J* = 8.2 Hz), 6.83 (d, 1H, *J* = 2.0 Hz), 6.75 (dd, 1H, *J* = 2.0 Hz, *J* = 8.4 Hz), 5.26 (s, 1H), 4.01 (d, 2H, *J* = 7.7 Hz), 2.01 (m, 1H), 1.49-1.21 (m, 8H), 0.95-0.80 (m, 6H). <sup>13</sup>C NMR (62.5 MHz, CD<sub>2</sub>Cl<sub>2</sub>): ppm 155.39, 143.18, 142.12, 130.32, 122.01, 121.48, 120.46, 119.50, 116.64, 109.34, 108.74, 95.96, 48.00, 39.45, 31.24, 29.09, 24.72, 23.45, 14.17, 11.06. FDMS: *m/z* 328.3. Elemental analysis: Calculated C, 72.82; H, 7.33; N, 4.25. Found C, 72.73; H, 7.35; N, 4.19.

**2-Chloro-7-trifluoromethanesulfonyl-9-(2-ethylhexyl)carbazole (38)**

A 250 mL Schlenk flask was charged with chlorohydroxycarbazole **37** (4 g, 12.1 mmol), dimethylaminopyridine (1.48 g, 12.1 mmol) and 40 mL of anhydrous pyridine. The

mixture was cooled to 0 °C and trifluoromethanesulfonic anhydride (3.07 mL, 18.2 mmol) was added dropwise. The resulting mixture was slowly allowed to warm to room temperature. The mixture was stirred for 24 h and then quenched by brine to destroy excess of anhydride. The mixture was extracted with diethylether and the extract was successively washed with brine, aqueous CuSO<sub>4</sub> (0.1M) and again with brine and then dried over MgSO<sub>4</sub>. The crude product so obtained was purified by chromatography on silica gel with 0-10 % ethyl acetate in hexane as eluent to give the compound **38** as a light brown viscous oil (5.05 g, 90 %). <sup>1</sup>H-NMR (250 MHz, CD<sub>2</sub>Cl<sub>2</sub>): ppm 8.10 (d, 1H, *J* = 8.6 Hz), 8.02 (d, 1H, *J* = 8.3 Hz), 7.44 (d, 1H, *J* = 1.6 Hz), 7.31 (d, 1H, *J* = 2.1 Hz), 7.25 (dd, 1H, *J* = 1.7 Hz, *J* = 8.3 Hz), 7.16 (dd, 1H, *J* = 2.2 Hz, *J* = 8.6 Hz), 4.13 (d, 2H, *J* = 7.6 Hz), 1.86 (m, 1H), 1.47-1.15 (m, 8H), 0.96-0.80 (m, 6H). <sup>13</sup>C-NMR (62.5 MHz, CD<sub>2</sub>Cl<sub>2</sub>): ppm 148.29, 142.81, 141.66, 132.66, 122.47, 121.85, 121.71, 120.85, 120.56, 112.69, 110.01, 103.04, 48.27, 39.61, 31.25, 29.07, 24.71, 23.32, 14.06, 10.97. FDMS: *m/z* 461.5.

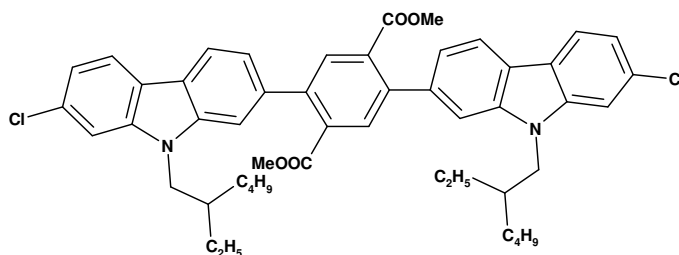
**2-Chloro-9-(2-ethylhexyl)-7-(4,4,5,5-tetramethyl-[1,3,2]dioxaborolan-2-yl)carbazole (39)**



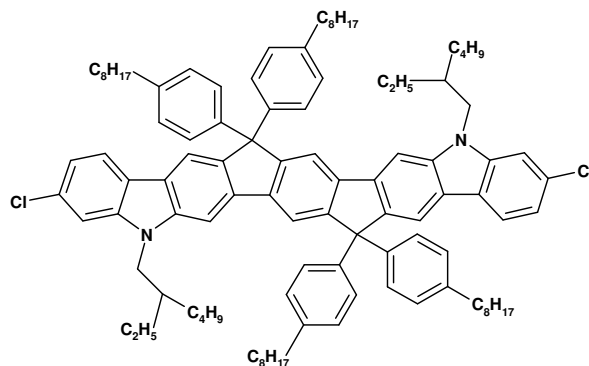
An oven dried 100 mL flask was charged successively with compound **38** (4 g, 8.51 mmol), 30 mL of anhydrous 1,2-dichloroethane, 63 mg of PdCl<sub>2</sub>(dppf), 3.82 mL of triethylamine and 2.61 mL of 4,4,5,5-tetramethyl-1,3,2-dioxaborolane. The mixture was stirred under argon for overnight at 80 °C and then poured in 50 mL of distilled water. The aqueous layer was extracted with dichloromethane and then dried over MgSO<sub>4</sub>. The crude dark oil was purified by chromatography on silica gel with 0-30 % ethyl acetate in hexane as eluent to give the compound **39** as a light yellow viscous oil (2.78 g, 73.5 %). <sup>1</sup>H-NMR (250 MHz, CD<sub>2</sub>Cl<sub>2</sub>): ppm 8.07 (d, 1H, *J* = 7.6 Hz), 8.02 (d, 1H, *J* = 8.3 Hz), 7.85 (s, 1H), 7.62 (d, 1H, *J* = 7.8 Hz), 7.41 (d, 1H, *J* = 1.7 Hz), 7.18 (dd, 1H, *J* = 1.7 Hz, *J* = 8.3 Hz), 4.18 (m, 2H), 2.07 (m, 1H), 1.49-1.19 (m, 20H), 0.93-0.80 (m, 6H). <sup>13</sup>C-

NMR (62.5 MHz, CD<sub>2</sub>Cl<sub>2</sub>): ppm 142.24, 141.22, 132.15, 125.65, 124.91, 121.85, 121.54, 119.74, 119.49, 115.99, 109.66, 84.19, 47.77, 39.57, 31.07, 28.90, 25.15, 25.10, 24.75, 23.43, 14.24, 11.11. FDMS: m/z 439.8.

**2,5-Bis-[7-chloro-9-(2-ethylhexyl)-carbazole-2-yl]-terephthalic acid dimethyl ester (41)**



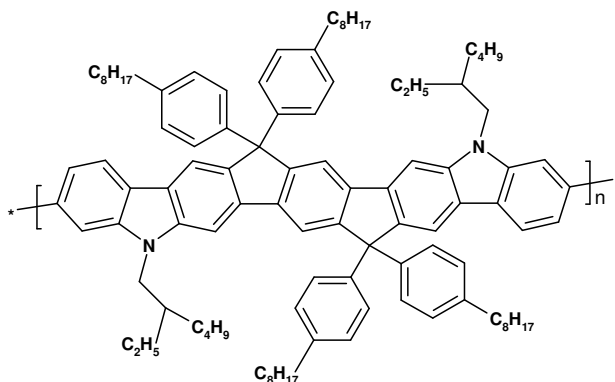
2-Chloro-9-(2-ethylhexyl)-7-(4,4,5,5-tetramethyl-[1,3,2]dioxaborolan-2-yl)carbazole (**39**) (2.77 g, 6.30 mmol), 2,5-dibromo-terephthalic acid dimethyl ester (**40**) (1.0 g, 2.84 mmol), and K<sub>2</sub>CO<sub>3</sub> (785 mg, 5.70 mmol) were dissolved in THF (20 mL) and water (5 mL) mixture in a 50 mL Schlenk flask. The solution was purged with argon for 20 min., and then Pd(PPh<sub>3</sub>)<sub>4</sub> (100 mg, 0.03 equiv) was added and the reaction mixture was heated with stirring at 85 °C. The reaction was followed by TLC and was worked up after 13 h. The cooled mixture was extracted with dichloromethane, and the extract was washed with brine and then dried over MgSO<sub>4</sub>. The crude product so obtained was purified by chromatography on silica gel with 0-10 % ethyl acetate in hexane as eluent. The product **41** was isolated as a yellow solid (2.3 g, 96 %). <sup>1</sup>H-NMR (300 MHz, CD<sub>2</sub>Cl<sub>2</sub>): ppm 8.12 (d, 2H, *J* = 8.04 Hz), 8.05 (d, 2H, *J* = 8.29 Hz), 7.93 (s, 2H), 7.47-7.42 (m, 4H), 7.31-7.19 (m, 4H), 4.26-4.11 (m, 4H), 3.64 (s, 6H), 2.22-1.96 (m, 2H), 1.50-1.17 (m, 16H), 0.93 (t, 6H, *J* = 7.42, 7.42 Hz), 0.85 (t, 6H, *J* = 7.07 Hz, 7.07 Hz). <sup>13</sup>C-NMR (75 MHz, CD<sub>2</sub>Cl<sub>2</sub>): ppm 167.68, 141.32, 140.69, 140.58, 137.14, 132.99, 131.30, 130.76, 120.99, 120.50, 120.43, 119.41, 119.27, 118.66, 108.58, 108.49, 46.98, 38.58, 30.17, 27.95, 23.68, 22.34, 13.03, 9.98. FDMS: m/z 818.2. Elemental analysis: Calculated C, 73.43; H, 6.65; N, 3.43. Found C, 73.38; H, 6.81; N, 3.28.

Ladder-type dichloropentaphenylene **43**

(a) A solution of 4-octylbromobenzene (2.89 mL, 12.2 mmol) in dry THF (50 mL) in a 100 mL Schlenk flask was cooled to  $-78^{\circ}\text{C}$  in an acetone/dry ice bath. *n*-Butyllithium in hexane (7.5 mL, 1.6 M, 12.0 mmol) was then added and the mixture was stirred for 20 min. Then solution of 2,5-bis-[7-chloro-9-(2-ethylhexyl)-carbazole-2-yl]-terephthalic acid dimethyl ester (**41**) (2.0 g, 2.44 mmol) in dry THF (10 mL) was added dropwise with stirring and then it was slowly allowed to warm to room temperature. The reaction mixture was stirred overnight and then quenched with brine. The mixture was extracted with diethyl ether, and the extract was washed with brine and dried over  $\text{MgSO}_4$ . The crude product was chromatographed on silica with 0-5 % ethyl acetate in hexane as eluent to give the diol **42** as a thick colorless viscous oil (3.17 g, 82 %). (b) The diol **42** (1.0 g, 0.66 mmol) was dissolved in dichloromethane (10 mL) and  $\text{BF}_3 \cdot \text{etherate}$  (0.2 mL) was added with stirring at room temperature. The colorless solution turned deep blue immediately upon addition of boron trifluoride. The mixture was stirred overnight at room temperature and then quenched by adding 50 mL of methanol. The monomer **43** was started precipitating as a light yellow solid. The mixture was further stirred for 2 h and then solid was collected by filtration, washed with methanol, and dried. The product was redissolved in dichloromethane and precipitated again by addition of methanol. Isolated yield of compound **43** = 0.86 g (88 %).  $^1\text{H-NMR}$  (300 MHz,  $\text{CD}_2\text{Cl}_2$ ): ppm 7.98 (s, 2H), 7.93-7.86 (m, 4H), 7.69 (s, 2H), 7.37 (d, 2H,  $J = 1.64$  Hz), 7.29 (d, 8H,  $J = 7.31$  Hz), 7.17-7.08 (m, 10H), 4.31-4.06 (m, 4H), 2.57 (t, 8H,  $J = 7.78$  Hz), 2.32-2.00 (m, 2H), 1.79-1.12 (m, 64H), 1.06-0.76 (m, 24H).  $^{13}\text{C-NMR}$  (300 MHz,  $\text{CD}_2\text{Cl}_2$ ): ppm 152.81, 144.54, 144.47, 144.42, 142.67, 141.86, 140.88, 139.08, 131.41, 128.68, 128.54, 122.90, 121.89, 121.28, 119.47, 117.94, 109.50, 100.78, 64.49, 48.17, 39.47, 35.86, 32.26, 31.93,

31.05, 29.87, 29.83, 29.61, 28.98, 24.77, 23.44, 23.03, 14.24, 11.07. FDMS:  $m/z$  1481.3. Elemental analysis: Calculated C, 84.45; H, 8.86; N, 1.89. Found C, 84.51; H, 8.90; N 1.71.

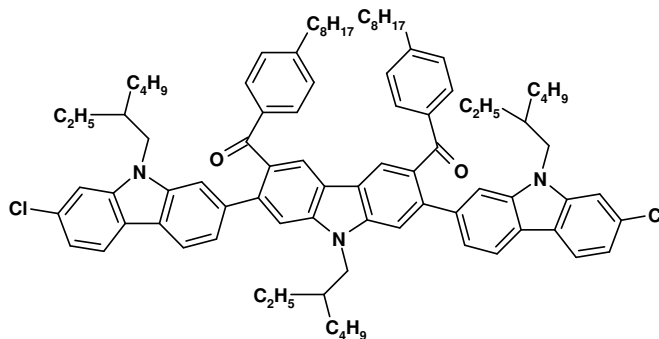
#### Nitrogen-bridged Poly(ladder-type pentaphenylene) **44**



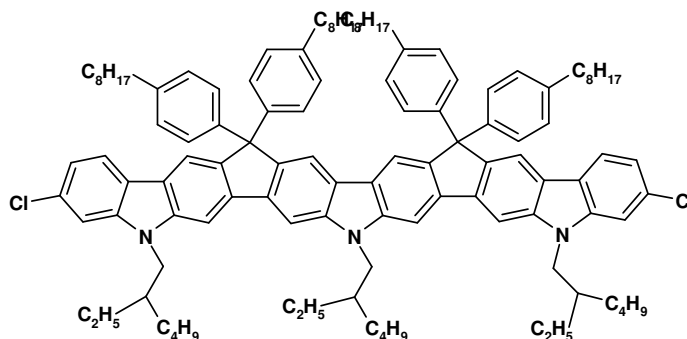
Bis(1,5-cyclooctadiene)nickel (132 mg, 2.4 equiv), cyclooctadiene (0.059 mL, 2.4 equiv), and 2,2'-bipyridine (76 mg, 2.4 equiv) were dissolved in dry toluene (2 mL) and dry N,N-dimethylformamide (2 mL) in a Schlenk tube within a glovebox. The mixture was heated at 60 °C with stirring under argon for 20 min to generate the catalyst, and then a solution of the monomer **43** (0.3 g, 0.20 mmol) in dry toluene (8 mL) was added. The reaction was heated at 80 °C for 2 days, where upon the solution became so viscous that it ceased to stir. Then a mixture of toluene (4 mL) and bromobenzene (0.1 mL) was added and the mixture was heated at 80 °C for an additional 12 h. The mixture was then poured into a mixture of methanol and concentrated hydrochloric acid (1:1, 200 mL) and stirred for 4 h. The precipitated yellow solid was redissolved in THF (10 mL) and added drop wise to methanol (100 mL). The resulting solid was filtered off and subjected to Soxhlet extraction for two days in acetone. The residue was then redissolved in THF and precipitated from mixture of methanol and ammonia (4:1, 200 mL), filtered, washed with methanol, and dried. Isolated yield of polymer **44** = 197 mg (70 %). <sup>1</sup>H-NMR (250 MHz, CD<sub>2</sub>Cl<sub>2</sub>): ppm 8.36-7.50 (m, 12H), 7.33 (d, 8H,  $J = 7.18$  Hz), 7.13 (d, 8H,  $J = 7.22$  Hz), 2.78-2.43 (m, 8H), 2.40-2.04 (m, 2H), 1.81-1.05 (m, 64H), 1.04-0.71 (m, 24H). GPC analysis:  $M_n = 4.6 \times 10^4$  gmol<sup>-1</sup> and  $D = 2.5$  (against PPP standard). Elemental analysis: Calculated C, 88.71; H, 9.31; N, 1.99. Found C, 88.61; H, 9.14; N, 1.71.



**2,7-Bis[7-chloro-9-(2'-ethylhexyl)carbazole-2''-yl]-9'-(2'''-ethylhexyl)-3,6-bis(4-octylbenzoyl)carbazole **45****



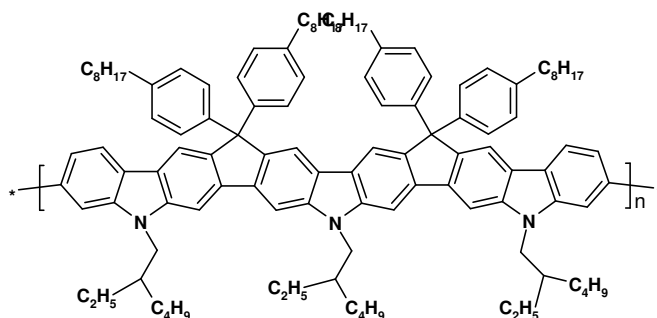
The carbazole boronic ester **39** (1.11g, 2.52 mmol), diketone **16** (1.0 g, 1.14 mmol), and  $K_2CO_3$  (314 mg, 2.28 mmol) were dissolved in THF (10 mL) and water (3 mL) mixture in a 50 mL Schlenk flask. The solution was purged with argon for 20 min., and then  $Pd(PPh_3)_4$  (40 mg, 0.03 equiv) was added and the reaction mixture was heated with stirring at 85 °C. The reaction was followed by TLC and was worked up after 24 h. The cooled mixture was extracted with dichloromethane, and the extract was washed with brine and then dried over  $MgSO_4$ . The crude product so obtained was purified by chromatography on silica with 0-10 % ethyl acetate in hexane as eluent. The product **45** was isolated as a yellow solid (1.1 g, 72 %).  $^1H$ -NMR (250 MHz,  $CD_2Cl_2$ ) ppm 8.28 (s, 2H), 7.97 (m, 4H), 7.70 (d, 4H,  $J = 8.1$  Hz), 7.66 (s, 2H), 7.35 (m, 6H), 7.17 (dd, 2H,  $J = 1.6$  Hz,  $J = 8.3$  Hz), 7.11 (d, 4H,  $J = 8.1$  Hz), 4.39 (d, 2H,  $J = 8.1$  Hz), 4.02 (d, 4H,  $J = 7.6$  Hz), 2.54 (t, 4H,  $J = 7.6$  Hz), 2.26 (m, 1H), 1.94 (m, 2H), 1.55-0.8 (br m, 72H).  $^{13}C$ -NMR (62.5 MHz,  $CD_2Cl_2$ ): ppm 198.12, 148.82, 143.17, 142.37, 141.50, 141.45, 139.97, 136.27, 132.23, 131.61, 130.56, 128.50, 122.50, 121.57, 121.43, 121.37, 121.27, 120.37, 119.57, 111.78, 110.72, 109.48, 48.24, 48.01, 39.84, 39.56, 36.22, 32.24, 31.46, 31.30, 31.17, 29.69, 29.55, 29.08, 28.97, 24.75, 24.58, 23.46, 23.03, 14.25, 14.17, 11.11, 11.05 (3 peaks are overlapping). FDMS:  $m/z$  1335.4. Elemental analysis: Calculated C, 80.93; H, 8.93; N, 3.15. Found C, 80.15; H, 8.51; N, 3.10.

Ladder-type dichlorohexaphenylene **46**

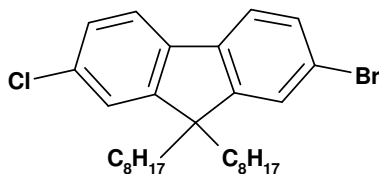
(a) A solution of 4-octylbromobenzene (0.32 mL, 1.35 mmol) in dry THF (20 mL) in a 100 mL Schlenk flask was cooled to  $-78^{\circ}\text{C}$  in an acetone/dry ice bath. *n*-Butyllithium in hexane (0.88 mL, 1.6 M, 1.42 mmol) was then added and the mixture was stirred for 20 min. Then solution of the diketone **45** (0.6 g, 0.45 mmol) in dry THF (10 mL) was added dropwise with stirring and then it was slowly allowed to warm to room temperature. The reaction mixture was stirred overnight and then quenched with brine. The mixture was extracted with diethyl ether, and the extract was washed with brine and dried over  $\text{MgSO}_4$ . The crude product was chromatographed on silica gel with 0-5 % ethyl acetate in hexane as eluent to give the diol as a thick viscous oil (0.72 g, 93 %). (b) The diol (0.7 g, 0.41 mmol) was dissolved in dichloromethane (10 mL) and  $\text{BF}_3$ ·etherate (0.2 mL) was added with stirring at room temperature. The colorless solution turned deep brown immediately upon addition of boron trifluoride. The mixture was stirred overnight at room temperature and then quenched by adding 20 mL of methanol. The monomer **46** was started precipitating as a light yellow solid. The mixture was further stirred for 2 h and then solid was collected by filtration, washed with methanol, and dried. The product was redissolved in dichloromethane and precipitated again by addition of methanol. Isolated yield of compound **46** = 0.62 g (91 %).  $^1\text{H-NMR}$  (250 MHz,  $\text{CD}_2\text{Cl}_2$ ): ppm 8.00 (s, 2H), 7.95 (s, 2H), 7.89 (d, 2H,  $J = 8.3$  Hz), 7.59 (s, 4H), 7.25 (d, 8H,  $J = 7.9$  Hz), 7.11 (m, 4H), 7.07 (d, 8H,  $J = 7.9$  Hz), 3.89 (s, 6H), 2.53 (t, 8H,  $J = 7.7$  Hz), 2.08 (m, 3H), 1.65-0.75 (br m, 102H).  $^{13}\text{C-NMR}$  (62.5 MHz,  $\text{CD}_2\text{Cl}_2$ ): ppm 145.83, 145.79, 145.74, 144.82, 144.41, 142.08, 141.67, 141.55, 139.50, 138.86, 131.44, 128.72, 128.50, 123.73, 122.71, 121.62, 120.74, 119.33, 117.61, 109.58, 100.52, 100.44, 63.98, 46.91, 46.64, 39.29, 35.94, 32.30, 31.87, 31.07, 29.96, 29.88, 29.65, 29.12, 29.04, 28.95, 28.83, 24.76, 24.71, 24.57, 23.40, 23.31, 23.08, 14.28, 11.29, 11.25, 11.18. FDMS:  $m/z$  1680.2.

Elemental analysis: Calculated C, 84.34; H, 8.94; N, 2.50. Found C, 84.18; H, 8.89; N, 2.49.

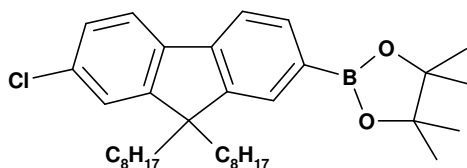
### Nitrogen-bridged poly(ladder-type polyhexaphenylene) **47**



Bis(cyclooctadiene)nickel(0) (78 mg, 2.4 equiv.), cyclooctadiene (0.035 mL, 2.4 equiv), and 2,2'-bipyridine (45 mg, 2.4 equiv) were dissolved in toluene (2 mL) and N,N-dimethylformamide (2 mL) in a Schlenk flask within a glovebox. The mixture was heated at 60 °C with stirring under argon for 20 min to generate the catalyst, and then a solution of the monomer **46** (0.2 g, 0.12 mmol) in toluene (6 mL) was added. The reaction was heated at 80 °C for 2 days, where upon the solution became so viscous that it ceased to stir. Then a mixture of toluene (4 mL) and bromobenzene (0.1 mL) was added and the mixture was heated at 80 °C for an additional 12 h. The polymer solution was then poured into a mixture of methanol and concentrated hydrochloric acid (1:1, 200 mL) and stirred for 4 h. The precipitated yellow solid was redissolved in THF (10 mL) and added dropwise to methanol (100 mL). The resulting solid was filtered off and subjected to Soxhlet extraction for two days in acetone. The residue was then redissolved in THF and precipitated from mixture of methanol and ammonia (4:1, 200 mL), filtered, washed with methanol, and dried. Isolated yield of polymer **47** = 160 mg (83 %). <sup>1</sup>H-NMR (250 MHz, CD<sub>2</sub>Cl<sub>2</sub>): ppm 8.2-6.6 (br m, 30H), 5.0-3.5 (br s, 6H), 2.8-2.4 (br m, 11H), 2.0-0.30 (br m, 102H). GPC analysis: Mn = 2.3 × 10<sup>4</sup> gmol<sup>-1</sup> and D = 2.4 (against PPP standard). Elemental analysis: Calculated C, 88.53; H, 9.09; N, 2.38. Found C, 85.24; H, 9.47; N, 2.43.

**2-Bromo -7- chloro-9,9-dioctylfluorene (48)**

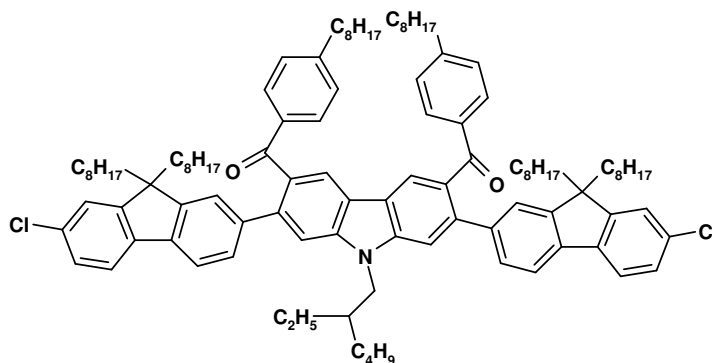
To 5.59 g of chlorobromofluorene **47** in a 100 mL round bottomed flask, 0.30 g of tetrabutylammoniumchloride, 5 g of sodium hydroxide, 10 mL of water and 20 mL of DMSO were added. To this, 14 mL of octylbromide was added and heated at 80 °C till the color of the solution turned yellow. The reaction was cooled to room temperature, the product was extracted into hexane, washed with 2M HCl, followed by aqueous NaHCO<sub>3</sub> and dried over MgSO<sub>4</sub>. The octyl bromide was distilled off using the Kugelrohr and then the crude was chromatographed on silica gel using hexane as eluent to give compound **48** as white solid. Isolated yield = 7.9 g (78 %). <sup>1</sup>H-NMR (300 MHz, CD<sub>2</sub>Cl<sub>2</sub>): ppm 7.61 (dd, 1H, *J* = 7.47, 1.17 Hz), 7.56 (dd, 1H, *J* = 7.91, 0.56 Hz), 7.52-7.43 (m, 2H), 7.36-7.27 (m, 2H), 2.04-1.87 (m, 4H), 1.40-0.94 (m, 20H), 0.83 (t, 6H, *J* = 6.98, 6.98 Hz), 0.70-0.46 (m, 4H). <sup>13</sup>C-NMR (75 MHz, CD<sub>2</sub>Cl<sub>2</sub>): ppm 153.20, 152.78, 139.56, 139.14, 133.59, 130.44, 127.59, 126.65, 123.71, 121.66, 121.51, 121.17, 56.10, 40.49, 32.14, 30.22, 29.55, 24.04, 22.98, 14.21. FDMS: *m/z* 503.4. Elemental analysis: Calculated C, 69.11; H, 8.00. Found C, 68.88; H, 8.01.

**2-Chloro-9,9-dioctyl-7-(4,4,5,5-tetramethyl-[1,3,2]dioxaborolan-2-yl)fluorene (49)**

To 2.0 g of **48** (3.96 mmol) in a 100 mL Schlenk flask, 40 mL of dry THF was added and cooled to -78 °C in an acetone/dry ice bath. To this, 2.72 mL of 1.6 M *n*-Butyllithium was added (1.1 equivalent) and stirred for 30 min. Then 0.89 mL (1.1 equiv) of 2-isopropoxy-4,4,5,5-tetramethyl-1,3,2-dioxaborolane was added and allowed to warm to room temperature. Reaction mixture was stirred for 40 h at room temperature and then

the reaction was quenched with brine, extracted into diethylether, washed with brine and dried over  $\text{MgSO}_4$ . The crude was chromatographed on silica gel using 0-5 % ethylacetate in hexane as eluent to give colorless viscous oil. Isolated yield = 1.42 g (65 %).  $^1\text{H-NMR}$  (300 MHz,  $\text{CD}_2\text{Cl}_2$ ): ppm 7.75 (dd, 1H,  $J = 7.52, 0.94$  Hz), 7.72 (s, 1H), 7.68 (dd, 1H,  $J = 7.52, 0.65$  Hz), 7.66 (d, 1H,  $J = 7.91$  Hz), 7.35 (d, 1H,  $J = 1.52$  Hz), 7.31 (dd, 1H,  $J = 8.01, 1.94$  Hz), 2.14-1.85 (m, 4H), 1.36 (s, 12H), 1.29-0.91 (m, 20H), 0.81 (t, 6H,  $J = 6.97, 6.97$  Hz), 0.69-0.42 (m, 4H).  $^{13}\text{C-NMR}$  (75 MHz,  $\text{CD}_2\text{Cl}_2$ ): ppm 153.69, 150.03, 143.28, 139.98, 134.02, 133.59, 129.17, 127.36, 123.74, 121.43, 119.35, 84.14, 55.78, 40.51, 32.13, 30.25, 29.55, 29.53, 25.11, 24.06, 22.96, 14.19. FDMS:  $m/z$  549.9.

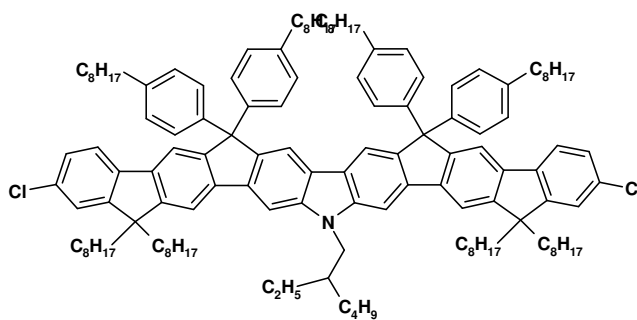
**2,7-Bis(7-chloro-9,9-dioctyl-fluoren-2'-yl)-9'-(2''-ethylhexyl)-3,6-bis(4-octylbenzoyl) carbazole (50)**



The fluoreneboronic ester **49** (1.39 g, 2.52 mmol), carbazole diketone **16** (1.0 g, 1.14 mmol), and  $\text{K}_2\text{CO}_3$  (314 mg, 2.28 mmol) were dissolved in THF (10 mL) and water (5 mL) in a 50 mL Schlenk flask. The solution was purged with argon for 20 min, and then  $\text{Pd}(\text{PPh}_3)_4$  (40 mg, 0.03 equiv) was added and the reaction was heated with stirring at 85 °C. The reaction was followed by TLC and worked up after 12 h. The cooled reaction mixture was extracted with dichloromethane and the extract was washed with brine and then dried over  $\text{MgSO}_4$ . The crude product so obtained was purified by chromatography on silica gel with 0-5 % ethyl acetate in hexane as eluent. The product **50** was isolated as yellow viscous liquid (1.3 g, 73 %).  $^1\text{H-NMR}$  (250 MHz,  $\text{CD}_2\text{Cl}_2$ ): ppm 8.25 (s, 2H), 7.69 (d, 4H,  $J = 8.25$  Hz), 7.64-7.58 (m, 6H), 7.45 (d, 2H,  $J = 7.75$  Hz), 7.31-7.28 (m, 6H), 7.12 (d, 4H,  $J = 8.25$  Hz), 4.39 (d, 2H,  $J = 7.25$  Hz), 2.57 (t, 4H,  $J = 7.5$  Hz), 2.27

(m, 1H), 1.81 (m, 8H), 1.55-0.75 (br m, 104H).  $^{13}\text{C}$ -NMR (62.5 MHz,  $\text{CD}_2\text{Cl}_2$ ): ppm 198.28, 153.61, 151.22, 149.00, 143.36, 141.38, 141.06, 139.88, 139.57, 136.32, 133.29, 132.31, 130.81, 128.77, 128.70, 127.58, 124.75, 123.87, 122.56, 121.60, 121.28, 120.19, 111.50, 55.86, 48.26, 40.67, 40.09, 36.47, 32.45, 32.41, 32.34, 31.62, 31.53, 30.64, 29.94, 29.86, 29.79, 29.75, 29.09, 25.31, 24.87, 24.30, 23.64, 23.23, 23.17, 14.43, 14.34, 11.31. FDMS:  $m/z$  1556.4. Elemental analysis: Calculated C, 83.25; H, 9.25; N, 0.90. Found C, 83.39; H, 8.90; N, 0.71.

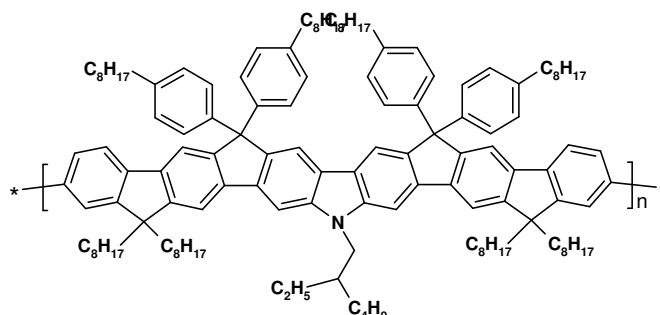
### Ladder-type dichlorohexaphenylene **51**



(a) A solution of 4-octylbromobenzene (0.59 mL, 2.50 mmol) in dry THF (40 mL) in a 100 mL schlenk flask was cooled to  $-78^\circ\text{C}$  in an acetone/dry ice bath. *n*-Butyllithium in hexane (1.63 mL, 1.6 M, 2.62 mmol) was then added and the mixture was stirred for 20 min. Then a solution of the diketone **50** (1.3 g, 0.835 mmol) in dry THF (20 mL) was added dropwise with stirring and the solution was slowly allowed to warm to room temperature. The mixture was stirred overnight and then quenched with brine and extracted with diethyl ether, and the extract was washed with brine and dried over  $\text{MgSO}_4$ . The crude product was chromatographed on silica gel with 0-5 % ethyl acetate in hexane as eluent to give the diol as thick viscous oil (1.56 g, 96 %). (b) The diol (1.0 g, 0.51 mmol) was dissolved in dichloromethane (10 mL), and  $\text{BF}_3\cdot\text{etherate}$  (0.5 mL) was added with stirring at room temperature. The colorless solution turned deep brown immediately upon addition. The mixture was stirred overnight at room temperature and then quenched by adding 30 mL of methanol. The compound **51** was started precipitating as light yellow solid. The mixture was further stirred for 2 h and then solid was collected by filtration, washed with methanol, and dried. The product was redissolved in

dichloromethane and precipitated again by addition of methanol. Isolated yield of monomer **51** = 0.72 g (72 %).  $^1\text{H}$  NMR (250 MHz,  $\text{CD}_2\text{Cl}_2$ ): ppm 7.90 (s, 2H), 7.83 (s, 2H), 7.78 (s, 2H), 7.66 (s, 2H), 7.55 (d, 2H,  $J = 8.1$  Hz), 7.34 (d, 2H,  $J = 1.6$  Hz), 7.27 (dd, 2H,  $J = 1.7$  Hz,  $J = 8.1$  Hz), 7.18 (d, 8H,  $J = 8.2$  Hz), 7.05 (d, 8H,  $J = 8.2$  Hz), 4.53-4.21 (m, 2H), 2.62-2.43 (t, 8H,  $J = 7.5$  Hz), 2.41-2.23 (m, 1H), 2.21-1.92 (m, 8H), 1.70-0.52 (m, 134H).  $^{13}\text{C}$  NMR (62.5 MHz,  $\text{CD}_2\text{Cl}_2$ ): ppm 153.66, 152.47, 151.14, 144.82, 144.28, 142.56, 141.87, 140.95, 140.50, 140.44, 138.94, 133.01, 128.81, 128.63, 127.47, 123.81, 121.20, 118.02, 117.90, 114.79, 100.44, 64.56, 55.73, 41.10, 39.84, 36.03, 32.45, 32.36, 32.06, 31.32, 30.58, 30.06, 30.01, 29.79, 29.26, 25.27, 24.46, 23.76, 23.23, 23.15, 14.66, 14.44, 14.39, 11.50. FDMS:  $m/z$  1903.5. Elemental analysis: Calculated C, 85.84; H, 9.69; N, 0.74. Found C, 85.67; H, 9.56; N, 0.55.

### Nitrogen-bridged poly(ladder-type hexaphenylene) **52**

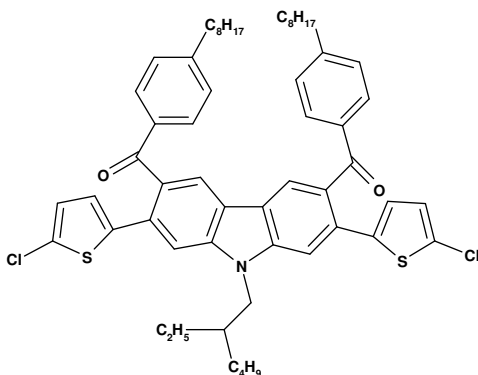


Bis(1,5-cyclooctadiene)nickel(0) (106 mg, 2.4 equiv), cyclooctadiene (0.044 mL, 2.4 equiv), and 2,2'-bipyridine (60 mg, 2.4 equiv) were dissolved in dry toluene (2 mL) and dry *N,N*-dimethylformamide (4 mL) in a Schlenk flask within a glovebox. The reaction mixture was heated at 60 °C with stirring under argon for 20 min to generate the catalyst, and then a solution of the monomer **51** (0.3 g, 0.157 mmol) in dry toluene (6 mL) was added. The reaction was heated at 80 °C for 2 days, whereupon the solution became so viscous that it ceased to stir. Then a solution of toluene (4 mL) in bromobenzene (0.1 mL) was added and the mixture was heated at 80 °C for an additional 12 h. The polymer solution was then poured into a mixture of methanol and concentrated hydrochloric acid (1:1, 200 mL) and stirred for 4 h. The precipitated yellow solid was redissolved in THF (10 mL) and added dropwise to methanol (100 mL). The resulting solid was filtered off and subjected to Soxhlet extraction for two days in acetone. The residue was then

redissolved in THF and precipitated from mixture of methanol and ammonia (4:1, 200 mL), filtered, washed with methanol, and dried. Isolated yield of polymer **52** = 220 mg (77 %). GPC analysis:  $M_n = 2.3 \times 10^4 \text{ g mol}^{-1}$  and  $D = 1.7$  (against PPP standard). Elemental analysis: Calculated C, 89.17; H, 10.07; N, 0.76. Found C, 89.00; H, 9.91; N, 0.53.

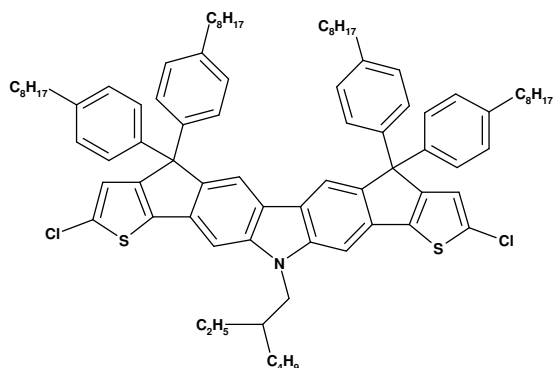
### 2,7-bis(5-chloro-thiophen-2'-yl)-9-(2''-ethylhexyl)-3,6-(4-octylbenzoyl)carbazole

(**55a**)

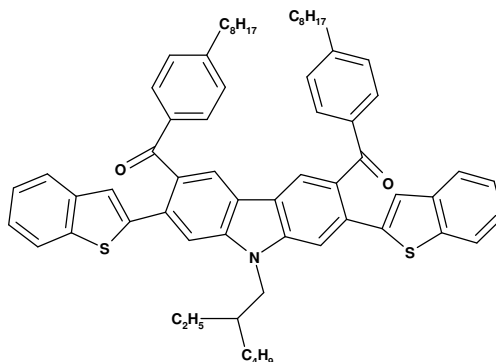


4-Chlorothiopheneboronic acid (0.73 g, 4.53 mmol), diketone **16** (1.65 g, 1.89 mmol), and  $K_2CO_3$  (512 mg, 3.76 mmol) were dissolved in THF (30 mL) and water (7 mL) in a 100 mL Schlenk flask. The solution was purged with argon for 20 min, and then tetrakis(triphenylphosphine)palladium (46 mg, 0.02 equiv) was added and the reaction was heated with stirring at  $85^\circ \text{C}$ . The reaction was followed by TLC and was worked up after 36 h. The cooled mixture was extracted with dichloromethane, and the extract was washed with brine and then dried over  $MgSO_4$ . The crude product so obtained was purified by chromatography on silica gel with 0-30 % ethyl acetate in hexane as eluent. The product **55a** was isolated as a colorless solid (1.68 g, 94 %).  $^1\text{H-NMR}$  (250 MHz,  $CD_2Cl_2$ ): ppm 8.15 (s, 2H), 7.64 (d, 4H,  $J = 8.16 \text{ Hz}$ ), 7.54 (s, 2H), 7.18 (d, 4H,  $J = 8.14 \text{ Hz}$ ), 6.74 (m, 4H), 4.31 (d, 2H,  $J = 7.45 \text{ Hz}$ ), 2.63 (t, 4H,  $J = 7.6 \text{ Hz}$ ), 2.16 (m, 1H), 1.7-1.2 (m, 32H), 1.7-1.2 (m, 35H), 0.99 (t, 3H,  $J = 7.39$ ), 0.93-0.80 (m, 9H).  $^{13}\text{C-NMR}$  (62.5 MHz,  $CD_2Cl_2$ ): ppm 197.72, 149.29, 142.98, 141.88, 136.02, 131.96, 131.62, 130.42, 130.40, 128.73, 127.20, 127.10, 122.41, 121.91, 111.38, 48.17, 39.83, 36.31, 32.25, 31.48, 31.26, 30.46, 29.77, 29.59, 29.04, 24.80, 23.42, 23.04, 14.24, 14.14, 11.09. FDMS:  $m/z$  944.2.

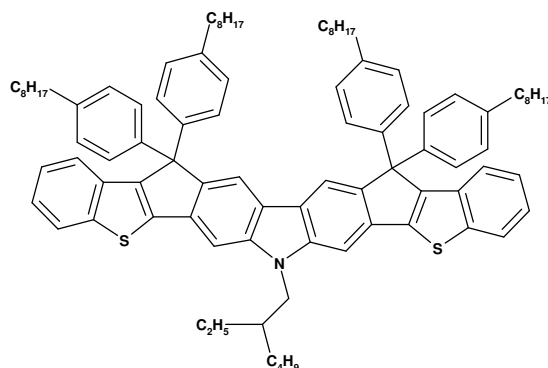


Carbazole-thiophene fused molecule **57a**

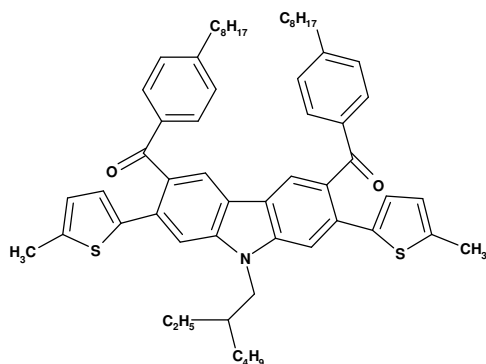
(a) A solution of 4-octylbromobenzene (1.19 mL, 5.0 mmol) in dry THF (40 mL) in a 100 mL Schlenk flask was cooled to  $-78\text{ }^{\circ}\text{C}$  in an acetone/dry ice bath. *n*-Butyllithium in hexane (3.30 mL, 1.6 M, 5.29 mmol) was then added and the mixture was stirred for 20 min. Then a solution of the diketone **55a** (1.59 g, 1.68 mmol) in dry THF (20 mL) was added drop wise with stirring and the solution was slowly allowed to warm to room temperature. The mixture was stirred overnight and then quenched with brine. The product was extracted into diethyl ether, and the extract was washed with brine and dried over  $\text{MgSO}_4$ . The crude product was chromatographed on silica gel with 0-2 % ethyl acetate in hexane as eluent to give the diol **56a** as a thick viscous oil (2.00 g, 90 %) (b) The diol **56a** (2.0 g, 1.51 mmol) was dissolved in 1, 2-dichloroethane (20 mL), and  $\text{BF}_3$ ·etherate (0.5 mL) was added with stirring at room temperature. The colorless solution turned deep blue immediately upon addition. The mixture was stirred 4 h at room temperature, and then quenched by adding 50 mL of methanol. The crude product was chromatographed on silica gel with 0-2 % ethyl acetate in hexane as eluent to give the product **57a** as a red solid. Isolated yield **57a** = 1.2 g (61 %).  $^1\text{H-NMR}$  (250 MHz,  $\text{CD}_2\text{Cl}_2$ ): ppm 7.85 (s, 2H), 7.36 (s, 2H), 7.12 (d, 8H,  $J = 8.13$  Hz), 7.04 (d, 8H,  $J = 8.13$  Hz), 6.93 (s, 2H), 4.21 (m, 2H), 2.53 (t, 8H,  $J = 7.72$  Hz), 2.24-2.06 (m, 1H), 1.77-1.05 (m, 56H), 1.06-0.70 (m, 18H).  $^{13}\text{C-NMR}$  (62.5 MHz,  $\text{CD}_2\text{Cl}_2$ ): ppm 154.57, 144.31, 142.56, 142.06, 141.66, 139.41, 135.16, 131.58, 128.74, 128.01, 123.24, 121.57, 117.82, 100.16, 63.59, 48.25, 39.60, 35.83, 32.26, 31.87, 31.11, 29.81, 29.61, 28.98, 24.79, 23.49, 23.04, 14.25, 11.12. FDMS:  $m/z$  1290.5. Elemental analysis: Calculated C, 80.08; H, 8.36; N, 1.09; S, 4.97. Found C, 79.99; H, 8.22; N, 0.98; S, 4.81.

2,7-Bis(benzothiophen-2-yl)-9-(2-ethylhexyl)-3,6-(4-octylbenzoyl)carbazole (**55b**)

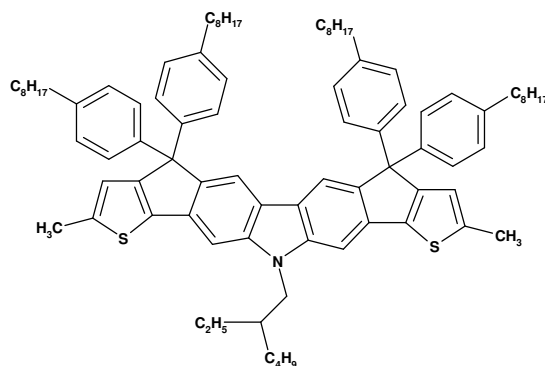
2-Benzothiopheneboronic acid (0.491 g, 2.76 mmol), diketone **16** (1.00 g, 1.15 mmol), and  $\text{K}_2\text{CO}_3$  (317 mg, 2.3 mmol) were dissolved in THF (10 mL) and water (3 mL) in a 100 mL Schlenk flask. The solution was purged with argon for 20 min, and then tetrakis(triphenylphosphine)palladium (28 mg, 0.02 equiv) was added and the reaction was heated with stirring at  $85^\circ\text{C}$ . The reaction was followed by TLC and was worked up after 12 h. The cooled mixture was extracted with dichloromethane, and the extract was washed with brine and then dried over  $\text{MgSO}_4$ . The crude product so obtained was purified by chromatography on silica gel with 0-10 % ethyl acetate in hexane as eluent. The product **55b** was isolated as a colorless solid (0.9 g, 81 %).  $^1\text{H-NMR}$  (250 MHz,  $\text{CD}_2\text{Cl}_2$ ): ppm 8.21 (s, 2H), 7.82-7.60 (m, 10H), 7.38-7.25 (m, 4H), 7.22 (s, 2H), 7.14 (d, 4H,  $J = 8.18$  Hz), 4.37 (d, 2H,  $J = 7.35$  Hz), 2.57 (t, 4H,  $J = 7.66$  Hz), 2.31-2.11 (m, 1H), 1.67-1.08 (m, 32H), 1.00 (t, 3H,  $J = 7.35, 7.35$  Hz), 0.94-0.80 (m, 9H).  $^{13}\text{C-NMR}$  (62.5 MHz,  $\text{CD}_2\text{Cl}_2$ ): ppm 197.83, 149.17, 143.38, 142.99, 140.56, 140.52, 136.09, 132.57, 132.31, 130.38, 128.66, 124.82, 124.71, 124.43, 123.97, 122.44, 122.28, 122.06, 111.93, 48.20, 39.89, 36.27, 32.25, 31.43, 31.29, 29.74, 29.56, 29.08, 24.83, 23.44, 23.04, 14.24, 14.17, 11.11. FDMS:  $m/z$  977.3. Elemental analysis: Calculated C, 81.18; H, 7.54; N, 1.43; S, 6.57. Found C, 80.93; H, 7.55; N, 1.22; S, 6.59.

Carbazole-benzothiophene fused molecule **57b**

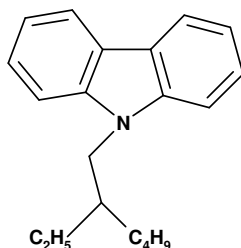
(a) A solution of 4-octylbromobenzene (0.55 mL, 2.33 mmol) in dry THF (40 mL) in a 100 mL Schlenk flask was cooled to  $-78^{\circ}\text{C}$  in an acetone/dry ice bath. *n*-Butyllithium in hexane (1.53 mL, 1.6 M, 2.46 mmol) was then added and the mixture was stirred for 20 min. Then a solution of the diketone **55b** (0.77 g, 0.79 mmol) in dry THF (20 mL) was added dropwise with stirring and the solution was slowly allowed to warm to room temperature. The mixture was stirred overnight and then quenched with brine. The product was extracted into diethyl ether, and the extract was washed with brine and dried over  $\text{MgSO}_4$ . The crude product was chromatographed on silica gel with 0-5 % ethyl acetate in hexane as eluent to give the diol **56b** as a thick viscous oil (0.95 g, 88 %). (b) The diol **56b** (0.80 g, 0.59 mmol) was dissolved in 1,2-dichloroethane (10 mL), and  $\text{BF}_3$ -etherate (0.5 mL) was added with stirring at room temperature. The colorless solution turned deep blue immediately upon addition. The mixture was stirred 4 h at room temperature, and then quenched by adding 50 mL of methanol. The crude product was chromatographed on silica gel with 0-5 % ethyl acetate in hexane as eluent to give the product **57b** as a light yellow solid. Isolated yield **57b** = 0.70 g (89 %).  $^1\text{H-NMR}$  (250 MHz,  $\text{CD}_2\text{Cl}_2$ ): ppm 7.98 (s, 2H), 7.94-7.86 (m, 2H), 7.63-7.46 (m, 4H), 7.31-7.15 (m, 12H), 7.04 (d, 8H,  $J = 7.60$  Hz), 4.37-4.24 (m, 2H), 2.52 (t, 8H,  $J = 7.76$  Hz), 2.33-2.13 (m, 1H), 1.68-1.09 (m, 56H), 1.09-0.79 (m, 18H).  $^{13}\text{C-NMR}$  (62.5 MHz,  $\text{CD}_2\text{Cl}_2$ ): ppm 149.79, 149.04, 144.81, 143.28, 142.42, 142.13, 141.74, 136.13, 135.17, 129.03, 125.34, 124.75, 124.58, 123.01, 122.78, 117.37, 101.29, 63.87, 48.71, 40.07, 36.22, 32.63, 32.19, 31.57, 30.25, 30.18, 29.98, 29.43, 25.25, 23.91, 23.42, 14.68, 14.63, 11.57. FDMS:  $m/z$  1320.9. Elemental analysis: Calculated C, 85.46; H, 8.62; N, 1.06; S, 4.85. Found C, 85.19; H, 8.56; N, 0.95; S, 4.74.

**2,7-Bis(5-methyl-thiophen-2-yl)-9-(2-ethylhexyl)-3,6-(4-octylbenzoyl)carbazole (55c)**

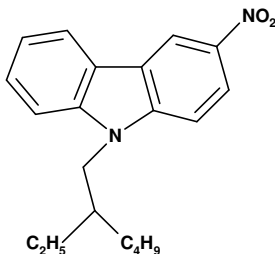
4-Methylthiopheneboronic acid (0.737 g, 5.19 mmol), diketone **16** (1.88 g, 2.16 mmol), and  $\text{K}_2\text{CO}_3$  (583 mg, 4.28 mmol) were dissolved in THF (20 mL) and water (5 mL) in a 100 mL Schlenk flask. The solution was purged with argon for 20 min, and then tetrakis(triphenylphosphine)palladium (52 mg, 0.02 equiv) was added and the reaction was heated with stirring at 85 °C. The reaction was followed by TLC and was worked up after 24 h. The cooled mixture was extracted with dichloromethane, and the extract was washed with brine and then dried over  $\text{MgSO}_4$ . The crude product so obtained was purified by chromatography on silica gel with 0-30 % ethyl acetate in hexane as eluent. The product **55c** was isolated as a colorless viscous liquid. (1.23 g, 61 %).  $^1\text{H-NMR}$  (250 MHz,  $\text{CD}_2\text{Cl}_2$ ): ppm 8.08 (s, 2H), 7.66 (d, 4H,  $J = 8.18$  Hz), 7.56 (s, 2H), 7.17 (d, 4H,  $J = 8.19$  Hz), 6.75 (d, 2H,  $J = 3.48$  Hz), 6.63-6.48 (m, 2H), 4.30 (d, 2H,  $J = 7.44$  Hz), 2.62 (t, 4H,  $J = 7.64$  Hz), 2.42 (s, 6H), 2.27-2.08 (m, 1H), 1.69-1.16 (m, 32H), 0.99 (t, 3H,  $J = 7.36$ , 7.36 Hz), 0.94-0.82 (m, 9H).  $^{13}\text{C-NMR}$  (62.5 MHz,  $\text{CD}_2\text{Cl}_2$ ): ppm 198.18, 148.99, 143.00, 141.27, 140.84, 136.20, 132.65, 131.77, 130.44, 128.98, 128.63, 127.67, 126.20, 121.95, 121.44, 111.01, 48.07, 39.80, 36.30, 32.25, 31.49, 31.28, 29.78, 29.60, 29.09, 24.84, 23.45, 23.04, 15.38, 14.25, 14.18, 11.11. FDMS:  $m/z$  904.1

Carbazole-thiophene fused molecule **57c**

(a) A solution of 4-octylbromobenzene (0.70 mL, 2.95 mmol) in dry THF (40 mL) in a 100 mL Schlenk flask was cooled to  $-78^{\circ}\text{C}$  in an acetone/dry ice bath. n-Butyllithium in hexane (1.95 mL, 1.6 M, 3.12 mmol) was then added and the mixture was stirred for 20 min. Then a solution of the diketone **55c** (0.90 g, 0.99 mmol) in dry THF (20 mL) was added dropwise with stirring and the solution was slowly allowed to warm to room temperature. The mixture was stirred overnight and then quenched with brine. The product was extracted into diethyl ether, and the extract was washed with brine and dried over  $\text{MgSO}_4$ . The crude product was chromatographed on silica gel with 0-2 % ethyl acetate in hexane as eluent to give the diol **56c** as a thick viscous oil (1.22 g, 96 %) (b) The diol **56c** (1.0 g, 0.77 mmol) was dissolved in 1,2-dichloroethane (20 mL), and  $\text{BF}_3$ -etherate (0.5 mL) was added with stirring at room temperature. The colorless solution turned deep blue immediately upon addition. The mixture was stirred 4 h at room temperature, and then quenched by adding 50 mL of methanol. The crude product was chromatographed on silica gel with 0-2 % ethyl acetate in hexane as eluent to give the product **57c** as a yellow solid. Isolated yield **57c** = 0.72 g (75 %).  $^1\text{H-NMR}$  (250 MHz,  $\text{CD}_2\text{Cl}_2$ ): ppm 7.80 (s, 2H), 7.33 (s, 2H), 7.13 (d,  $J = 8.14$  Hz, 8H), 7.03 (d,  $J = 8.06$  Hz, 8H), 6.71 (s, 2H), 4.35-4.09 (m, 2H), 2.62-2.44 (m, 14H), 2.26-2.05 (m, 1H), 1.75-1.05 (m, 56H), 1.09-0.73 (m, 18H).  $^{13}\text{C-NMR}$  (62.5 MHz,  $\text{CD}_2\text{Cl}_2$ ): ppm 156.44, 144.89, 143.73, 143.38, 141.70, 141.55, 139.46, 135.79, 128.58, 128.09, 121.70, 120.99, 117.57, 99.65, 62.81, 39.60, 35.83, 32.26, 31.90, 31.15, 29.82, 29.61, 29.01, 24.79, 23.50, 23.04, 16.62, 14.24, 11.13. FDMS:  $m/z$  1247. Elemental analysis: Calculated C, 84.62; H, 9.12; N, 1.12; S, 5.13. Found C, 84.56; H, 8.98; N, 1.07; S, 4.99.

**9-(2-ethylhexyl)carbazole**

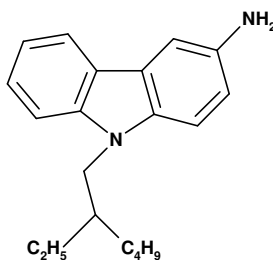
A 100 mL Schlenk flask was charged with carbazole (1.00 g, 5.9 mmol), NaH (0.33 g, 8.26 mmol) and 40 mL of DMF. The resulting mixture was stirred for 30 min. 2-Ethylhexylbromide (1.29 mL, 7.08 mmol) was then added under argon and the mixture was stirred overnight at room temperature. The reaction was quenched with 20 mL of water and extracted three times with diethyl ether (40 mL each). The combined organic fractions were washed with brine and dried over  $\text{MgSO}_4$ . The solvent was removed under reduced pressure and the residue was purified by column chromatography (Silica gel, 2 % ethyl acetate in hexane as eluent) Isolated yield = 92 %.  $^1\text{H-NMR}$  (250 MHz,  $\text{CDCl}_3$ ): ppm 8.04 (d, 2H,  $J = 7.7$  Hz), 7.33 (m, 4H), 7.15 (d, 2H,  $J = 7.7$  Hz), 4.11 (d, 2H,  $J = 7.5$  Hz), 2.02 (m, 1H), 1.21-1.31 (m, 8H), 0.82-0.89 (m, 6H). FDMS:  $m/z$  279.5.

**3-Nitro-9-(ethylhexyl)carbazole**

$\text{Cu}(\text{NO}_3)_2 \cdot 2.5\text{H}_2\text{O}$  (0.41 g, 1.76 mmol) was added to a mixture of acetic acid (4 mL) and acetic anhydride (8 mL) at room temperature. The mixture was stirred for 10 min, and then 9-(2-ethylhexyl)carbazole (1 g, 3.55 mmol) was added slowly in portions over 5 min. Heat was generated during the addition, and an additional 4 mL of acetic acid was added. The mixture was stirred at this temperature for 15 min and then poured into distilled water (200 mL). Then the aqueous layer was extracted with DCM and dried over  $\text{MgSO}_4$  and purified by column chromatography. Isolated yield = 72 %.  $^1\text{H-NMR}$  (250

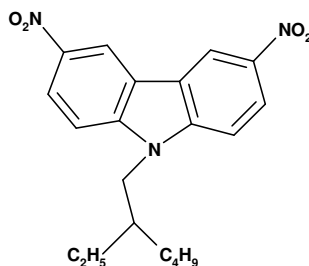
MHz, CD<sub>2</sub>Cl<sub>2</sub>): ppm 9.02 (d, 1H,  $J = 2.2$  Hz), 8.36 (dd, 1H,  $J = 2.3$  Hz,  $J = 9.1$  Hz), 8.18 (d, 1H,  $J = 7.8$  Hz), 7.62-7.41 (m, 3H), 7.35 (t, 1H,  $J = 7.4$  Hz), 4.23 (d, 2H,  $J = 7.5$  Hz), 2.07 (m, 1H), 1.49-1.19 (m, 8H), 0.96-0.81 (m, 6H) <sup>13</sup>C-NMR (62.5 MHz, CD<sub>2</sub>Cl<sub>2</sub>): ppm 144.26, 142.41, 140.77, 127.58, 123.02, 122.67, 121.62, 121.10, 120.90, 117.30, 110.40, 108.96, 48.06, 39.69, 31.23, 29.04, 24.68, 23.33, 14.09, 10.97. FDMS:  $m/z$  324.6.

### 3-Amino-9-(2-ethylhexyl)carbazole (59)



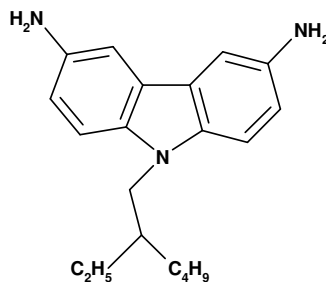
Palladium on charcoal (10 %, 356 mg) was added in portions to a hot solution of 3-nitro-9-(2-ethylhexyl)carbazole (2.7 g, 8.32 mmol) and hydrazine hydrate (3.1 mL) in ethanol (60 mL) and the mixture was heated under reflux for 2 h. The cooled mixture was filtered off and the filtrate was concentrated to give the title product **59**. Isolated yield = 72 %. <sup>1</sup>H-NMR (250 MHz, CD<sub>2</sub>Cl<sub>2</sub>): ppm 7.97 (d, 1H,  $J = 7.8$  Hz), 7.43-7.30 (m, 3H), 7.22 (d, 1H,  $J = 8.6$  Hz), 7.12 (ddd, 1H,  $J = 1.5$  Hz,  $J = 6.6$  Hz,  $J = 8.0$  Hz), 6.88 (dd, 1H,  $J = 2.3$  Hz,  $J = 8.6$  Hz), 4.10 (d, 2H,  $J = 7.2$  Hz), 3.64 (s, 2H), 2.03 (m, 1H), 1.44-1.14 (m, 8H), 0.95-0.80 (m, 6H). <sup>13</sup>C-NMR (62.5 MHz, CD<sub>2</sub>Cl<sub>2</sub>): ppm 141.77, 139.84, 135.70, 125.70, 123.75, 122.57, 120.50, 118.22, 115.70, 109.99, 109.30, 105.91, 47.78, 39.84, 31.39, 29.23, 24.79, 23.50, 14.23, 11.11. FDMS:  $m/z$  294.2. Elemental analysis: Calculated C, 81.59; H, 8.90; N, 9.51. Found C, 81.54; H, 8.89; N, 9.58.

### 3,6-Dinitro-9-(2-ethylhexyl)carbazole



$\text{Cu}(\text{NO}_3)_2 \cdot 2.5\text{H}_2\text{O}$  (1.19 g, 5.1 mmol) was added into a mixture of acetic acid (5 mL) and acetic anhydride (10 mL) at room temperature. The mixture was stirred for 10 min, and added 9-(2-ethylhexyl)carbazole (1 g, 3.55 mmol) slowly in portions over 5 min. Heat was generated during the addition, and an additional 5 mL of acetic acid was added. The mixture was stirred at this temperature for 15 min and then poured into distilled water (200 mL). The yellow precipitate was then collected by filtration, washed with water and dried under vacuum. The product was recrystallized from ethanol. Isolated yield = 70 %.  $^1\text{H-NMR}$  (250 MHz,  $\text{CDCl}_3$ ): ppm 9.08 (d, 2H,  $J = 2.2$  Hz), 8.4 (dd, 2H,  $J = 2.2$  Hz,  $J = 9.2$  Hz), 7.5 (d, 2H,  $J = 9.2$  Hz), 4.28 (d, 2H,  $J = 7.5$  Hz), 2.02 (m, 1H), 1.21-1.31 (m, 8H), 0.82-0.89 (m, 6H).  $^{13}\text{C-NMR}$  (62.5 MHz,  $\text{CDCl}_3$ ): ppm 145.61, 142.16, 123.14, 122.81, 117.91, 110.44, 48.78, 39.86, 31.24, 29.04, 24.71, 23.32, 14.09, 10.98. FDMS:  $m/z$  369.2. Elemental analysis: Calculated C, 64.67; H, 6.78; N, 11.31. Found C, 64.94; H, 6.37; N, 11.39.

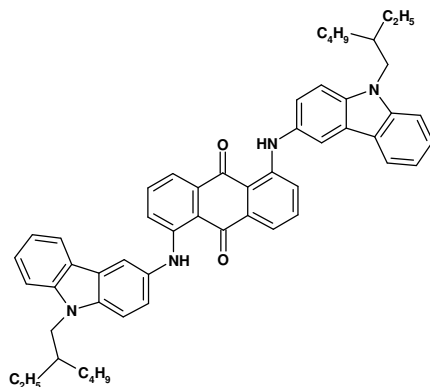
### 3,6-Diamino-9-(2-ethylhexyl)carbazole (60)



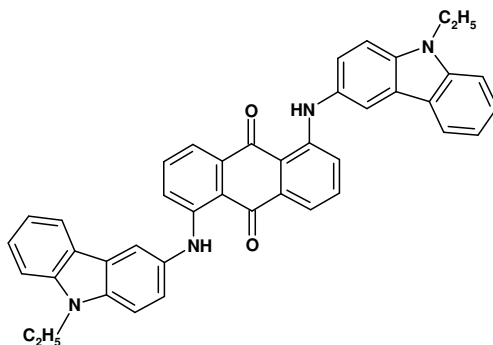
Palladium on charcoal (10 %, 115 mg) was added in portions to a hot solution of 3,6-dinitrocarbazole (0.5 g, 1.35 mmol) and hydrazine hydrate (1 mL) in ethanol (40 mL) and the mixture was heated under reflux for 2 h. The cooled mixture was filtered off and the filtrate was concentrated to give 200 mg of title product. Isolated yield = 77 %.  $^1\text{H-NMR}$  (250 MHz,  $\text{CDCl}_3$ ): ppm 7.25 (d, 2H,  $J = 2.2$  Hz), 7.08 (d, 2H,  $J = 8.5$  Hz), 6.8 (dd, 2H,  $J = 2.5$  Hz,  $J = 8.5$  Hz), 3.9 (d, 2H,  $J = 9.0$  Hz), 3.50 (br s, 4H), 1.94 (m, 1H), 1.18-1.28 (m, 8H), 0.82-0.89 (m, 6H).  $^{13}\text{C-NMR}$  (62.5 MHz,  $\text{CDCl}_3$ ): ppm 139.08, 136.33, 123.14, 115.67, 109.80, 105.88, 47.83, 39.87, 31.37, 29.20, 24.75, 23.45, 14.16, 11.06. FDMS:  $m/z$  309.6. Elemental analysis: Calculated C, 77.63; H, 8.79; N, 13.58. Found C, 77.50; H, 8.69; N, 13.57.



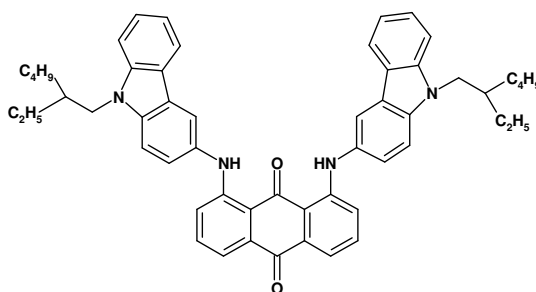
## 1,5-Bis[9-(2-ethylhexyl)carbazol-3-ylamino]anthraquinone (61)



3-Amino-9-(2-Ethylhexyl)carbazole (2.2 g, 7.48 mmol), 1,5-dichloroanthraquinone (861 mg, 3.1 mmol), Pd<sub>2</sub>(dba)<sub>3</sub> (76 mg), BINAP (153 mg), cesium carbonate (3.98 g) and toluene (15 mL) were mixed together and heated at 100 °C for 24 h. The reaction was quenched with water (10 mL) and then extracted with 100 mL of DCM, washed with brine and dried over MgSO<sub>4</sub>. Evaporation of solvent under vacuum resulted in a violet residue. The residue was purified by column chromatography using ethyl acetate/hexane as eluent. Isolated yield = 72 %. <sup>1</sup>H-NMR (250 MHz, CD<sub>2</sub>Cl<sub>2</sub>): ppm 11.46 (s, 2H), 8.12-8.03 (m, 4H), 7.70 (dd, 2H, *J* = 1.0 Hz, *J* = 7.2 Hz), 7.55-7.41 (m, 10H), 7.37 (dd, 2H, *J* = 1.0 Hz, *J* = 8.6 Hz), 7.23 (ddd, 2H, *J* = 1.9 Hz, *J* = 6.1 Hz, *J* = 7.9 Hz), 4.22 (d, 4H, *J* = 7.4 Hz), 2.11 (m, 2H), 1.35 (m, 16H), 0.95 (t, 6H, *J* = 7.4 Hz), 0.87 (t, 6H, *J* = 7.0 Hz). <sup>13</sup>C-NMR (62.5 MHz, CD<sub>2</sub>Cl<sub>2</sub>): ppm 184.61, 150.08, 140.77, 138.25, 135.41, 134.05, 130.04, 125.20, 123.15, 122.69, 121.59, 119.56, 118.06, 117.87, 116.46, 115.49, 112.71, 109.10, 108.55, 46.82, 38.71, 30.25, 28.06, 23.69, 22.31, 13.02, 9.95. FDMS: *m/z* 792.3. Elemental analysis: Calculated C, 81.78; H, 7.12; N, 7.06. Found C, 82.05; H, 7.05; N, 7.18.

**1,5-Bis[9-ethyl-carbazol-3-ylamino]anthraquinone (61a)**

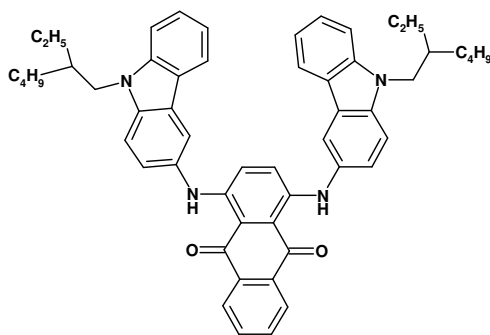
3-Amino-9-ethyl-carbazole (1.66 g, 7.94 mmol), 1,5-dichloroanthraquinone (1.00 g, 3.61 mmol), Pd<sub>2</sub>(dba)<sub>3</sub> (88 mg), BINAP (178 mg), cesium carbonate (4.63 g) and toluene (15 mL) were mixed together and heated at 100 °C for 24 h. The reaction was quenched with water (10 mL) and then extracted with DCM, washed with brine solution and dried over MgSO<sub>4</sub>. Evaporation of solvent under vacuum resulted in a violet residue. The residue was purified by recrystallization from ethanol. Isolated yield = 63 %. <sup>1</sup>H-NMR (250 MHz, CD<sub>2</sub>Cl<sub>2</sub>): ppm 11.46 (s, 2H), 8.12-8.03 (m, 4H), 7.70 (d, 2H, *J* = 7.3 Hz), 7.55-7.41 (m, 10H), 7.35 (d, 2H, *J* = 8.6 Hz), 7.23 (t, 2H, *J* = 6.4 Hz), 4.43 (q, 4H, *J* = 7.2 Hz), 1.47 (t, 6H, *J* = 7.0 Hz). FDMS: *m/z* 624.8.

**1,8-Bis[9-(2-ethylhexyl)carbazol-3-ylamino]anthraquinone (62)**

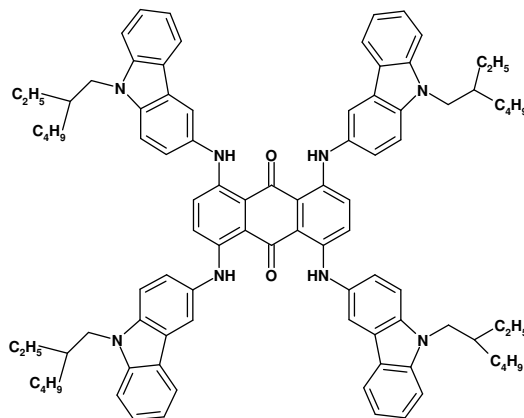
3-Amino-9-(2-ethylhexyl)carbazole (509 mg, 1.73 mmol), 1,8-dichloroanthraquinone (200 mg, 0.72 mmol), Pd<sub>2</sub>(dba)<sub>3</sub> (17.5 mg), BINAP (35 mg), cesium carbonate (926 mg) and toluene (5 mL) were mixed together and heated at 80 °C for 24 h. The reaction was quenched with water (5 mL) and then extracted with DCM, washed with brine solution and dried over MgSO<sub>4</sub>. Evaporation of solvent under vacuum resulted in a violet residue which was purified by column chromatography using 0-20 % ethyl acetate/hexane as

eluent. Isolated yield = 76 %.  $^1\text{H-NMR}$  (250 MHz,  $\text{CD}_2\text{Cl}_2$ ): ppm 11.43 (s, 2H), 8.10-8.04 (m, 4H), 7.63 (dd, 2H,  $J = 2.8$  Hz,  $J = 5.7$  Hz), 7.54-7.40 (m, 12H), 7.22 (ddd, 2H,  $J = 2.1$  Hz,  $J = 6.0$  Hz,  $J = 7.9$  Hz), 4.16 (d, 4H,  $J = 7.5$  Hz), 2.07 (m, 2H), 1.48-1.18 (m, 16H), 0.96-0.80 (m, 12H). FDMS:  $m/z$  793.1.

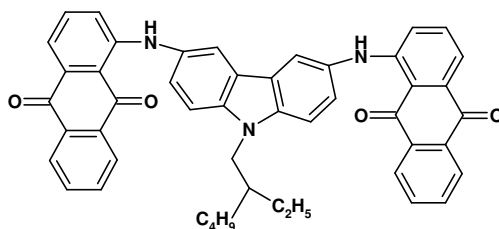
### 1,4-Bis[9-(2-ethylhexyl)carbazol-3-ylamino]anthraquinone (63)



3-Amino-9-(2-ethylhexyl)carbazole (509 mg, 1.73 mmol), 1,4-dichloroanthraquinone (200 mg, 0.722 mmol),  $\text{Pd}_2(\text{dba})_3$  (17.5 mg), BINAP (35 mg), cesium carbonate (926 mg) and toluene (5 mL) were mixed together and heated at  $80^\circ\text{C}$  for 24 h. The reaction mixture was quenched with water (5 mL) and extracted with DCM, washed with brine solution and dried over  $\text{MgSO}_4$ . Evaporation of solvent under vacuum resulted in a violet residue which was purified by column chromatography using 0-20 % ethyl acetate/hexane as eluent. Isolated yield = 80 %.  $^1\text{H-NMR}$  (250 MHz,  $\text{CD}_2\text{Cl}_2$ ): ppm 12.53 (s, 2H), 8.41 (dd, 2H,  $J = 3.3$  Hz,  $J = 5.9$  Hz), 8.04 (d, 2H,  $J = 7.7$  Hz), 8.00 (s, 2H), 7.76 (dd, 2H,  $J = 3.3$  Hz,  $J = 5.9$  Hz), 7.51-7.36 (m, 10H), 7.19 (t, 2H,  $J = 7.2$  Hz), 4.16 (d, 4H,  $J = 7.5$  Hz), 2.07 (m, 2H), 1.48-1.18 (m, 16H), 0.96-0.80 (m, 12H).  $^{13}\text{C-NMR}$  (62.5 MHz,  $\text{CD}_2\text{Cl}_2$ ): ppm 182.94, 145.85, 141.87, 139.21, 135.00, 132.64, 131.19, 126.54, 126.33, 125.51, 124.04, 123.75, 122.66, 120.69, 119.17, 117.18, 110.75, 110.13, 109.66, 47.90, 39.81, 31.36, 29.17, 24.78, 23.43, 14.16, 11.06. FDMS:  $m/z$  793.2. Elemental analysis: Calculated C, 81.78; H, 7.12; N, 7.06. Found C, 81.96; H, 6.98; N, 7.00.

**1,4,5,8-Tetra[9-(2-ethylhexyl)carbazol-3-ylamino]anthraquinone (64)**

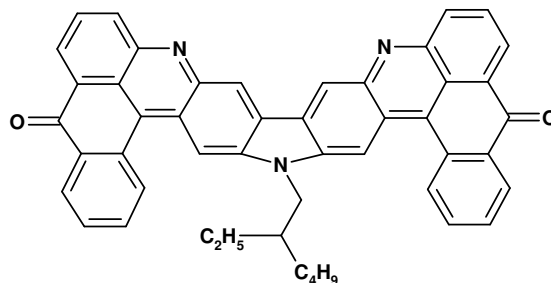
3-Amino-9-(2-ethylhexyl)carbazole (303 mg, 1.44 mmol), 1,4,5,8-tetrachloroanthraquinone (100 mg, 0.289 mmol),  $\text{Pd}_2(\text{dba})_3$  (15 mg), BINAP (29 mg), cesium carbonate (745 mg) and toluene (5 mL) were mixed together and heated at 100 °C for 72 h. The reaction was quenched with water (10 mL) and then extracted with DCM, washed with brine solution, and dried over  $\text{MgSO}_4$ . Evaporation of the solvent under vacuum resulted in a violet residue. The residue was purified by recrystallization from ethanol. Isolated yield = 42 %.  $^1\text{H-NMR}$  (250 MHz,  $\text{CD}_2\text{Cl}_2$ ): ppm 12.14 (s, 4H), 8.03 (d, 8H,  $J = 7.8$  Hz), 7.45 (m, 18H), 7.17 (m, 6H), 4.16 (s, 8H), 2.05 (m, 4H), 1.47-1.15 (m, 32H), 0.98-0.76 (m, 24H). FDMS:  $m/z$  1378.0. Elemental analysis: Calculated C, 81.94; H, 7.61; N, 8.13. Found C, 82.17; H, 7.66; N, 7.97.

**3,6-Bis(1-anthraquinonylamino)-9-(2-ethylhexyl)carbazole (65)**

3,6-Diamino-9-(2-ethylhexyl)carbazole (100 mg, 0.32 mmol), 1-chloroanthraquinone (170 mg, 0.70 mmol),  $\text{Pd}_2(\text{dba})_3$  (5.9 mg), BINAP (12 mg), cesium carbonate (312 mg),

and toluene (5 mL) were mixed together and heated at 100 °C for 24 h. The reaction mixture was quenched with water (5 mL) and was extracted with DCM, washed with brine, and dried over MgSO<sub>4</sub>. Evaporation of solvent under vacuum resulted in a violet residue. The residue was purified by column chromatography using 0-10 % ethyl acetate/hexane as eluent. Isolated yield = 80 %. <sup>1</sup>H-NMR (250 MHz, CD<sub>2</sub>Cl<sub>2</sub>): ppm 11.44 (s, 2H), 8.34 (dd, 2H, *J* = 1.3 Hz, *J* = 7.7 Hz), 8.25 (dd, 2H, *J* = 1.7 Hz, *J* = 7.4 Hz), 8.03 (d, 2H, *J* = 1.6 Hz), 7.86-7.72 (m, 4H), 7.64 (dd, 2H, *J* = 1.4 Hz, *J* = 6.9 Hz), 7.55-7.36 (m, 8H), 4.25 (d, 1H, *J* = 7.4 Hz), 2.15 (m, 1H), 1.49-1.21 (m, 8H), 0.97 (t, 3H, *J* = 7.4 Hz), 0.89 (t, 3H, *J* = 7.0 Hz). <sup>13</sup>C-NMR (62.5 MHz, CD<sub>2</sub>Cl<sub>2</sub>): ppm 185.43, 183.69, 151.30, 139.92, 135.29, 135.20, 134.91, 134.31, 133.47, 131.10, 127.06, 126.91, 124.73, 123.41, 120.17, 117.71, 117.20, 113.77, 110.52, 110.47, 48.07, 39.88, 31.34, 29.16, 24.81, 23.43, 14.16, 11.09. FDMS: *m/z* 722.1. Elemental analysis: Calculated C, 79.87; H, 5.45; N, 5.82. Found C, 80.09; H, 5.28; N, 5.87.

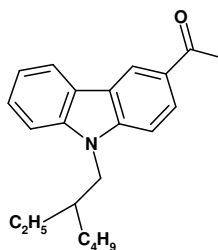
### Ring closed product 66



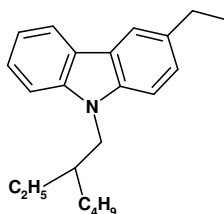
Compound **65** (500 mg, 0.69 mmol) was dissolved in sulfuric acid (10 mL) and heated at 150 °C for 6 h. The reaction was quenched with ice water and then extracted with dichloromethane. The organic layer was washed with NaOH, 2N HCl, Saturated NaHCO<sub>3</sub> and finally with brine. Evaporation of solvent under vacuum resulted in a black residue. The residue was purified by column chromatography using 0-50 % ethyl acetate/hexane as eluent to give the title compound **66** as a black solid. Isolated yield = 24 %. <sup>1</sup>H-NMR (250 MHz, CD<sub>2</sub>Cl<sub>2</sub>): ppm 8.57 (dd, 2H, *J* = 1.1 Hz, *J* = 7.1 Hz), 8.39 (dd, 2H, *J* = 0.9 Hz, *J* = 8.4 Hz), 8.08 (s, 4H), 7.87 (dd, 2H, *J* = 7.2 Hz, *J* = 8.4 Hz), 7.58 (dd, 2H, *J* = 1.1 Hz, *J* = 7.8 Hz), 7.08 (d, 2H, *J* = 7.9 Hz), 6.34 (t, 2H, *J* = 7.1 Hz), 5.93 (t, 2H, *J* = 7.7 Hz),

4.61 (d, 2H,  $J = 7.7\text{Hz}$ ), 2.28 (s, 1H), 1.70-1.20 (m, 8H), 1.13-0.99 (m, 3H), 0.82 (t, 3H,  $J = 6.9\text{ Hz}$ ).  $^{13}\text{C}$ -NMR (62.5 MHz,  $\text{CD}_2\text{Cl}_2$ ): ppm 181.63, 148.53, 145.19, 137.80, 135.47, 134.92, 132.31, 129.92, 129.60, 129.02, 128.95, 128.62, 128.31, 128.27, 127.40, 127.06, 120.67, 119.86, 117.81, 117.05, 48.78, 41.35, 41.18, 31.57, 31.46, 29.24, 29.13, 25.23, 25.13, 23.34, 23.24, 14.02, 11.26, 11.17. FDMS:  $m/z$  686.2.

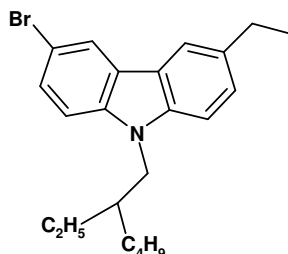
### 3-Acetyl-9-(2-ethylhexyl)carbazole (69)



The 9-(2-ethylhexyl)carbazole (2.8 g, 10 mmol) and  $\text{AlCl}_3$  (1.33 g, 10 mmol) were dissolved in 1,2-dichloroethane (10 mL) and acetyl chloride (0.71 mL, 10 mmol) was added slowly at room temperature. The mixture was stirred for overnight at  $50^\circ\text{C}$  and then quenched with ice. The inorganic precipitate was dissolved in 2M HCl and the product was extracted with dichloromethane. The organic fractions were dried over  $\text{MgSO}_4$  and solvent was removed under reduced pressure. The product was purified by chromatography on silica gel with 0-10 % ethyl acetate in hexane as eluent to give the colorless viscous oil. Isolated yield = 46%.  $^1\text{H}$ -NMR (250 MHz,  $\text{CD}_2\text{Cl}_2$ ): ppm 8.74 (d, 1H,  $J = 1.4\text{ Hz}$ ), 8.17 (d, 1H,  $J = 7.8\text{ Hz}$ ), 8.10 (dd, 1H,  $J = 1.7\text{ Hz}$ ,  $J = 8.7\text{ Hz}$ ), 7.59-7.40 (m, 3H), 7.35-7.25 (m, 1H), 4.21 (d, 2H,  $J = 7.5\text{ Hz}$ ), 2.69 (s, 3H), 2.11 (m, 1H), 1.50-1.15 (m, 8H), 0.97-0.80 (m, 6H).  $^{13}\text{C}$ -NMR (250 MHz,  $\text{CD}_2\text{Cl}_2$ ): ppm 197.44, 143.97, 141.99, 129.11, 126.68, 126.48, 123.42, 122.77, 121.95, 120.76, 120.17, 110.01, 109.05, 47.93, 39.71, 31.29, 29.10, 26.81, 24.72, 23.37, 14.12, 11.01. FDMS:  $m/z$  321.5.

**3-Ethyl-9-(2-ethylhexyl)carbazole (70)**

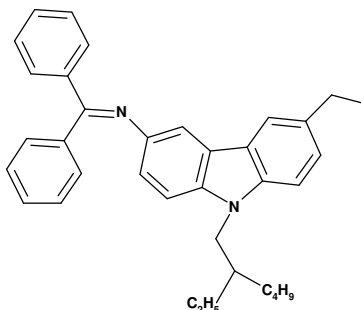
The 3-acetyl-(2-ethylhexyl)carbazole (1.33 g, 4.14 mmol), hydrazine hydrate (0.60 mL, 12.42 mmol), KOH (0.92 g, 16.5 mmol) and triethylene glycol (20 mL) was mixed together and heated to 180 °C for 2 h. Then the condenser was replaced by distillation apparatus and reaction mixture was again heated at 220 °C for additional 6 h. The reaction mixture was cooled and quenched by brine. The product was extracted in diethyl ether. The combined organic fractions were washed with brine and dried over MgSO<sub>4</sub>. The solvent was removed under reduced pressure and the residue was purified by chromatography on silica gel with 0-2 % ethyl acetate in hexane as eluent to give the colorless viscous oil. Isolated yield = 82 %. <sup>1</sup>H-NMR (250 MHz, CD<sub>2</sub>Cl<sub>2</sub>): ppm 8.06 (d, 1H, *J* = 7.7 Hz), 7.92 (s, 1H), 7.47-7.30 (m, 4H), 7.23-7.14 (m, 1H), 4.15 (d, 2H, *J* = 7.7 Hz), 2.83 (q, 2H, *J* = 7.5 Hz), 2.06 (m, 1H), 1.50-1.19 (m, 11H), 0.98-0.81 (m, 6H) <sup>13</sup>C-NMR (62.5 MHz, CD<sub>2</sub>Cl<sub>2</sub>): ppm 141.55, 139.79, 135.14, 126.23, 125.66, 123.06, 122.93, 120.36, 119.21, 118.70, 109.34, 109.18, 47.77, 39.78, 31.35, 29.22, 29.19, 24.75, 23.46, 16.72, 14.17, 11.05 FDMS: *m/z* 307.6.

**3-Bromo-6-ethyl-9-(2-ethylhexyl)carbazole (71)**

N-Bromosuccinimide (0.58 g, 3.3 mmol) was dissolved in DMF (10 mL) and added dropwise at room temperature to a stirred solution of 3-ethyl-9-(2-ethylhexyl)carbazole (0.96 g, 3.1 mmol) in DMF (10 mL). Then the reaction mixture was stirred overnight. The

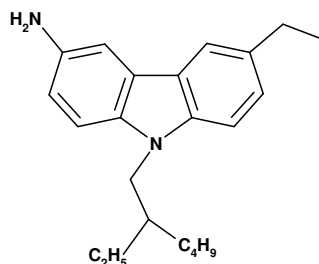
reaction was quenched by addition of ice water. The product was extracted with diethyl ether. The combined organic fractions were washed with brine and dried over magnesium sulphate. The solvent was removed under reduced pressure and the residue was purified by chromatography on silica gel with 0-2 % ethyl acetate in hexane as eluent to give the colorless viscous oil. Isolated yield = 92 %.  $^1\text{H-NMR}$  (250 MHz,  $\text{CD}_2\text{Cl}_2$ ): ppm 8.18 (d, 1H,  $J = 1.9$  Hz), 7.86 (s, 1H), 7.50 (dd, 1H,  $J = 1.9$  Hz,  $J = 8.7$  Hz), 7.36-7.31 (m, 2H), 7.28 (d, 1H,  $J = 8.7$  Hz), 4.13 (d, 2H,  $J = 7.7$  Hz), 2.82 (q, 2H,  $J = 7.6$  Hz), 2.02 (m, 1H), 1.46-1.18 (m, 11H), 0.94-0.80 (m, 6H).  $^{13}\text{C-NMR}$  (62.5 MHz,  $\text{CD}_2\text{Cl}_2$ ): ppm 140.18, 140.10, 135.71, 128.18, 127.11, 124.72, 123.09, 122.05, 119.36, 111.31, 110.91, 109.49, 47.91, 39.74, 31.31, 29.15, 24.71, 23.41, 16.60, 14.14, 11.02. FDMS: m/z 387.7.

### 3-Benzophenone-imine-6-ethyl-9-(2-ethylhexyl)carbazole (72)

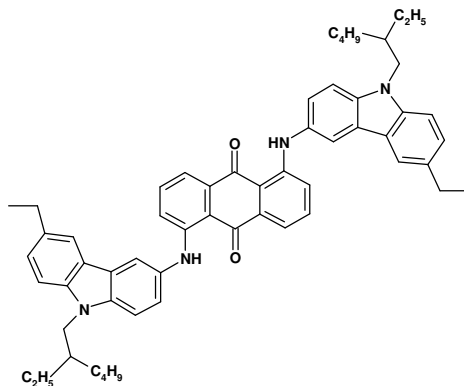


3-Bromo-6-ethyl-9-(2-ethylhexyl)carbazole (0.50 g, 1.29 mmol), benzophenone imine (0.26 mL, 1.53 mmol),  $\text{Pd}_2(\text{dba})_3$  (11.7 mg),  $\text{P}(\text{t-Bu})_3$  (35mg),  $\text{t-BuONa}$  (184 mg) and toluene (5 mL) were mixed together and heated at 80 °C for 24 h. The reaction was quenched with water (5 mL) and the organic products extracted into 100 mL of DCM, washed with brine solution and dried over  $\text{MgSO}_4$ . Evaporation of solvent under vacuum resulted in a yellow residue. It was not purified for further reaction. (Crude yield = 95 %). FDMS: m/z 487.0.



**3-Amino-6-ethyl-9-(2-ethylhexyl)carbazole (73)**

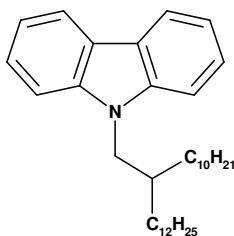
The imine adduct **72** (0.5 g) was dissolved in THF (10 mL) and 2M HCl (2 mL) was added at room temperature. The mixture was stirred for 30 minutes and the product was extracted with dichloromethane. The organic fractions were dried over MgSO<sub>4</sub> and solvent was removed under reduced pressure. The product was purified by chromatography on silica gel with 0-5 % ethyl acetate in hexane as eluent to give the yellow solid. Isolated yield = 96 %. <sup>1</sup>H-NMR (250 MHz, CD<sub>2</sub>Cl<sub>2</sub>): ppm 7.79 (s, 1H), 7.36 (d, 1H, *J* = 2.2 Hz), 7.28-7.22 (m, 2H), 7.19 (d, 1H, *J* = 8.6 Hz), 6.86 (dd, 1H, *J* = 2.3 Hz, *J* = 8.6 Hz), 4.07 (d, 1H, *J* = 7.7 Hz), 3.63 (s, 2H), 2.80 (q, 2H, *J* = 7.6 Hz), 2.00 (m, 1H), 1.44-1.18 (m, 11H), 0.96-0.80 (m, 6H). <sup>13</sup>C-NMR (62.5 MHz, CD<sub>2</sub>Cl<sub>2</sub>): ppm 140.30, 139.57, 136.02, 134.32, 126.08, 123.64, 122.59, 119.19, 115.51, 109.88, 109.05, 105.86, 47.81, 39.85, 31.37, 29.23, 24.76, 23.50, 16.78, 14.23, 11.09. FDMS: *m/z* 322.8. Elemental analysis: Calculated C, 81.94; H, 9.38; N, 8.69. Found C, 81.69; H, 9.20; N, 8.66.

**1,5-Bis[3-ethyl-9-(2-ethylhexyl)carbazol-6-ylamino]anthraquinone (74)**

3-Amino-6-ethyl-9-(2-Ethylhexyl)carbazole (0.8 g, 2.49 mmol), 1,5-dichloroanthraquinone (287 mg, 1.03 mmol), Pd<sub>2</sub>(dba)<sub>3</sub> (26 mg), BINAP (51 mg),

cesium carbonate (1.32 g), and toluene (5 mL) were mixed together and heated at 100 °C for 24 h. The reaction was quenched with water (5 mL) and the organic layer taken into 50 mL of DCM, washed with brine solution, and dried over MgSO<sub>4</sub>. Evaporation of solvent under vacuum resulted in a violet residue. The residue was purified by column chromatography using 0-5 % ethyl acetate/hexane as eluent. Isolated yield = 70 %. <sup>1</sup>H-NMR (250 MHz, CD<sub>2</sub>Cl<sub>2</sub>): ppm 11.46 (s, 2H), 8.04 (s, 2H), 7.89 (s, 2H), 7.69 (d, 2H, *J* = 7.2 Hz), 7.52-7.30 (m, 12H), 4.18 (d, 4H, *J* = 7.5 Hz), 2.83 (q, 4H, *J* = 7.6 Hz), 2.09 (m, 2H), 1.50-1.20 (m, 22H), 1.00-0.80 (m, 12H). <sup>13</sup>C-NMR (62.5 MHz, CD<sub>2</sub>Cl<sub>2</sub>): ppm 185.71, 151.26, 140.38, 139.63, 136.53, 135.37, 135.15, 130.88, 126.72, 124.07, 123.70, 122.76, 119.36, 119.01, 117.52, 116.54, 113.79, 110.12, 109.43, 47.96, 39.85, 31.36, 29.18, 24.78, 23.45, 16.65, 14.17, 11.07. FDMS: *m/z* 849.4. Elemental analysis: Calculated C, 82.04; H, 7.60; N, 6.60. Found C, 82.38; H, 7.40; N, 6.56.

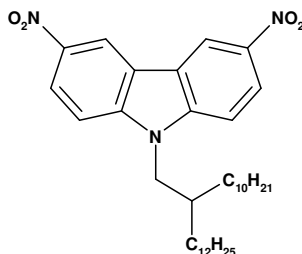
### 9-(2-Decyltetradecyl)carbazole



A 250 mL Schlenk flask was charged with carbazole (2.00 g, 11.9 mmol), NaH (0.66 g, 16.5 mmol) and 80 mL of DMF. The resulting mixture was stirred for 30 min. 2-Decyltetradecanebromide (6.00 g, 14.28 mmol) was then added under argon and the mixture was stirred overnight at room temperature. The reaction was then quenched with 20 mL of water and extracted three times with diethyl ether (50 mL each). The combined organic fractions were washed with brine and dried over MgSO<sub>4</sub>. The solvent was removed under reduced pressure and the residue was purified by column chromatography (Silica gel, hexane as eluent) Isolated yield = 88 %. <sup>1</sup>H-NMR (250 MHz, CD<sub>2</sub>Cl<sub>2</sub>): ppm 8.20 (d, 2H, *J* = 7.7 Hz), 7.61-7.48 (m, 4H), 7.33 (t, 2H, *J* = 7.2 Hz), 4.24 (d, 2H, *J* = 7.4 Hz), 2.25 (s, 1H), 1.60-1.20 (m, 40H), 1.04 (t, 6H, *J* = 6.5Hz). <sup>13</sup>C-NMR (62.5 MHz,

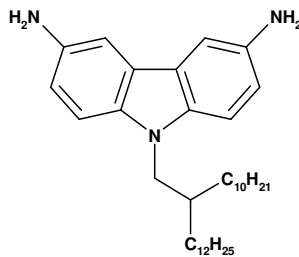
CD<sub>2</sub>Cl<sub>2</sub>): ppm 141.48, 126.03, 123.27, 120.65, 119.18, 109.54, 48.20, 38.44, 32.56, 32.48, 30.55, 30.30, 30.23, 30.16, 30.02, 29.97, 27.16, 23.33, 14.55. FDMS: m/z 503.9.

### 3,6-Dinitro-9-(2-decyltetradecyl)carbazole



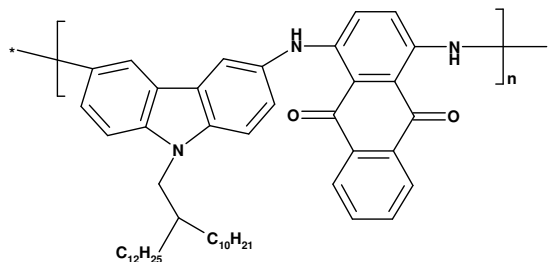
Cu(NO<sub>3</sub>)<sub>2</sub>·2.5 H<sub>2</sub>O (2.21 g, 9.52 mmol) was added into a mixture of acetic acid (10 mL) and acetic anhydride (20 mL) at room temperature. The mixture was stirred for 10 min, and then 9-(2-Decyltetradecyl)carbazole (4.00 g, 7.93 mmol) was added slowly in portions over 5 min. Heat was generated during the addition, and an additional 10 mL of acetic acid was added. The mixture was stirred at this temperature for 15 min and then poured into distilled water (200 mL). The yellow precipitate was collected by filtration, washed with water and dried under vacuum. The product was recrystallized from ethanol. Isolated yield = 70 %. <sup>1</sup>H-NMR (250 MHz, CD<sub>2</sub>Cl<sub>2</sub>): ppm 9.10 (d, 2H, *J* = 2.1 Hz), 8.46 (dd, 2H, *J* = 2.2 Hz, *J* = 9.1 Hz), 7.55 (d, 2H, *J* = 9.1 Hz), 4.29 (d, 2H, *J* = 7.6 Hz), 2.12 (s, 1H), 1.40-1.12 (m, 40H), 0.87 (t, 6H, *J* = 6.4 Hz). <sup>13</sup>C-NMR (62.5 MHz, CD<sub>2</sub>Cl<sub>2</sub>): ppm 145.63, 142.20, 123.15, 122.84, 117.98, 110.45, 49.15, 38.39, 32.28, 32.16, 30.16, 30.02, 29.95, 29.91, 29.81, 29.73, 29.69, 26.84, 23.07, 14.26. FDMS: m/z 594.2. Elemental analysis: Calculated C, 72.57; H, 9.64; N, 7.05. Found C, 72.77; H, 9.32; N, 7.13.

### 3,6-Diamino-9-(2-decyltetradecyl)carbazole (75)



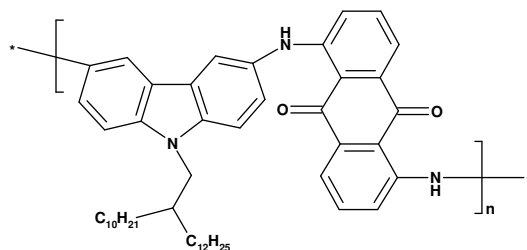
Palladium on charcoal (10 %, 173 mg) was added in portions to a hot solution of 3,6-dinitro-9-(2-decyltetradecyl)carbazole (1.2 g, 2.02 mmol) and hydrazine hydrate (1.5 mL) in ethanol (60 mL) and then mixture was heated under reflux for 2 h. The cooled mixture was filtered off and the filtrate was concentrated to give the title product **75**. Isolated yield = 70 %.  $^1\text{H-NMR}$  (250 MHz,  $\text{CD}_2\text{Cl}_2$ ) ppm 7.27 (d, 2H,  $J = 2.1$  Hz), 7.13 (d, 2H,  $J = 8.6$  Hz), 6.83 (dd, 2H,  $J = 2.2$  Hz,  $J = 8.6$  Hz), 4.01 (d, 2H,  $J = 7.4$  Hz), 3.48 (br s, 4H), 2.04 (s, 1H), 1.40-1.10 (m, 40H), 0.88 (t, 1H,  $J = 6.5$  Hz).  $^{13}\text{C-NMR}$  (62.5 MHz,  $\text{CD}_2\text{Cl}_2$ ): ppm 139.03, 136.33, 123.12, 115.65, 109.79, 105.87, 48.16, 38.42, 32.32, 32.23, 30.37, 30.04, 29.99, 29.95, 29.75, 29.73, 26.94, 23.08, 14.27. FDMS:  $m/z$  534.4. Elemental analysis: Calculated C, 80.99; H, 11.14; N, 7.87. Found C, 80.82; H, 11.02; N, 7.78.

### Polymer 76



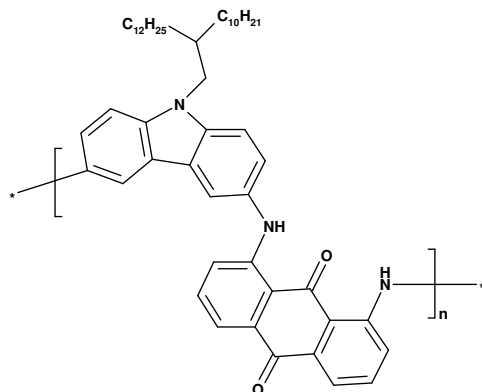
The 3,6-diamino-9-(2-decyltetradecyl)carbazole (192 mg, 0.36 mmol), 1,4-dichloroanthraquinone (100 mg, 0.36 mmol),  $\text{Pd}_2(\text{dba})_3$  (9 mg), BINAP (18 mg), cesium carbonate (462 mg), and toluene (5 mL) were mixed together and heated at  $100^\circ\text{C}$  for 72 h. Then a solution of 1-chloroanthraquinone (10 mg) in 2 mL of toluene was added and the reaction mixture was again heated at  $100^\circ\text{C}$  for an additional 6 h. The reaction mixture was precipitated in methanol. The solid was filtered off and redissolved in THF then reprecipitated from methanol. The polymer obtained was subjected to soxhlet extraction for 24 h and then dried. Isolated yield = 71 %. GPC analysis  $M_n = 7 \times 10^3$  g/mol and PDI = 2.98 (PS standard). Elemental analysis: Calculated C, 81.37; H, 8.60; N, 5.69. Found C, 75.53; H, 8.07; N, 4.98.

## Polymer 77



The 3,6-diamino-9-(2-decyltetradecyl)carbazole (96 mg, 0.18 mmol), 1,5-dichloroanthraquinone (50 mg, 0.18 mmol),  $\text{Pd}_2(\text{dba})_3$  (4.5 mg), BINAP (9 mg), cesium carbonate (231 mg), and toluene (3 mL) were mixed together and heated at  $100^\circ\text{C}$  for 72 h. Then a solution of 1-chloroanthraquinone (5 mg) in 1 mL of toluene was added and the reaction mixture was heated at  $100^\circ\text{C}$  for an additional 6 h. The reaction mixture was precipitated in methanol. The solid was filtered off and redissolved in THF and again precipitated from methanol. The polymer so obtained was subjected to soxhlet extraction for 24 h and then dried. Isolated yield = 62 %. GPC analysis:  $M_n = 5.6 \times 10^3$  g/mol and PDI = 2.53 (PS standard). Elemental analysis: Calculated C, 81.37; H, 8.60; N, 5.69. Found C, 79.80; H, 8.09; N, 5.13.

## Polymer 78



The 3,6-diamino-9-(2-decyltetradecyl)carbazole (96 mg, 0.18 mmol), 1,8-dichloroanthraquinone (50 mg, 0.18 mmol),  $\text{Pd}_2(\text{dba})_3$  (4.5 mg), BINAP (9 mg), cesium carbonate (231 mg), and toluene (3 mL) were mixed together and heated at  $100^\circ\text{C}$  for 72 h. Then a solution of 1-chloroanthraquinone (5 mg) in 1 mL of toluene was added and the reaction mixture was again heated at  $100^\circ\text{C}$  for an additional 6 h. The reaction mixture

was precipitated in methanol. The solid was filtered off and redissolved in THF and again precipitated from methanol. The polymer obtained was subjected to soxhlet extraction for 24 h and then dried. Isolated yield = 52 %. GPC analysis:  $M_n = 5.0 \times 10^3$  g/mol and PDI = 2.30 (PS standard). Elemental analysis: Calculated C, 81.37; H, 8.60; N, 5.69. Found C, 74.53; H, 7.97; N, 4.70.